

SOME ANALYTICAL AND EXPERIMENTAL INVESTIGATIONS TO PREDICT THE BEHAVIOUR OF SOILS UNDER THE RAILWAY TRACKS

*A Thesis Submitted
in Partial Fulfilment of the Requirements
for the Degree of*

DOCTOR OF PHILOSOPHY

by

JAGDISH T. SHAHU

VOLUME II

Chapter IV	GEOTECHNICAL TESTING FOR EVALUATION OF STRENGTH, STRESS-STRAIN-PORE PRESSURE BEHAVIOUR
Chapter V	DESIGN METHODOLOGY
Chapter VI	CONCLUSIONS AND RECOMMENDATIONS
	REFERENCES
	APPENDICES

**DEPARTMENT OF CIVIL ENGINEERING
INDIAN INSTITUTE OF TECHNOLOGY KANPUR**

February, 1993

3 JUN 1994
CENTRAL LIBRARY
INDIAN KANPUR

Doc. No. A. 117836

CE-1993-D-SHA-SOM

TO
AMMA AND DADA

12319

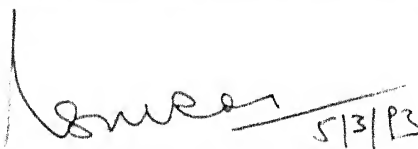
CERTIFICATE

This is to certify that the thesis entitled, "SOME ANALYTICAL AND EXPERIMENTAL INVESTIGATIONS TO PREDICT THE BEHAVIOUR OF SOILS UNDER THE RAILWAY TRACKS", by Mr. Jagdish T. Shahu, for the award of the Degree of Doctor of Philosophy, of Indian Institute of Technology, Kanpur is a record of bonafide research work carried out by him under our supervision and guidance. The results embodied in this thesis have not been submitted to any other university or institute for the award of any degree or diploma.


(YUDHBIR)

Professor

Department of Civil Engineering
Indian Institute of Technology, Kanpur


(N. S. V. Kameswara Rao)

Professor

Department of Civil Engineering
Indian Institute of Technology, Kanpur

February, 1993

ACKNOWLEDGEMENTS

The author feels immense gratitude and indebtedness to Prof. Yudhbir for his invaluable guidance, numerous suggestions, criticisms and encouragement. In the same breath, author expresses his profound gratitude to Prof. N. S. V. Kameswara Rao for his useful advice and encouragement.

Special thanks are due to Prof. M. R. Madhav for his advice and interest in this work. Thanks are also due to Prof. P. K. Basudhar and Dr. S. Chandra for their kind help.

Author is thankful to Mr. Joyis Thomas for his help in conducting unconfined tests. Sincere thanks are due to Mr. R. P. Trivedi, Mr. A. K. Srivastava, Shri Gulab Chand and Shri Parshuram of Geotechnical engineering laboratory for their day to day help. Careful tracing work of Mr. B. K. Jain is very much appreciated. Help of RDSO is appreciated.

Thanks are due to all friends, especially Miss Pratima Agarwal for her help in time of need.

Special appreciations to his wife, Prabha, for her constant patience and endurance. To his beloved child, Sunny, whose lovely smile has always been a source of strength after a long spell of hard work.

Finally, it were his parents who made many sacrifices due to author's involvement in the present work, but are no more to share the joy of this moment. It is to his parents, Amma and Dada, that this piece of work is gratefully dedicated.

CONTENT

	Page
TITLE PAGE	i
DEDICATION	ii
CERTIFICATE	iii
ACKNOWLEDGEMENTS	iv
CONTENT	v
LIST OF TABLES	xii
LIST OF FIGURES	xv
NOTATION	xxx
SYNOPSIS	xxxxx
CHAPTER 1 INTRODUCTION	1
1.1 General	1
1.2 Present problem	2
1.3 Scope of the present investigation	6
CHAPTER 2 LITERATURE REVIEW	8
2.1 Introduction	8
2.2 Literature related to analytical studies for stress determination	9
2.2.1 Empirical approaches	9
2.2.2 Finite element and other computer oriented approaches	16
2.3 Literature related to geotechnical testing for evaluation of strength, stress - strain - pore pressure behaviour	21
2.3.1 Total stress/fatigue studies	21
2.3.2 Effective stress studies	24
2.3.2.1 Saturated soils	25
2.3.2.2 Non-saturated soils	34

2.4 Literature related to track formation design	38
2.5 Literature related to other important aspects	50
2.5.1 Effect of train speed on stresses	50
2.5.2 Characterization of track foundation	51
2.5.3 Soil improvement methods	57
2.5.4 Field measurements and model testing	58
2.6 Summary	61
CHAPTER 3 MATHEMATICAL MODELLING OF RAILWAY TRACK	64
3.1 Introduction	64
3.2 Rigorous elastic method (ELASTIC.F model)	65
3.2.1 Introduction	65
3.2.2 Theoretical background	65
3.2.3 Description of rigorous elastic method (ELASTIC.F model)	67
3.2.4 Limitations	72
3.2.5 Comparison of results	73
3.2.6 Results and discussion	73
3.3 Two dimensional finite element analysis	90
3.3.1 Introduction	90
3.3.2 Description of two dimensional finite element routines	90
3.3.3 Two dimensional finite element model for railway track (2D8N model)	93
3.3.4 Selection of finite element mesh	102
3.3.5 Limitations	119
3.3.6 Comparison of results	122
3.3.7 Results and discussion	122
3.4 Three dimensional finite element analysis	136
3.4.1 Introduction	136
3.4.2 Description of three dimensional finite element routines	136
3.4.3 Track modelling	140
3.4.3.1 Track outline	140
3.4.3.2 Boundary conditions	142
3.4.3.3 Rail element	142
3.4.3.4 Sleepers	146

3.4.4	Selection of finite element mesh	147
3.4.5	Limitations	152
3.4.6	Evaluation of parameters used in constitutive relationship	153
3.4.7	Comparison of results	159
3.4.8	Parametric studies	159
3.4.9	Results and discussion	160
3.5	Comparison of results	183
3.5.1	FAST track	183
3.5.2	So (1978) track	186
3.5.3	Vienna arsenal single sleeper and Derby panel full Scale model tests	189
3.5.4	Field measurements by RDSO on Indian railways	200
3.5.4.1	Tests conducted on section No. 2 on Ambala-Ludhiana section (1964-67)	200
3.5.4.2	Tests conducted on section No. 6 on Ambala-Ludhiana section (1964-67)	202
3.5.4.3	Tests conducted on a dead-end siding near canal bed site at RDSO, Lucknow	202
3.5.4.4	Field measurement of formation pressure due to long haul train trials at Mandah road station, Allahabad division.	202
3.5.5	Empirical formulae available in literature	202
3.6	Comparison of the three models	206
CHAPTER 4	GEOTECHNICAL TESTING FOR EVALUATION OF STRENGTH, STRESS-STRAIN-PORE PRESSURE BEHAVIOUR	210
4.1	Introduction	210
4.2	Explanation of selected terms	211
4.3	Geotechnical nature of Campus silt	212
4.3.1	General	212
4.3.2	Particle size distribution and Atterberg limits	212
4.3.3	Compaction characteristics	216

4.5	Relevance of tests performed with present problem	216
4.6	Technique of testing	221
4.6.1	Equipment used	221
4.6.2	Sample preparation	221
4.6.3	Total stress tests	222
4.6.3.1	Series A1 - Unconsolidated undrained tests without pore pressure measurement	222
4.6.3.2	Series A2 - Unconfined cyclic tests	223
4.6.3.3	Series A3 - Unconfined cyclic softened tests	234
4.6.4	Effective stress tests	225
4.6.4.1	Pore pressure measurement in partially saturated soils	225
4.6.4.2	Series B1 - Unconsolidated undrained tests with pore water pressure measurement	225
4.6.4.3	Series B2 - Unconsolidated undrained cyclic tests with pore water pressure measurement	226
4.6.4.4	Series B3 - Undrained static and cyclic tests with pore water pressure measurement on samples with back pressure saturation	228
4.7	Presentation of test results	230
4.7.1	Total stress tests	230
4.7.1.1	Series A1 - Unconsolidated undrained tests without pore pressure measurement	230
4.7.1.2	Series A2 - Unconfined cyclic tests	230
4.7.1.3	Series A3 - Unconfined cyclic softened tests	244
4.7.2	Effective stress tests	252
4.7.2.1	Series B1 - Unconsolidated undrained tests with pore water pressure measurement	252

4.7.2.2	Series B2 - Unconsolidated undrained cyclic tests with pore water pressure measurement	270
4.7.2.3	Series B3 - Undrained static and cyclic tests with pore water pressure measurement on samples with back pressure saturation	271
4.8	Interpretation and Discussion	292
4.8.1	Introduction	292
4.8.2	Total stress behaviour (static and cyclic)	292
4.8.2.1	Unconfined tests	292
4.8.2.2	Confined tests	305
4.8.3	Effective stress behaviour for static tests	309
4.8.3.1	Quasi saturated behaviour	309
4.8.3.2	Samples exhibiting quasi saturated response	314
4.8.3.3	Stress - strain, pore pressure - strain response with varying confining stress	325
4.8.3.4	Failure envelope	328
4.8.3.5	Comparison of other results	332
4.8.3.5.1	Comparison with Cruz et al. (1985)	332
4.8.3.5.2	Comparison with data for Canyon dam clay	334
4.8.3.5.3	Comparison in terms of total stress behaviour of compacted soils	349
4.8.4	Effective stress behaviour of Campus silt under cyclic load condition and evaluation of threshold stress	354
4.8.4.1	Plastic strain development	354
4.8.4.2	Pore pressure response during cyclic loading	369

4.8.4.3	Evaluation of threshold stress and threshold stress ratio	375
4.8.4.3.1	Plastic strain criterion	376
4.8.4.3.2	Pore pressure during cyclic loading criterion	379
4.8.4.4	Guidelines for evaluation of threshold stress ratio	382
CHAPTER 5	DESIGN METHODOLOGY	391
5.1	Introduction	391
5.2	Broad outline of design methodology	393
5.2.1	Estimation of induced stresses on the subgrade	393
5.2.2	Evaluation of threshold stress	397
5.2.3	Design of depth of formation	398
5.3	Rigorous design	398
5.4	Simplified design	404
5.5	Design example for Campus silt	406
5.5.1	Rigorous design	408
5.5.2	Simplified design	409
CHAPTER 6	CONCLUSIONS AND RECOMMENDATIONS	414
6.1	General	414
6.2	Mathematical modelling	414
6.3	Geotechnical testing	418
6.3.1	Unconfined tests	419
6.3.2	Effective stress static tests	420
6.3.3	Effective stress cyclic tests	424
6.4	Recommendations for further studies	428
REFERENCES		430

Appendices		439
A1	Details of TRACK 1	439
A2	Details of TRACK 2 [Same as FAST TRACK, Selig et al. (1979)]	441
A3	So (1978) TRACK and the range of parameters used	443
A4	Details of Derby and Vienna TRACKS	445
A5	Details of TRACKS tested in India	448
B1	Testing of 2D8N finite element routine	452
B2	Testing of 3D20N finite element routine	458

LIST OF TABLES

Table No.	Name of Table	Page
1.1	Status of formation treatment methods	4
2.1	Track equipment standards by SNCF	48
2.2	Track formation quality by SNCF	48
3.1	Range of Young's modulus for different soils [(Bowles (1984))]	74
3.2	Empirical correlation between formation coefficient 'C' and Young's modulus of subgrade, 'E'	74
3.3	Results of parametric studies (ELASTIC.F model)	76
3.4(a)	Meshes used in trials for rectangular mesh selection	104
3.4(b)	Compartment dimensions of meshes used in trials for rectangular mesh selection	105
3.4(c)	Results of trials for rectangular mesh selection	113
3.5	Results of parametric studies (2D8N model)	124
3.6	Beam problem -- 2D8N vis - a - vis 3D20N	138
3.7(a)	Meshes used in trials for 3-D mesh selection	148
3.7(b)	Compartment dimensions for meshes used in trials for 3-D mesh selection	149

3.7(c)	Result of trials for 3-D mesh selection	150
3.8	Summary of cyclic plate load test results (tests carried out on Sandilla-Rahimabad section near Lucknow)	156
3.9	Results of parametric studies (3D20N model)	170
3.10	Comparison of results for section no. 2, Ambala-Ludhiana section	201
3.11	Comparison of results for section no. 6, Ambala - Ludhiana section	203
3.12	Track properties for canal bed site, Lucknow	203
3.13	Comparison of results for canal bed site, Lucknow	204
3.14	Comparison of results for Mandah road station, Allahabad division	204
3.15	Comparison of results with empirical formulae	205
3.16	Comparison of 3 models in terms of results predicted	207
3.17	Comparison of CPU time on Convex 220	209
4.1	Index properties for Campus silt	215
4.2	Summary of total tests conducted	218
4.3	Details of total stress UU tests (tests with cell pressure > 0)	232
4.4	Details of series A2 tests	233
4.5	Details of series A3 tests	251

4.6	Details of effective stress tests on Campus silt (static tests)	267
4.7	Details of effective stress tests on Campus silt (cyclic and static tests)	268
4.8	Calculation of ultimate stress from Eq. (28.1) from Lambe and Whitman (1978) for Campus silt	323
4.9	Calculation of ultimate stress from Eq. (28.1) from Lambe and Whitman (1978) for Canyon dam clay	324
4.10	Critical state data for Campus silt (static tests)	336
4.11	Critical state data for Campus silt (cyclic and static tests)	337
4.12	Calculation for Roscoe surface	346
4.13	Additional data related to cyclic tests on Campus silt	358
4.14	Value of coefficients in plastic strain model	364

LIST OF FIGURES

	Page
1.1 Track structure	5
2.1 Method of Odemark	12
2.2 Comparison of stress - strain curves of single loading	26
2.3 Peak strength after ten cycles of loading for series I	27
2.4 Comparison of stress-strain curves of single loading and repeated loading	28
2.5 Mohr envelope for compacted soil	37
2.6 Design charts [Rubin et al. (1970)]	39
2.7 Decision diagram for road bed depth	42
2.8(a) Relationship between tie spacing and road bed pressure	43
2.8(b) Relationship between ballast depth, the kind of tie and road bed pressure	43
2.9(a) Relationship between roadbed pressure, liquid limit and mud pumping. (Applied rail pressure is 5 t and ordinary wooden tie is used)	44
2.9(b) Relationship between roadbed pressure, CBR and mudpumping. Applied rail pressure is 5 t and standard wooden tie is used)	44
2.10 Maximum dynamic vertical stresses exerted on the subgrade	46

2.11	Track depression vs. Load relationship for different tracks	54
2.12	Bearing area of sleeper	56
3.1	Measurement of X in Equation 3.7	68
3.2	Sleeper and load configuration for double wheel load case	68
3.3	Assumed load distribution below the sleeper	70
3.4	Assumed load distribution below the sleeper	70
3.5	Variation of σ_{vt} with E_s for TRACK 1 (ELASTIC.F model)	79
3.6	Variation of σ_{vt} with total depth of construction for TRACK 1 (ELASTIC.F model)	80
3.7	Variation of σ_v inside the subgrade for $E_s = 10$ MPa for different d_t (ELASTIC.F model)	81
3.8	Variation of σ_v with depth for different d_t (ELASTIC.F model)	82
3.9	Variation of σ_v with depth for different E_s (ELASTIC.F model)	84
	Variation of σ_v inside the subgrade for $d_t = 1.0$ m for different E_s (ELASTIC.F model)	85
	Variation of σ_{vt} for different proportioning of ballast and subballast depth for $d_t = 1.0$ m (ELASTIC.F model)	86
	Variation of σ_{vt} with formation coefficient 'C' for $d_t = 0.4$ m (ELASTIC.F model)	86

3.13	Variation of σ_{vt} with tie spacing for different track conditions (ELASTIC.F model)	88
3.14	Variation of σ_{vt} with moment of inertia of rail, I_r (ELASTIC.F model)	88
3.15	Variation of σ_{vt} with Young's modulus of ballast (ELASTIC.F model)	89
3.16	Variation of σ_{vt} with Young's modulus of subballast (ELASTIC.F model)	89
3.17	Notations used (2D8N model)	94
3.18	Track structure and the referred directions	94
3.19	Track sections	96
3.20	Sleeper section	98
3.21	Wheel configuration	98
3.22	Load distribution - when load is between the sleepers	100
3.23	Load distribution - when load is on the sleeper	100
3.24	Load distribution - Present problem	100
3.25	Track formation originally used for calculations	103
3.26	Discretization for mesh A (2D8N model)	106
3.27	Discretization for mesh B (2D8N model)	107
3.28	Discretization for mesh C (2D8N model)	108
3.29	Variation of σ_1 with depth for TRACK 2 (2D8N model)	110

3.30	Variation of σ_3 with depth for TRACK 2 (2D8N model)	111
3.31	Variation of δ with depth for TRACK 2 (2D8N model)	112
3.32	Scheme for rectangular mesh discretization	114
3.33	Variation of δ with depth for TRACK 2 by different rectangular mesh discretizations (2D8N model)	116
3.34	Variation of σ_1 with depth computed by using different rectangular mesh discretizations for TRACK 2 (2D8N model)	117
3.35	Variation of σ_3 with depth computed by using different rectangular mesh discretizations for TRACK 2 (2D8N model)	118
3.36	Proposed modification to 2D8N model	121
3.37	Variation of displacement with depth for TRACK 1 (2D8N model)	126
3.38(a)	Variation of σ_1 with depth for TRACK 1 (2D8N and modified 2D8N model)	127
3.38(b)	Variation of σ_3 with depth for TRACK 1 (2D8N model)	128
3.38(c)	Variation of τ_{\max} with depth for TRACK 1 (2D8N model)	129
3.39	Variation of major and minor principal stress along the sleeper on top of subgrade for TRACK 1 (2D8N model)	131
3.40	Variation of σ_{1t} and σ_{3t} with E_s for different depths of subballast (2D8N model)	132

3.41	Variation of displacement on top of sleeper with E_s for different depths of subballast (2D8N model)	133
3.42	Variation of σ_{1t} with d_b/d_t (2D8N model)	135
3.43	Notations used (3D20N model)	141
3.44	Displacement under the rail seat versus depth for different rail conditions for TRACK 2	144
3.45	σ_1 versus depth for different rail conditions for TRACK 2	145
3.46	Mesh C' discretization	151
3.47	E_s versus depth below formation level - wave propagation test results on Sandilla - Rahimabad section	155
3.48	Variation of displacement under the rail seat with depth for TRACK 1 (3D20N model)	162
3.49(a)	Variation of σ_1 with depth for TRACK 1 (3D20N model)	163
3.49(b)	Variation of σ_3 with depth for TRACK 1 (3D20N model)	164
3.50	Variation of major principal stress along the sleeper at different depths for TRACK 1 (3D20N model)	165
3.51	Variation of rail deflection along the rail direction for TRACK 1 (3D20N model)	166
3.52	Stresses on top of subgrade along the sleeper for single wheel load with joint element (3D20N model)	167

3.53	Stress distribution in actual track system	173
3.54	Assumed stress distribution in equivalent track system	173
3.55	Elastic plates	175
3.56	Variation of σ_{1t} with Young's modulus of subballast, E_{sb} for reference track (3D20N model)	177
3.57	Variation of σ_{1t} with Young's modulus of ballast, E_b for reference track (3D20N model)	177
3.58	Variation of σ_{1t} with I_r for TRACK 1 (3D20N model)	178
3.59	Variation of σ_{1t} with tie spacing for TRACK 1 (3D20N model)	179
3.60	Variation of σ_{1t} with m	180
3.61	Comparison of results - Vertical displacement with depth for FAST track	184
3.62	Comparison of results for vertical stress with depth for FAST track	185
3.63	Comparison of results for vertical stress along the sleeper at 18 cm depth for FAST track	187
3.64	Comparison of results for rail displacement along rail direction for FAST track	188
3.65	Comparison of results with So (1978)	190
3.66	Comparison of results with So (1978)	190

3.67	Comparison of results with So (1978)	190
3.68	Structures tested at Vienna and Derby [Janin et al. (1983b)]	192
3.69	Comparison of results for total resilient displacement for Derby panel tests	193
3.70	Comparison of results for major principal stress for Derby panel tests	194
3.71	Comparison of results in terms of vertical stresses for Vienna and Derby tests	196
3.72	Comparison of results for horizontal stresses for vienna structure No. 2	197
3.73	Comparison of results for transverse stresses for Derby structures	198
3.74	Comparison of results with Rosalie elasto plastic model	199
4.1	Particle size distribution	213
4.2	Index properties	214
4.3	Water content - dry density relationship	217
4.4	Stress - strain relationship for static unconfined test	231
4.5	Stress - strain relationship for cyclic test ($R_f = 6.6 \%$)	234
4.6	Stress - strain relationship for cyclic test ($R_f = 18.7 \%$)	235
4.7	Stress - strain relationship for cyclic test ($R_f = 29.7 \%$)	236

4.8	Stress - strain relationship for cyclic test ($R_f = 36.5 \%$)	237
4.9	Stress - strain relationship for cyclic test ($R_f = 46.0 \%$)	238
4.10	Stress - strain relationship for cyclic test ($R_f = 54.2 \%$)	239
4.11	Stress - strain relationship for cyclic test ($R_f = 64.0 \%$)	240
4.12	Stress - strain relationship for cyclic test ($R_f = 71.3 \%$)	241
4.13	Stress - strain relationship for cyclic test ($R_f = 73.7 \%$)	242
4.14	Stress - strain relationship for cyclic test ($R_f = 76.6 \%$)	243
4.15	Stress - strain relationship for static softened test	245
4.16	Stress - strain relationship for cyclic softened test ($R_f = 18.9 \%$)	246
4.17	Stress - strain relationship for cyclic softened test ($R_f = 37.1 \%$)	247
4.18	Stress - strain relationship for cyclic softened test ($R_f = 54.4 \%$)	248
4.19	Stress - strain relationship for cyclic softened test ($R_f = 70.7 \%$)	249
4.20	Stress - strain relationship for cyclic softened test ($R_f = 82.2 \%$)	250

4.21	Dry density versus water content relationship for effective stress tests	253
4.22	Cell pressure versus initial pore water pressure	254
4.23	Stress - strain relation for $S = (86.5 - 87.2) \%$	255
4.24	Pore pressure - strain relation for $S = (86.5 - 87.2) \%$	256
4.25	Effective stress ratio - strain relation for $S = (86.5 - 87.2) \%$	257
4.26	Effective stress path for $S = (86.5 - 87.2) \%$	258
4.27	Stress - strain relation for $S = (92.0 - 94.6) \%$	259
4.28	Pore pressure - strain relation for $S = (92.0 - 94.6) \%$	260
4.29	Effective stress ratio - strain relation for $S = (92.0 - 94.6) \%$	261
4.30	Effective stress path for $S = (92.0 - 94.6) \%$	262
4.31	Stress - strain relation for $S = (95.1 - 96.1) \%$	263
4.32	Pore pressure - strain relation for $S = 95.1 - 96.1) \%$	264
4.33	Effective stress ratio - strain relation for $S = (95.1 - 96.1) \%$	265
4.34	Effective stress path for $S = (95.1 - 96.1) \%$	266

4.35	Stress - strain , pore pressure strain relationship for test with $R_f = 18.52 \%$	272
4.36	Stress - strain , pore pressure strain relationship for test with $R_f = 31.82 \%$	273
4.37	Stress - strain , pore pressure strain relationship for test with $R_f = 37.68 \%$	274
4.38	Stress - strain , pore pressure strain relationship for test with $R_f = 31.37 \%$	275
4.39	Effective stress path for test with $R_f = 18.52 \%$	276
4.40	Effective stress path for test with $R_f = 31.82 \%$	277
4.41	Effective stress path for test with $R_f = 37.68 \%$	278
4.42	Effective stress path for test with $R_f = 31.37 \%$	279
4.43	Stress - strain relation for tests with back saturation	280
4.44	Pore - pressure - strain relation for tests with back saturation	281
4.45	Effective stress ratio - strain relation for tests with back saturation	282
4.46	Effective stress path for tests with back saturation	283
4.47	Stress - strain relation for tests with back saturation	285

4.48	Pore - pressure - strain relation for tests with back saturation	286
4.49	Effective stress ratio - strain relation for tests with back saturation	287
4.50	Effective stress path for tests with back saturation	288
4.51	Stress - strain relation for tests with back saturation for (a) $R_f = 20.05 \%$ (b) $R_f = 14.53 \%$	290
4.52	Stress - strain relation for tests with back saturation for (a) $R_f = 27.78 \%$ (b) $R_f = 15.83 \%$ (c) $R_f = 28.38 \%$	291
4.53	Increase in water content from initial state with R_f	294
4.54	Increase in water content due to cyclic loading with R_f	295
4.55	Variation of s_u with δ_w	296
4.56	Variation of s_u with R_f	297
4.57	Variation of plastic strain with δ_w	298
4.58	Stress - strain relation for all unconfined cyclic tests	300
4.59	Variation of E_u/E_i and E_{us}/E_i with R_f	301
4.60	Stress - strain relation for all unconfined softened tests	302
4.61	Variation of Young's modulus with water content	303

4.62	Variation of $\log (E)$ with water content	304
4.63	Variation of s_u with water content	306
4.64	Effect of confining pressure on stress - strain behaviour	307
4.65	Total stress failure envelopes	308
4.66	Variation of B with S for (a) Campus silt (b) Canyon dam clay (c) Chiew larn clay	310
4.67	Comparison of stress-strain and pore pressure - strain behaviour (a) dry of optimum (b) wet of optimum	312
4.68	Comparison of peak failure envelope	313
4.69	Variation of $\Delta u_{\max}/\sigma_c'$ with σ_c'	316
4.70	Variation of $\Delta u_{\max}/(\sigma_1 - \sigma_3)$ with σ_c'	317
4.71	Normalized stress paths for Campus silt	318
4.71(a)	Explanation for Figure 4.71	319
4.72	Normalized stress paths for Canyon dam clay [Casagrande and Poulos (1964)]	320
4.73	Variation of $(\sigma_1 - \sigma_3)/2$ at failure with σ_c'	321
4.74	Effect of confining pressure on (a) pore pressure - strain behaviour (b) Stress - strain behaviour	326
4.75	Effect of confining pressure on stress strain behaviour	327
4.76	Effective stress failure envelope	329

4.77	Effective stress failure envelope (enlarged view)	330
4.78	Typical stress - strain, pore pressure - strain and stress path for group IV soil [Cruz et al. (1985)]	333
4.79	Variation of P_i' with w_f	335
4.80	Variation of P_f' with w_f	339
4.80(a)	Variation of P' with w	340
4.81	Variation of P_f' with q_f	341
4.82	q/P_e' versus P'/P_e' relationship for Campus silt	343
4.83	q/P_e' versus P'/P_e' relationship for Canyon dam clay	344
4.84	q_f/P_e' versus P_f'/P_e' relationship	345
4.85	Pore pressure parameter A_f versus OCR	348
4.86	Water content versus strength relationship at failure	351
4.87	Variation of s_u with $(w-w_{opt})/I_p$	353
4.88	Increase in plastic strain with cyclic loading ($\sigma_c' = 20-22$ kPa)	356
4.89	Increase in plastic strain with cyclic loading ($\sigma_c' = 40$ kPa)	357
4.90	Increase in plastic strain with cyclic loading (high confining pressure)	359
4.91	Plastic strain versus R_f for unconfined cyclic tests	360

4.92	Cyclic load triaxial tests - permanent strain versus No. of cycles [Janin et al. (1983a)]	362
4.93	Development of permanent axial strain in cyclic triaxial undrained compression tests on lacustrine clay from Hamilton, Ontario [after Wilson and Greenwood (1974)]	363
4.94	C_p versus R_f	366
4.95	Pore pressure rise with number of cycles	370
4.96	Normalized effective stress path for cyclic tests with high confining pressure	371
4.97	Normalized pore pressure rise with axial strain	373
4.98	q/P_e' versus P'/P_e' relationship for cyclic tests	374
4.99	Rise in plastic strain during 100 cycles versus R_f	377
4.100	$(\sigma_1 - \sigma_3)_{At\Delta u_{max}} / (\sigma_1 - \sigma_3)_{max}$ and R_{TS} versus σ_c'	381
4.101	Threshold stress ratio versus I_p relationship	384
4.102	Threshold stress versus σ_c' relationship for compacted saturated Campus silt	386
4.103	Threshold stress versus σ_c' relationship for compacted Angul clay [Yudhbir et al. (1992)]	387
4.104	Threshold stress versus σ_c' relationship for NC marine clay [Rehman (1977)]	388

4.105	Threshold stress versus σ_c' relationship	389
5.1	Induced stress ($\sigma_1 - \sigma_3$) versus m	394
5.2	Induced stress (σ_1) versus m	395
5.3	Threshold stress versus total depth of formation	399
5.4	Flow chart	401
5.5	Design chart	402
5.6	Flow chart for simplified design	407
5.7	Cross-section of a typical formation	412
B1.1	Comparison of exact and FE solutions - stress profiles under the load - 2-D case	453
B1.2	Comparison of exact and FE solutions for vertical stress distribution - 2-D case	454
B1.3	Comparison of exact and FE solutions for Lateral pressure distribution - 2-D case	455
B1.4	Comparison of exact and FE solutions for shear stress distribution - 2-D case	456
B1.5	Finite element mesh for 2-D analysis	457
B2.1	Comparison of exact and FE solutions for Vertical stress profile - 3-D case	459
B2.2	Comparison of exact and FE solutions for vertical pressure distribution - 3-D case	460

NOTATION

a, b	= intercept and slope of line (used with subscript)
a_1	= angle of distribution of pressure in ballast
A, B	= Skempton's pore pressure parameters
b	= width of sleeper
\bar{b}	= bearing factor = $F / 2 S$
c_v	= coefficient of consolidation
c'	= cohesion in terms of effective stresses
C	= formation coefficient
C_p	= value of $\log(\epsilon_p)$ at $N = 1$
CBR	= California bearing ratio
CSL	= critical state line
CLRS	= critical level of repeated stress
d_b	= actual depth of ballast
d_{sb}	= actual depth of subballast
d_b^*	= modified depth of ballast
d_{sb}^*	= modified depth of subballast
d_t	= total depth of formation ($d_b + d_{sb}$)
D_p	= value of first gradient of bilinear log-log plot between ϵ_p and N

e	= maximum horizontal tensile strain at the base of stabilized layers
e_e	= elastic strain
e_f	= vertical strain at failure
e_0	= initial void ratio
E	= tangent Young's modulus
E_b	= Young's modulus of elasticity of ballast
E_{equ}	= Young's modulus of equivalent system
E_f	= Young's modulus of filling material
E_i	= tangent Young's modulus of shear failure (before repeated loading)
E_p	= value of second gradient of bilinear log-log plot between ϵ_p and N
E_r	= Young's modulus of elasticity of rail
E_s	= Young's modulus of elasticity of subgrade
E_{sb}	= Young's modulus of elasticity of subballast
E_t	= Young's modulus of elasticity of tie (sleeper)
E_{t1}, E_{t2}	= Young's modulus of elasticity for discrete sleeper system and continuous sleeper system
E_u	= tangent young's modulus of shear failure (after repeated loading but no softening)
E_{us}	= tangent Young's modulus of shear failure (after repeated loading and softening)
EI	= flexural stiffness

F	= bearing area per sleeper
G	= track gauge
GDS	= Geotechnical Digital System
i	= speed impact factor to be multiplied by σ_t to obtain σ_{speed}
I	= moment of inertia
I_p	= plasticity index
I	= moment of inertia per rail
I_{t1}, I_{t2}	= moment of inertia of discrete sleeper and continuous sleeper respectively
K_f 'line	= line in effective stress plot joining maximum failure shear stress points
k_n	= normal joint stiffness
k_s	= shear joint stiffness (for 2-D case)
k_{s1}	= shear joint stiffness (in x-direction in 3-D case)
k_{s2}	= shear joint stiffness (in y-direction in 3-D case)
K	= ratio of pulsating load causing failure to the static failure strength
K_n	= Newmark's influence factor
K_0	= coefficient of earth pressure at rest
l	= length of sleeper
L	= effective bearing length of sleeper

L_b	=	base length of ballast track
L1-L10	=	load areas
L1'-L10'	=	load areas
m	=	modular ratio as a measure of ballast, subballast and subgrade
M	=	slope of critical state line
\bar{M}	=	moment force on rail
\bar{m} , \bar{n}	=	parameters used in Newmark's equations
N	=	number of load cycle
N_f	=	total number of repetitions required for track for failure
N_r	=	total number of repetitions in the track life
N_s	=	value of N where change in gradient from D_p to E_p occurs
OCR	=	overconsolidation ratio
OMC, w_{opt}	=	optimum moisture content
ORE	=	Office for Research and Experiments, International union of railways, Utrecht
p_s	=	stress below the sleeper where y_r is calculated
P'	=	$(\sigma_1' + 2\sigma_3')/3$
P_e'	=	Hvorslev's equivalent consolidation pressure
P_s	=	load on individual sleeper
q	=	$(\sigma_1' - \sigma_3')$

$q(x)$	=	externally applied load
q_1	=	intensity of pressure on rectangular load area
Q	=	vertical wheel load
\bar{Q}_1	=	initial range load
Q_1	=	load number one under which stresses are needed
Q_2	=	load number two -- far side load of axle
R	=	reaction of sleeper
R_f	=	cyclic stress ratio
R_{TH}	=	threshold stress ratio
RDSO	=	Research, Design and Specifications Organization, Ministry of Indian Railways
s	=	a factor which depends on track quality
s_u	=	undrained shear strength
\bar{S}	=	spacing between the sleepers
S	=	degree of saturation
SNCF	=	French railway organization
t	=	thickness of sleeper
\bar{t}	=	statistical safety factor
u, k	=	modulus of railroad reaction or Modulus of elasticity of rail support
u_a	=	pore air pressure
		track modulus in the elastic range

u_i	= track modulus in the initial range
Δu	= pore water pressure change
$(\Delta u)_{cyc}$	= cumulative pore water pressure built up in total 100 cycles
Δu_0	= equilibrium pore water pressure when cell pressure was applied. Also called as initial pore water pressure
UU	= unconsolidated undrained
v_o	= specific volume of sample
V	= train speed
w	= water content
w_l	= liquid limit
w_1	= final water content after softening
Δw	= change in water content during series A2 tests
δw	= difference between water content after 100 cycles and softening, and water content at equilibrium state (i.e. water content after softening of as compacted sample)
W_1	= moment of resistance of rail foot
W_2	= moment of resistance of rail head
x	= horizontal distance of point from the load position on the rail where deflection is needed
X	= a parameter that varies with the degree of saturation of sample

x_1	= horizontal distance of point from the load position on the rail where zero bending moment occurs
y_f	= distance between the neutral axis of rail and rail flange
y_r	= deflection of rail
y_s	= deflection of sleeper under total load Q
y_{s1}	= deflection of sleeper under initial load Q_1
y_t	= vertical deflection of sleeper due to reaction force 'R' of sleeper
z	= rail deflection
z_d	= depth of point from surface at which stresses are required
ZLV	= Zimmermann's Wheel load
α, β	= coefficients in pore pressure rate vs. time relationship
δ	= displacement
$\delta \epsilon_p$	= cumulative plastic strain due to 100 cycles only
ϵ_p	= strain rate per unit time
ϵ_p	= plastic strain
ϵ_y	= strain in y-direction
ϕ'	= angle of shearing resistance in terms of effective stresses
ϕ^b	= term relating the contribution of matrix suction to the shearing resistance

γ_d	=	dry density
$\eta(\xi), \mu(\xi)$	=	coefficients as a function of ξ
κ	=	slope of swelling line in consolidation test
λ	=	slope of virgin consolidation line in volume change plot
ν	=	Poisson's ratio
θ	=	stress dispersion angle in equivalent system
θ_1	=	stress dispersion angle in ballast
θ_2	=	stress dispersion angle in subballast
ρ_s	=	static rigidity of track
σ	=	total mean stress
σ_c'	=	initial effective stress ; Initial consolidation pressure
σ_{dyn}	=	dynamic stress level in terms of deviator stress during repeated / cyclic loading
σ_{min}	=	minimum stress level maintained in terms of deviator stress during repeated / cyclic loading
σ_{r1}	=	stresses in rail foot
σ_{r2}	=	stresses in rail head
σ_s	=	maximum pressure at the bottom of sleeper
σ_t	=	static stress at any point in the track
σ_{ult}	=	ultimate failure stress in terms of deviator stress
σ_{vmean}	=	average pressure on top of subgrade

σ_{vt}	= vertical pressure on top of subgrade under the rail seat
σ_z	= maximum pressure at any point in subgrade after applying increment for given speed
$(\sigma_z)_c$	= vertical stress at corner of any rectangular area due to uniformly distributed load on that area
σ_1	= major principal stress
σ_2	= minor principal stress
σ_3	= cell pressure, minor principal stress
σ_{1t}	= maximum major principal stress on top of subgrade
σ_{3t}	= maximum minor principal stress on top of subgrade
(σ_1'/σ_3')	= effective stress ratio
τ	= undrained shear strength of partially saturated soil
τ_{max}	= maximum shear stress on top of subgrade
ξ	= x / L_b

Subscript

f	= failure
TS	= at threshold stress level
cyc	= cyclic
sr	= stress ratio
v	= vertical

p	=	plastic
cal	=	calculated
exp	=	experimental
i	=	initial
cs	=	critical state
max	=	maximum
dyn	=	dynamic
sta	=	static
bm	=	beam
sb	=	subballast
b	=	ballast

Name of Student : Jagdish Jelangrao Thahu Roll No : 8720363
Degree for which submitted : Ph.D Department : Civil Enng.

Thesis title : Some Analytical and Experimental Investigations to predict the Behaviour of Soils under the Railway Tracks.

Names of thesis supervisors :

1. Dr. Gudhlin
2. Dr. N. S. V. Kameswara Rao

Month and year of thesis submission : February, 1993

SYNOPSIS

Railway is the most important mode of transportation of both men and materials in India. To increase the transportation efficiency, heavier, longer and faster trains are needed. The track-foundation-soil system is one of the key factors in bringing about these changes. The present method of design of railway formation is based on empirical basis which gives uneconomical design. Moreover, this method does not help decision making in respect of suitability of existing tracks for heavier and faster trains.

When trains pass over the track, subgrade gets subjected to cyclic stress. If this stress is greater than a certain level of stress called threshold stress for soil, cumulative permanent deformations are produced leading to ballast penetration into the subgrade progressively causing the subgrade failure. In some instances, ballast penetration up to 1 m depth into the subgrade has been observed in the field.

The present study to predict the behaviour of soils under the railway formations subjected to cyclic loading has been carried out in three steps viz. (i) mathematical modelling for determination of induced stresses in the subgrade based on

elastic method, 2-D finite element method and 3-D finite element method, (ii) geotechnical testing to evolve a suitable laboratory testing procedure for formation design and to evaluate threshold stress, and (iii) formulation of formation design methodology.

The work contained in the thesis has been organized into six chapters. In Chapter One, the topic has been introduced and the scope of the present study has been outlined. The available literature related to analytical studies for stress determination (empirical, finite element and other computer oriented approaches) ; geotechnical testing for total stress and effective stress studies on both saturated and non saturated soils ; track formation design ; and other important aspects such as effect of train speed on stresses, characterization of track foundation, soil improvement methods, field measurements and model testing has been reviewed in Chapter Two.

Mathematical modelling carried out in this study, is described in detail in Chapter Three. Three models with increasing sophistication viz. ELASTIC.F , 2D8N and 3D20N model have been developed for calculating major and minor principal stresses in the track structure.

ELASTIC.F model consists of determining the stresses at sleeper-ballast interface by considering the rail as a beam on elastic foundation and then using Odemark's method and Newmark's solution for calculating stresses in the subgrade. 2D8N model is a two-dimensional linear, elastic finite element

model which uses 8-noded rectangular elements. Also, a semi-analytical modification to this model is suggested which invokes two trials of 2D8N model. 3D20N model is a three-dimensional linear, elastic finite element model which uses 20-noded brick element and models rail as one-dimensional beam element. Performance of this model is very similar to 'MULTA' model [Selig et al. (1979)] which is like a closed form solution.

Parametric studies using all the three models have been carried out to evaluate the relative importance of each track component. It is observed that depth of formation and type of subgrade are the most important factors.

Results predicted by all the three models have been compared with predicted results by other models ; measured results in the field by ORE (Office of Research and Experiments, International Union of Railways) and Indian Railways ; and full scale model test results by ORE . It has been observed that all the three models predict quite satisfactory results. Comparisons have been also made with values predicted by semi-empirical methods and it is shown that these methods overpredict by as much as 2 to 4 times the measured results.

It is shown that vertical and horizontal stresses predicted by elastic analysis compare well with those obtained by elasto-plastic analysis which takes into consideration 'no tension' condition in granular media. A non-dimensional parameter 'm' has been introduced as a measure of ballast,

subballast and subgrade characteristics (i.e the formation quality).

Chapter four deals with the geotechnical testing carried out on alluvial silt for evaluation of strength, stress-strain-pore pressure behaviour during static and cyclic loading. Total six series of tests viz. total stress static shear tests, unconfined cyclic tests, unconfined cyclic softened tests, effective stress static shear tests, cyclic undrained tests on quasi saturated samples with pore pressure measurement at high confining pressure and cyclic undrained tests on back saturated samples with pore pressure measurement at low cell pressure simulating the track loading conditions, have been carried out.

Relationship between incremental plastic strain, $\delta\epsilon_p$ after 100 cycles on unconfined compacted samples and corresponding increase in incremental water content on softening has been indicated. The explanation of mudpumping problems encountered by Indian railways under the tracks in alluvial soil deposits has been well brought out by observing the significant degradations in both stiffness and strength following the transient loading and softening.

A simple procedure to ensure quasi saturated response for partially saturated sample is given. It has been shown that stress - strain, pore pressure - strain response and effective stress paths for compacted samples follow non-normalized behaviour with respect to consolidation stress. It is observed that evaluation of failure envelope by Marsal's procedure gives

satisfactory results.

Stress - strain, pore pressure - strain , stress path and other results for IITK Campus silt show remarkable similarities with group IV soils [Cruz et al. (1985)] and with Canyon dam clay [Casagrande and Hirschfeld (1960) ; Casagrande and Poulos (1964)] in all aspects of behaviour of compacted samples. Effective stress data available for Campus silt and Canyon dam clay on compacted samples has been examined in the general framework of critical state model. It has been brought out that compacted soil samples behave like overconsolidated soils with different values of past maximum pressure (produced due to compaction, depending upon moulding water content and dry density for a given compaction energy). It has been observed that compacted soils, when tested at a degree of saturation above a certain value which ensures quasi-saturation, behave like over consolidated soils up to effective confining stresses below that needed for complete saturation and like normally consolidated when tested at effective confining stresses greater than that needed for full saturation.

Guidelines given by Yudhbir and Wood (1989) have been followed in drawing Virgin consolidation line, Critical state line, Recompression lines, Tension cut off etc. It has been observed that these lines show reasonable fit with actual experimental data.

The generalized relationship, initially proposed by Leroueil et al. (1992) between $(\omega - \omega_{opt})/I_p$ and s_u has been modified. This relationship may be used for estimating

undrained strength of compacted clays at OMC or wet of OMC.

A generalized relationship to relate cumulative plastic strain during cyclic loading with number of cycles has been proposed and the values of coefficients required in this relationship for different types of soils have been evaluated. It is observed that end points of cyclic load tests on compacted samples would lie on Hvorslev surface as observed by Hyde and Ward (1984) for normally and overconsolidated soils.

Procedure to evaluate threshold stress on the basis of cumulative plastic strain data is suggested. Rubin et al. (1970) also suggested a similar procedure on the basis of drained cyclic tests. Threshold stress has also been evaluated from the equilibrium line concept suggested by Sangrey (1968).

A generalized relationship between threshold stress ratio, R_{TS} and plasticity index, I_p has been developed for a variety of soils (compacted, stiff, normally consolidated etc.) at low and relatively high effective confining stresses. Relationship of the form $(\sigma_1 - \sigma_3)_{TS} = a + b \sigma_c'$ has also been given for a variety of soil types at low effective stress ranges.

In Chapter Five, a rational design methodology based on stresses induced and threshold stress evaluated from above study has been proposed. A detailed step by step procedure (flow chart) has been outlined and a simplified method for routine design of formation depth has been recommended.

The conclusions arrived at on the basis of present study and the recommendations for the further studies are given in Chapter Six.

CHAPTER 4

GEOTECHNICAL TESTING FOR EVALUATION OF STRENGTH, STRESS-STRAIN-PORE PRESSURE BEHAVIOUR

4.1 INTRODUCTION

Geotechnical testing is done in order to investigate the causes of failure of subgrade and to evolve the proper laboratory testing procedure for evaluation of threshold stress. In this study, geotechnical testing is carried out on compacted, partially saturated/ saturated alluvial silty soil. Over most part of northern and north western India, these alluvial soils form the subgrade foundation material under the railway tracks.

In Sec. 4.2, few selected terms which are used frequently during this chapter are explained. Section 4.3 gives the geotechnical properties of the silty soil. Broad review of type of tests and total tests performed are given in Sec. 4.4. In Sec. 4.5, relevance of tests performed with the present problem is discussed. Methodology and techniques used in performing tests are discussed in Sec. 4.6. In Sec. 4.7, test results are presented. Interpretation and discussion of test results are given in Sec. 4.8.

4.2 EXPLANATION OF SELECTED TERMS

Certain selected terms which are frequently used in this chapter are explained below.

1. Unconfined static softened test. In this test, compacted sample is mounted on triaxial cell and it is allowed to suck the water freely till equilibrium is reached. Then, it is failed in unconfined compression test.

2. Unconfined cyclic softened test. In this test, compacted sample is mounted on triaxial cell and it is subjected to cyclic loading. Then, it is allowed to suck the water freely till equilibrium is reached followed by unconfined compression test.

3. Threshold stress. It is defined as the stress level above which the cyclic loading causes rapid permanent deformation and cumulative pore pressure built up leading to the failure below the static failure value.

4. Threshold stress ratio. It is the ratio of threshold stress to the ultimate static failure stress (threshold stress/ultimate static failure stress).

5. Effective stress ratio. It is the ratio of effective major principal stress to the effective minor principal stress (σ'_1/σ'_3).

4.2 EXPLANATION OF SELECTED TERMS

Certain selected terms which are frequently used in this chapter are explained below.

1. Unconfined static softened test. In this test, compacted sample is mounted on triaxial cell and it is allowed to suck the water freely till equilibrium is reached. Then, it is failed in unconfined compression test.

2. Unconfined cyclic softened test. In this test, compacted sample is mounted on triaxial cell and it is subjected to cyclic loading. Then, it is allowed to suck the water freely till equilibrium is reached followed by unconfined compression test.

3. Threshold stress. It is defined as the stress level above which the cyclic loading causes rapid permanent deformation and cumulative pore pressure built up leading to the failure below the static failure value.

4. Threshold stress ratio. It is the ratio of threshold stress to the ultimate static failure stress (threshold stress/ultimate static failure stress).

5. Effective stress ratio. It is the ratio of effective major principal stress to the effective minor principal stress (σ'_1/σ'_3).

4.3 GEOTECHNICAL NATURE OF CAMPUS SILT

4.3.1 General

The term Campus silt is used to describe the soils present on IIT Kanpur Campus. This sedimentary soil is abundantly found in Gangetic plains. In this research work, all tests are carried out on this soil. This material has been thoroughly investigated both in the laboratory and field over the past two decades as part of M.Tech. thesis research projects [see Prakasa Rao (1985) for a comparative review]. This soil is known to be fairly variable in its physical properties from site to site.

For testing purpose, soil is obtained from within the IITK campus. Total 3 batches of soil samples are used for testing purpose. These batches are obtained from the same area but at different period of time and from different pits.

4.3.2 Particle size distribution and Atterberg limits

Particle size distribution and index properties for all the three batches are shown in Figs. 4.1 and 4.2 respectively. The variation in particle size distribution between batch 1 and 2 soil is within the range of variation of particle size distribution for these soils. Physical characteristics for the 3 batches are given in Table 4.1. As batch 1 soil has higher clay content (40 %) as compared to batch 2 soil (18.5 %), plastic limit is higher for batch 1 soil (18 %) than for batch 2 soil (14 %) .

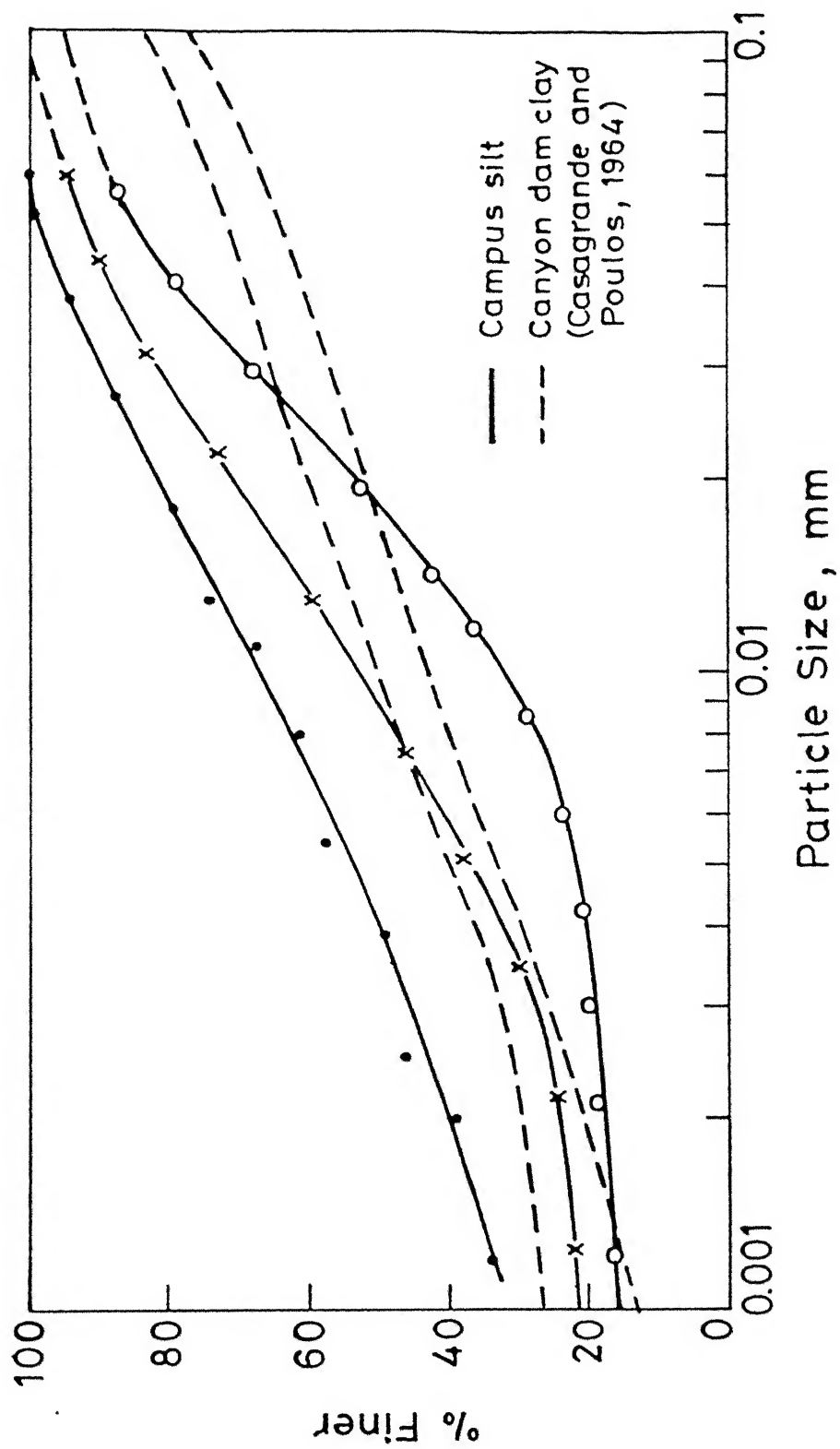


Fig. 4.1 Particle size distribution.



Fig. 4.2 Index properties.

4.3.3 Compaction characteristics

Compaction was carried out using Harvard miniature compactor as described in Sec. 4.6.2. Compaction was done using 25 tamps - 40 pounds spring - 3 layers (i.e 25 - 40 -3). Figure 4.3 shows water content - dry density relationship for Campus silt. Batch 1 soil was used for series A2 and A3 tests and was given 6 hr curing time after thorough mixing. Batch 2 and 3 soils were used for all other test series and samples were compacted and tested immediately after thorough mixing of soil sample.

For batch 1, the optimum moisture content and the maximum dry density are found to be 14.7 % and 18.26 kN/m^3 respectively while for batch 2 and 3, corresponding values are obtained as 14.0 % and 18.85 kN/m^3 . This variation may be due to the differences in particle size distribution and period of curing.

4.4 TESTS PERFORMED

Tests described in this chapter can be classified as total stress tests and effective stress tests. Summary of total tests conducted is given in Table 4.2.

4.5 RELEVANCE OF TESTS PERFORMED WITH PRESENT PROBLEM

Track is laid either in filling or cutting. When the track is laid in filling, soil subgrade is compacted and the formation is constructed over it, but when the track is laid in cutting, compaction of subgrade is not important. To develop

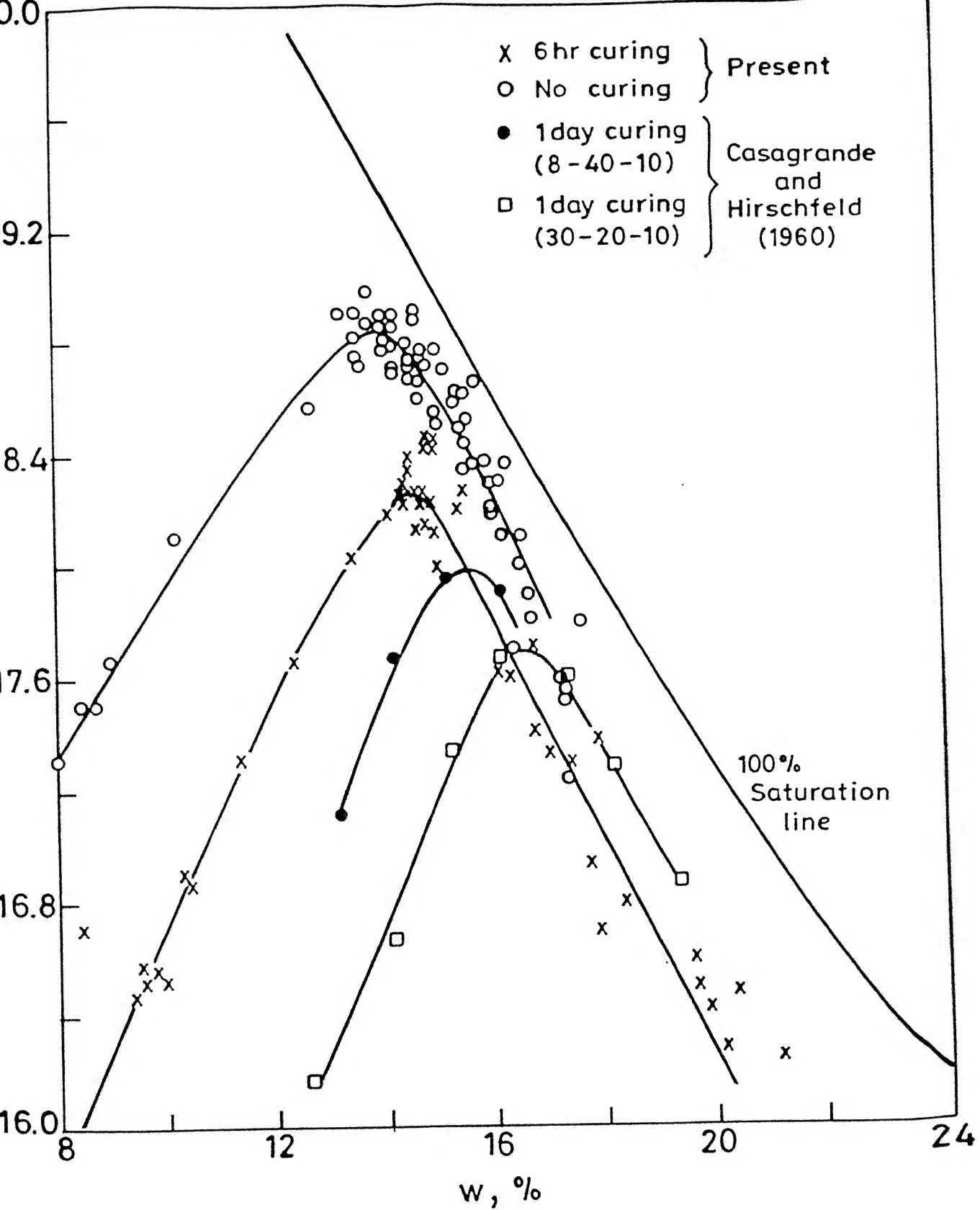


Fig. 4.3 Water content-dry density relationship.

Table 4.2 Summary of total tests conducted

S.No.	Series No.	Types of Test Conducted	No. of Tests	Static (S) or Cyclic (C)	S (%)	σ'_c (kPa)	σ_3 (kPa)	w_f (%)	How much wet of w_{opt} (%)
1	A1	Quick -- UU without pore pressure measurement.	22 14 11	S S S	(85-98)	---	0 (20-100) (300-900)	(13.5-17.5)	0-3
2	A2	Unconfined Cyclic	18 4	C-did not fail in cycling C- failed	>85	---	0	@ 14.7	at w_{opt}
3	A3	Unconfined Cyclic Softened	15 13 3 3	Measured C- s_u and E both C- only s_u S- s_u and E both S- only s_u	>85	---	0	w_f - 14.7 w_f - varying	$w_f = w_{opt}$
4	B1	Unconsolidated Undrained with pore pressure measurement	3 5 2	S S S	90 94 96	(392-720) (180-477) (86 -149)	(500-900) (300-900) (200-300)	13.5-13.8 14.5-15.0 15.2-16.0	@ w_{opt} 0.5-1.0 1.2-2.0
5	B2	Unconsolidated Undrained with pore pressure measurement	2 2	C C	94 96	(340-385) (153-285)	700 700	15.5 15.5-16.0	1.5-2.0
6	B3	Backsaturated Undrained with pore pressure measurement	2 2	S C	95-100 100	(20 - 22) (20 - 22)	500 500	16.5 16.5-17.0	2.5-3.0
			1	S	100	40	500	16.5	2.5
			3	C	100	40	500	16.5	

a methodology of testing, both proper control and sample producibility are needed. However, for these soils, it is very difficult to obtain reproducible undisturbed samples because variability in samples is known to exist even at the same site. In addition to this, these soils remain partially saturated in the field during most of the period in the year and water table fluctuation is common. Hence, in this study, the condition of compacted subgrade is simulated and tests are performed on compacted samples. The compaction control has been specified in terms of optimum density using Harvard miniature compactor.

For a typical track with 40 cm depth of formation, assuming water table at the top of subgrade, $\gamma_d = 17.5 \text{ kN/m}^3$ and overburden due to rail and sleeper equal to 4 kPa, the vertical stress on top of subgrade soil due to the dead load is 1 kPa (also see Fig. 5.3). Due to water table fluctuations, these soil deposits are very stiff. From the tests carried out on undisturbed samples, Srivastava (1977) has determined $K_0 = 1$ for these soils in the field. Thus, taking $K_0 = 1$, confinement pressure for element resting on top of soil is of the order of 1 kPa. Thus, track problem is essentially the low confinement problem. The worst case is zero confinement. With this view, unconfined cyclic tests in series A2 and A3 have been carried out.

Most of the trouble in the railway formation starts during the rainy season. It is known that this is because subgrade on which railway formation is built, gets softened / saturated due

to the penetration of rain water from top [Hall, (A)]. If the subgrade soil is heavily overconsolidated clay, the residual pore pressure due to cyclic loading is negative and the presence of free water leads to softening of clay [Bishop and Henkel, (1953)]. This softening of the clay may be the reason for mudpumping phenomenon observed in railway track. Hence with this view, the cyclic and cyclic softened tests have been carried out in series A2 and series A3 respectively. Also, it may be noted that Bishop and Henkel (1953) have described softened tests relevant to the study of effect of transient loading on formations and subgrades.

Investigation of the behaviour of soils in terms of only total stresses may be of some interest, but understanding of the changes in response of subgrade soil during cyclic loading, needs to be related to the effective stress changes [see Wood (1982)]. With this view, effective stress cyclic tests are carried out.

As the train would pass over the track, subgrade soil would be subjected to the cyclic loading under the undrained condition. But, then, subgrade would get the respite to dissipate the excess pore water pressure built up and to equilibriate with the surrounding before the next train passes. However, if the drainage condition of subgrade is poor as the case is with the most of the existing Indian tracks, either the partial drainage of subgrade would take place or no drainage at all would occur. The worst case is of 'no drainage' condition.

Thus, the most relevant geotechnical testing for track

problem must be carried out under low confinement pressure (10 - 20 kPa for a typical track) on saturated soil under no drainage condition. However, due to fluctuations of measurement system which are of the order of 5 kPa, tests have been conducted at $\sigma'_c = 20$ kPa and $\sigma'_c = 40$ kPa (series B3) so that results can be extrapolated to the required confinement pressure.

Total stress and effective stress static unconsolidated undrained tests (series A1 and B1) are carried out in order to evaluate the behaviour of soil in static conditions and to compare it with cyclic behaviour. Tests in series B2 are carried out to investigate the cyclic behaviour at high initial effective stresses and compare it with cyclic behaviour at low initial effective stresses.

4.6 TECHNIQUE OF TESTING

In this section, the methodology used for carrying out the tests is outlined. In general, procedure given in Bishop and Henkel (1962) is followed. For all tests (confined, unconfined, static or cyclic), two membranes were used to wrap the specimens. Specimens were covered with the side drains for quick equilibration of water inside the specimen.

4.6.1 Equipment used

All tests except unconfined tests are carried out in

Geotechnical Digital System (GDS), version 1.3. For carrying out tests in this system, GDS manual published in 1990 and Menzies (1988) are referred. GDS uses computer controlled Bishop and Wesley (1975) type triaxial cell. In this system, both static and cyclic triaxial tests can be performed. Three types of cyclic load waveform viz. triangular, sine and square can be applied. The maximum frequency of cyclic loading that can be applied is 1 cycle per minute. Both drained and undrained cyclic tests can be performed.

All tests were performed in such a way that maximum capacity of GDS system (1400 kPa) should not be exceeded.

4.6.2 Sample preparation

All tests were carried out on compacted samples. Compaction was done using the Harvard miniature compactor in split spoon mould (diameter = 3.8 cm and height = 7.6 cm). Soil was compacted in three layers and each layer was tamped by using 25 number of blows of 40 lbs Harvard miniature compactor.

4.6.3 Total stress tests

4.6.3.1 Series A1 - Unconsolidated undrained tests without pore pressure measurement

a. Unconfined compression : These are the conventional tests and are carried out as described in Bishop and Henkel (1962). Rate of loading applied was 14 mm/hr axial strain rate.

b. Triaxial compression : The required cell pressure was applied in one step and pore pressure reading was monitored. Specimen was subjected to this cell pressure for approximately 6 hours so that equilibration of water inside the specimen takes place. It was found that 6 hours were sufficient for this purpose. Then, specimen was loaded by applying the axial strain rate equal to 40 mm/hr without pore pressure measurement.

6.3.2 Series A2 - Unconfined cyclic tests

The cyclic stress ratio (R_f), is defined as

$$R_f = \left(\frac{\sigma_{\text{dyn}}}{\sigma_{\text{ult}} - \sigma_{\text{min}}} \right) \times 100 \quad (4.1)$$

σ_{dyn} = cyclic stress level during cyclic loading,

σ_{ult} = ultimate failure stress, and

σ_{min} = minimum stress level kept during the cyclic loading.

Minimum axial stress during cyclic load tests was kept equal to confining pressure (i.e. $\sigma_{\text{min}} = 0$). Knowing the ultimate failure stress by static test and the required cyclic stress ratio (R_f), cyclic stress level was calculated.

Before the start of cyclic loading, stress level equal to σ_{dyn} was reached. Unloading was done by reversing the motor. Further cyclic loading was applied by changing the stress level

between σ_{dyn} and minimum stress level by rotating the lever manually. After 100 cycles, the sample was loaded to failure. In machine operations, loading was done at the axial strain rate equal to 14 mm per hour.

4.6.3.3 Series A3 - Unconfined cyclic softened tests

Tests in this series are carried out exactly similar to tests in series A2 up to the level of 100 cycles of loading and unloading. Then, the sample was allowed to suck water freely from top and bottom till equilibrium and finally the sample was machine loaded till failure. This process of allowing water freely (after 100 cycles) till equilibrium is termed as softening.

For series A3 tests, following special arrangements were made. The sample in the triaxial cell was connected at top and bottom with two separate burettes filled with water through small intermediate tube. The water level of the burette connected to the bottom side was kept levelled with the bottom of the sample and the level of water in the top burette was kept levelled with middle of the sample. It is hoped that this arrangement would allow the sample to suck the water freely from the burette. By repeated trials, it was found out that the water content of the sample reached equilibrium after 12 hours.

4.6.4 Effective stress tests

4.6.4.1 Pore pressure measurement in partially saturated soils

Yudhbir and Korchoke (1987) reviewed the currently recommended experimental procedures for shear strength evaluation in partially saturated soils :

- (i) involving the measurement of pore air and pore water pressure and computation of κ parameter [Bishop et al. (1960)],
- (ii) determination of ϕ^b parameter through testing with variable constant values of matrix suction, $(u_a - u_w)$ [Fredlund et al. (1978) ; Ho and Fredlund (1982)], and
- (iii) The Marsal's approach [Marsal (1979)] where the response of partially saturated soils is investigated by raising the cell pressure up to a value where the air in the voids is totally dissolved and the soil behaves like a saturated material.

As the degree of saturation of the samples tested in the present study varied between 87 % to 96 % - the range in which water voids are known to be continuous [Cruz et al.(1985);Yudhbir and Korchoke (1987)], it was decided to test these samples following the methodology recommended for saturated soils with pore water pressure measurements [Bishop and Henkel (1962)].

4.6.4.2 Series B1 - Unconsolidated undrained tests with pore water pressure measurement

These tests are carried out in similar manner as series A1 triaxial compression tests except that in this series, pore

water pressure is measured. Pore water pressure measurements were carried out at the bottom of the sample. For tests carried out in this section, in addition to Bishop and Henkel (1962), Head (1982) and Baldi et al. (1988) were referred to.

The rate of loading applied was calculated according to procedure given in Bishop and Henkel (1962). From the Oedometer test, coefficient of consolidation, c_v for the Campus silt was determined. The average value of c_v in the stress range up to 800 kPa was found out to be $2.5 \text{ m}^2/\text{year}$. Thus, time to failure was equal to 2.5 hr. As the sample was partially saturated, it was decided to use the rate of loading equal to 14 mm/hr, slightly greater than this value .

Next, in IIT Kanpur, commercially available rubber membranes manufactured by Hindustan latex limited are used for wrapping the sample in the cell. The extension modulus and corrections for compressive strength due to barrelling effect for these membranes are 35 g/cm and 0.6 kPa respectively. It may be noted that extension modulus (35 g/cm) for these membranes are quite small as compared to conventional rubber membranes (394 g/cm) as reported in Bishop and Henkel (1962).

To minimize the air present in the system, hot water was circulated in the system before the start of every test.

4.6.4.3 Series B2 - Unconsolidated undrained cyclic tests with pore water pressure measurement

In this series, tests were performed in the similar way as series B1 tests up to the level of applying static compressive

stress equal to the required cyclic stress ratio (i.e. up to σ_{dyn}). This was followed by unloading up to $\sigma_{\text{dyn}}/2$. Then, cyclic loading was carried out by loading up to stress level equal to σ_{dyn} and unloading up to deviator stress equal to zero kPa. After completion of 100 cycles, sample was failed in shear with axial strain rate equal to 4 mm/hr. Sample was then removed and cut into 3 parts for water content determination.

All tests were conducted under the following general conditions.

- (i) Undrained test with pore water pressure measurement.
- (ii) Loading wave frequency = 1 cycles / min.
- (iii) Loading wave shape = Sine wave.
- (iv) Total number of cycles = 100.
- (v) Cell pressure = 700 kPa

Slow cyclic tests with frequency equal to 1 cycle per minute were preferred over fast cyclic tests (simulating prototype situation) because in slow tests, pore pressure measurements are reliable, can be easily monitored and are more likely to reflect the actual intentions of the soil [Wood (1982)].

While calculating the stresses on top of subgrade due to the train load, increase in stresses due to speed i.e. inertial effect due to cyclic loading had already been considered. Hence the cyclic tests carried out in series B2 and B3 are of quasi-static nature i.e. they neglect inertial effect.

The shape of loading wave chosen is sinusoidal because from the results of Netherland railways [Janin et al. (1982)], it is known that shape of loading wave would be in the form of 3 arcs of parabolas and from the choice available in GDS, sinusoidal is considered as the most relevant one.

The total number of cycles for all cyclic load tests is arbitrarily chosen as 100. The number of cycles used by various researchers varies from 4 to 10,000 because plastic strain increase and pore pressure rise during first few cycles are only important [see Wood (1982)].

4.6.4.4 Series B3 - Undrained static and cyclic tests with pore water pressure measurement on samples with back pressure saturation

After application of cell pressure in one step, back pressure was applied after few minutes and sample was allowed to saturate for approximately 24 hours. The purpose of applying the back pressure was to produce as nearly as possible full saturation by dissolving the air present in the sample voids into solution. For all tests, cell pressure equal to 500 kPa was applied. However, for tests with $\sigma_c' = 40$ kPa, back pressure equal to 460 kPa and for tests with $\sigma_c' = 20$ kPa, back pressure equal to 480 kPa was applied. After consolidation of sample, static tests were carried out in the same manner as series B1 tests while cyclic tests were carried out in the same manner as series B2 tests.

At low cyclic stresses, cyclic pore pressure would also be

very low while system fluctuations are more than these cyclic pore pressures hence pore pressures measured during cyclic loading for series B3 tests are considered unreliable and hence not plotted.

4.7 PRESENTATION OF TEST RESULTS

In this section, results of total stress tests and effective stress tests (both static and cyclic) are presented separately.

4.7.1 Total stress tests

Results of total stress tests are presented according to series in which they are conducted.

4.7.1.1 Series A1 - Unconsolidated undrained tests without pore pressure measurement

Stress-strain relation for this soil under unconfined condition is shown in Fig. 4.4. Inset shows the failure shape of the specimen after the test. Shaded portion shows the range for different test. E_i is the initial tangent modulus for this soil for unconfined condition.

Details of tests under higher cell pressure are given in Table 4.3 .

4.7.1.2 Series A2 - Unconfined cyclic tests

Total tests carried out in this series are shown in Table 4.4. The representative stress strain relationships for $R_f = 6.6, 18.7, 29.7, 36.5, 46.0, 54.2, 64.0, 71.3, 73.7$ and 76.6 are shown in Figs. 4.5 to 4.14. The initial Young's modulus and

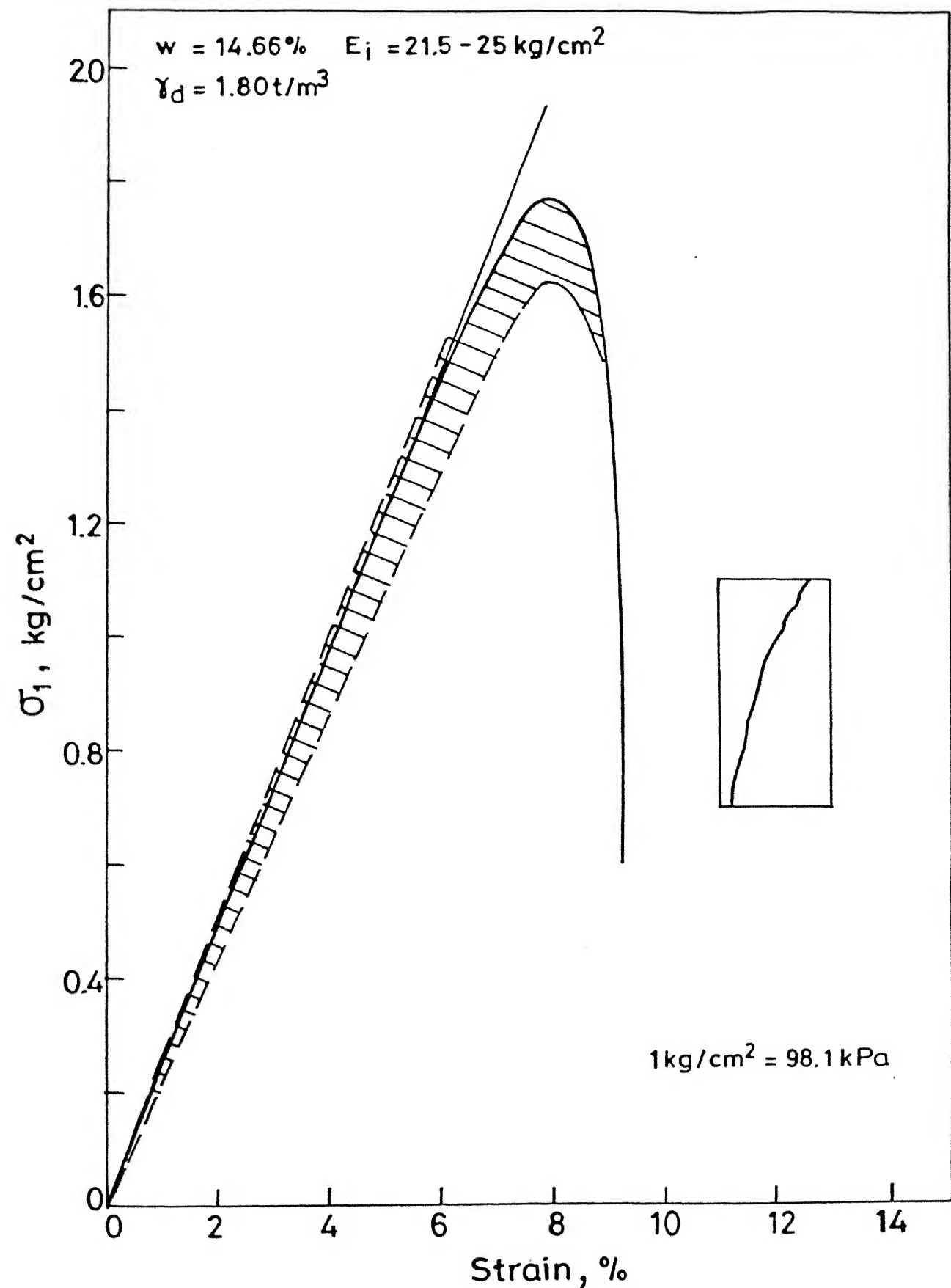


Fig. 4.4 Stress-strain relationship for static unconfined test.

Table 4.3 Details of total stress UU tests
(tests with cell pressure > 0)

Test No.	σ_3 (kPa)	w (%)	S (%)	γ_d kN/m ³	$\frac{(\sigma_1 - \sigma_3)_{\max}}{2}$ (kPa)	$\frac{(\sigma'_1 + \sigma'_3)_{\max}}{2}$ (kPa)
For w = (13.5 -- 15.0) %						
PCD1	900	14.00	92.26	18.90	615	1515
NEW9	700	14.05	90.90	18.80	435	1135
NP3	700	14.61	96.28	18.90	390	1090
NEW7	500	14.20	92.89	18.86	355	855
NP2	300	14.51	91.68	18.67	240	540
NEW6	300	14.50	92.62	18.73	220	520
R1	100	14.00	92.26	18.90	169	269
T49	100	14.00	91.75	18.87	166	266
CD2	100	14.29	90.79	18.70	172	272
T47	50	14.50	92.12	18.70	120	170
T45	50	14.25	92.50	18.80	125	175
T90	20	14.18	90.09	18.70	102	122
T91	20	14.21	90.28	18.70	102	122
T73	20	14.60	96.22	18.90	85	105
T43	20	15.00	96.52	18.77	74	94
For w = (15.0 - 16.5)%						
NEW14	700	15.51	92.21	18.33	300	1000
NP1	700	16.10	93.23	18.30	210	910
NEW13	500	16.00	92.65	18.18	220	720
NEW12	300	15.45	94.68	18.50	215	515
CY1	100	16.00	94.62	18.30	75	175
CY2	100	16.50	92.59	18.00	70	170
T44	20	16.27	97.42	18.37	58	78
T78	20	15.46	95.08	18.52	78	98
For w > 16.5 %						
PCD4	700	16.52	94.33	18.10	150	850
R2	100	17.60	95.42	17.80	35	135

Table 4.4 Details of series A2 tests

S. No	$R_f(\%)$	No. of tests	Remark
1	6.6	2	did not fail during cyclic loading
2	18.7	2	
3	29.7	2	
4	36.5	2	
5	46.0	2	
6	54.2	2	
7	64.0	2	
8	71.3	2	
9	76.6	2	
10	73.7	1	failed during cyclic loading
11	87.0	1	
12	92.0	1	
13	100.0	1	

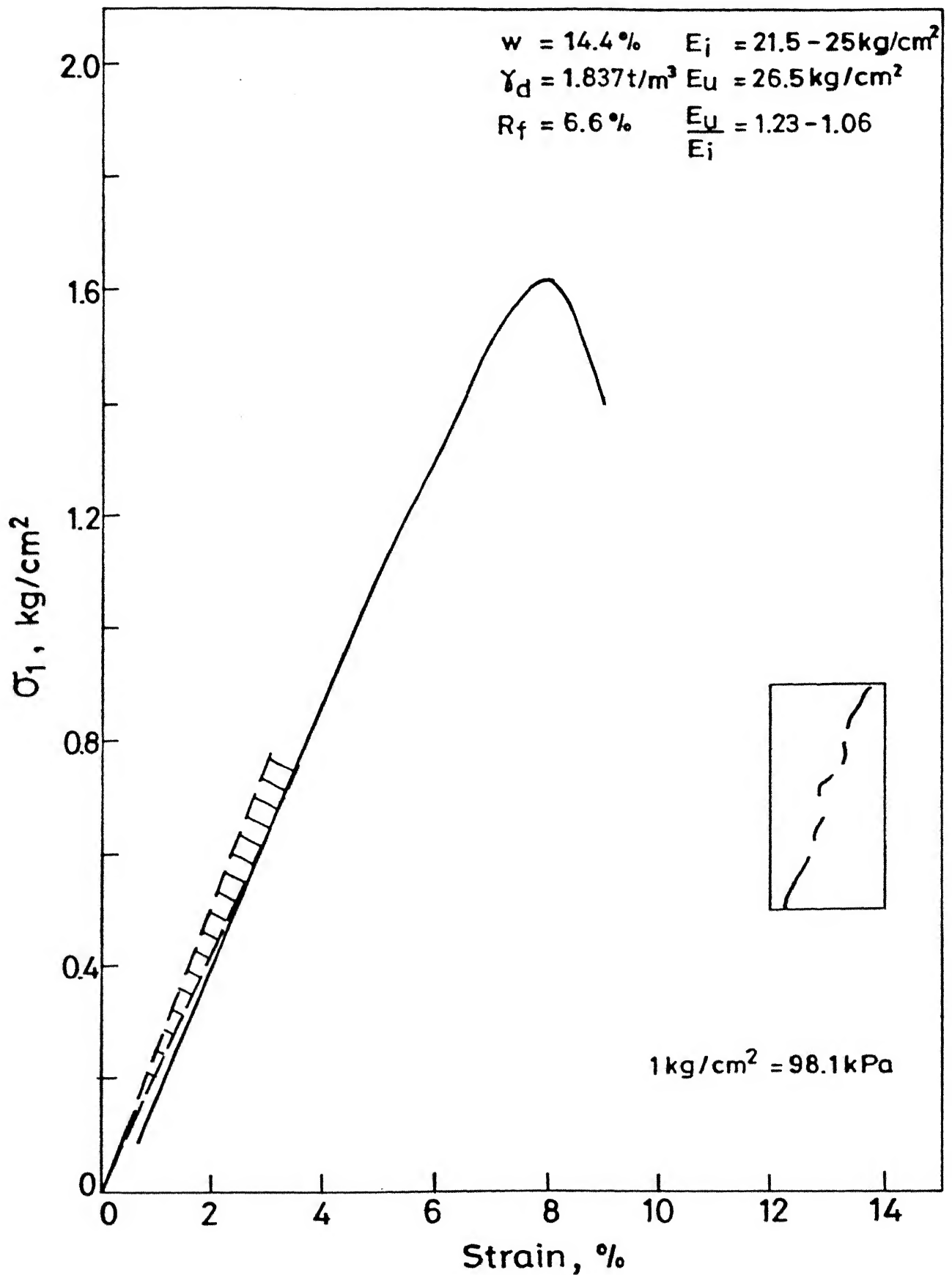


Fig. 4.5 Stress-strain relationship for cyclic test
($R_f = 6.6\%$)

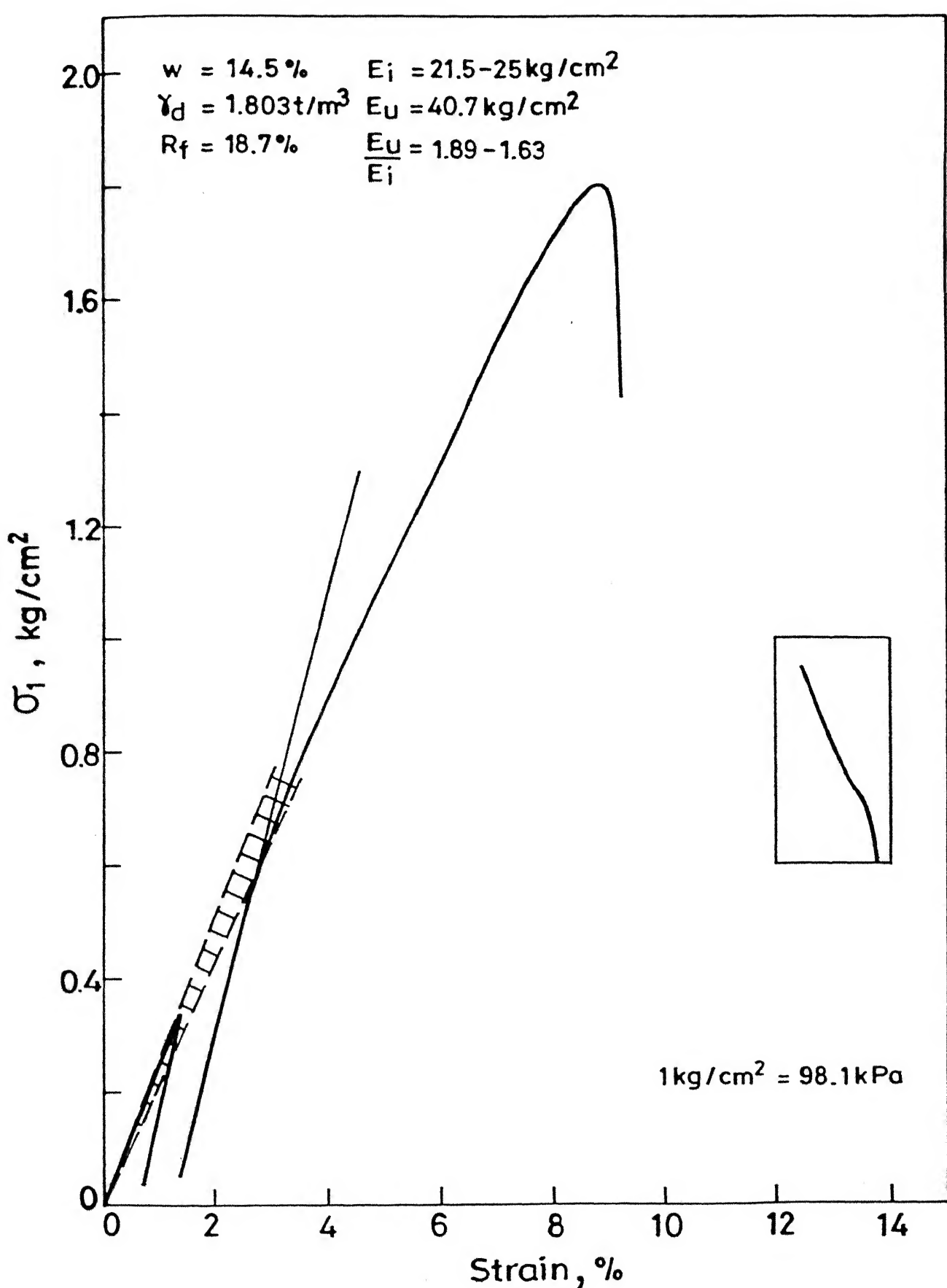


Fig. 4.6 Stress - strain relationship for cyclic test
($R_f = 18.7\%$)

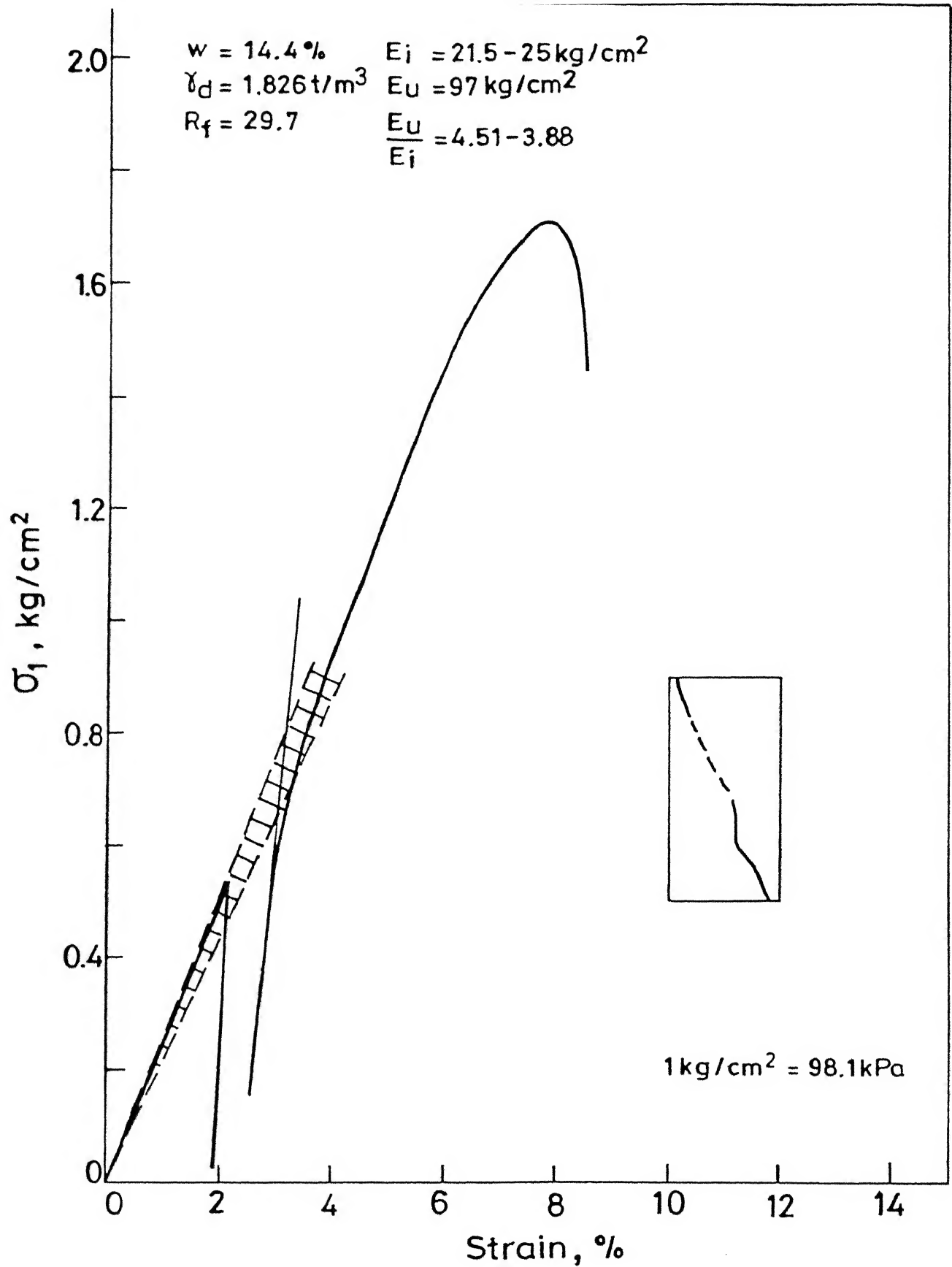


Fig. 4.7 Stress-strain relationship for cyclic test
($R_f = 29.7\%$)

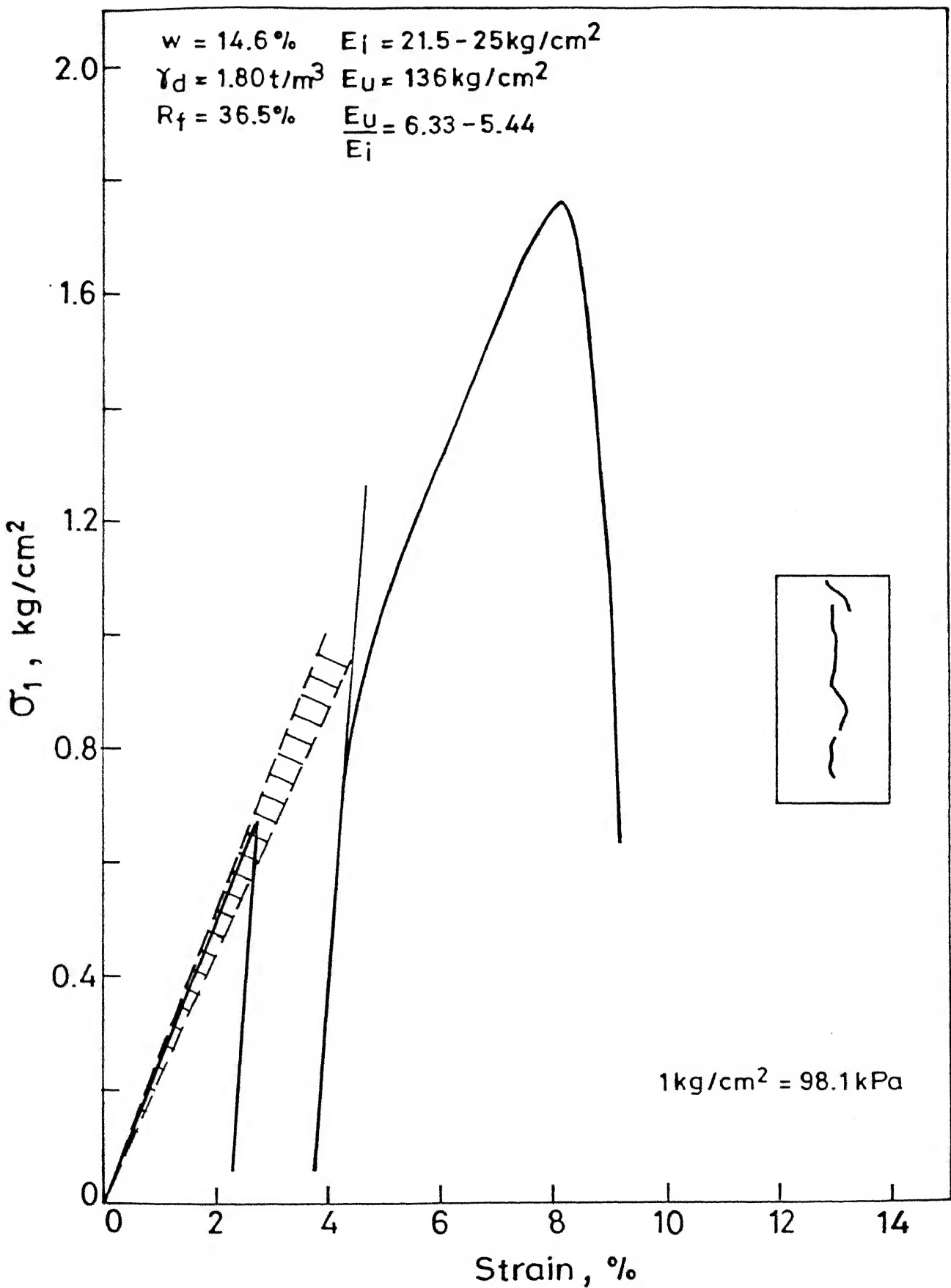


Fig. 4.8 Stress-strain relationship for cyclic test
($R_f = 36.5\%$)

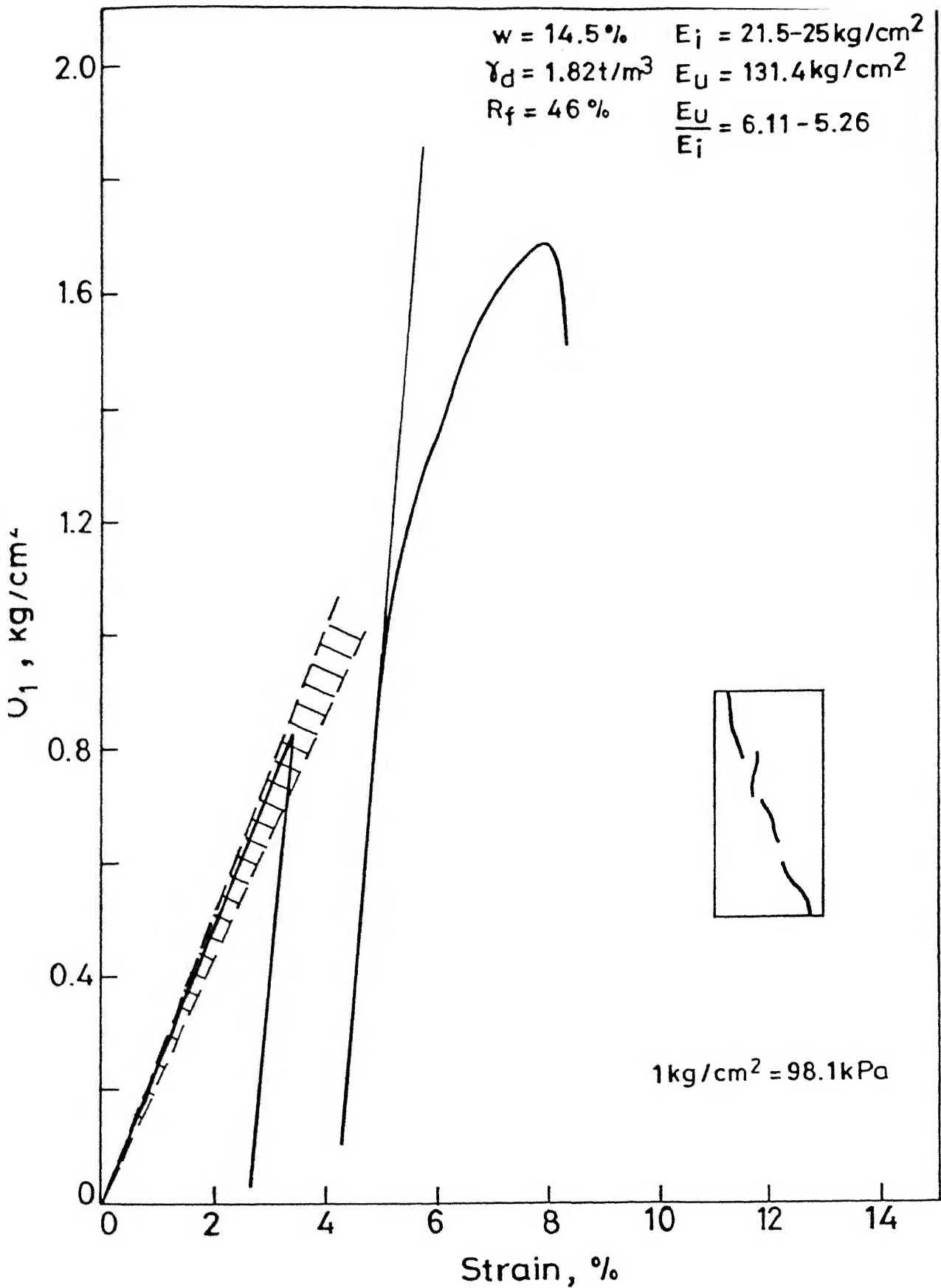


Fig. 4.9 Stress-strain relationship for cyclic test ($R_f = 46\%$)

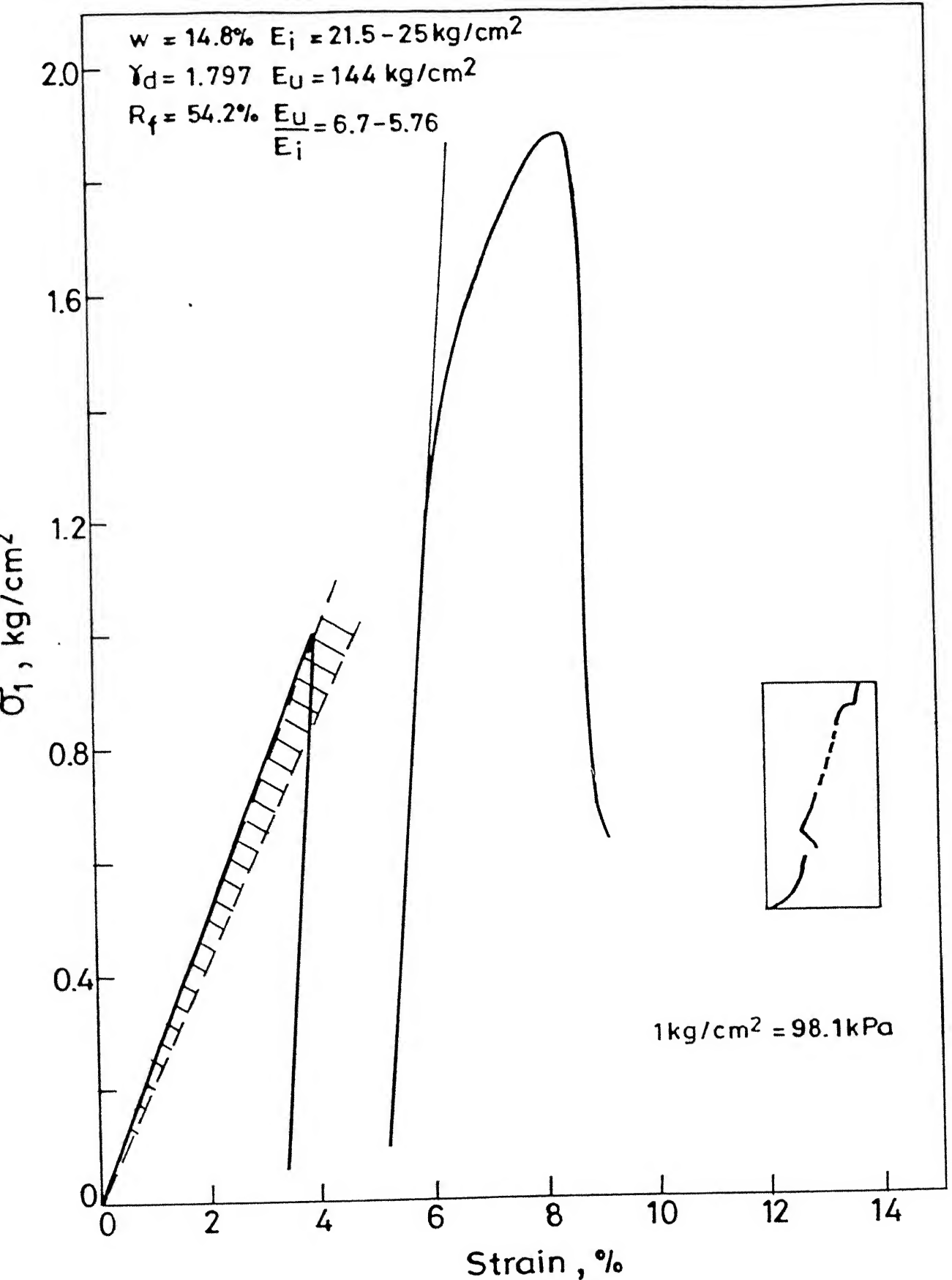


Fig. 4.10 Stress-strain relationship for cyclic test
($R_f = 54.2\%$)

$w = 14.4\%$ $E_i = 21.5 - 25 \text{ kg/cm}^2$
 $\gamma_d = 1.83 \text{ t/m}^3$ $E_u = 132 \text{ kg/cm}^2$
 $R_f = 64\%$ $\frac{E_u}{E_i} = 6.14 - 5.28$

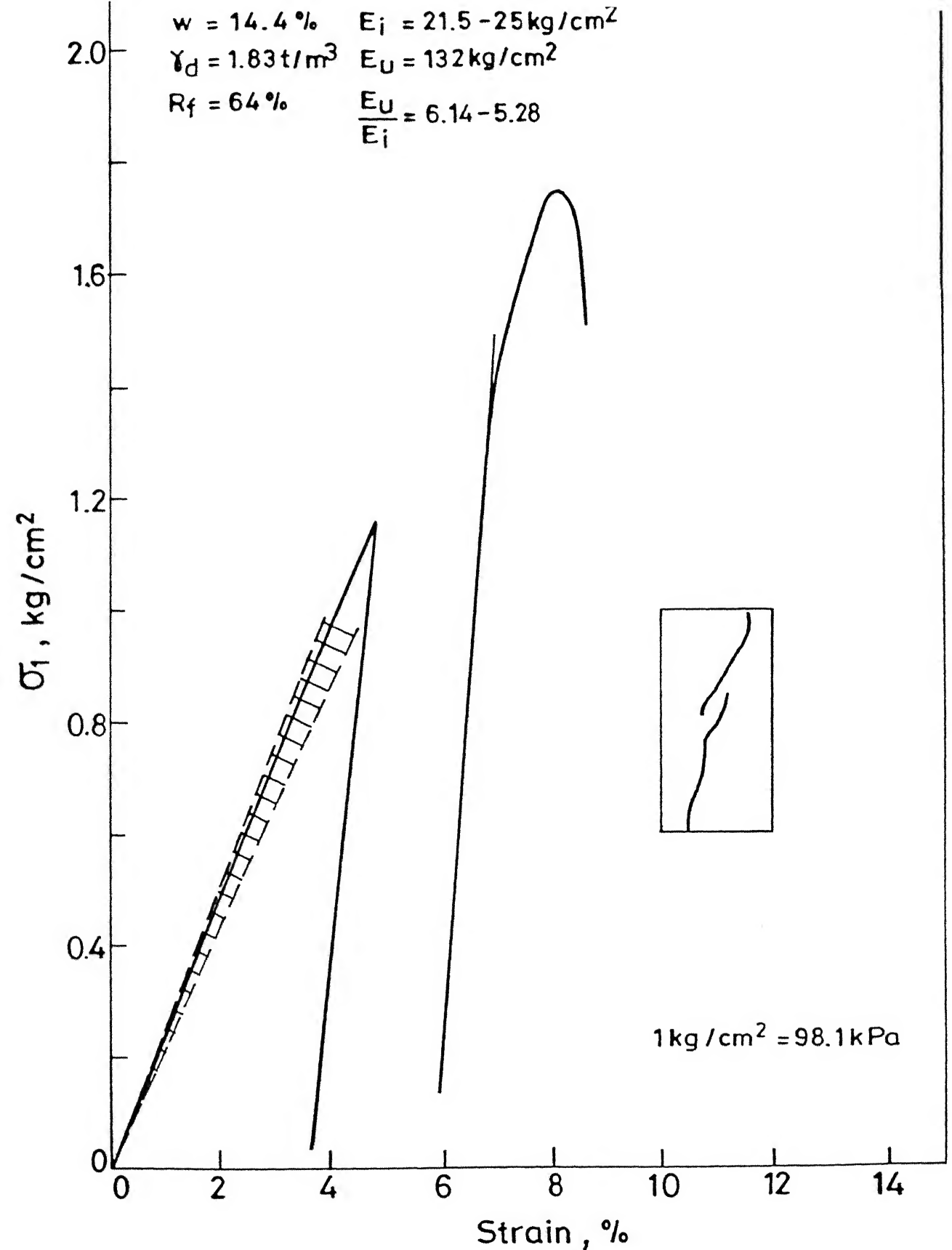


Fig. 4.11 Stress-strain relationship for cyclic test
 ($R_f = 64\%$)

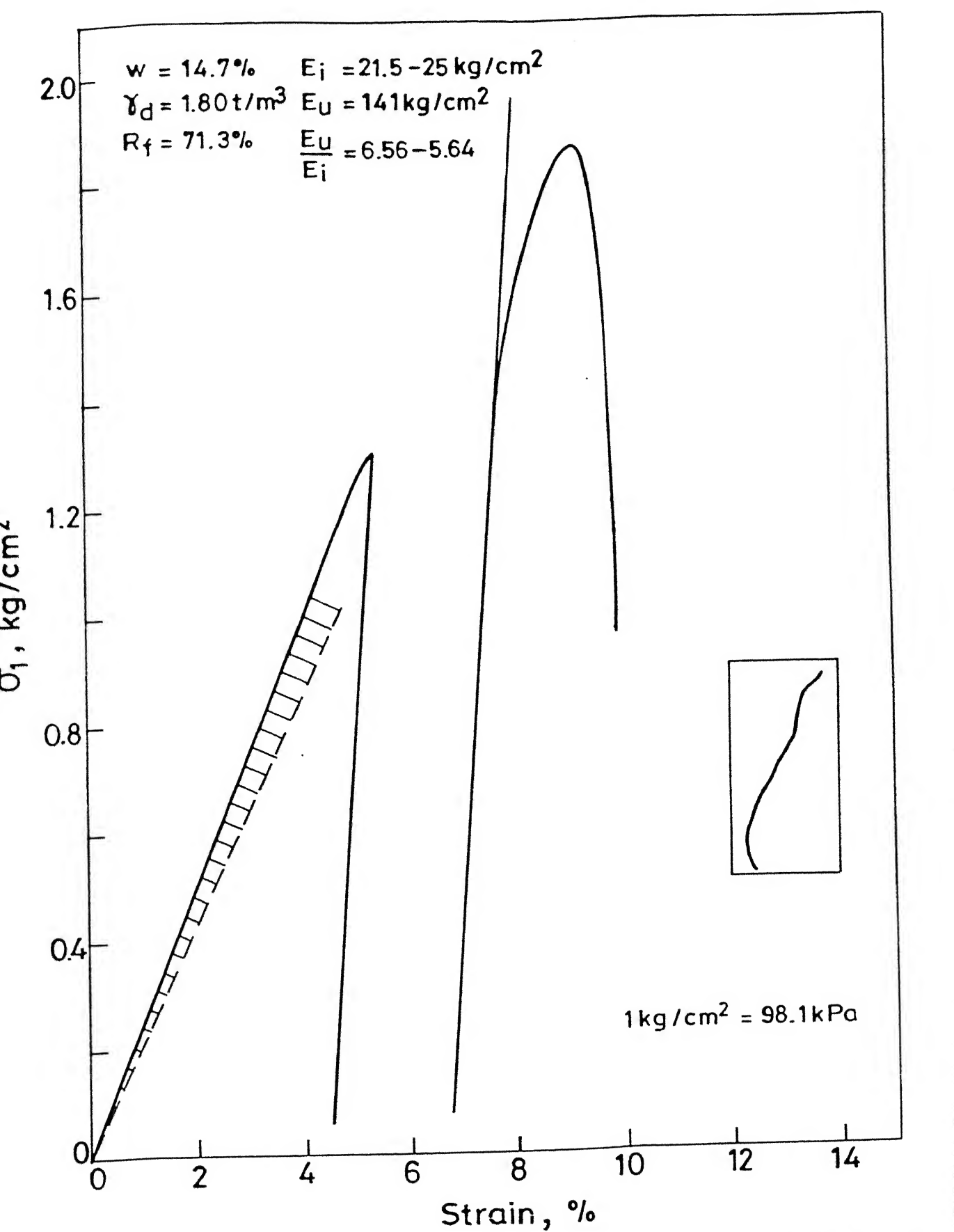


Fig. 4.12 Stress-strain relationship for cyclic test ($R_f = 71.3$)

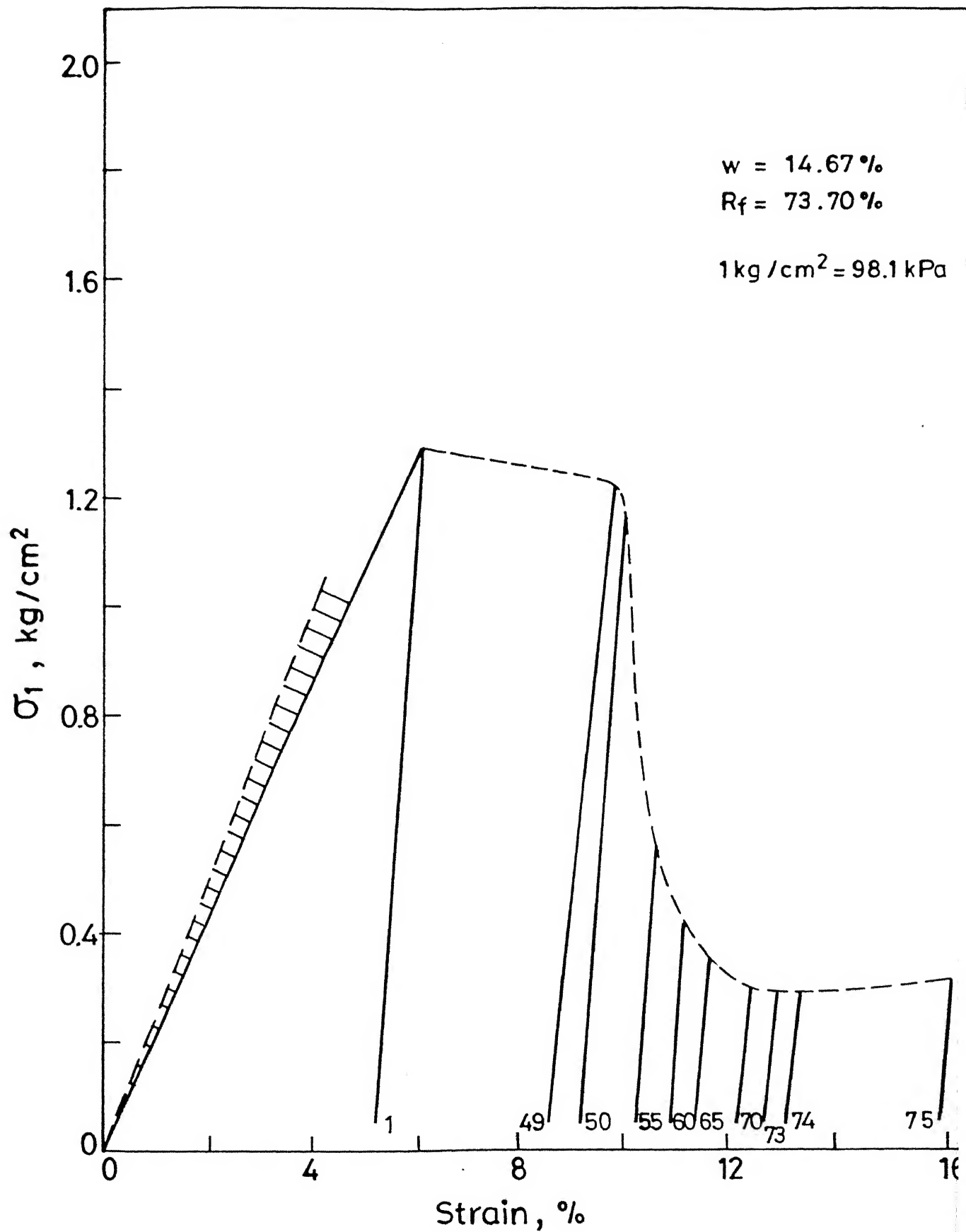


Fig. 4.13 Stress-strain relationship for cyclic test ($R_f = 73.70\%$)

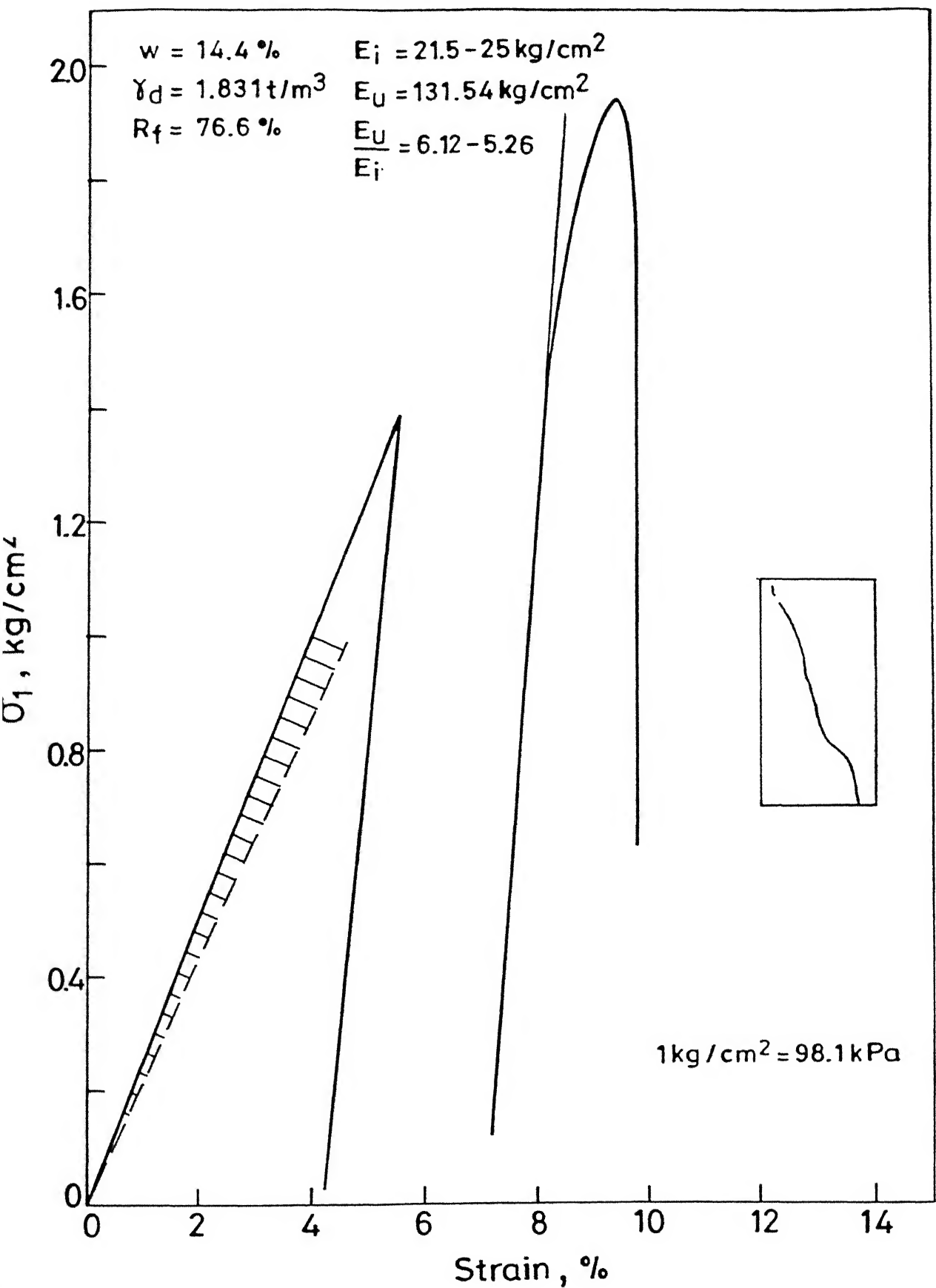


Fig. 4.14 Stress-strain relationship for cyclic test ($R_f = 76.6$)

the Young's modulus after 100 cycles were determined in each test.

In these figures, the initial shaded portion before the start of cycles shows the range followed by other comparable static tests. The first loop marked by dark line shows the loading and unloading carried out before the start of cyclic load test. 100 cycles given thereafter, are not shown. After 100 cycles, the sample was machine loaded to failure as shown by dark line while lighter line shows the tangent Young's modulus after 100 cycles.

It was found that cyclic loading at stress level R_f around 75 % led to failure.

4.7.1.3 Series A3 - Unconfined cyclic softened tests

For series A3, out of total 32 cyclic and 6 static tests conducted, one static and five cyclic representative tests for varying percentage stress ratio, $R_f = 18.9, 37.1, 54.4, 70.7$ and 82.2 are plotted in Figs. 4.15 to 4.20 respectively. For test with R_f equal to 82.2 percent (Fig. 4.20), failure had occurred due to cycling loading itself and then sample was allowed to suck the water. Water content (before and after softening) and ultimate strength were measured for all tests but stress strain relationship was recorded only for 15 tests. Table 4.5 gives the details of series A3 tests.

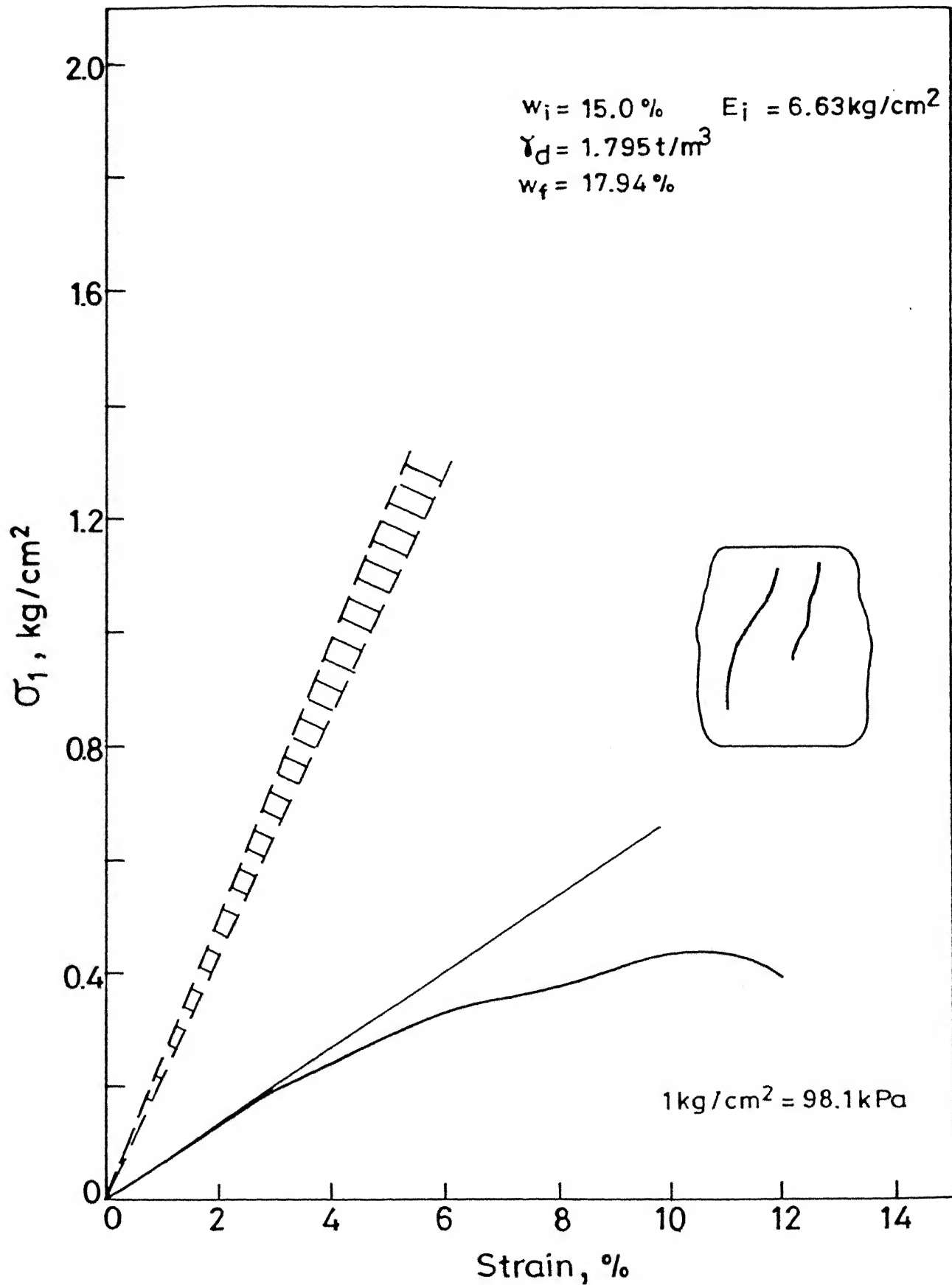


Fig. 4.15 Stress-strain relationship for static softened test.

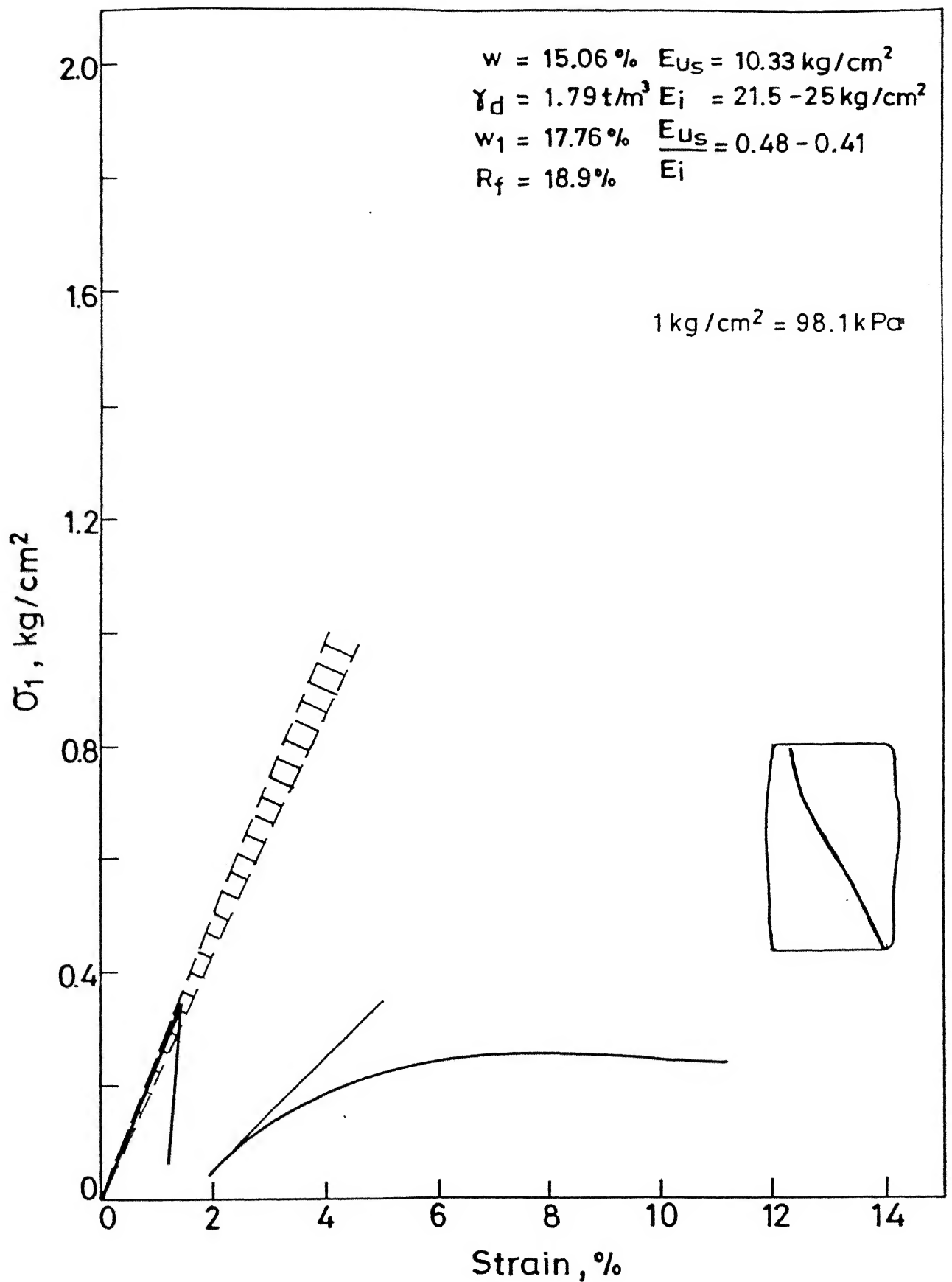


Fig. 4.16 Stress-strain relationship for cyclic softened test ($R_f = 18.9\%$)

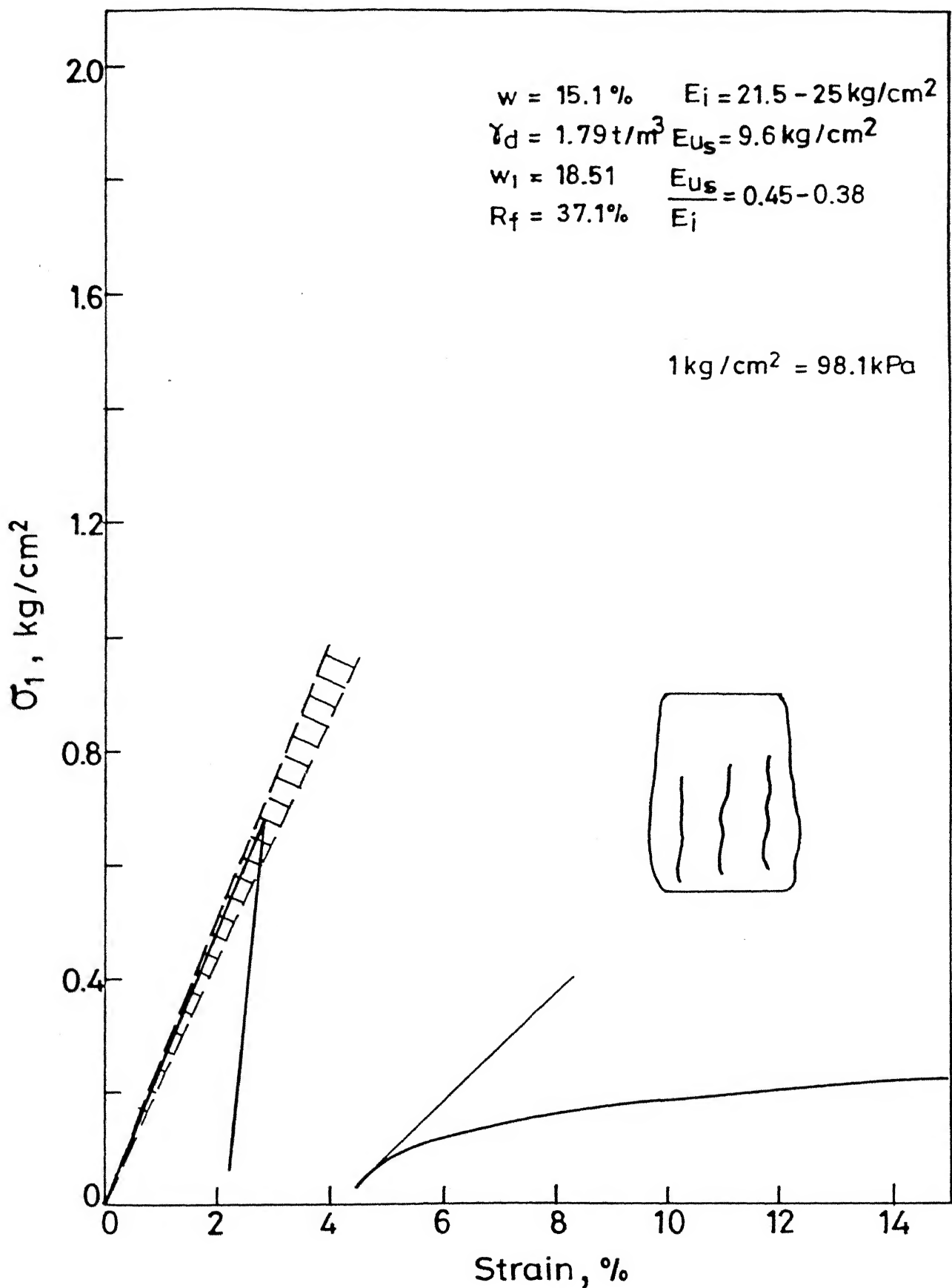


Fig. 4.17 Stress - strain relationship for cyclic softened test ($R_f = 37.1\%$)

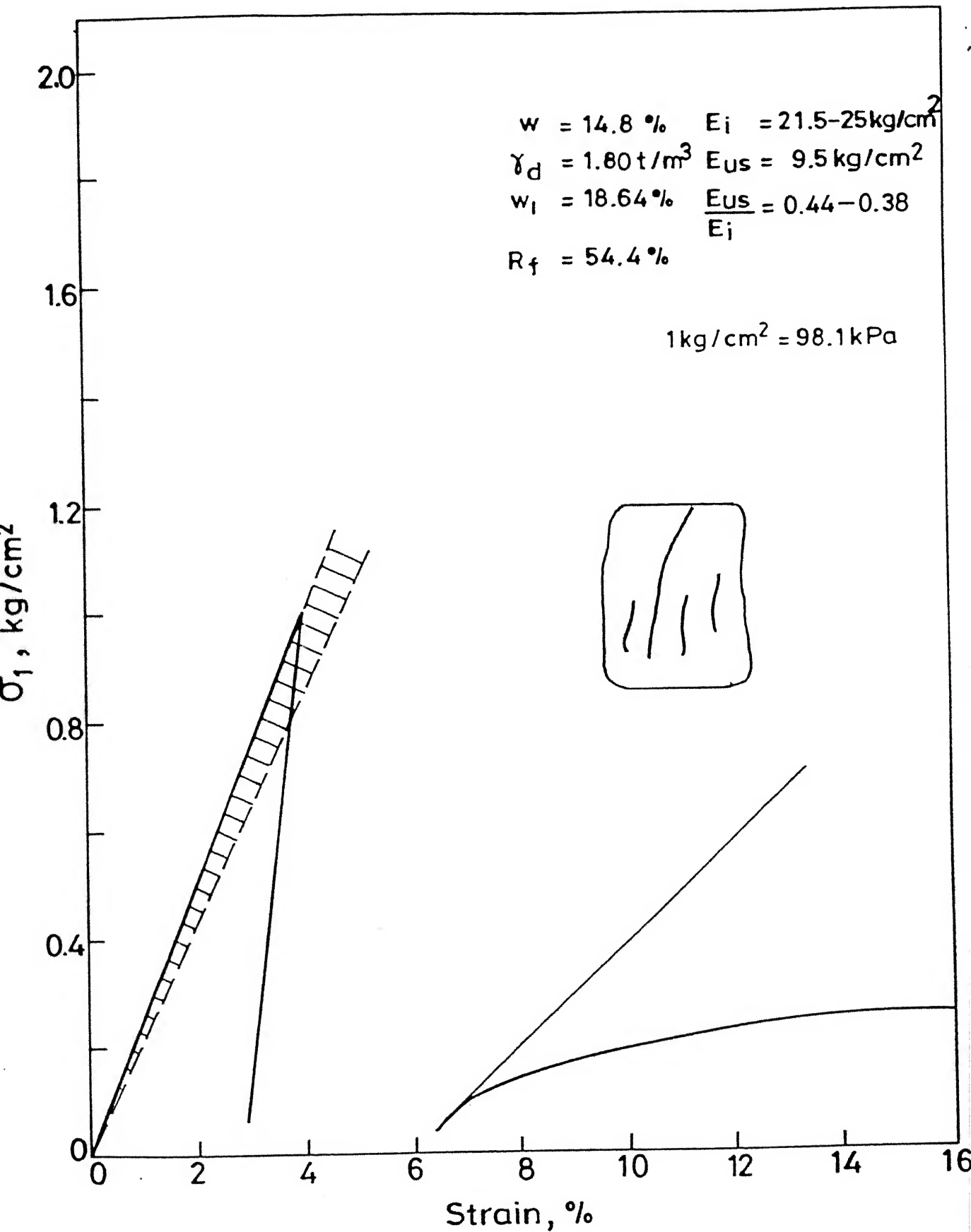


Fig. 4.18 Stress-strain relationship for cyclic softened te
 ($R_f = 54.4 \%$)

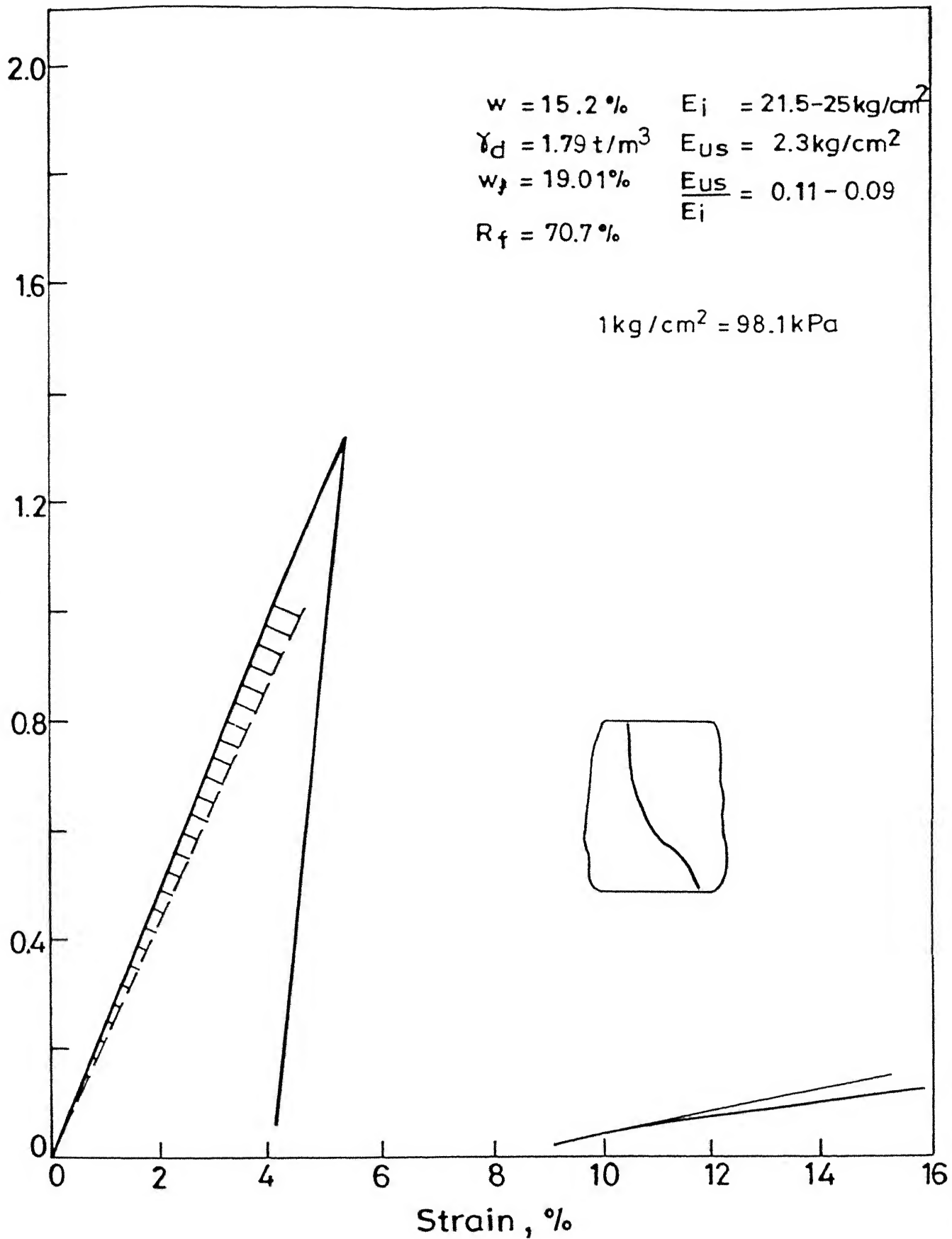


Fig. 4.19 Stress-strain relationship for cyclic softened test
($R_f = 70.7\%$)

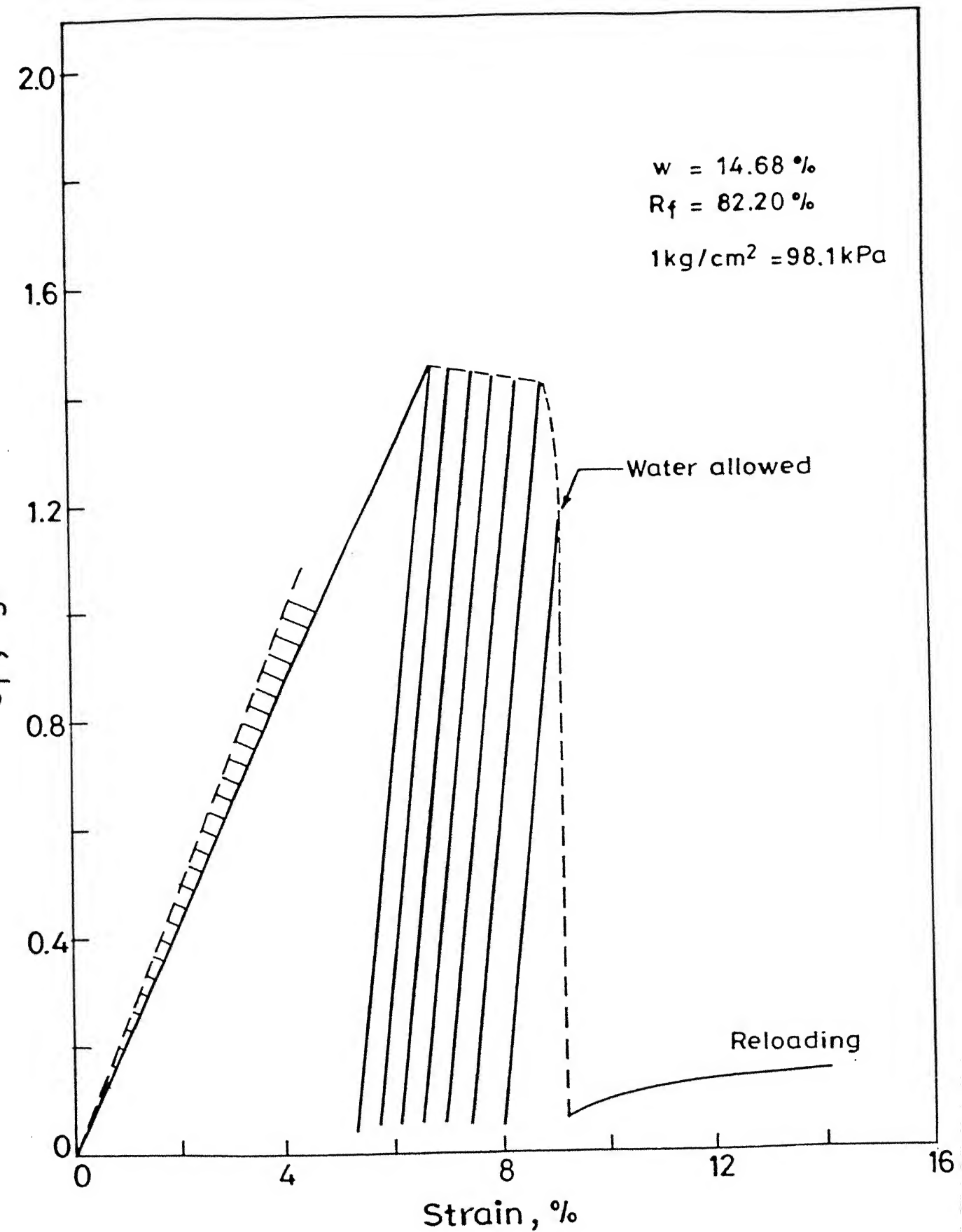


Fig. 4.20 Stress strain relationship for cyclic softened test
($R_f = 82.2\%$)

Table 4.5 Details of series A3 tests

S. No	R_f	No. of tests
1	0.0	6
2	11.0	3
3	14.0	1
4	18.9	3
5	23.3	1
6	27.6	4
7	37.1	3
8	41.5	1
9	45.0	2
10	47.0	1
11	50.0	1
12	54.4	1
13	59.1	1
14	63.0	3
15	66.4	2
16	70.7	1
17	74.0	1
18	52.5	1
19	72.0	1
20	82.2	1

CENTRAL LIBRARY
I. I. T. KANPUR

Acc No. A. 117836

4.7.2 Effective stress tests

Figure 4.21 shows the water content versus dry density data points for the effective stress tests. Results of these tests are also presented according to series in which they are carried out.

4.7.2.1 Series B1 - Unconsolidated undrained tests with pore water pressure measurement

Pore water pressure generated under increasing confining stress is shown in Fig. 4.22.

The effective stress tests are divided under 3 categories on the basis of degree of saturation viz. $S = 86.5-87.2 \%$, $92-94.6 \%$ and $95.1-96.1 \%$. Stress - strain, pore pressure - strain, effective stress ratio - strain relationship and effective stress path for $S = 86.5-87.2 \%$ are shown in Figs. 4.23 to 4.26 respectively. Figures 4.27 to 4.30 show corresponding relationships for $S = 92-94.6 \%$ and Figs. 4.31 to 4.34 show them for $S = 95.1-96.1 \%$.

Cyclic tests of series B2 are also shown in Figs. 4.27 to 4.34. For these tests, cyclic part is not given and only the post cyclic response under monotonic loading is indicated. The level of cyclic loading in these tests is marked as 1 whereas the end of cyclic loading is shown as 2.

For legend, curve names used in these figures and other test details, Tables 4.6 and 4.7 should be referred to. Separate legend and curve name are used for each test.

In this study, the term σ_c' - the initial effective

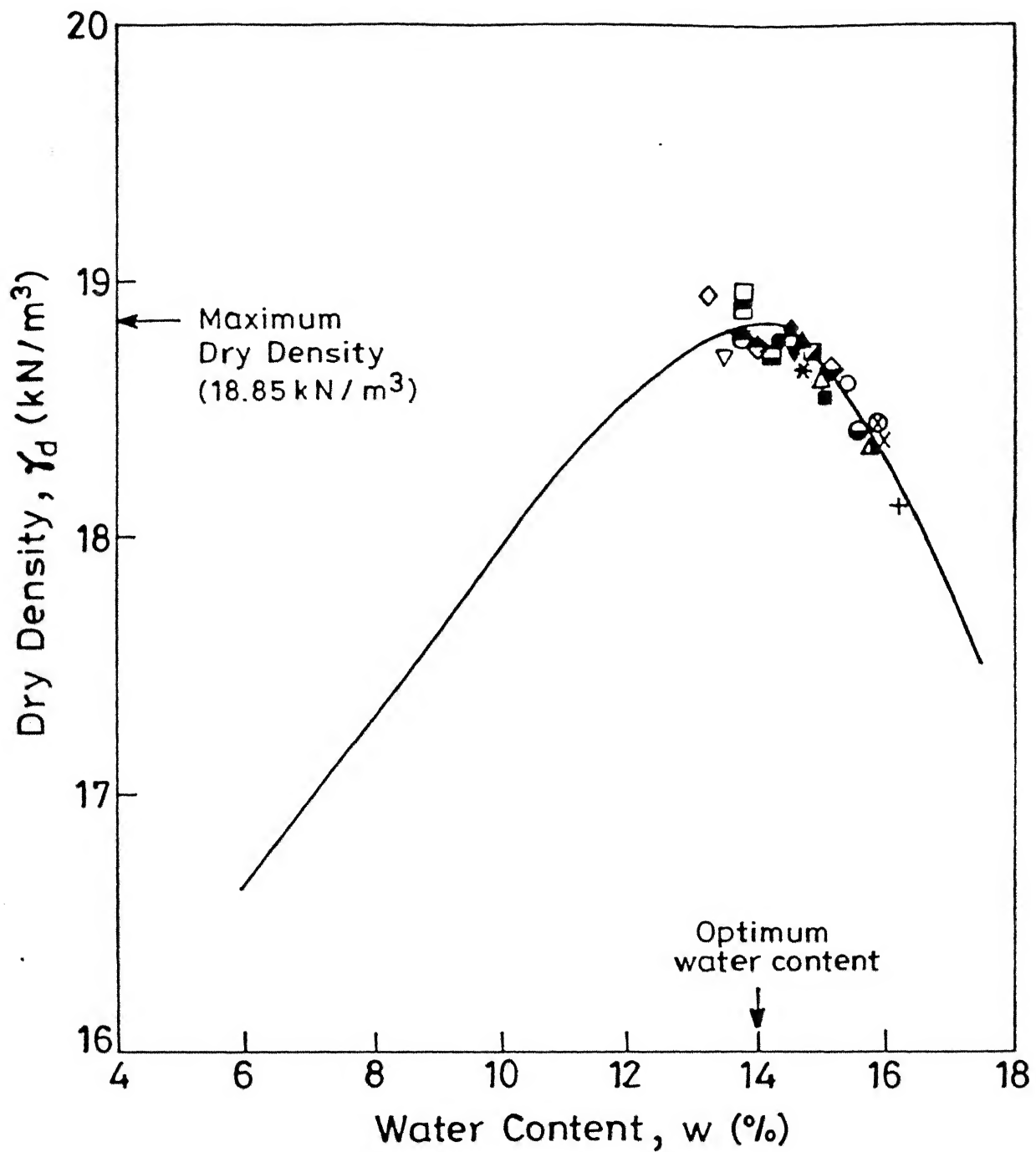


Fig. 4.21 Dry density versus water content relationship for effective stress tests.

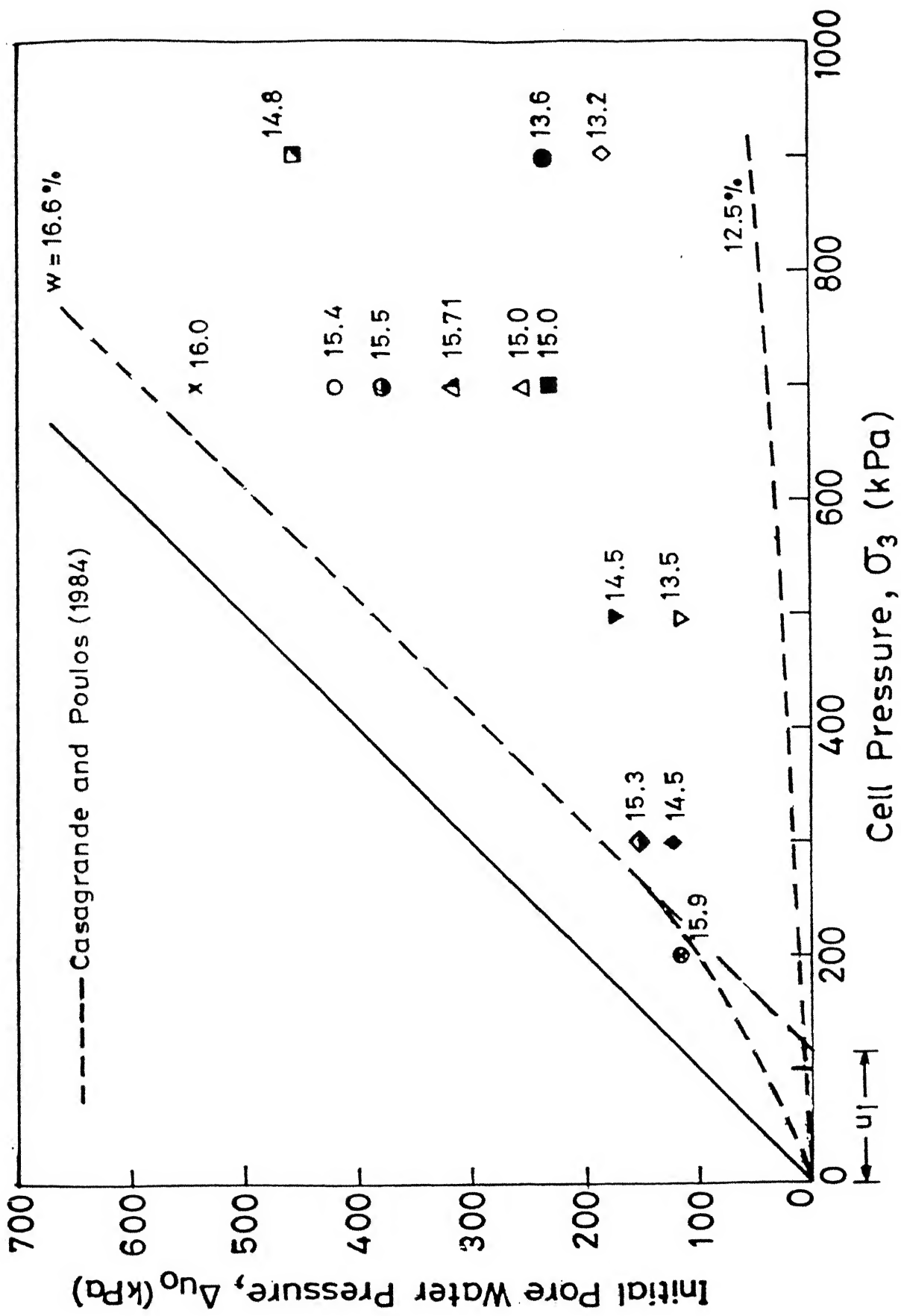


Fig. 4.22 Cell pressure versus initial pore water pressure.

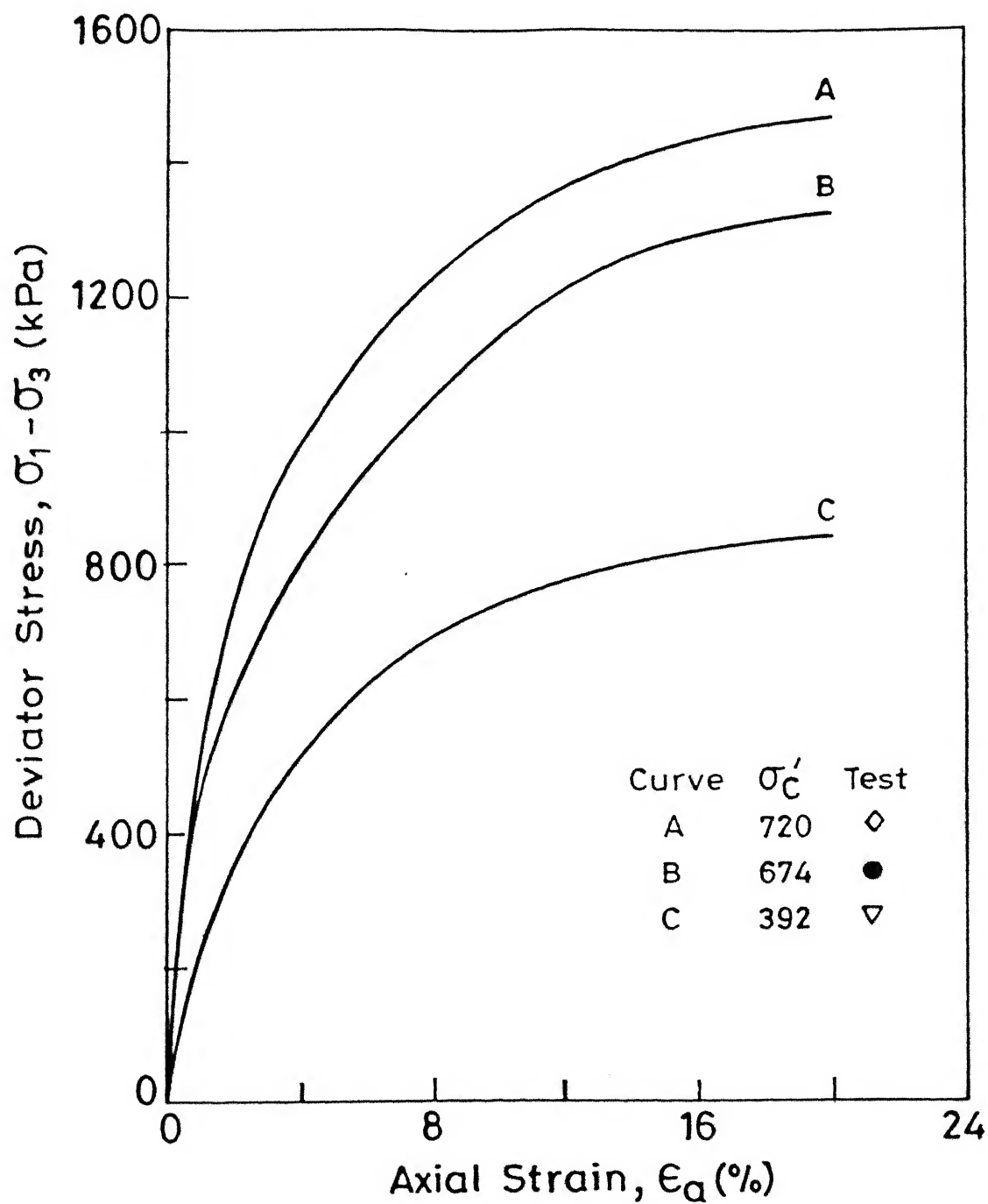


Fig. 4.23 Stress-strain relation for $S = (86.5 - 87.2)\%$.

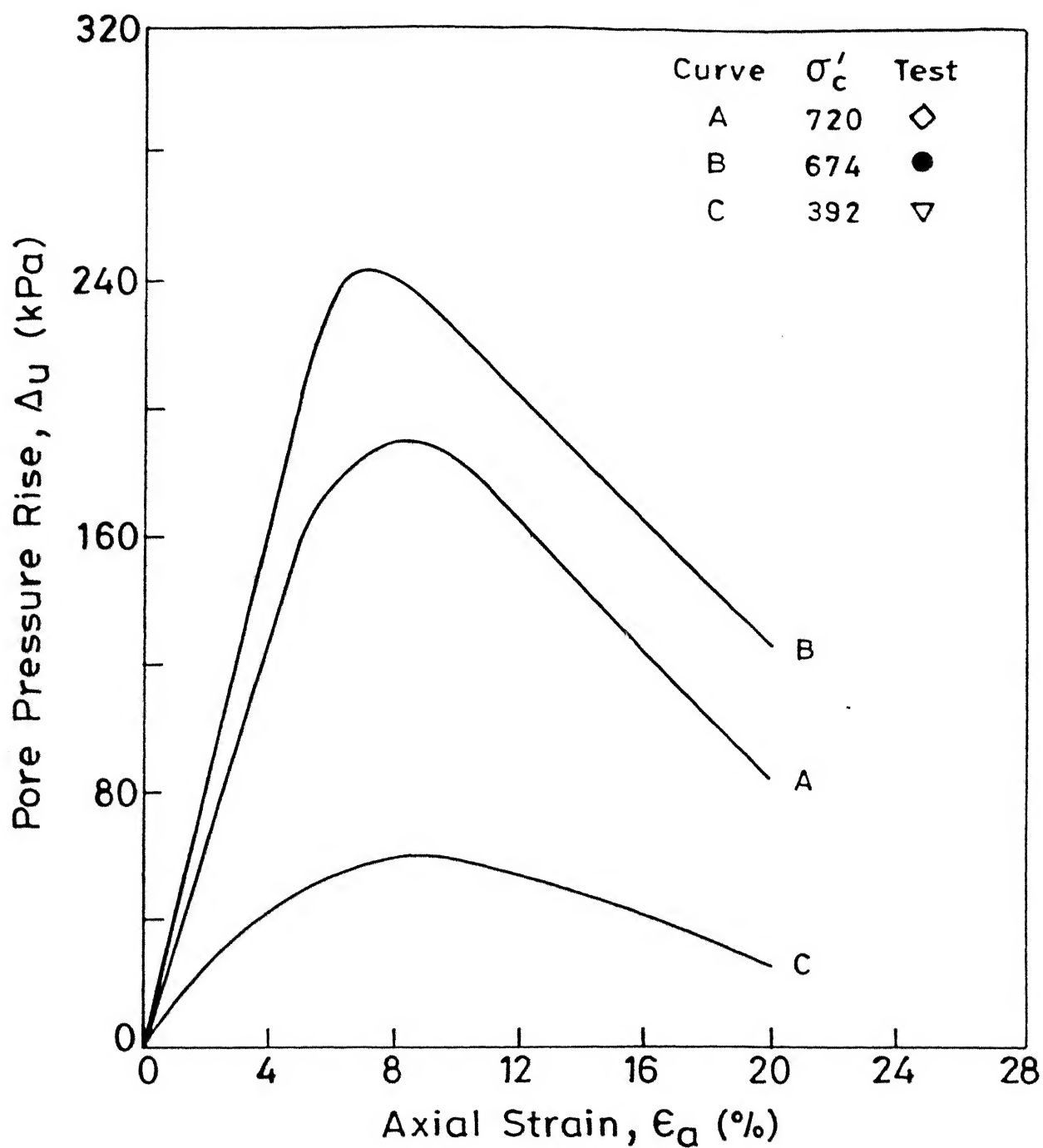


Fig. 4.24 Pore pressure-strain relation for $S=(86.5-87.2)$

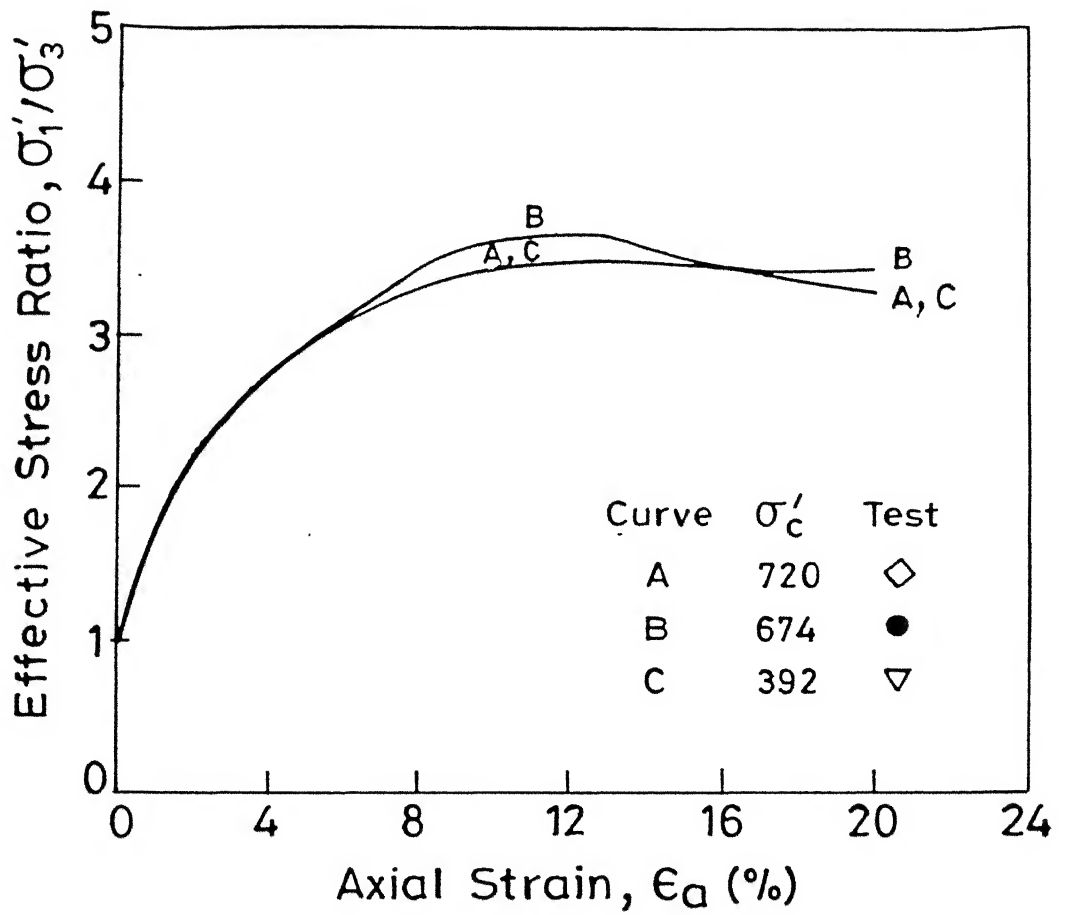


Fig. 4.25 Effective stress ratio-strain relation for $S = (86.5 - 87.2) \%$.

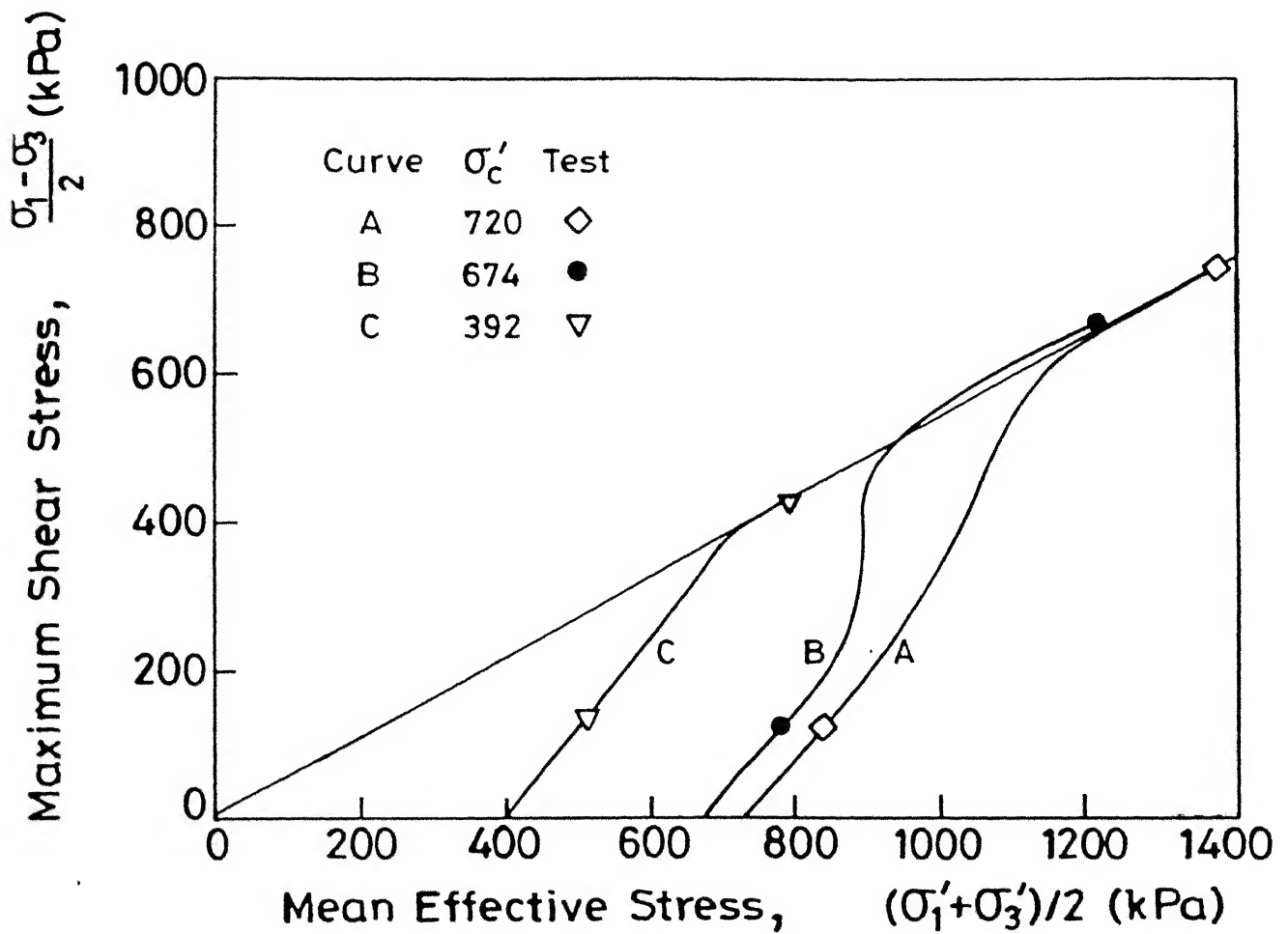


Fig. 4.26 Effective stress path for $S = (86.5-87.2)\%$

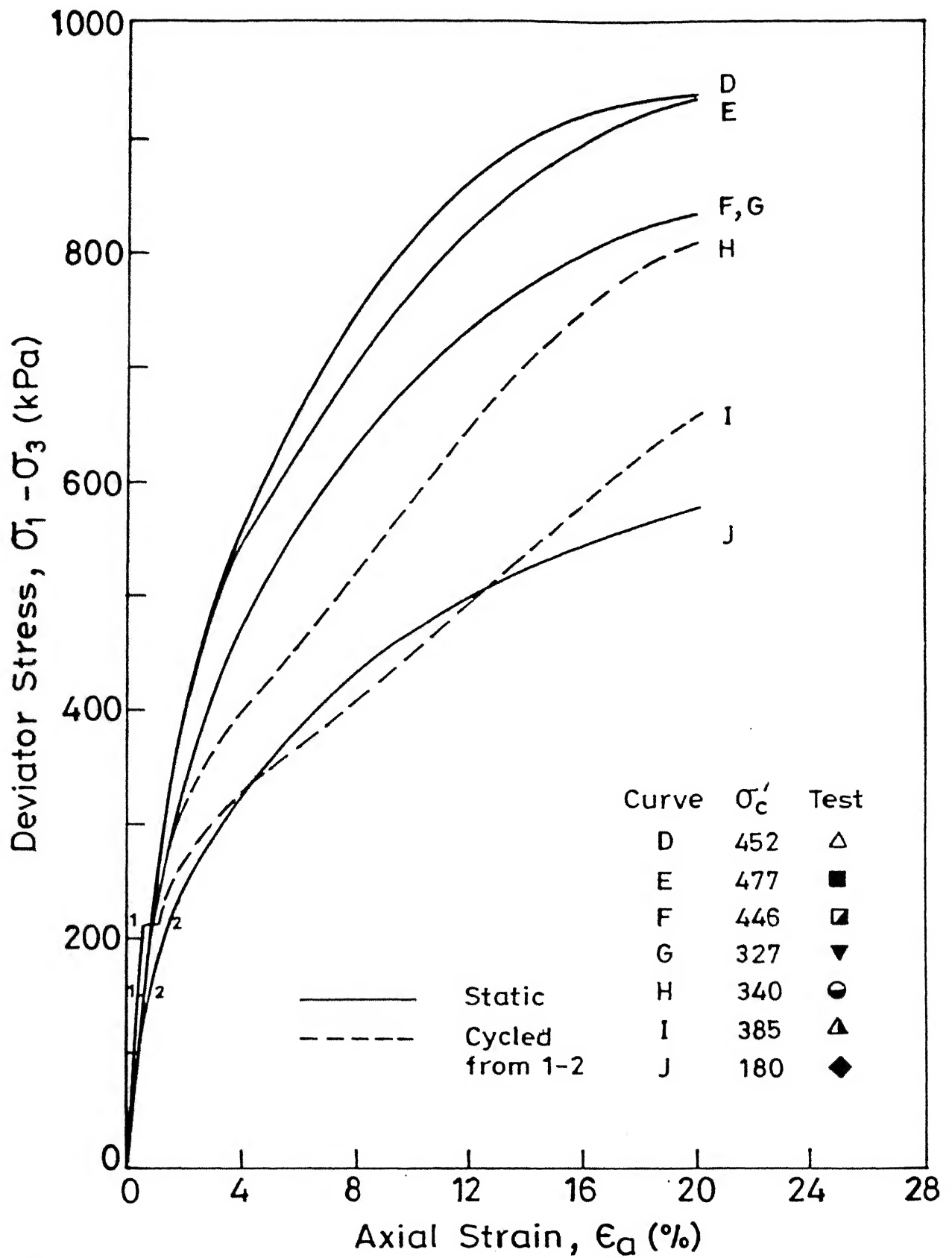


Fig. 4.27 Stress strain relation for $S = (92.0 - 94.6) \%$.

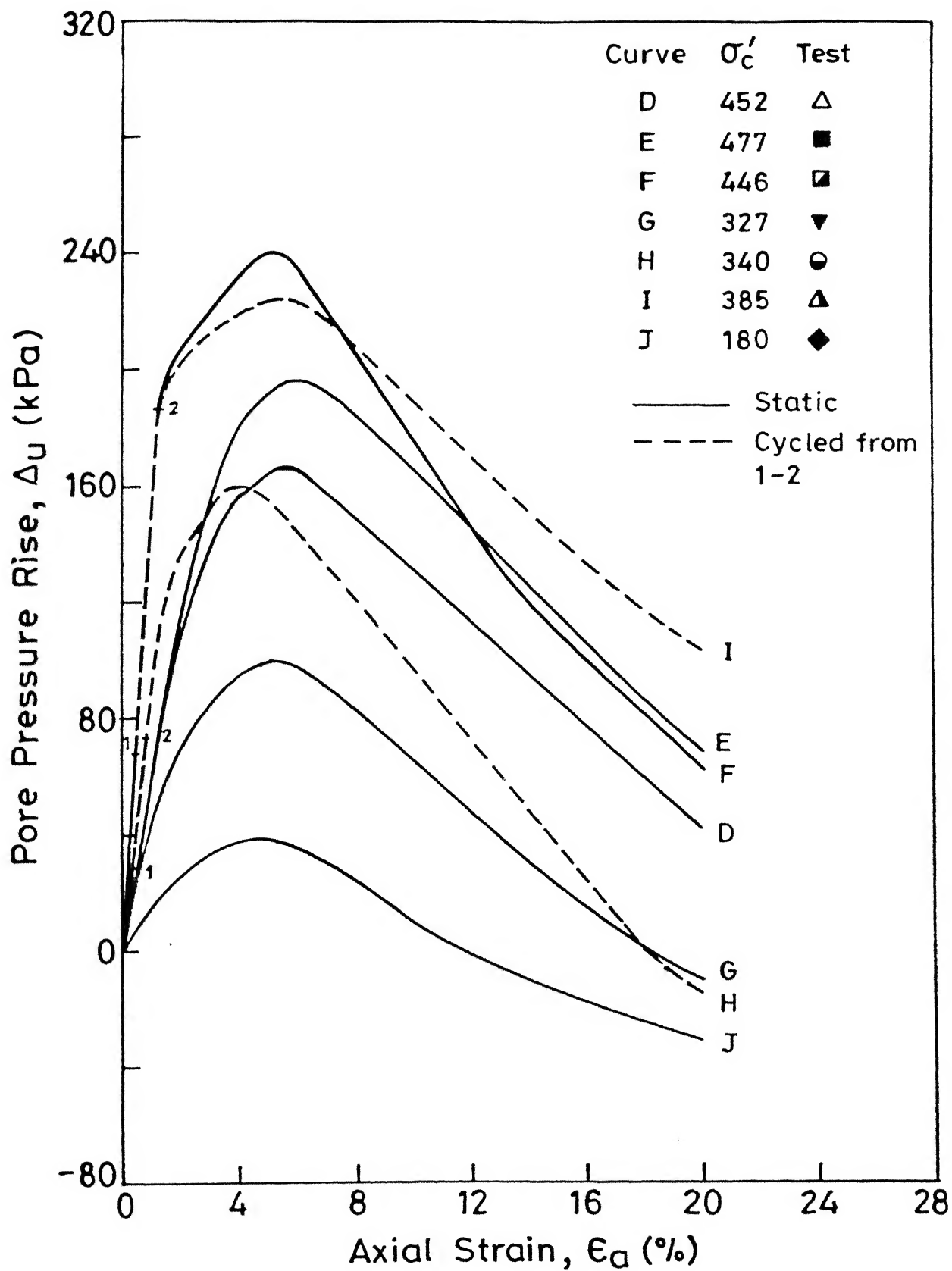


Fig. 4.28 Pore pressure-strain relation for $S = (92.0-94.6)$

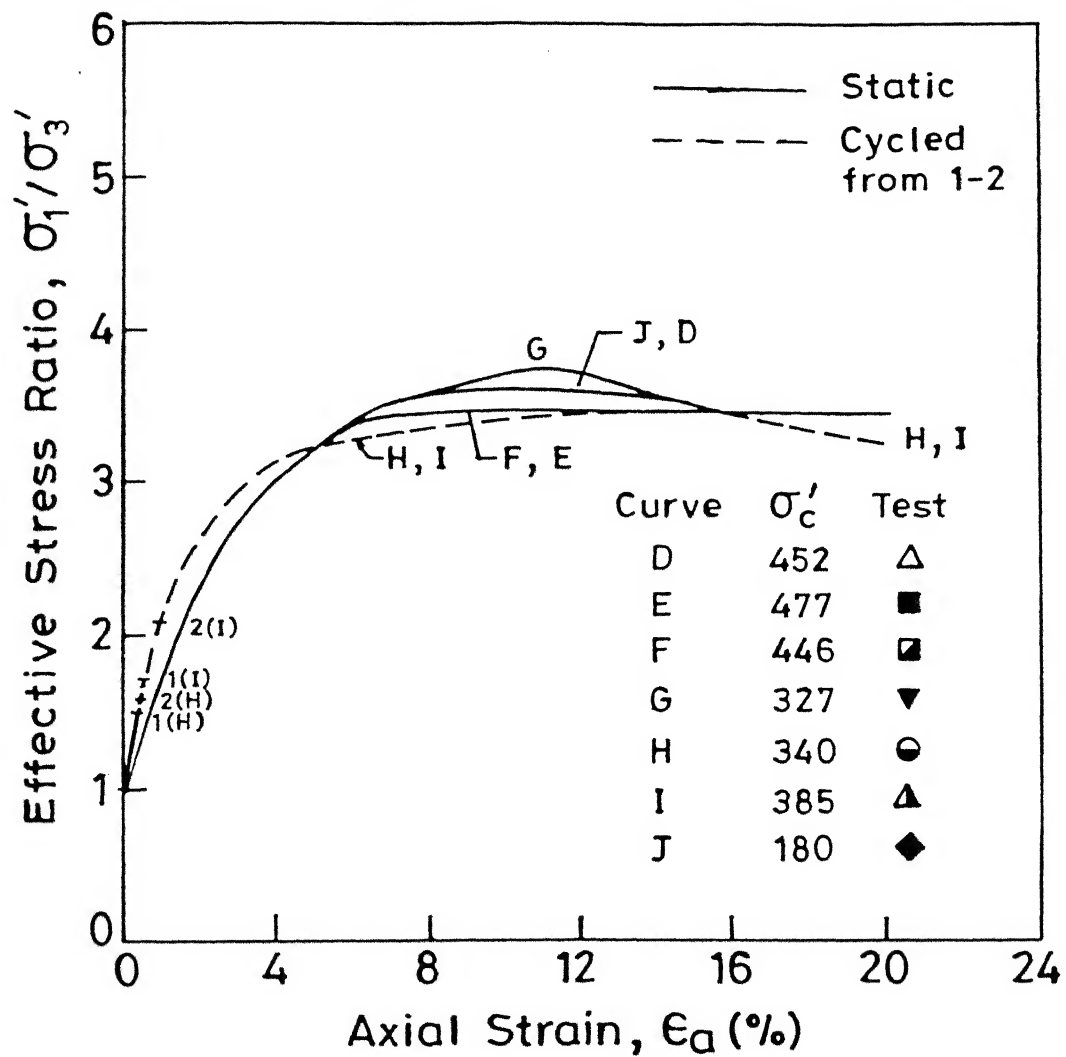


Fig. 4.29 Effective stress ratio-strain relation for $S = (92.0 - 94.6) \%$.

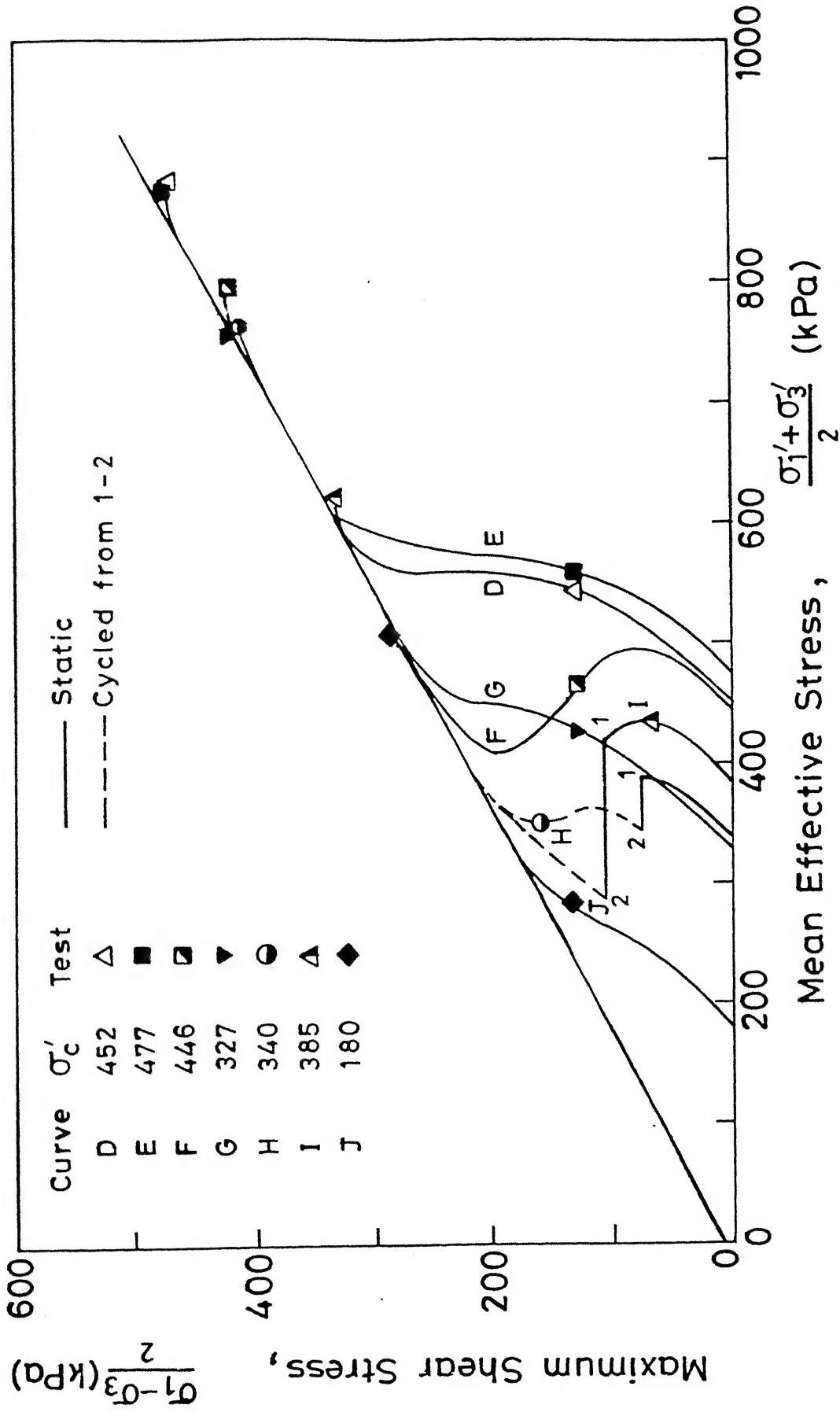


Fig.4.30 Effective stress path for $S = (92.0 - 94.6) \%$.

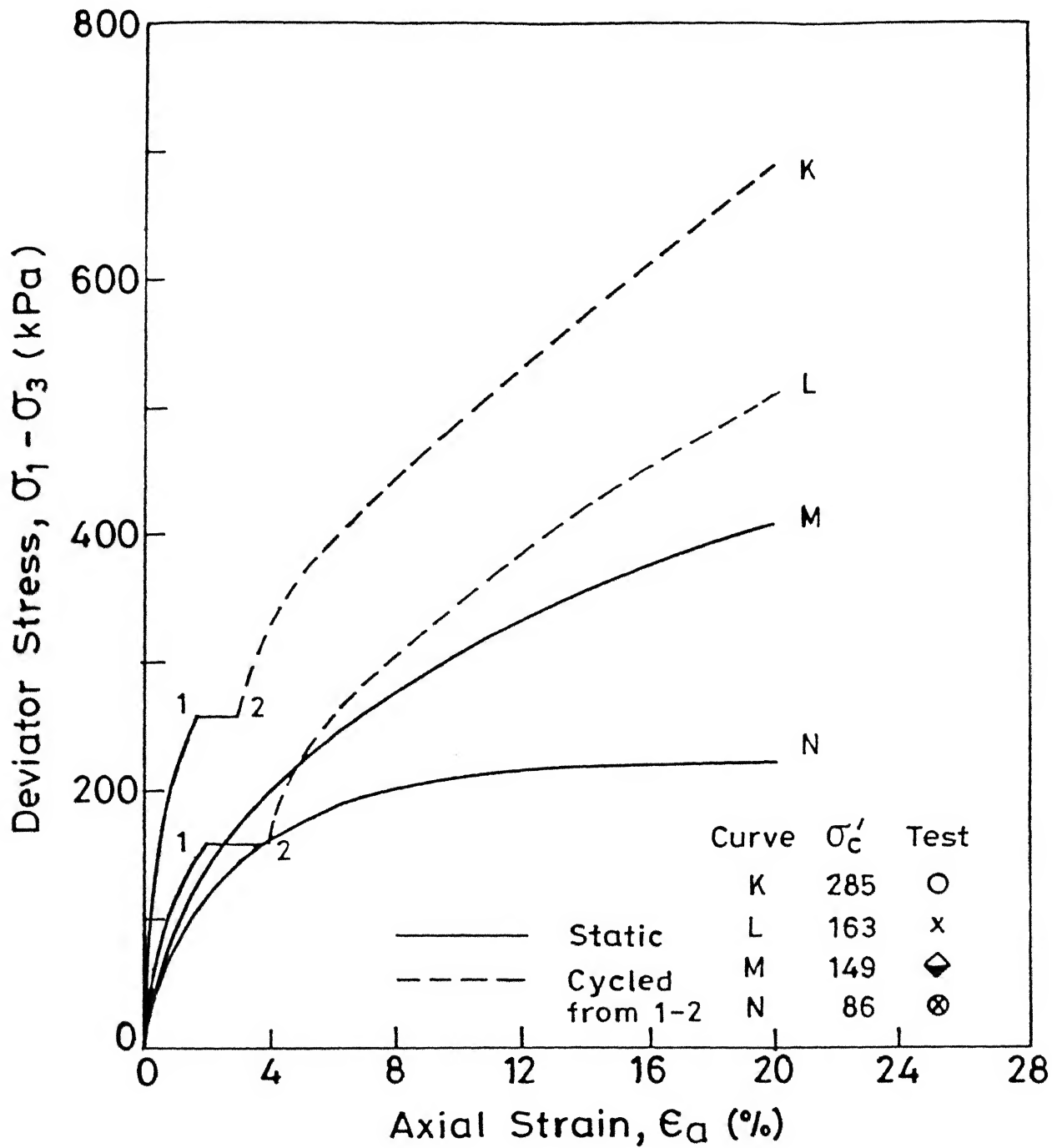


Fig. 4.31 Stress strain relation for $S = (95.1 - 96.1)\%$.

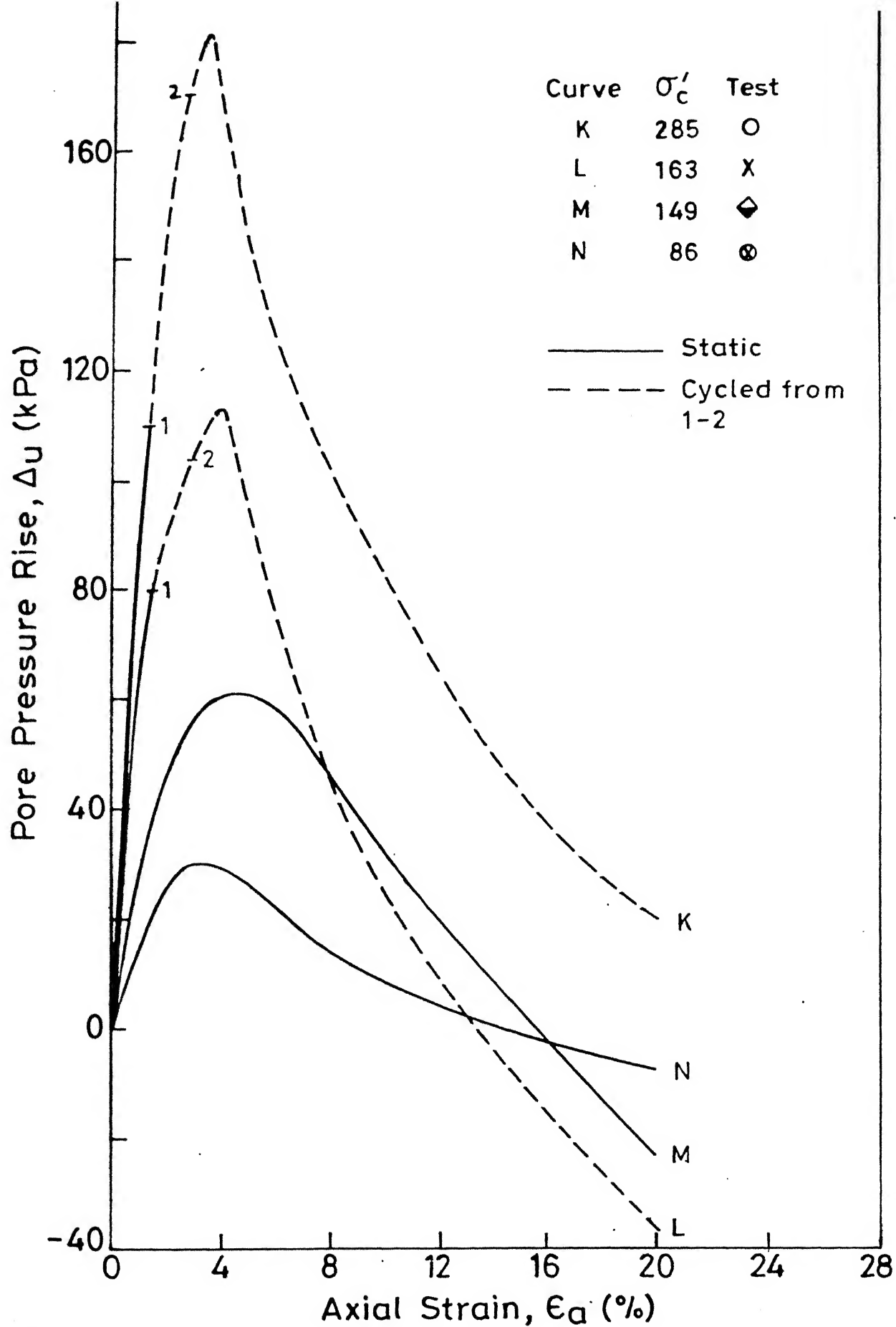


Fig. 4.32 Pore pressure - strain relation for $S = (95.1-96.1)$

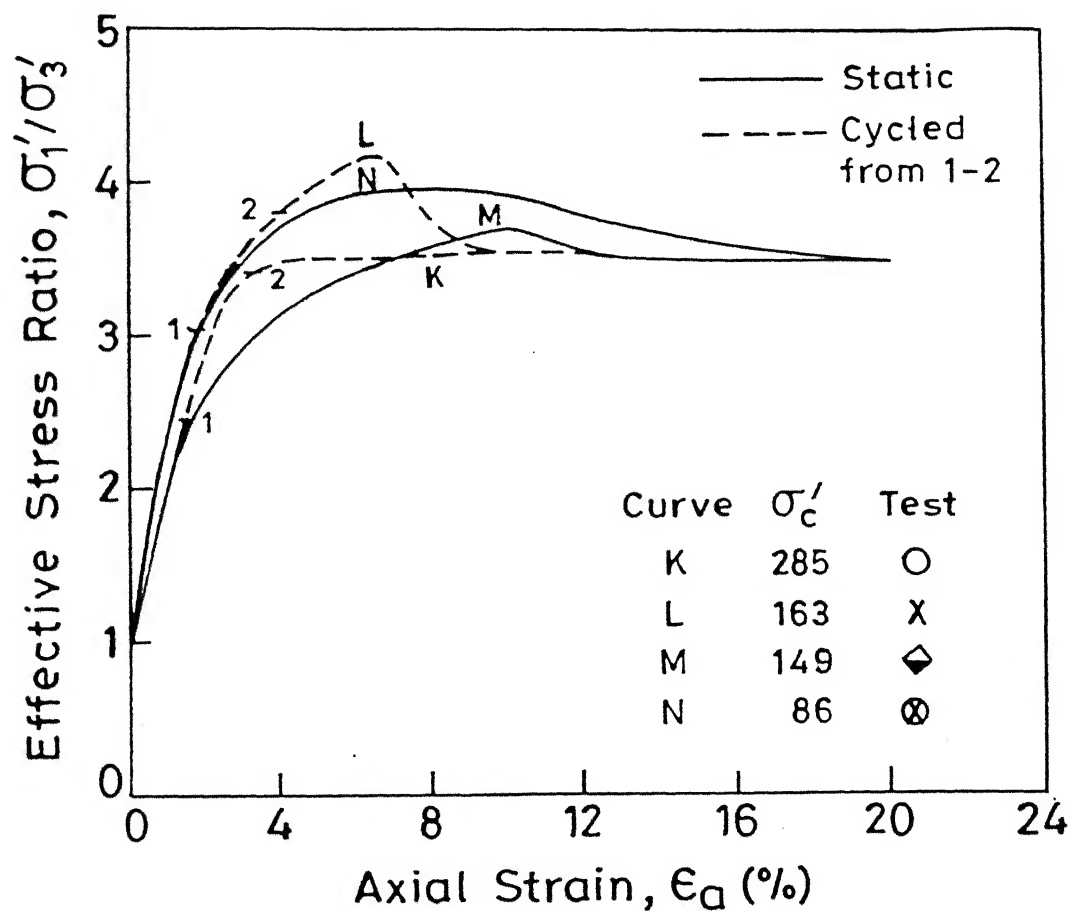


Fig. 4.33 Effective stress ratio - strain relation for $S = (95.1 - 96.1) \%$

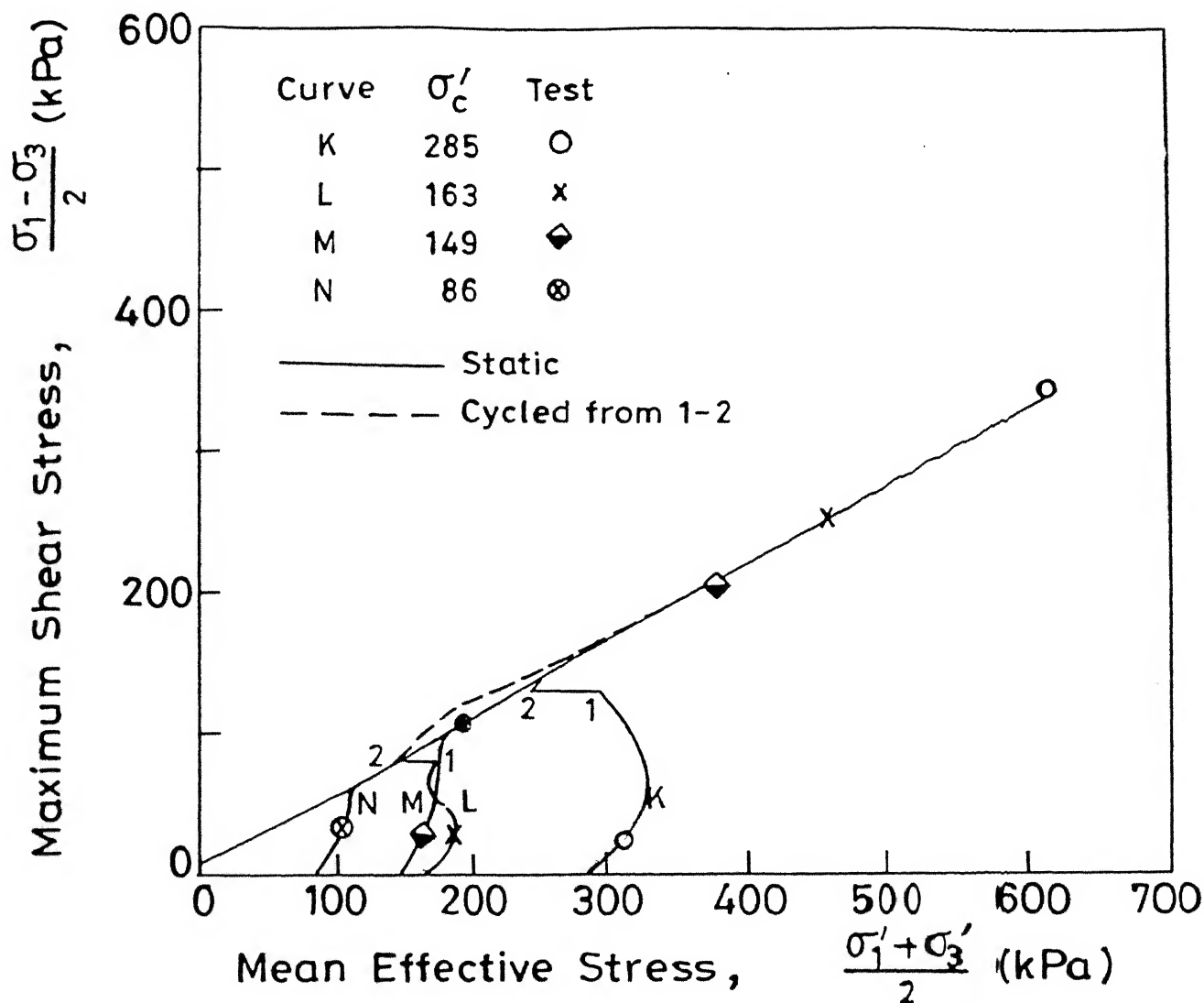


Fig. 4.34 Effective stress path for $S = (95.1-96.1)\%$.

Table 4.6 Details of effective stress tests on Campus silt (static tests).

Test No.	Test Legd	Test Curve	w_f C%	γ_d (kN/m ³)	S C%	σ_3 (kPa)	σ'_c (kPa)	Δu_o (kPa)	$\frac{(\sigma'_1 - \sigma'_3)}{2}$ (kPa)	$\frac{(\sigma'_1 + \sigma'_3)}{2}$ (kPa)	$\frac{(\sigma'_1 - \sigma'_3)}{2}$ sr	$\frac{(\sigma'_1 + \sigma'_3)}{2}$ (kPa)	$(\sigma'_1 / \sigma'_3)_{\max}$	$(\Delta u)_{\max}$ (kPa)	$\frac{\sigma'_1 - \sigma'_3}{2}$ at (Δu) _{max} (kPa)
NEW23	◇	A	13.24	18.90	87.25	900	720	180	740	1376	685	1249	3.43	190	619
NEW1	▽	C	13.52	18.74	86.52	500	392	108	423	789	394	724	3.39	60	356
NEW27	●	B	13.60	18.74	87.03	900	674	230	665	1213	590	1028	3.72	245	516
NEW30	◆	J	14.46	18.79	93.39	300	180	120	290	535	235	410	3.68	39	172
NEW29	▼	G	14.50	18.70	92.12	500	327	173	417	755	366	635	3.72	100	269
NEW26	▣	F	14.83	18.72	94.56	900	446	454	415	707	388	711	3.40	239	260
NEW32	△	D	14.98	18.54	92.46	700	452	248	472	882	420	749	3.56	167	317
NEW24	■	E	14.99	18.51	92.02	700	477	223	471	880	390	712	3.42	194	308
NEW25	◆	M	15.27	18.59	95.10	300	149	151	202	375	151	264	3.67	62	101
NEW28	⊗	N	15.89	18.39	95.48	200	86	114	110	202	110	184	3.98	30	75

Table 4.7 Details of effective stress tests on Campus Silt (Cyclic and Static Tests).

Test No.	Test Legd	Test curve	w_f C%	γ_d CKN/m ³	S C%	σ_3 (kPa)	σ'_c (kPa)	Δu_o (kPa)	$\frac{(\sigma_1 - \sigma_3)_{\max}}{2}$ (kPa)	$\frac{(\sigma'_1 + \sigma'_3)_{\max}}{2}$ (kPa)	$\frac{(\sigma_1 - \sigma_3)_{sr}}{2}$ (kPa)	$\frac{(\sigma'_1 + \sigma'_3)_{sr}}{2}$ (kPa)	$(\sigma'_1 / \sigma'_3)_{\max}$	$(\Delta u)_{\max}$ (kPa)	$\frac{\sigma_1 - \sigma_3}{2 \text{ at } (\Delta u)_{\max}}$ (kPa)	$\frac{\sigma_1 - \sigma_3}{2} \text{ cyc}$ (kPa)
HIGH σ'_c																
T103	O	K	15.39	18.60	96.02	700	285	415	345	610	300	540	3.50	181	155	130.0
T104	●	H	15.49	18.43	93.74	700	340	360	405	761	294	537	3.42	160	195	75.0
T105	▲	I	15.71	18.37	94.07	700	385	315	330	615	275	503	3.40	225	172	105.0
T106	X	L	15.99	18.39	96.08	700	163	537	255	455	122	198	4.21	113	108	80.0
$\sigma'_c = (20 - 22)$ KPa																
T107	+	R	16.17	18.10	92.33	500	20	480	75	181	30	49	4.16	5	34	S
T108	▲	P	16.66	18.75	95.13	500	22	478	212	388	32	49	4.75	5	64	S
T109	□	O	14.69	18.75	94.18	500	20	480	212	408	---	---	---	5	60	42.5
T110	*	Q	16.40	18.98	91.96	500	22	478	212	304	---	---	---	5	60	25.0
$\sigma'_c = 40$ KPa																
T115	■	T	13.50	18.90	88.97	500	40	460	230	416	52	89	3.81	7	7	S
T116	●	V	16.50	18.81	100.0	500	40	460	180	329	---	---	---	7	7	50.0
T117	◆	S	16.87	18.77	87.51	500	40	460	240	440	---	---	---	7	7	38.0
T119	□	U	14.00	18.70	100.0	500	40	460	222	406	50	83	4.03	7	7	63.0

* S - static test

cyc - indicates cyclic stress level

at $(\Delta u)_{\max}$ - indicates stress level where $(\Delta u)_{\max}$ occurs

confining stress - represents the difference between either the cell pressure and the pore pressures induced under undrained condition or the cell pressure and the back pressure against which the sample was allowed to consolidate. γ_d is the dry density before the start of the test. If the stress strain curve for test does not show any peak stress, then $(\sigma_1 - \sigma_3)_{\max}/2$ records the shear stress at 20 % axial strain. $(\sigma'_1 + \sigma'_3)_{\max}/2$ is the mean effective stress corresponding to maximum shear stress. $(\sigma'_1/\sigma'_3)_{\max}$ is the maximum value of effective stress ratio during the test. $(\Delta u)_{\max}$ is the maximum value of pore water pressure recorded during the test. Suffix 'sr' indicates corresponding values at maximum effective stress ratio.

It may be seen that for a particular degree of saturation, the resistance to shearing increases with increasing value of σ'_c (Figs. 4.23, 4.27 and 4.31).

Pore water pressure response during these tests is shown in Figs. 4.24, 4.28 and 4.32 respectively. It may be observed that in general, as σ'_c value increases, a higher value of maximum pore water pressure is reached. However, pore water pressure - strain response is very sensitive to the value of initial degree of saturation.

In Figs. 4.28 and 4.32, results of cycled samples are also given. The pore pressure increase due to cyclic loading ($N = 100$) is observed (1 to 2) and the response following the cyclic loading under monotonic increase in axial stress is indicated. It may be seen (Fig. 4.28) that the decrease in pore pressure with strain is higher for the cycled sample ($H, \sigma'_c = 340$ kPa)

as compared to sample G which was tested under static loading at comparable σ_c , (327 kPa).

The variations of σ_1'/σ_3' vs. axial strain are shown in Figs. 4.25, 4.29 and 4.33. In these figures, the response of cycled tests is also indicated. It may be noted that except for test indicated L in Fig. 4.33 which is cyclic test and has low σ_c' and for test N in same figure which has $\sigma_c' < 100$ kPa, $(\sigma_1'/\sigma_3')_{\max}$ is attained at an axial strain of around 12 % and the average value of $(\sigma_1'/\sigma_3')_{\max}$ is 3.55 (3.39 - 3.72) for all these tests.

Effective stress path curves for all these tests (see Figs. 4.26, 4.30 and 4.34) indicate a highly dilatant response during shear. The stress path approaches the failure envelope and then moves along it as the sample continues to dilate up to 20 % axial strain where the test is terminated. The point where the effective stress path approaches the failure envelope corresponds approximately to the state of stress where σ_1'/σ_3' is maximum.

4.7.2.2 Series B2 - Unconsolidated undrained cyclic tests with pore water pressure measurement

The cycled test experimental data referred to in the preceding series B1 tests, is now presented.

As seen previously (Figs. 4.26, 4.30 and 4.34), in the initial stages, the effective stress path moves quite close to the total stress path and only at a particular value of shear stress, the material begins to exhibit compressive response

(increase in induced positive pore pressure). It will be shown in a later section under discussion (Sec. 4.8.4.3.2), that corresponding to this point, $(\sigma_1 - \sigma_3)/2\sigma_c'$ is roughly 0.13 for this soil and at or below this level, the soil behaves almost like an elastic material during the cyclic loading. Four cycled tests described in this series were conducted with values of $(\sigma_1 - \sigma_3)/2$ greater than the corresponding elastic limit with R_f ranging from 18.52 to 31.37 % . The relative position of these tests on a stress path for a given σ_c' is shown in Fig. 4.41.

The stress - strain and pore pressure - strain relationships for these 4 tests with special emphasis on behaviour during cyclic loading are given in Figs. 4.35 to 4.38. The corresponding effective stress paths are given in Figs. 4.39 to 4.42.

The response during cyclic loading is similar to the results already reviewed in literature.

The cumulative increase in pore pressure during cyclic loading varied from 160, 225, 181 and 113 kPa corresponding to the tests cycled at points 1, 2, 3 and 4 (Fig. 4.41) as given in Table 4.7.

4.7.2.3 Series B3 - Undrained static and cyclic tests with pore water pressure measurement on samples with back pressure saturation.

Figures 4.43 to 4.46 depict the stress - strain, pore pressure -strain, effective stress ratio - strain relationship and effective stress path for samples with $\sigma_c' = 20$ and 22 kPa.

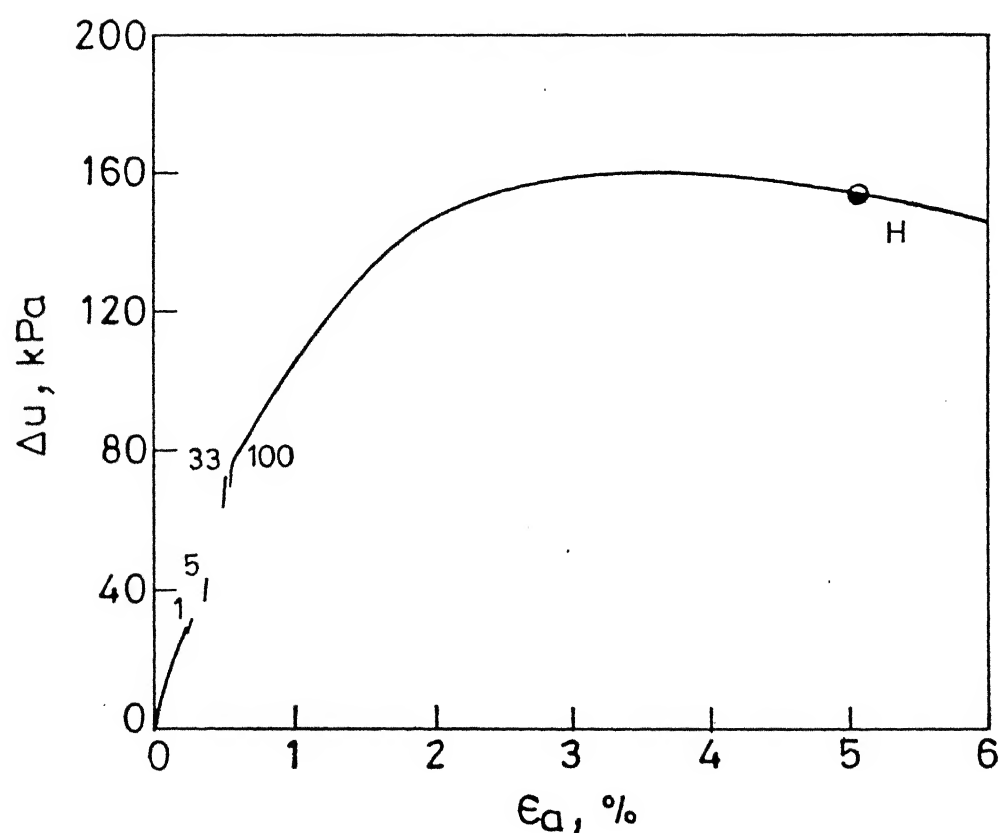
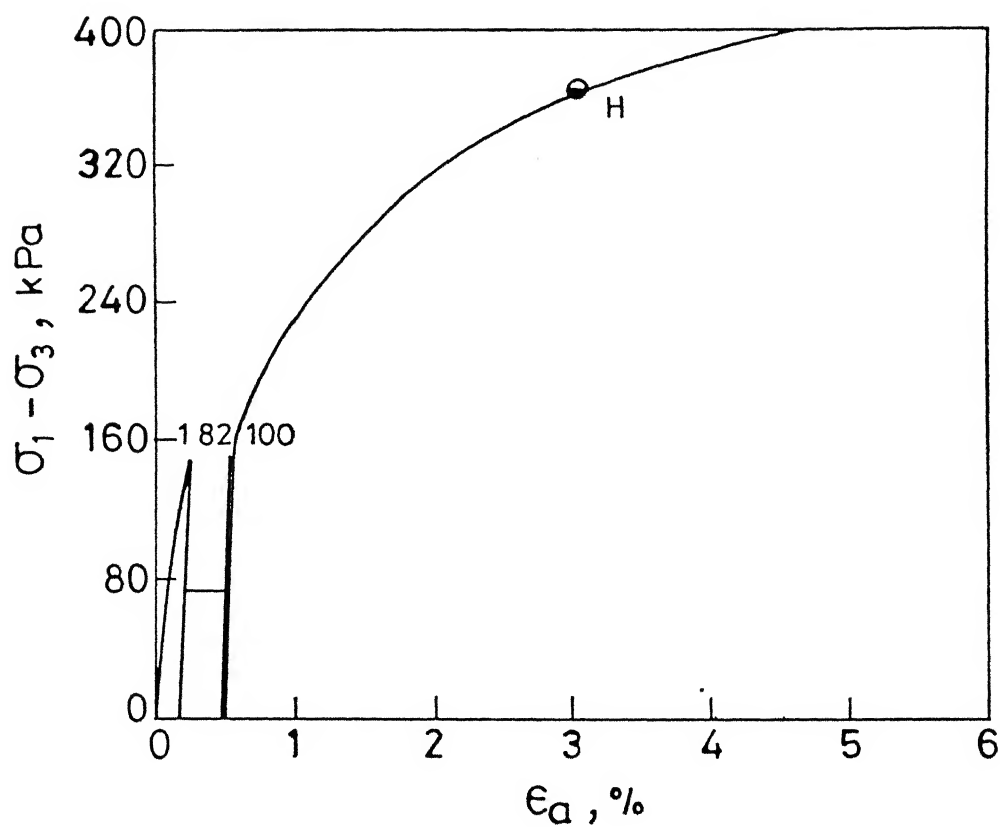


Fig. 4.35 Stress-strain, pore pressure-strain relationship for test with $R_f = 18.52\%$.

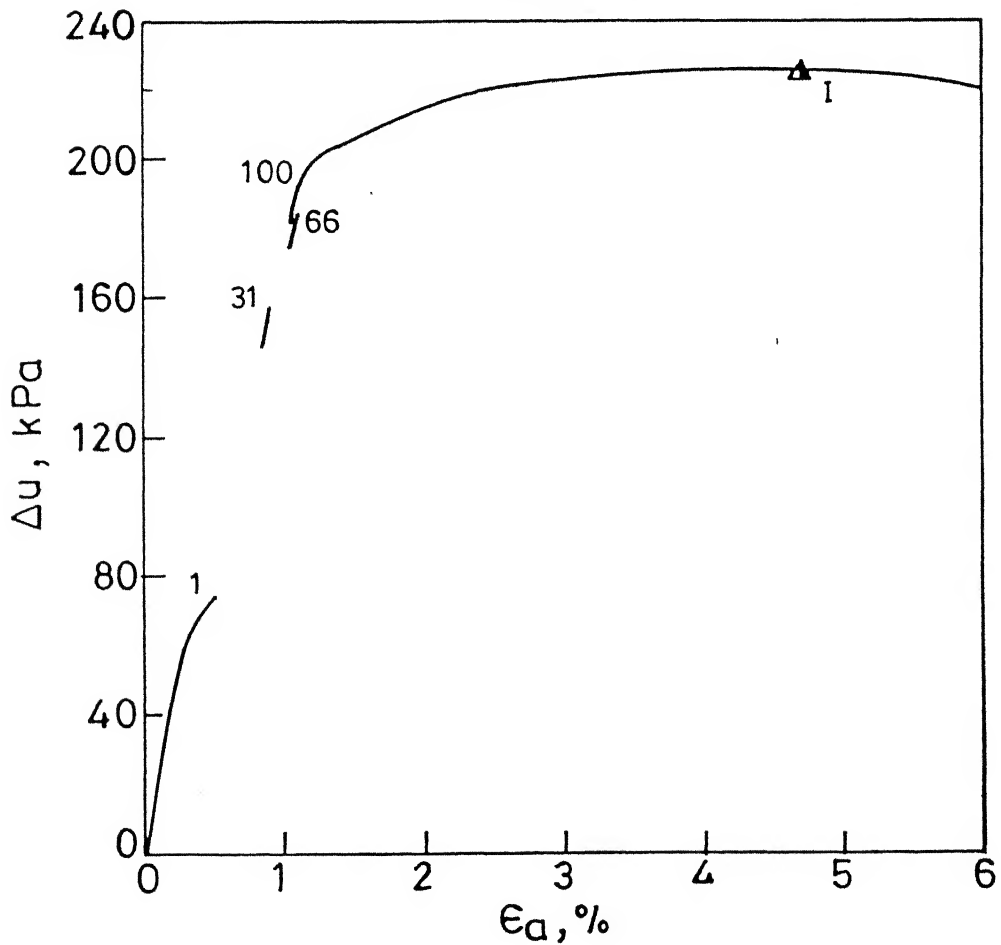
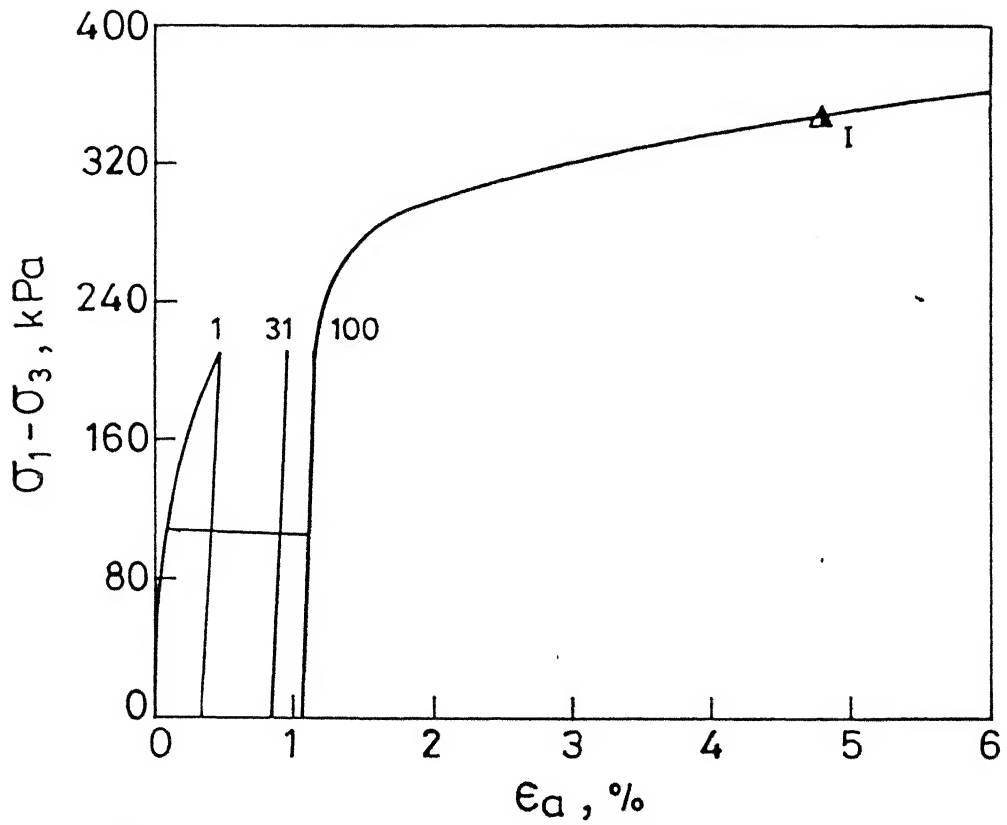


Fig. 4.36 Stress-strain, pore pressure-strain relationship for test with $R_f = 31.82\%$

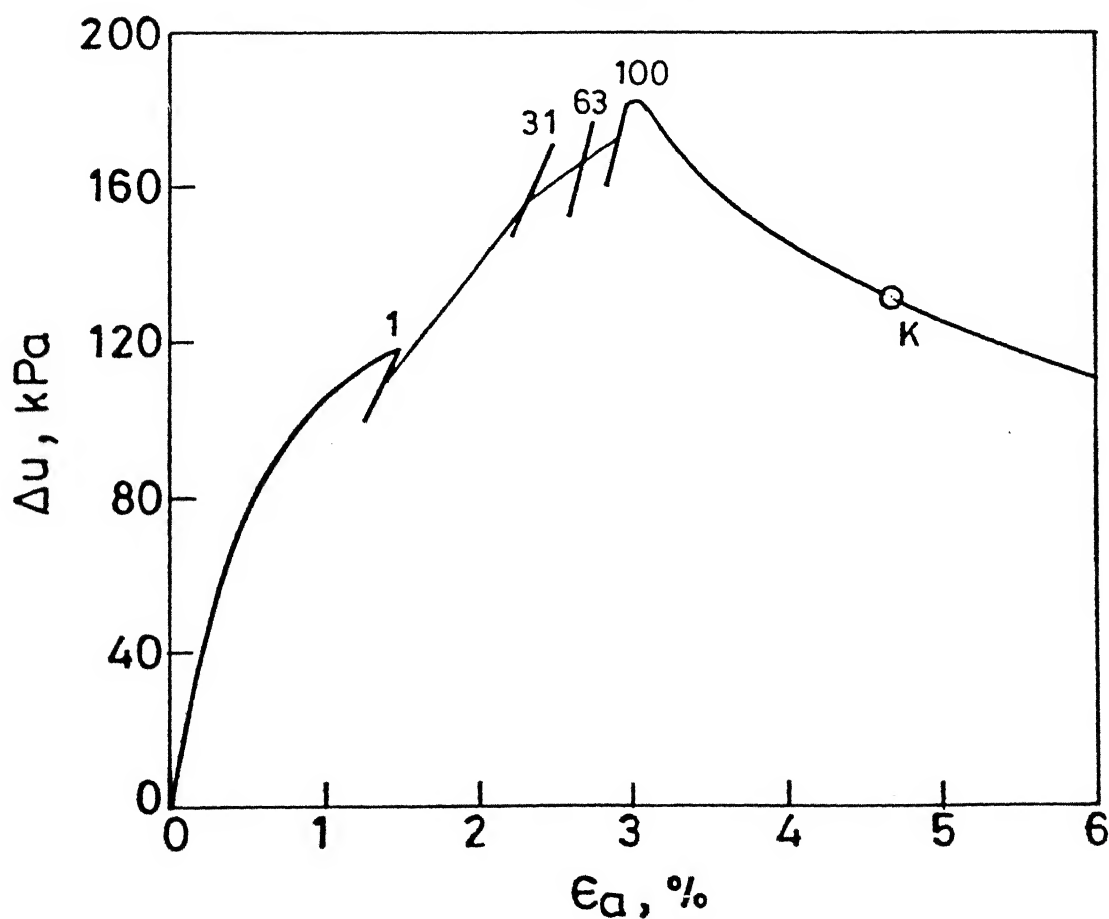
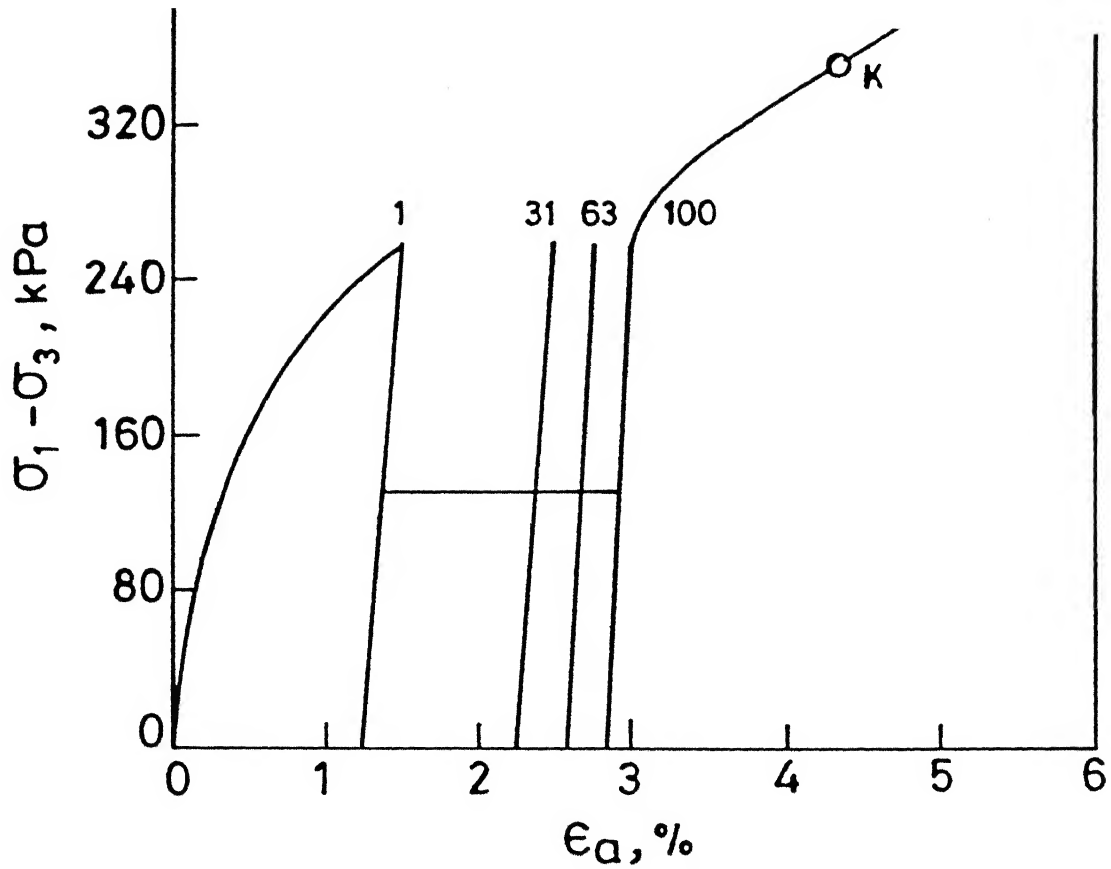


Fig. 4.37 Stress-strain, pore pressure-strain relationship for test with $R_f = 37.68\%$

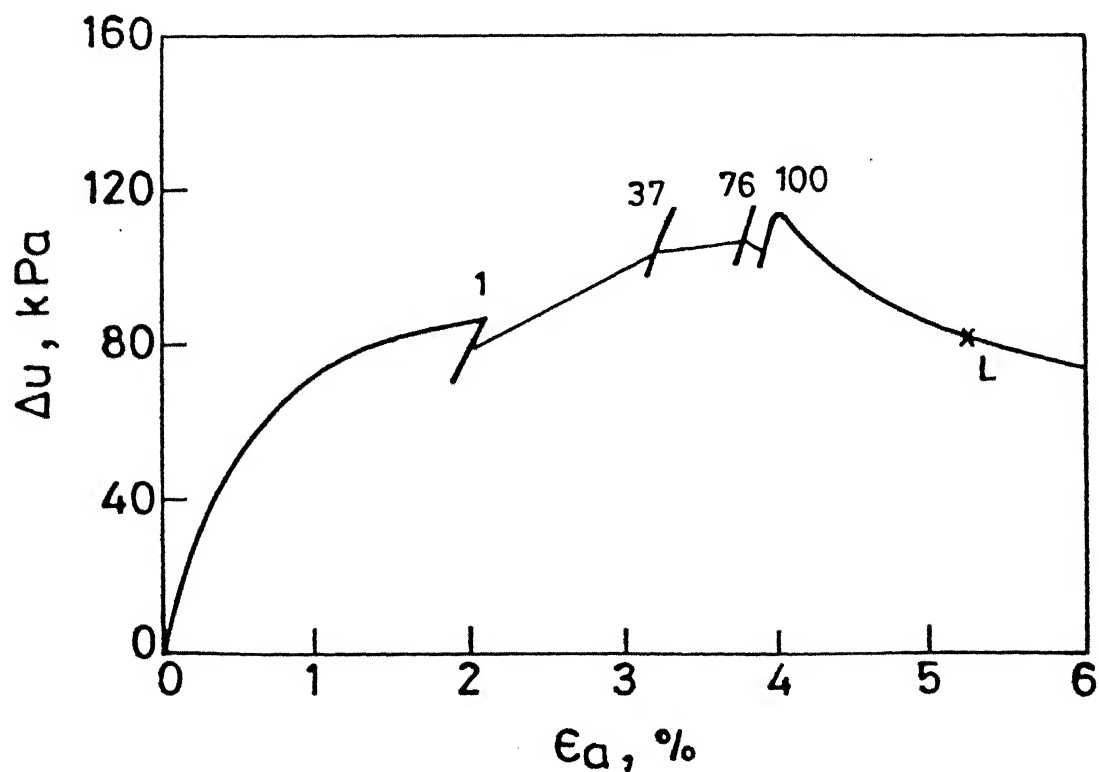
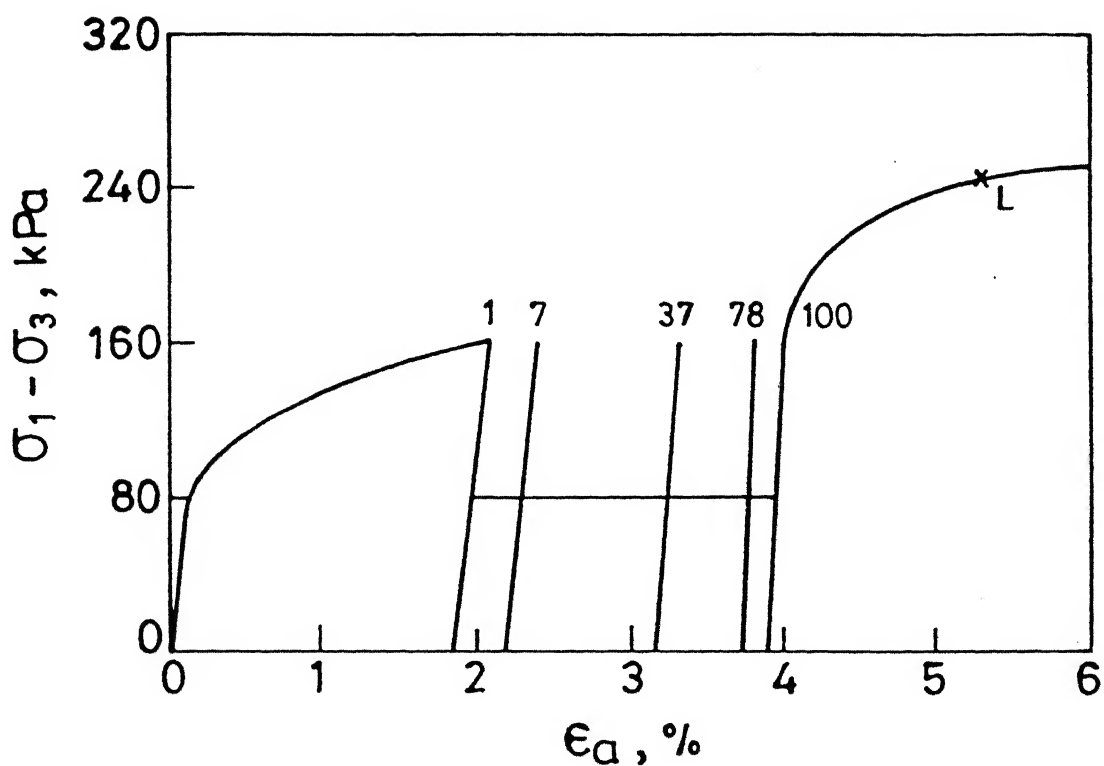


Fig. 4.38 Stress-strain, pore pressure - strain relationship for test with $R_f = 31.37\%$

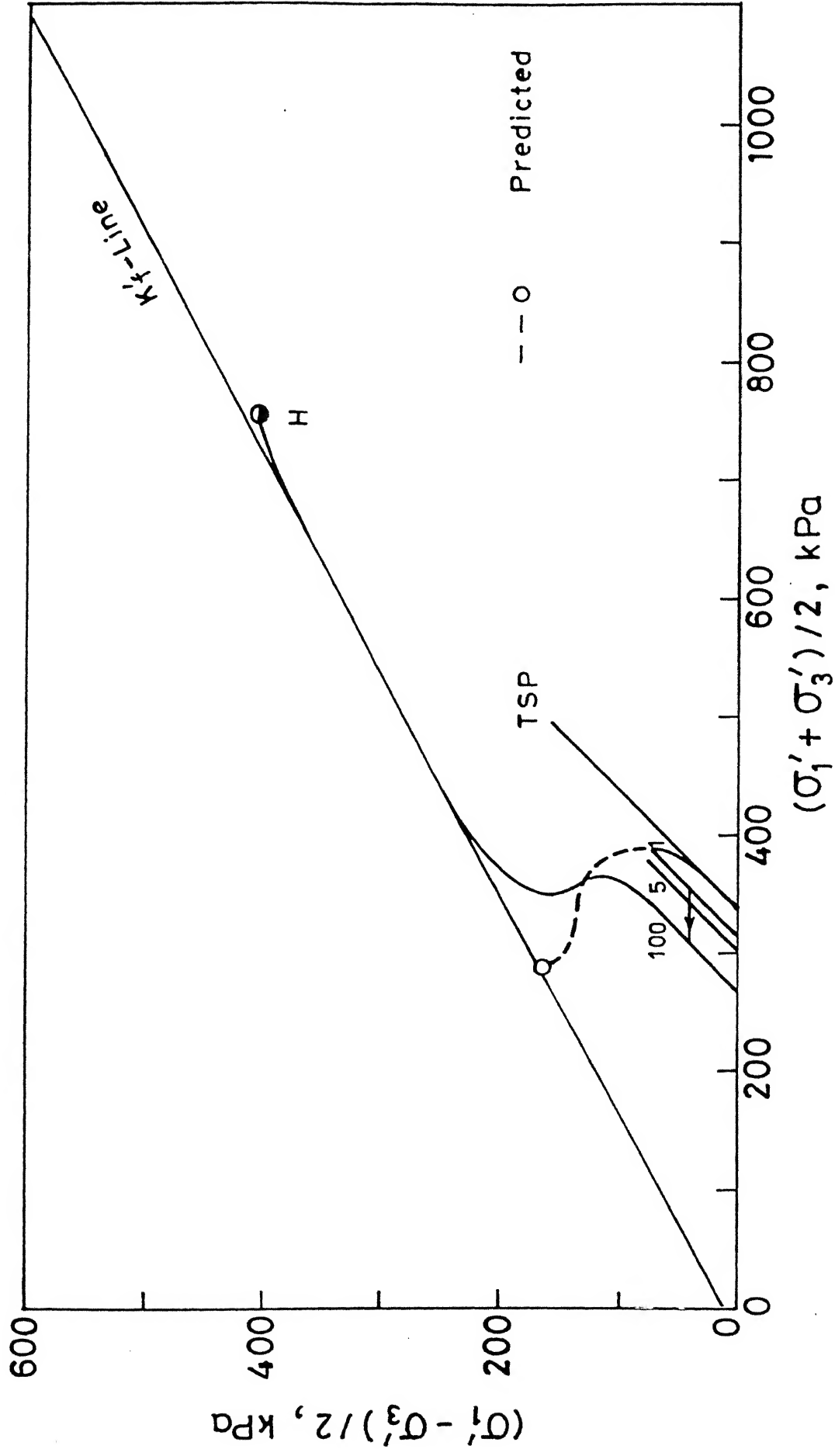


Fig. 4.39 Effective stress path for test with $R_f = 18.52\%$

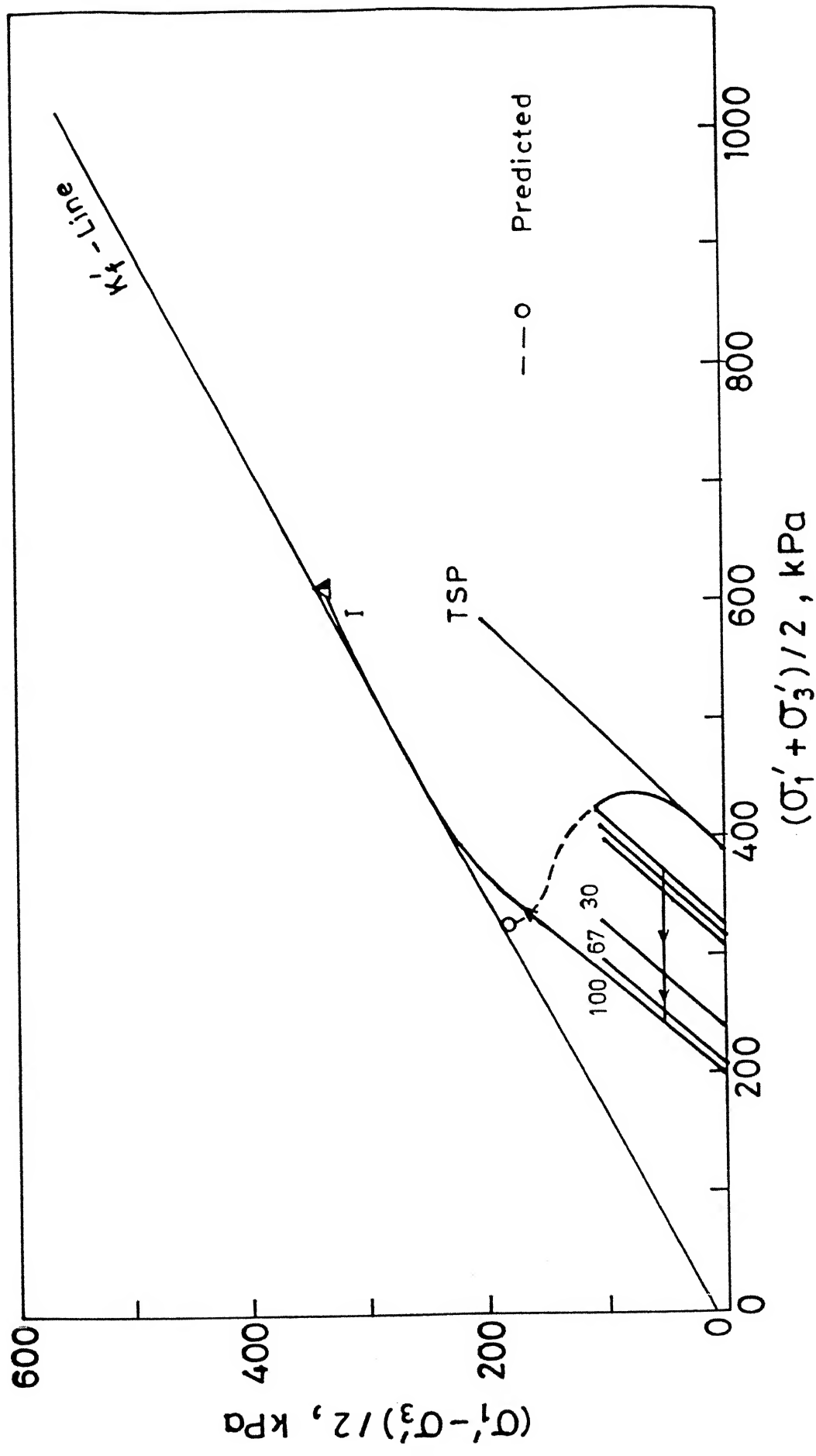


Fig. 4.40 Effective stress path for test with $R_f = 31.82\%$

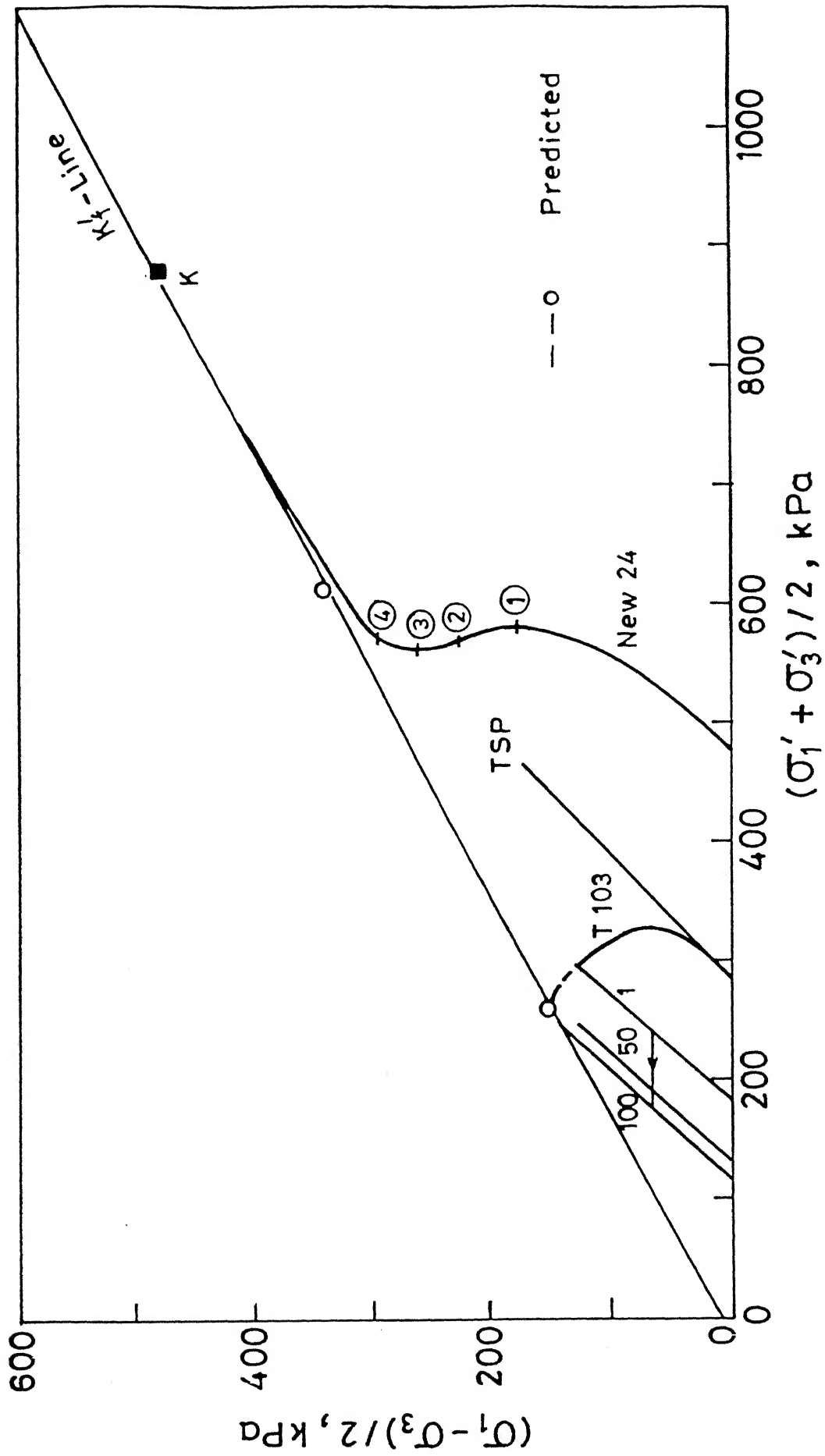


Fig.4.41 Effective stress path for test with $R_f = 37.68\%$

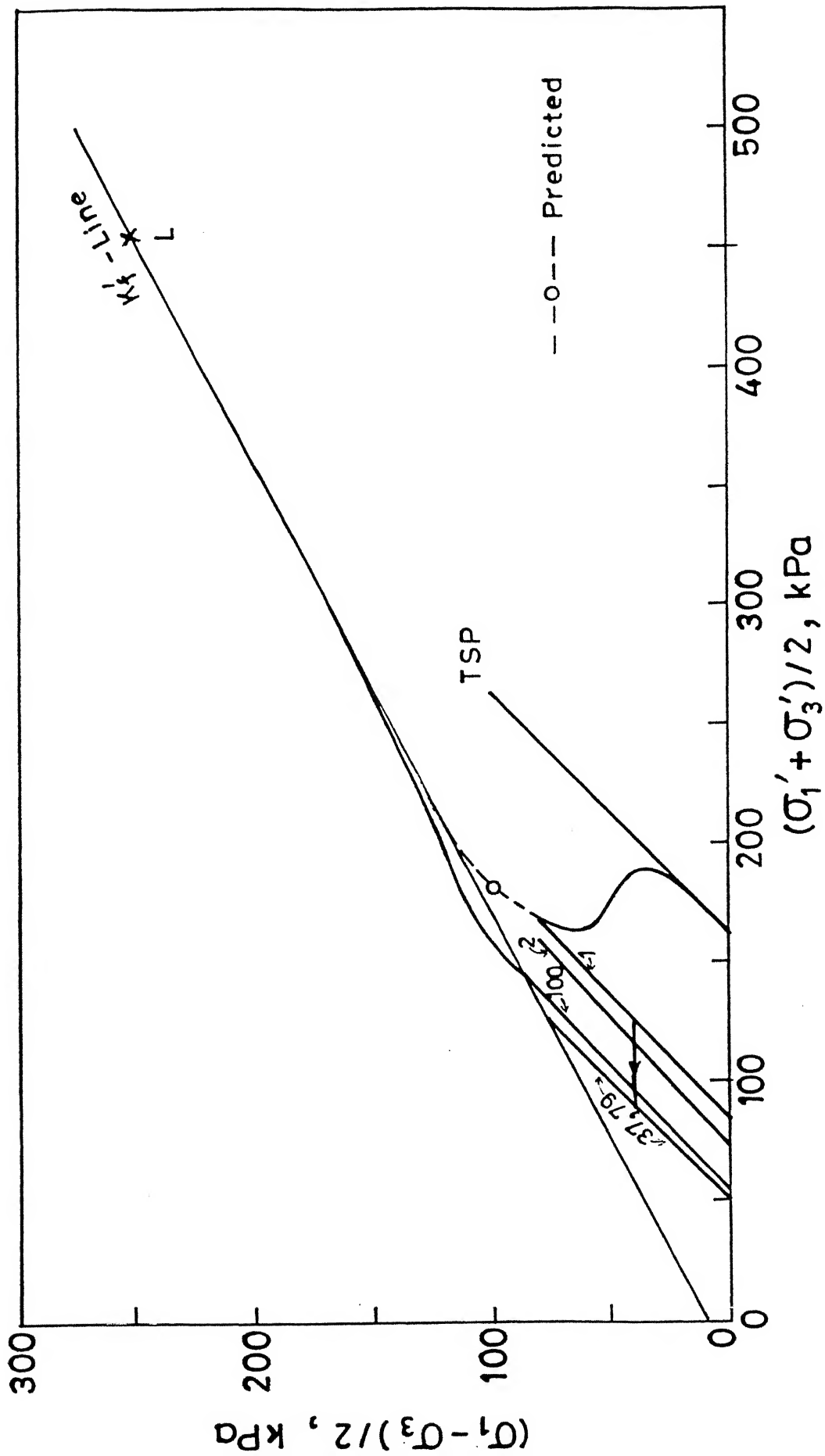


Fig. 4.42 Effective stress path for test with $R_f = 31.37\%$

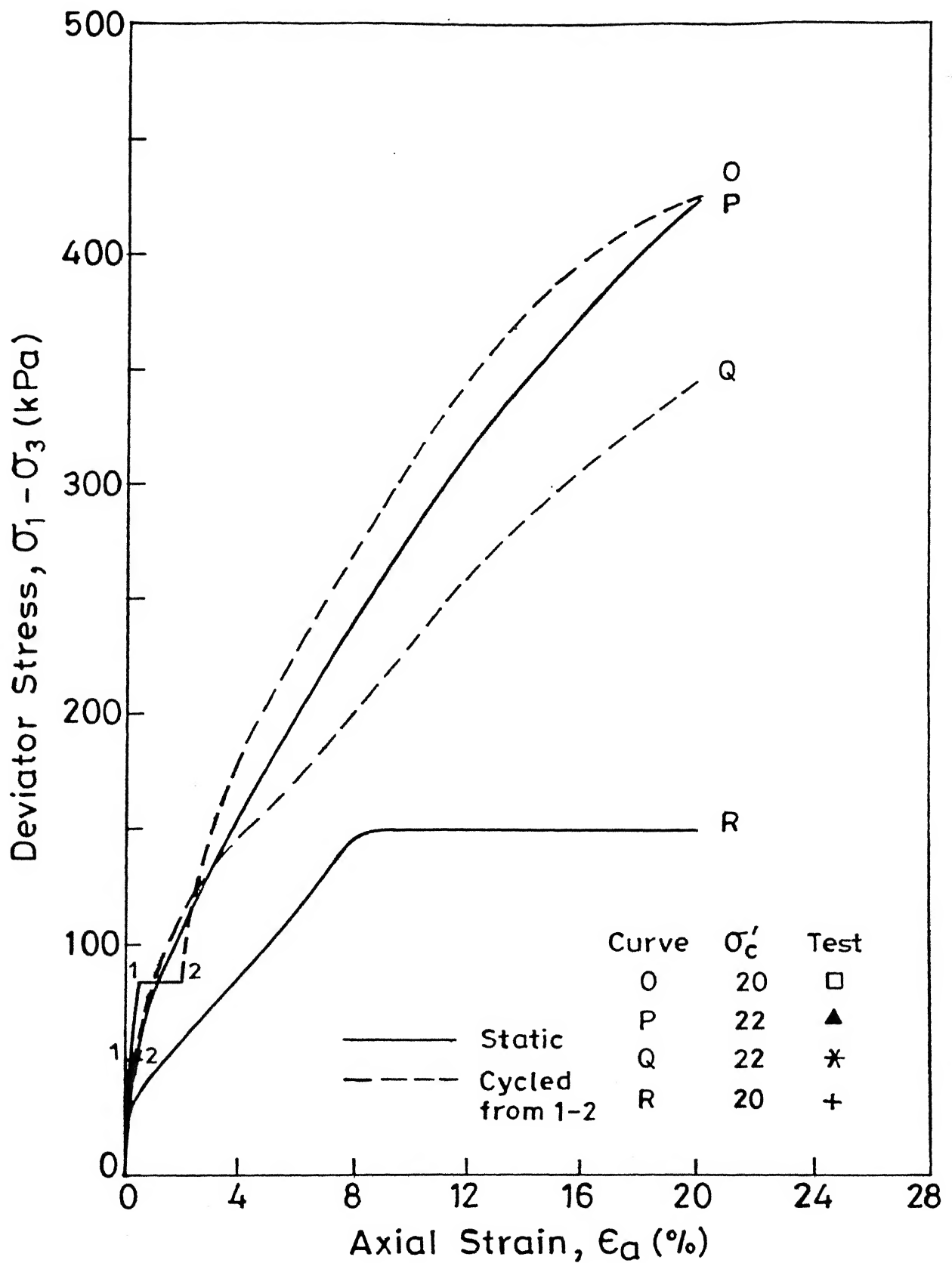


Fig.4.43 Stress-strain relation for tests with back saturation.

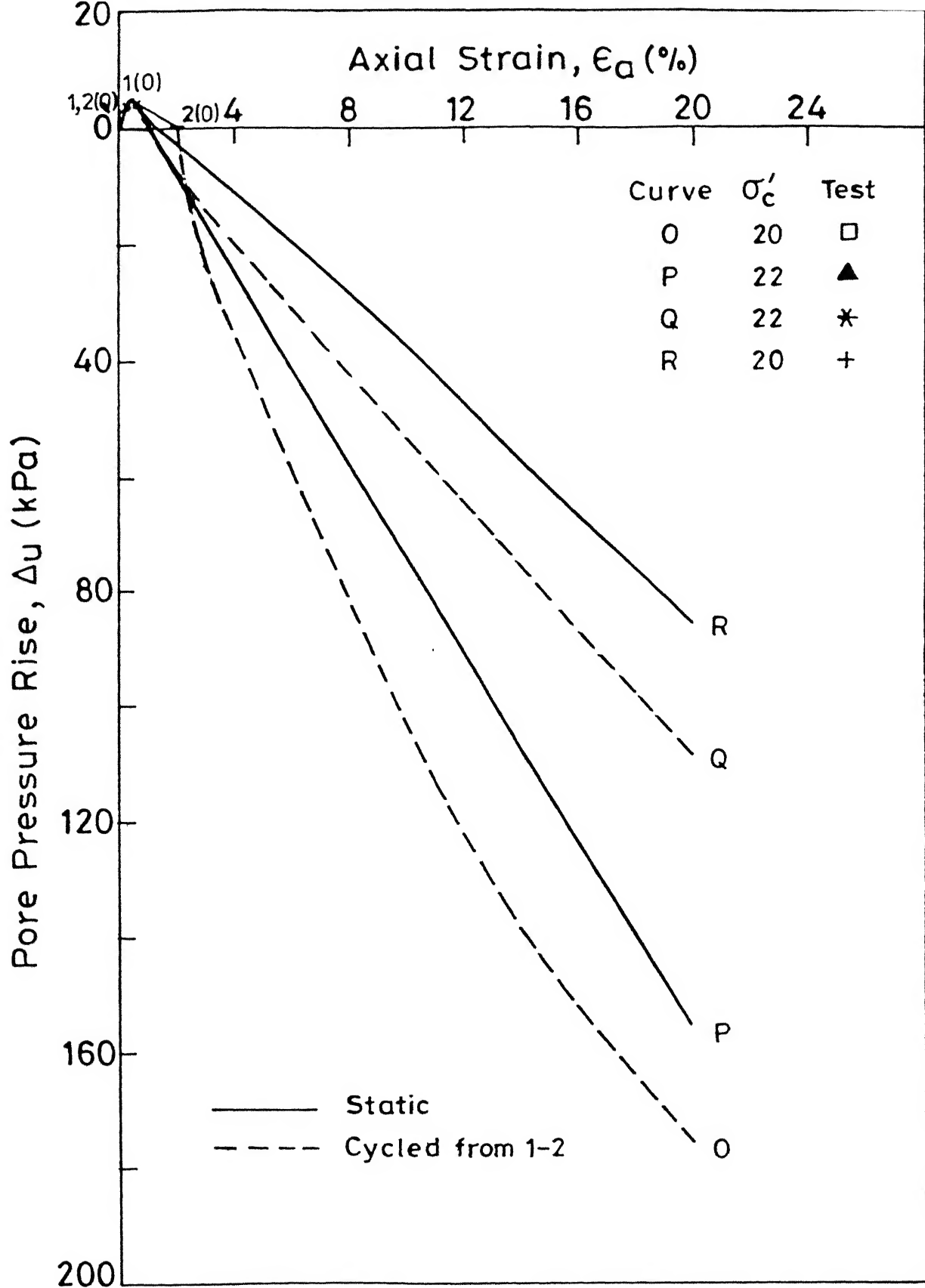


Fig. 4.44 Pore pressure - strain relation for tests with back saturation.

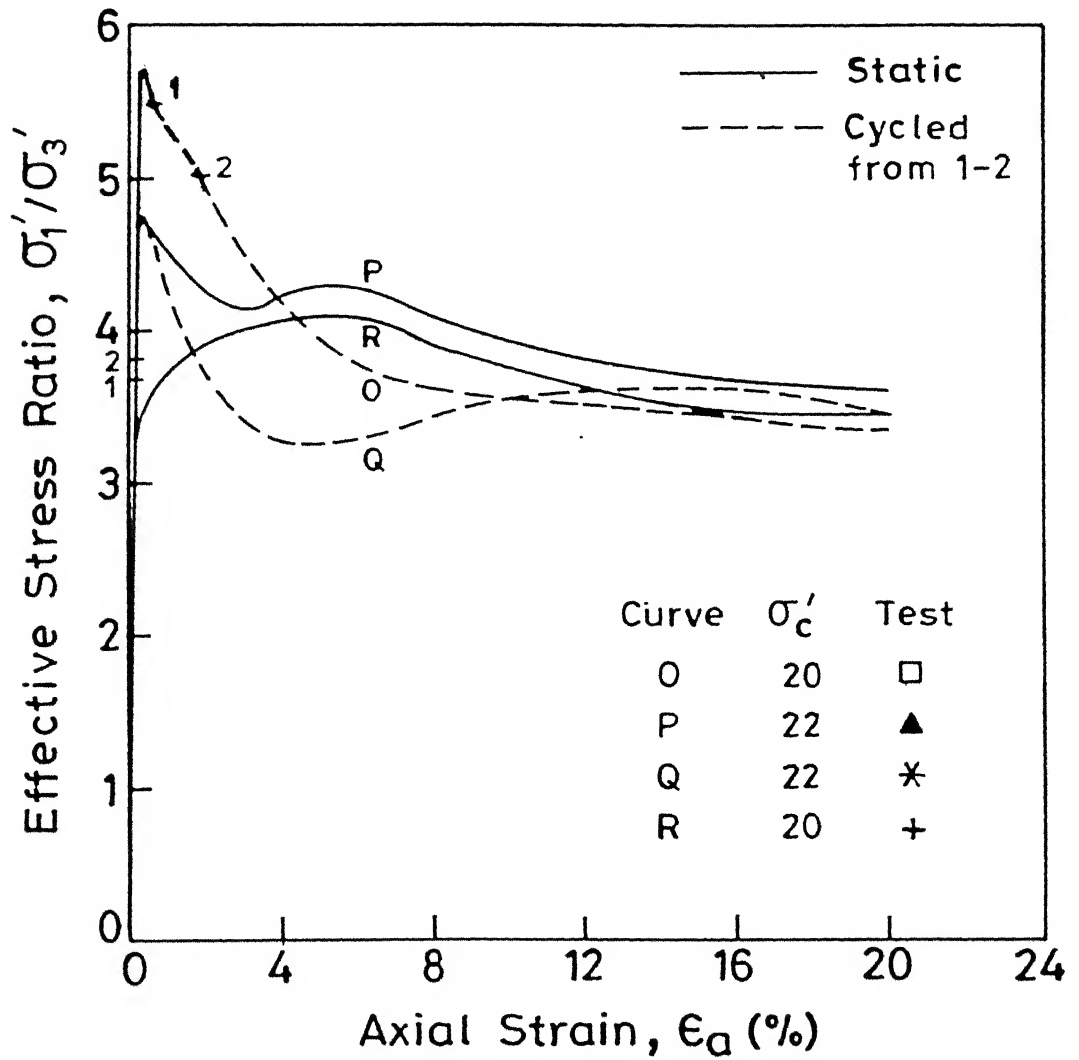


Fig. 4.45 Effective stress ratio-strain relation for tests with back saturation.

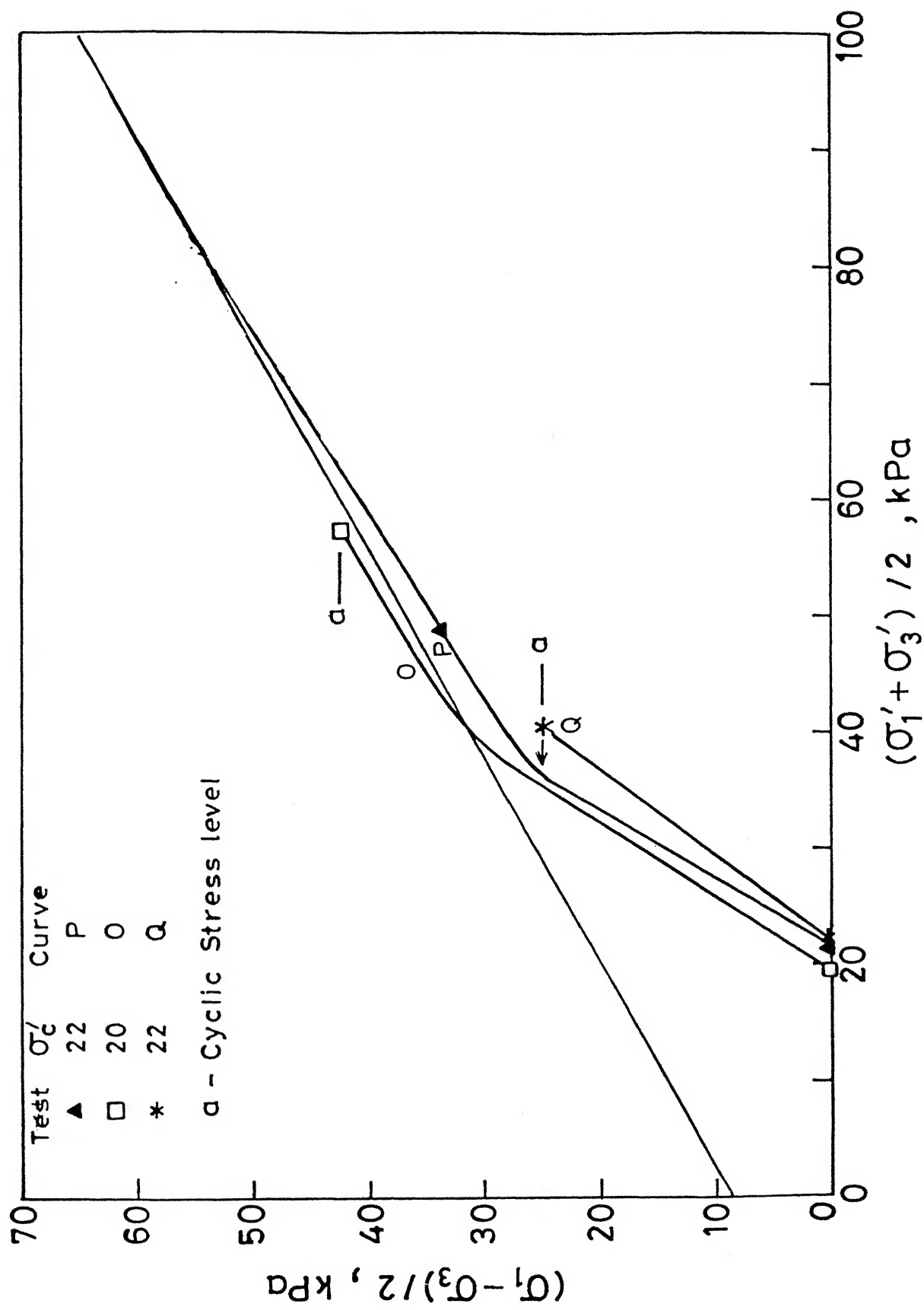


Fig. 4.46 Effective stress path for tests with back saturation.

Corresponding results for samples with $\sigma_c' = 40$ kPa are shown in Figs. 4.47 to 4.50. Test details are given in Table 4.7. These samples were compacted at optimum moisture content except for test shown as R (Fig. 4.43) which had a moulding water content 2.2 % higher than the optimum moisture content.

In general, the $(\sigma_1'/\sigma_3')_{\max}$ coincides with the occurrence of maximum positive pore pressure during the shear (see Figs. 4.44 and 4.45 for $\sigma_c' = 20-22$ kPa and Figs. 4.48 and 4.49 for $\sigma_c' = 40$ kPa). This may be contrasted with the test results for the series B1 and B2 where $(\sigma_1'/\sigma_3')_{\max}$ occurs at higher axial strain (approximately equal to 12 %) as compared to the development of maximum positive pore pressure at lower strain (approximately equal to 4 %).

The stress paths for these low σ_c' tests (Figs. 4.46 and 4.50) show highly dilatant response. A_f value varies from -0.37 for tests with $\sigma_c' = 20-22$ kPa to -0.32 for tests with $\sigma_c' = 40$ kPa. The corresponding values of A_f are -0.04, -0.06 and +0.05 for tests in series B1 at σ_c' values of 86, 150 and 452 kPa respectively. While the samples in series B3 were compacted at optimum moisture content and back saturated, the moulding water content (and the corresponding degree of saturation) for the tests with $\sigma_c' = 86, 150$ and 452 kPa was 15.89 % ($S = 95.5$ %), 15.27 % ($S = 95.1$ %) and 14.98 % ($S = 92.46$ %) respectively.

The stress level for applying the cyclic loading was fixed in the vicinity of the point of maximum positive pore pressure during undrained loading.

It is noted that the points of maximum (σ_1'/σ_3')

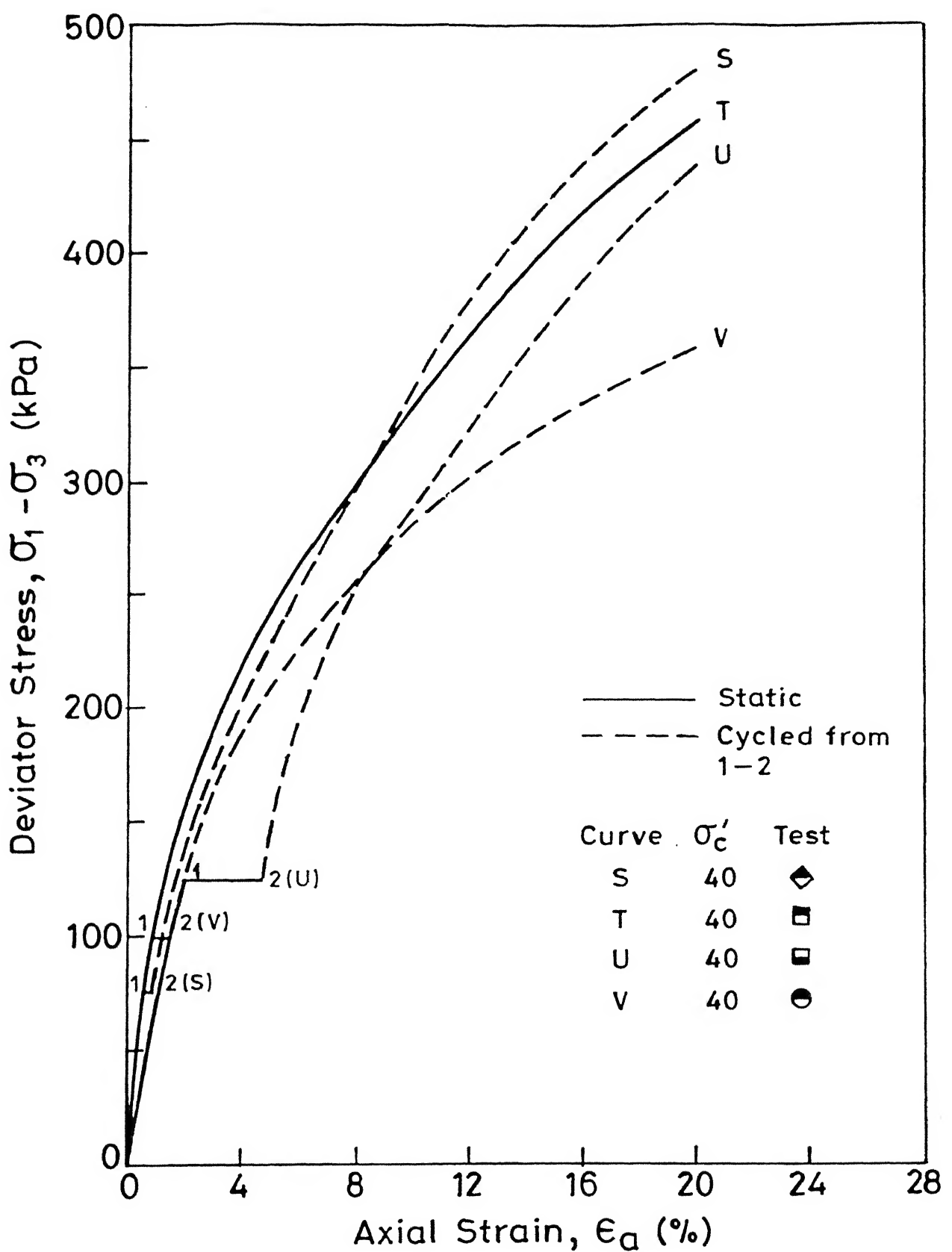


Fig. 4.47 Stress strain relation for tests with back saturation.

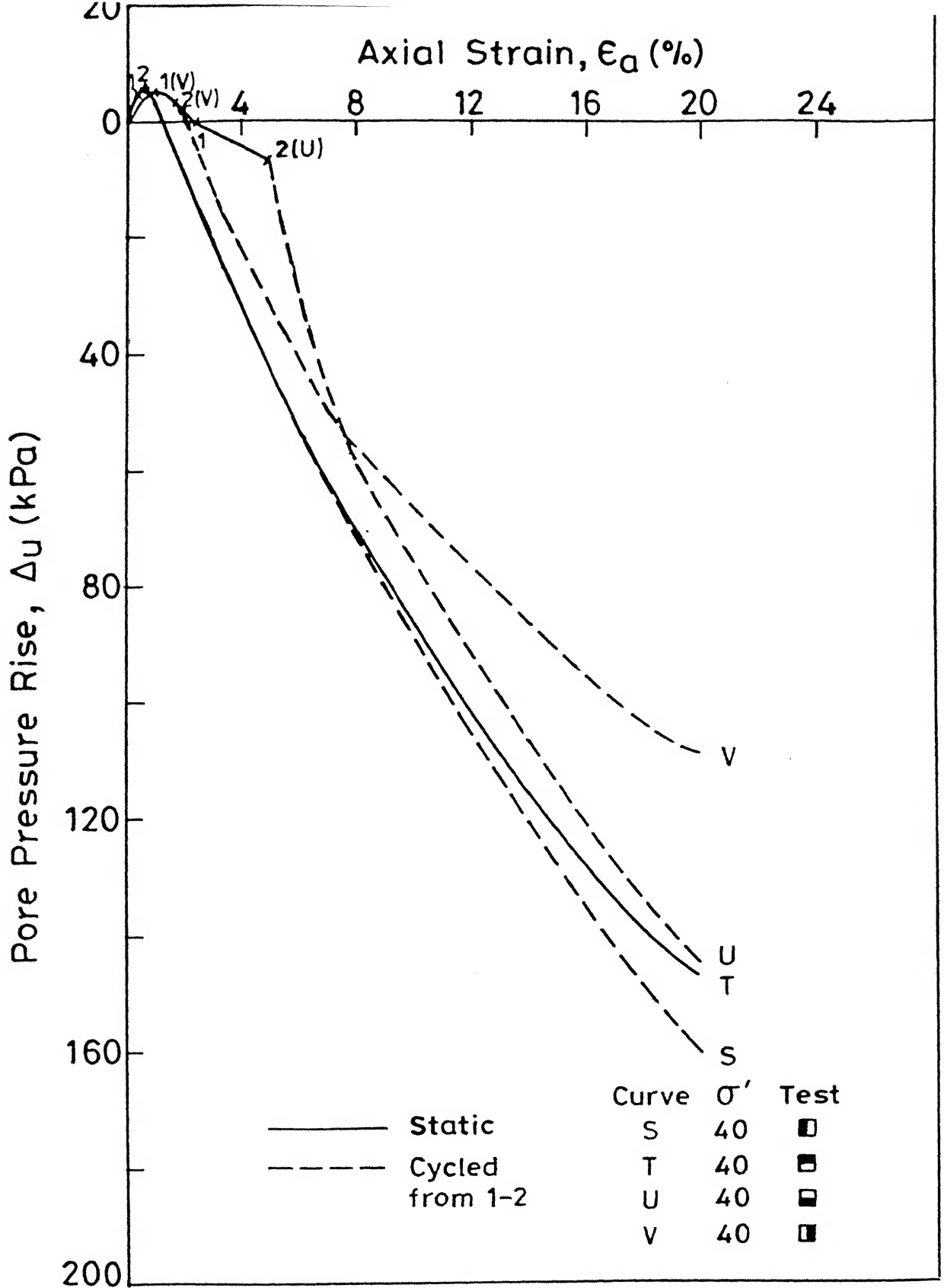


Fig.4.48 Pore pressure - strain relation for tests with back saturation.

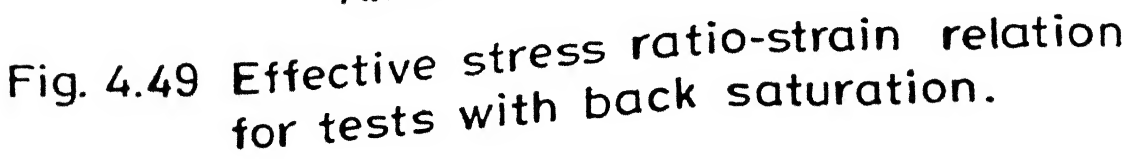


Fig. 4.49 Effective stress ratio-strain relation for tests with back saturation.

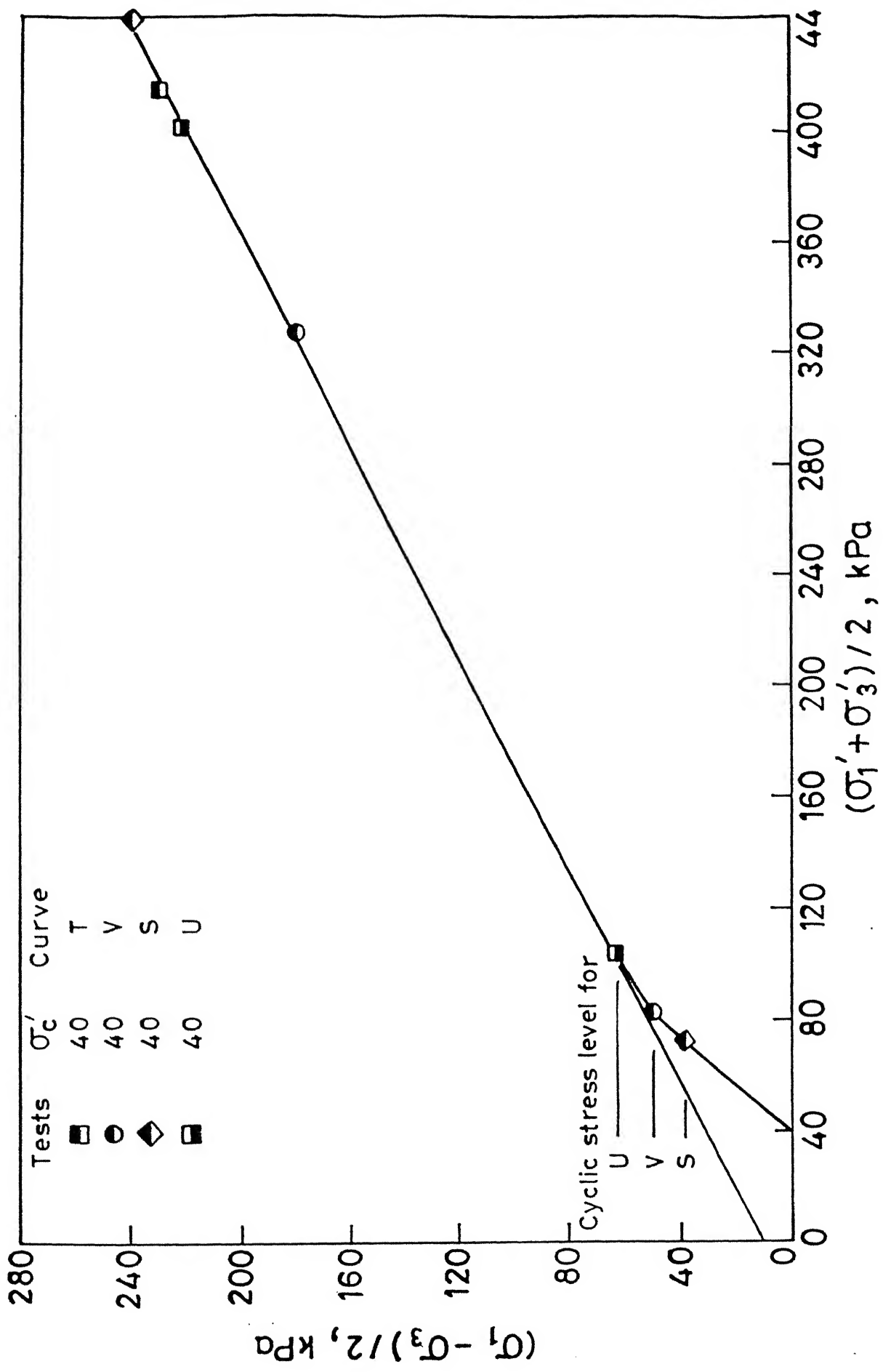


Fig. 4.50 Effective stress path for tests with back saturation.

approximately lie on the failure envelope obtained for tests conducted at higher values of σ_c' . The $(\sigma_1 - \sigma_3)_{\max}$ points for these tests also lie on the same failure envelope as shown later in Fig. 4.76 (also see Figs. 4.46 and 4.50).

The stress strain response with special emphasis on cyclic loading for tests with $\sigma_c' = 20-22$ kPa and 40 kPa is indicated in Figs. 4.51 and 4.52 respectively.

The pore pressure response during cyclic loading at these very low effective stresses was in the range of fluctuations of the measurements and as such is not given here. In case of tests with $\sigma_c' = 22$ kPa (see tests marked Q in Figs. 4.43 to 4.46), the sample showed increase in positive pore pressure during cyclic loading (about 1 kPa) whereas in case of test marked O in Figs. 4.43 to 4.46, the sample initially showed net small positive pore pressure followed by decrease in pore pressure with increasing number of cycles, the net decrease after 100 cycles was of the order of 4 kPa.

In case of tests with $\sigma_c' = 40$ kPa (tests marked S, U and V in Figs. 4.47 to 4.50), some positive increase in pore pressure during cycling was observed for the test marked S (about 1 kPa) whereas a net slight decrease (about 3 and 6 kPa) was observed in case of tests marked V and U after 100 cycles.

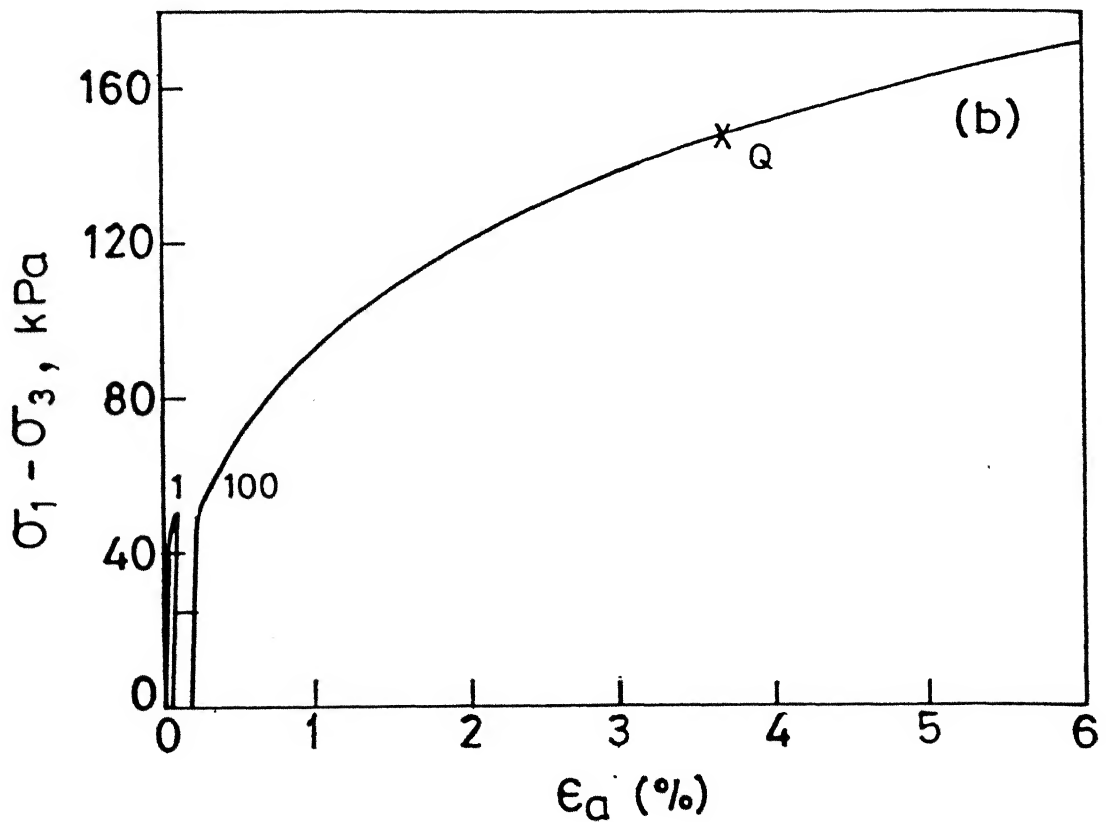
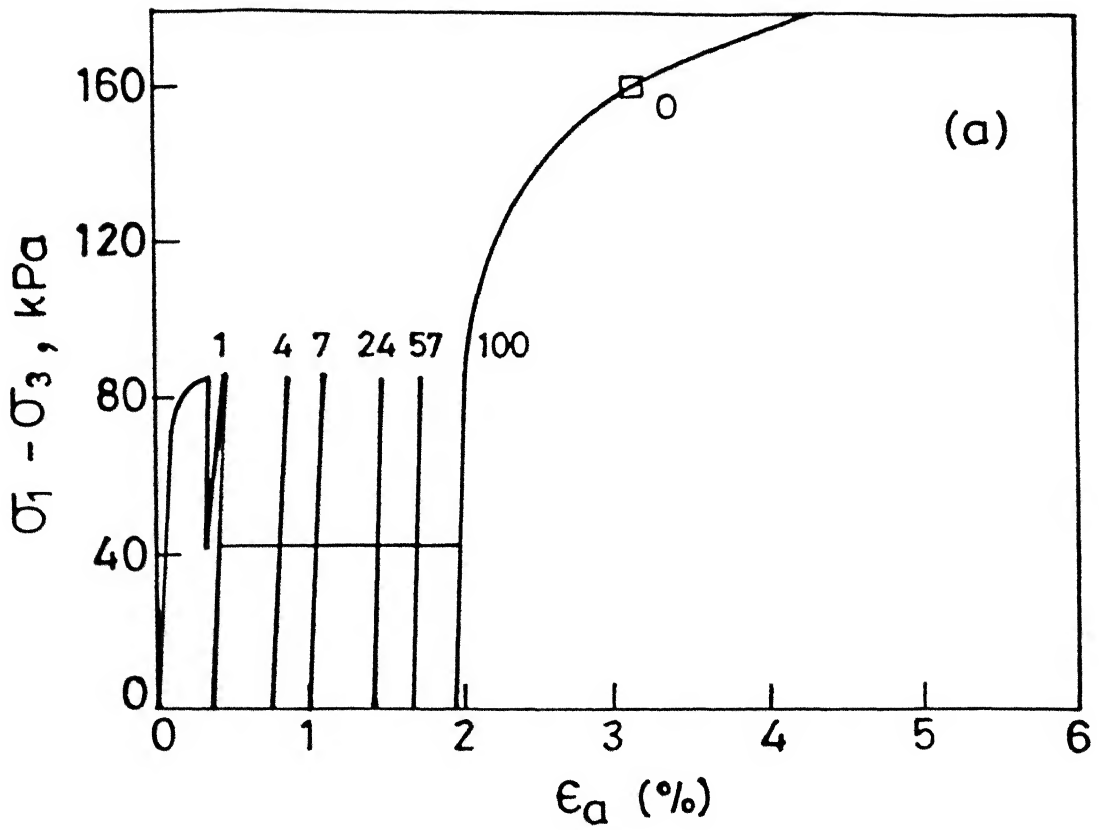


Fig. 4.51 Stress strain relation for tests with back saturation for (a) $R_f = 20.05\%$ (b) $R_f = 14.53\%$

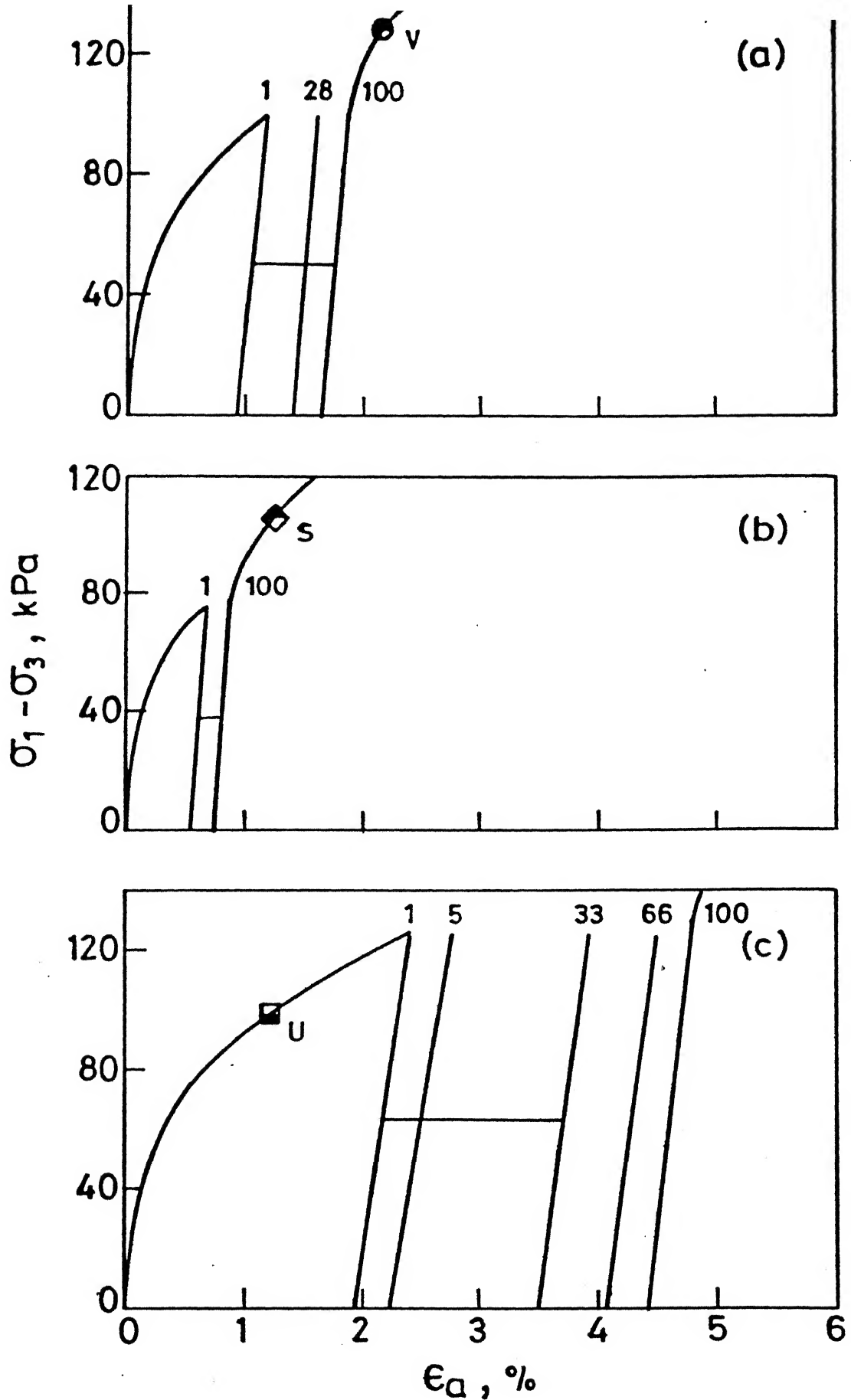


Fig. 4.52 Stress strain relation for tests with back saturation for (a) $R_f = 27.78\%$ (b) $R_f = 15.83\%$

4.8 INTERPRETATION AND DISCUSSION

4.8.1 Introduction

Interpretation and discussion of test results have been carried out under three sections viz. total stress behaviour (static and cyclic) ; effective stress behaviour for static tests ; and effective stress behaviour for cyclic load tests and evaluation of threshold stress. Total stress behaviour is described under unconfined and confined states. Unconfined behaviour is discussed under initially softened state (i.e softening without cyclic loading) referred to as equilibrium state vis-a-vis under softened state after cyclic loading at various values of R_f .

4.8.2 Total stress behaviour (static and cyclic)

4.8.2.1 Unconfined tests

As indicated earlier, these tests were designed following Bishop and Henkel (1953) to simulate the conditions experienced by soil under railway tracks at very low confining stress level under undrained loading conditions. Softening was to simulate the dissipation of cumulative pore pressures induced due to cyclic loading. Furthermore, the difficulties of pore pressure measurement were attempted to be overcome by examining the changes in water content during softening after cyclic loading.

Finally, changes in soil stiffness and strength following the cyclic loading for both softened and unsoftened states were examined.

Increase in water content, Δw , from initial state (for both equilibrium state and softened state tests) with the stress level (R_f) at which cyclic loading was conducted, is indicated in Fig. 4.53.

Bishop and Henkel (1953) presented data for water absorption by undisturbed over consolidated clay after transient undrained loading. Results in Fig. 4.54 tend to suggest that cumulative negative pore pressures during cyclic loading which would lead to water absorption during softening stage of compacted soil (compacted at optimum moisture content), increase with increasing values of R_f . The expected decrease in strength subsequent to absorption of water by compacted samples is indicated in Fig. 4.55. The effect of R_f value before softening is presented in Fig. 4.56.

In the absence of pore pressure data, development of plastic strains during cyclic loading before softening would be indirectly indicative of the negative pore water pressures developed in the sample. Figure 4.57 shows the relationship between incremental plastic strain, $\delta \epsilon_p$ after 100 cycles and the corresponding incremental increase in water content on softening. Such correlations, if developed on undisturbed samples for a subgrade soil under a track would offer a simple methodology to predict expected changes in water content due to cyclic loading on the basis of incremental plastic strain data

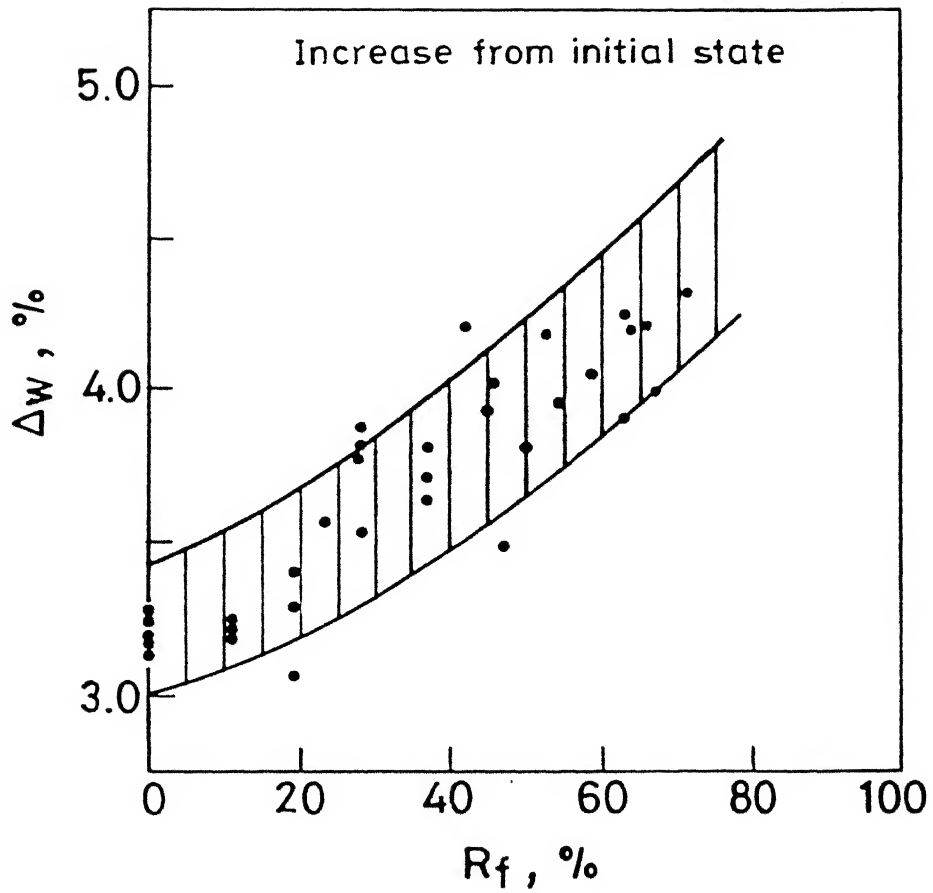


Fig. 4.53 Increase in water content from initial state with R_f .

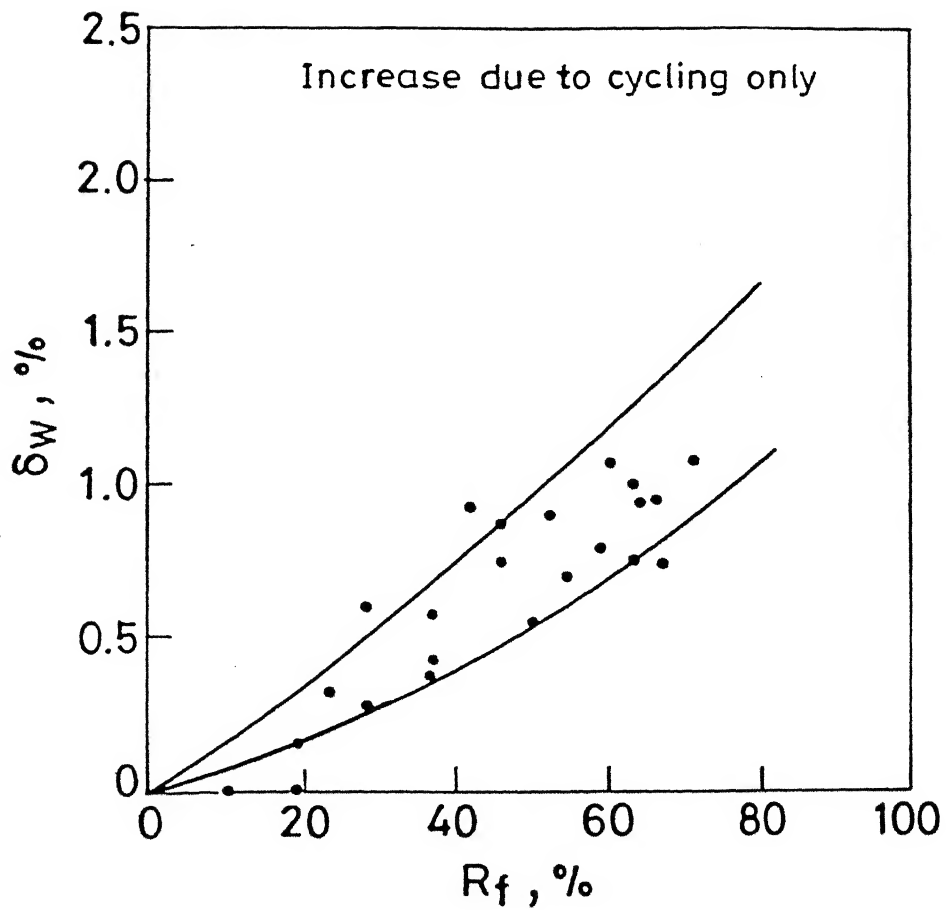


Fig. 4.54 Increase in water content due to cyclic loading with R_f .

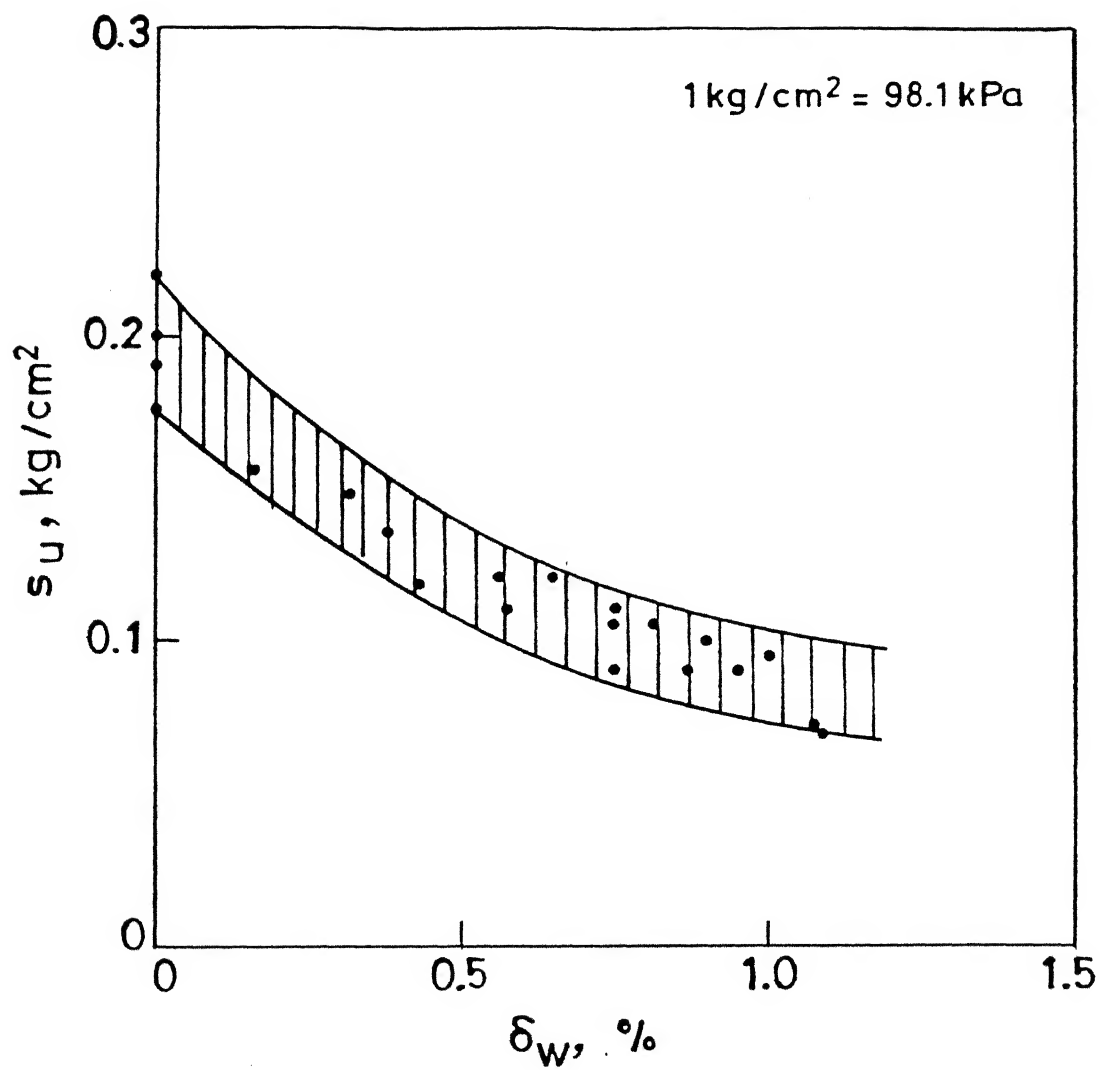


Fig. 4.55 Variation of s_u with δ_w .

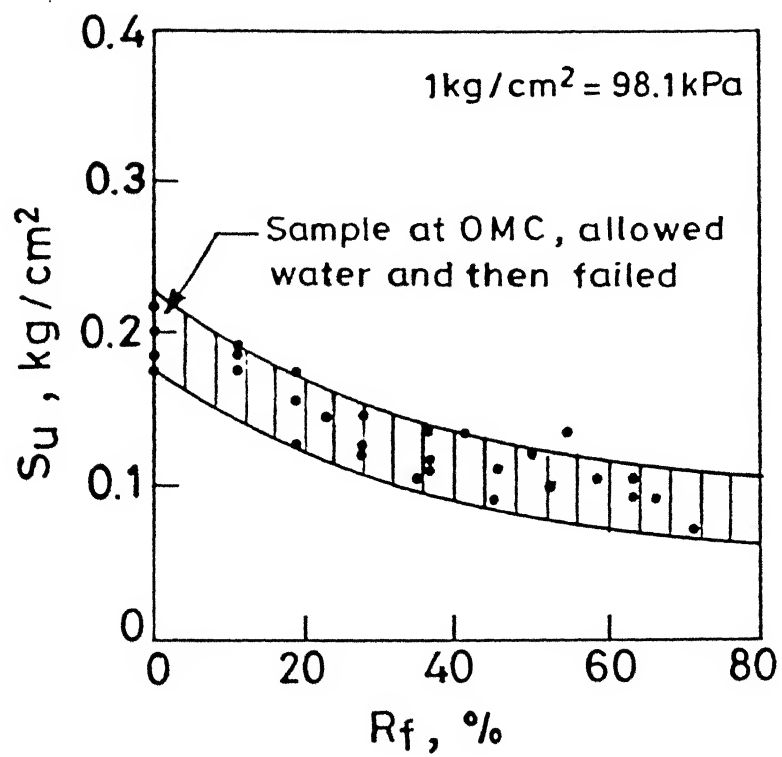


Fig. 4.56 Variation of s_u with R_f .

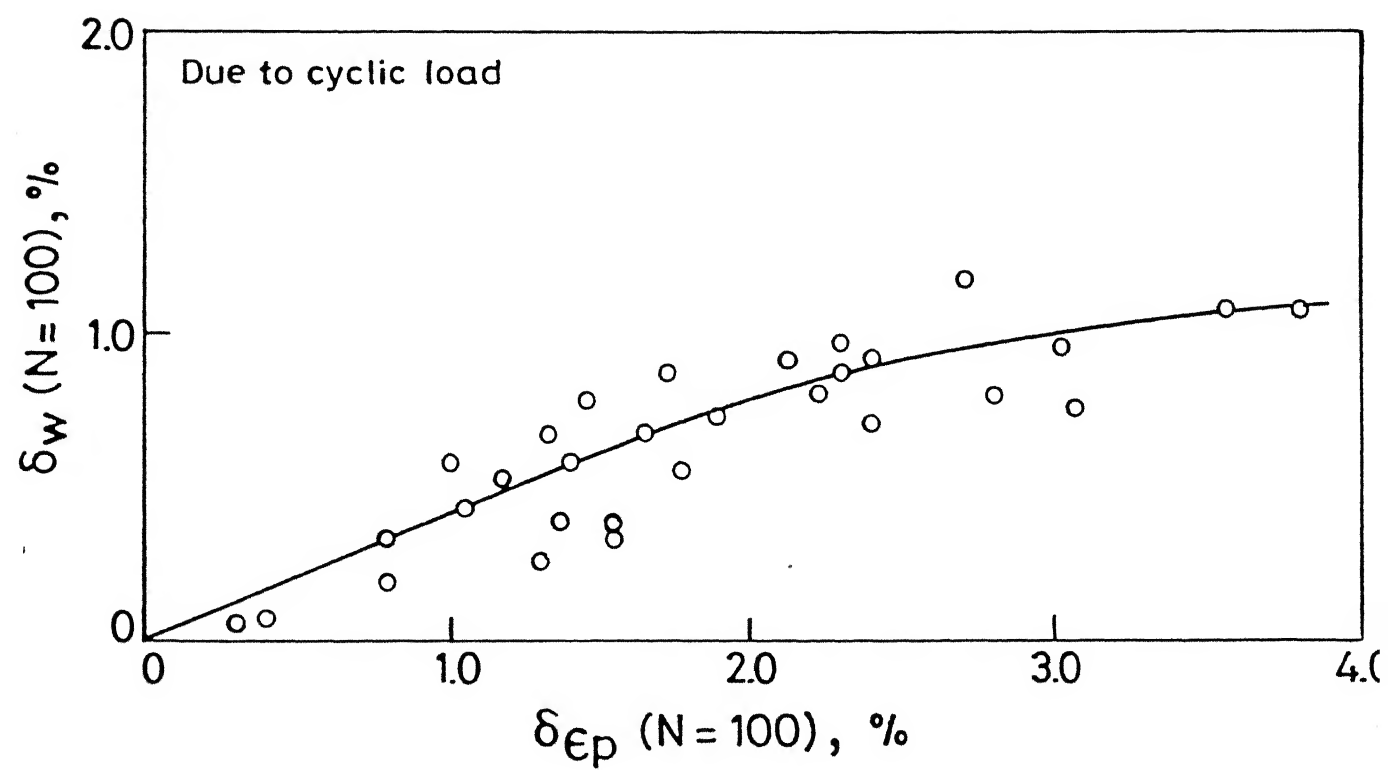


Fig. 4.57 Variation of plastic strain with δ_w .

obtained from total stress unconfined tests. The predicted change in water content could then be used to estimate the changes in undrained strength from relationship of the type shown in Fig. 4.55.

In addition to these changes in water content and undrained strength, soil samples subjected to undrained cyclic loading undergo changes in stiffness. Figure 4.58 shows the stress - strain response of compacted samples with and without cyclic loading ($N = 100$) at different R_f values. Up to certain value of R_f , the slope of the stress - strain curve (E value) increases after which no more stiffening takes place (Fig. 4.59) as a result of cyclic loading. Figure 4.59 shows reduction in E value for softened state. This reduction in the stiffness value on softening is the well known effect of reduction in effective stress [for example, see Andersen et al. (1976), Andersen et al. (1980) for soft clays subjected to cyclic undrained loading]. Figure 4.58 also suggests that the value of failure stress is practically independent of the cyclic history of the sample. Figure 4.60 compares the stress - strain response of softened samples (with and without cyclic loading) with the as compacted behaviour.

The variation of E value with water content under all the states investigated is depicted in Figs. 4.61 and 4.62. The significant influence of water content on the E value is well illustrated and underscores the importance of changes in water content produced due to softening after cyclic loading especially when water is freely available due to poor drainage

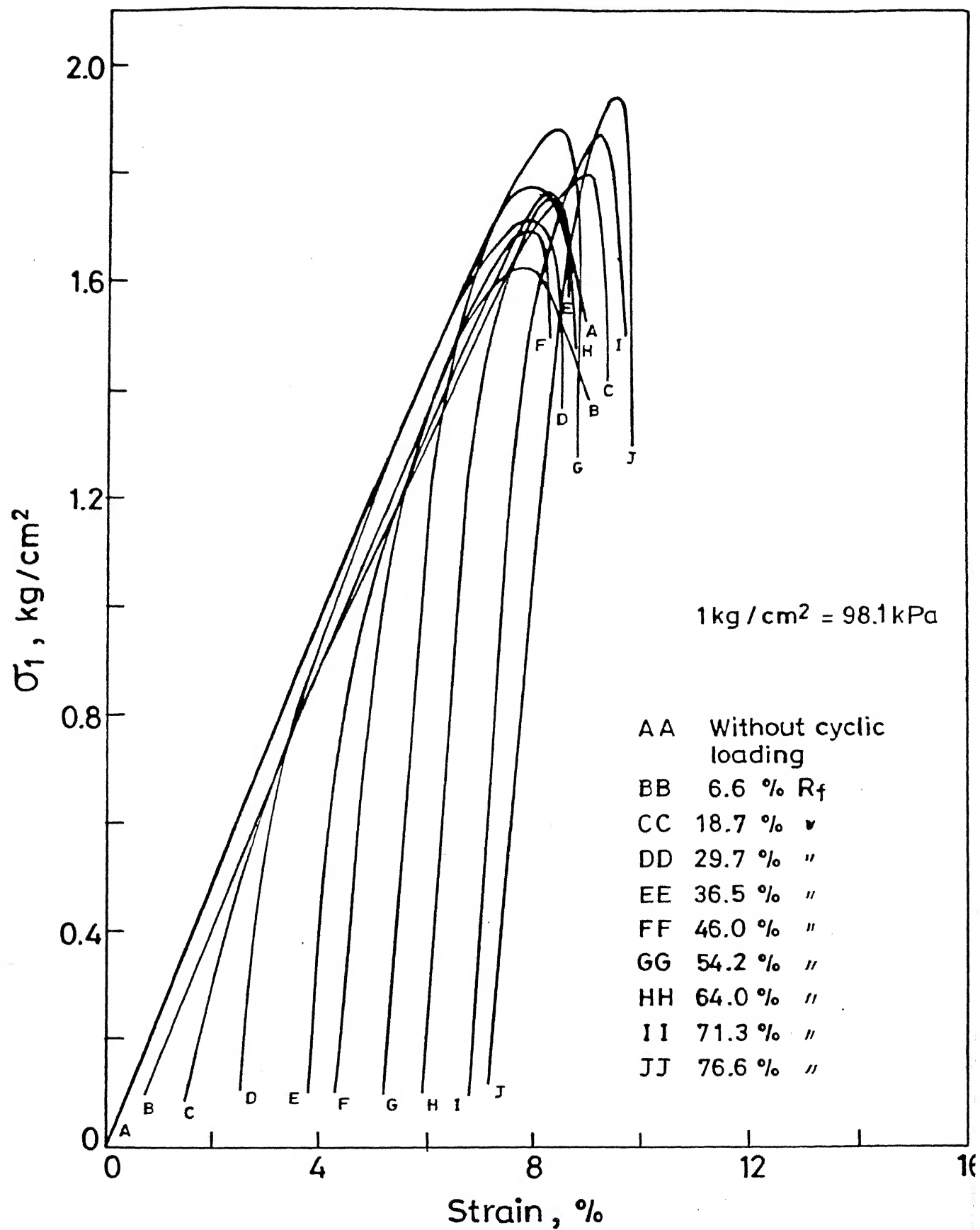


Fig. 4.58 Stress-strain relation for all unconfined

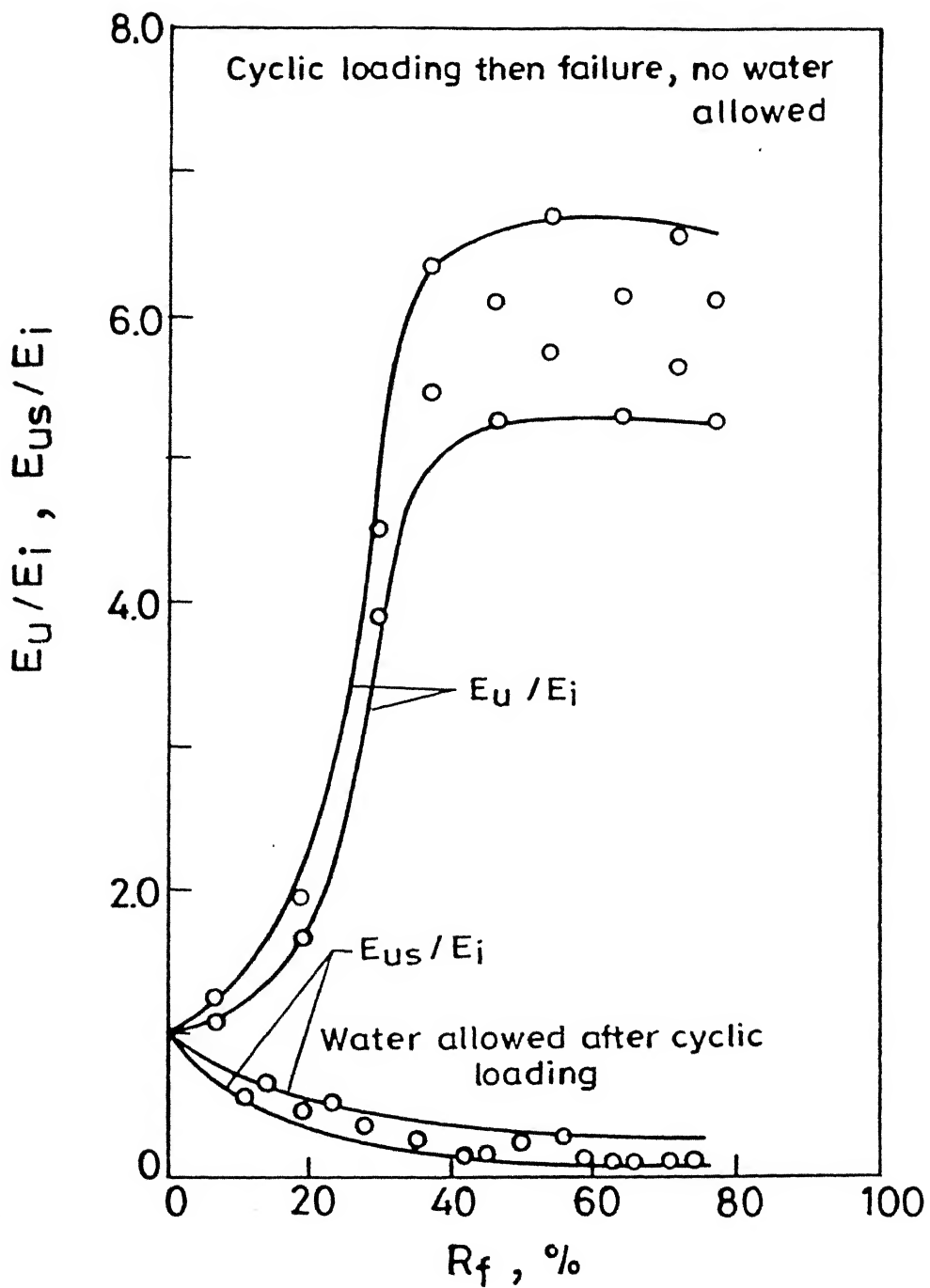


Fig. 4.59 Variation of E_U/E_i and E_{US}/E_i with R_f .

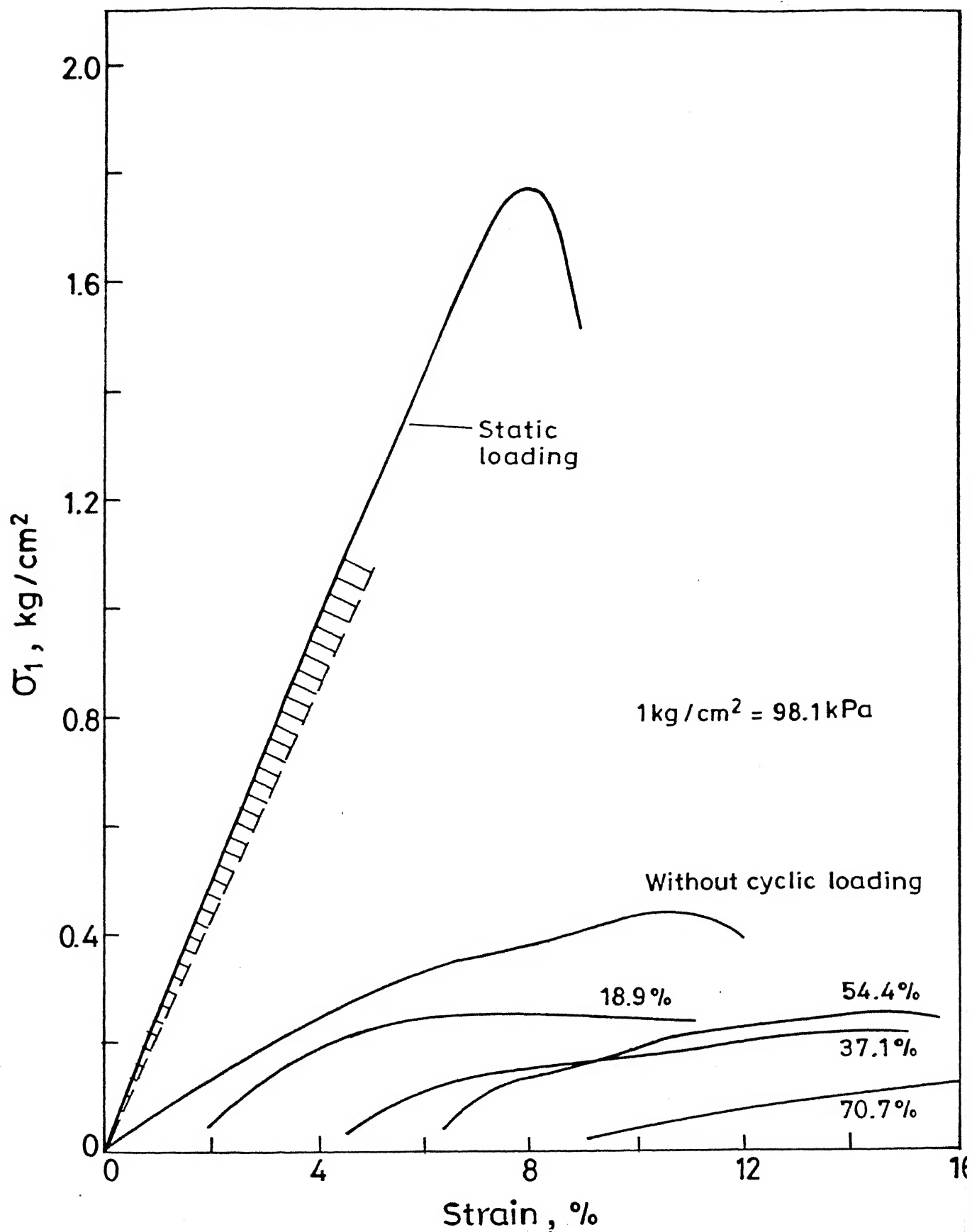


Fig. 4.60 Stress-strain relation for all unconfined softened tests.

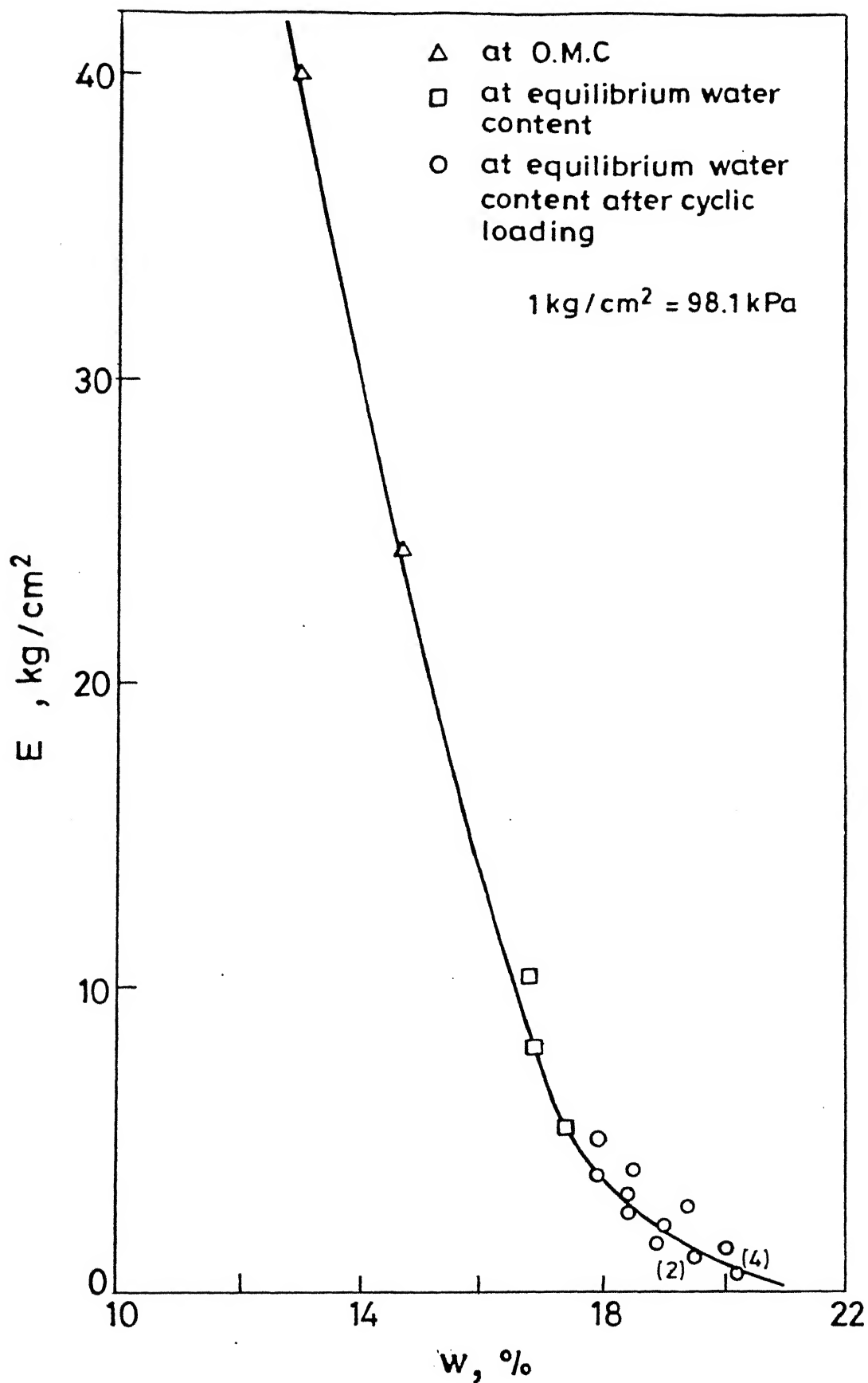


Fig. 4.61 Variation of Young's Modulus with water content.

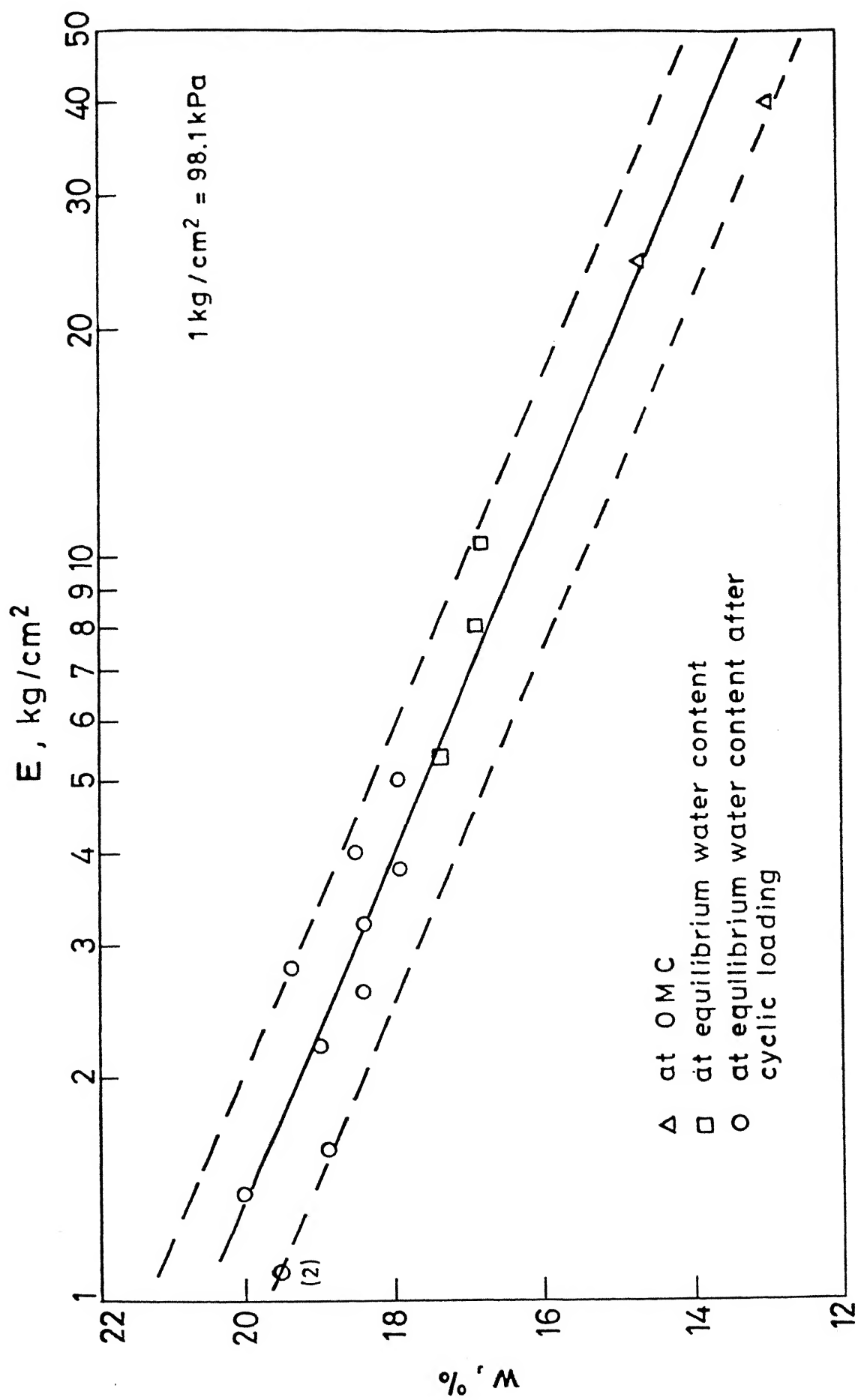


Fig. 4.62 Variation of $\log(E)$ with water content.

of the subgrade. Figure 4.63 displays the corresponding changes in strength with water content. These results are similar to the data presented by Bishop and Henkel (1953). Once again, the sensitivity of undrained shear strength of such a silty soil to the changes in water content is well brought out. These significant degradations in both strength and stiffness of compacted samples on softening following the transient loading are the clear explanation of the mud pumping problems encountered by the Indian railways under the tracks in such soil deposits also.

4.8.2.2 Confined tests

Even though the foundation problems under railway tracks fall in the category of very low effective confining stress soil behaviour, the known changes in response of partially saturated soils with increasing confining pressure need to be investigated.

Results of tests relevant to low confining stress (0 - 100 kPa) behaviour are compared in Fig. 4.64. Marked changes in degree of brittleness with increase in confining stress are noticed for these compacted samples. The changes in failure stress with increasing confining stress for samples compacted at different moulding water content are depicted in Fig. 4.65. The inset gives details at very low confining stress level. These results are similar to the behaviour of compacted partially saturated soils [Casagrande and Hirschfeld (1960), Casagrande and Poulos (1964) and Yudhbir and Korchoke (1987)].

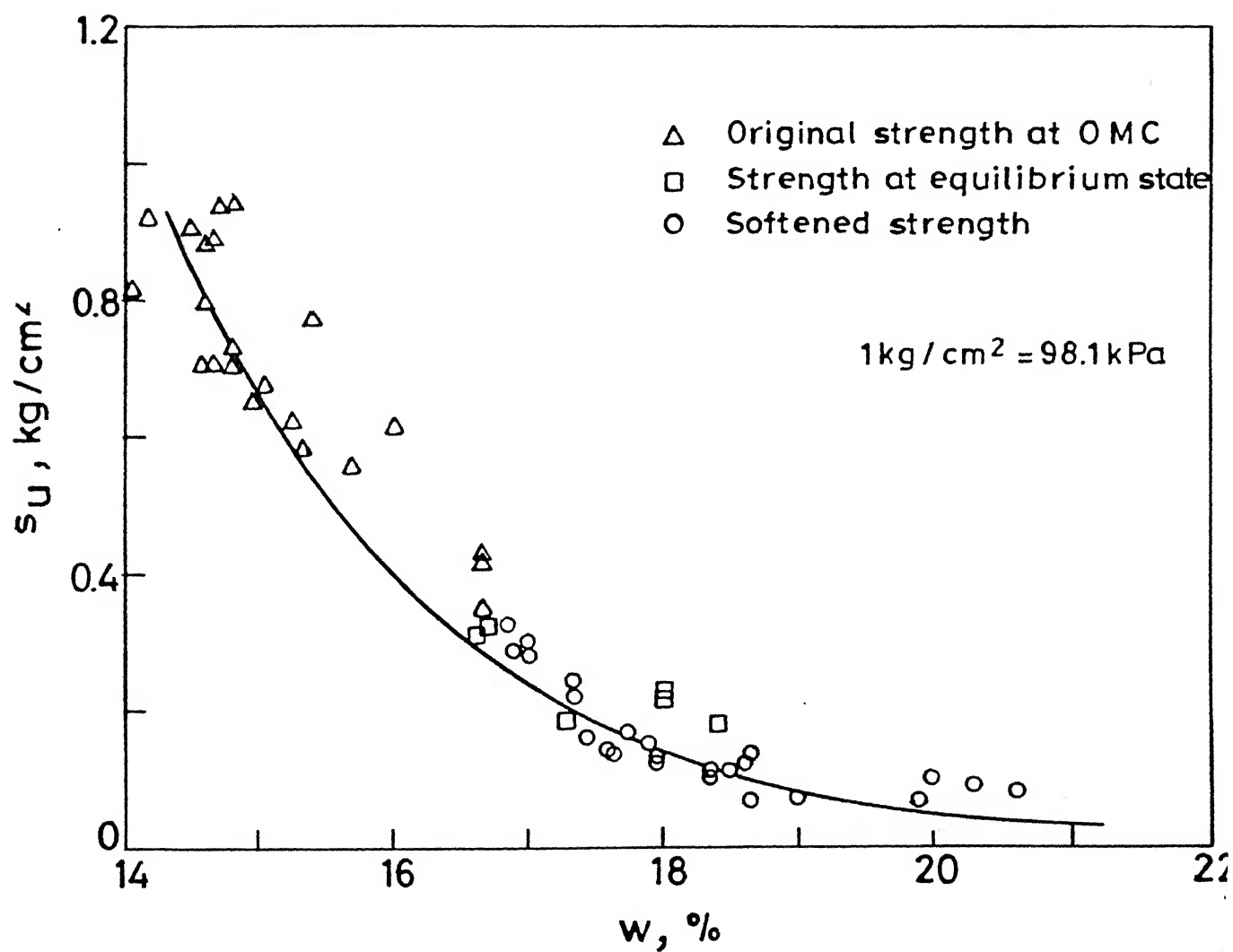


Fig. 4.63 Variation of s_u with water content.

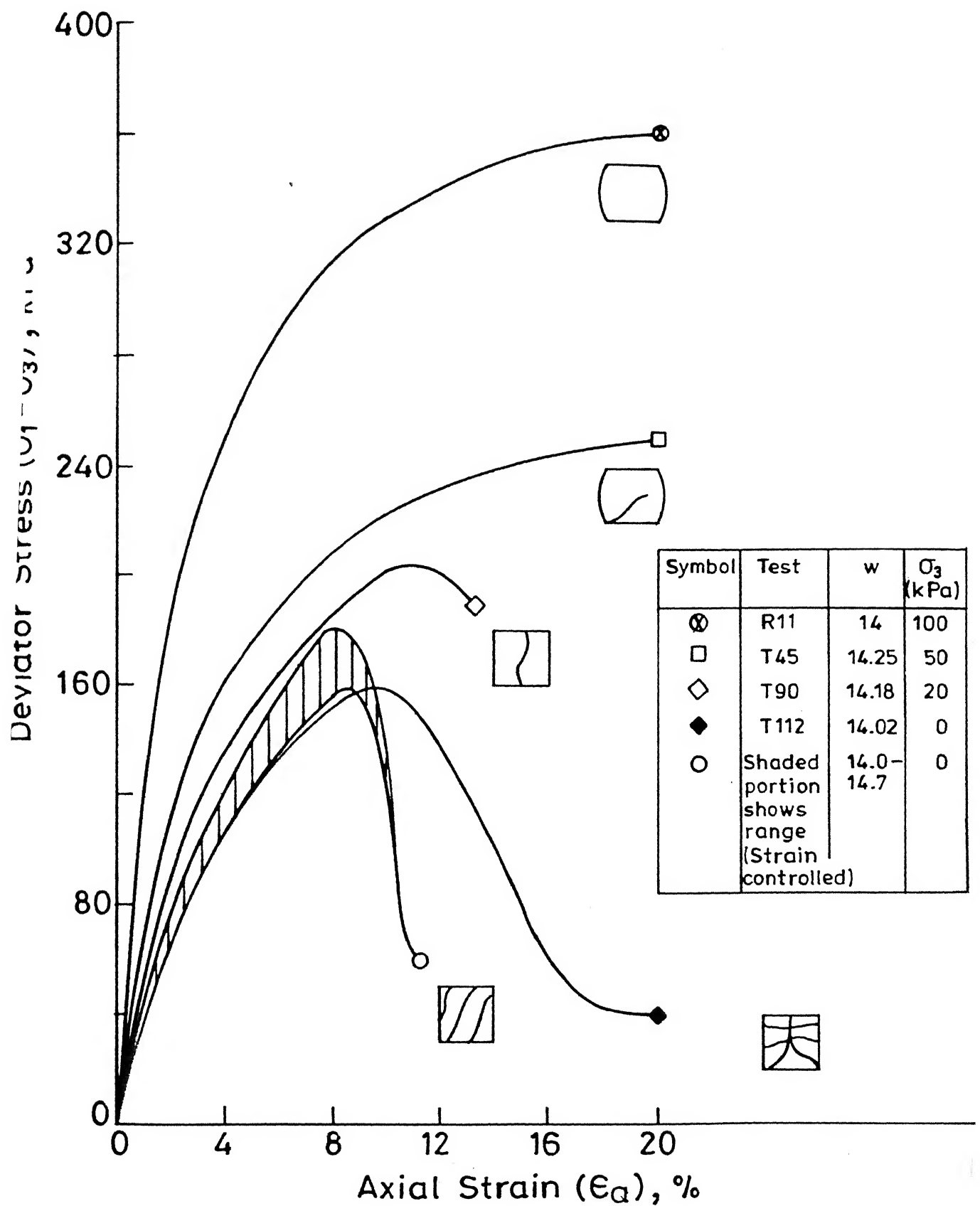


Fig. 4.64 Effect of confining pressure on stress-strain behaviour.

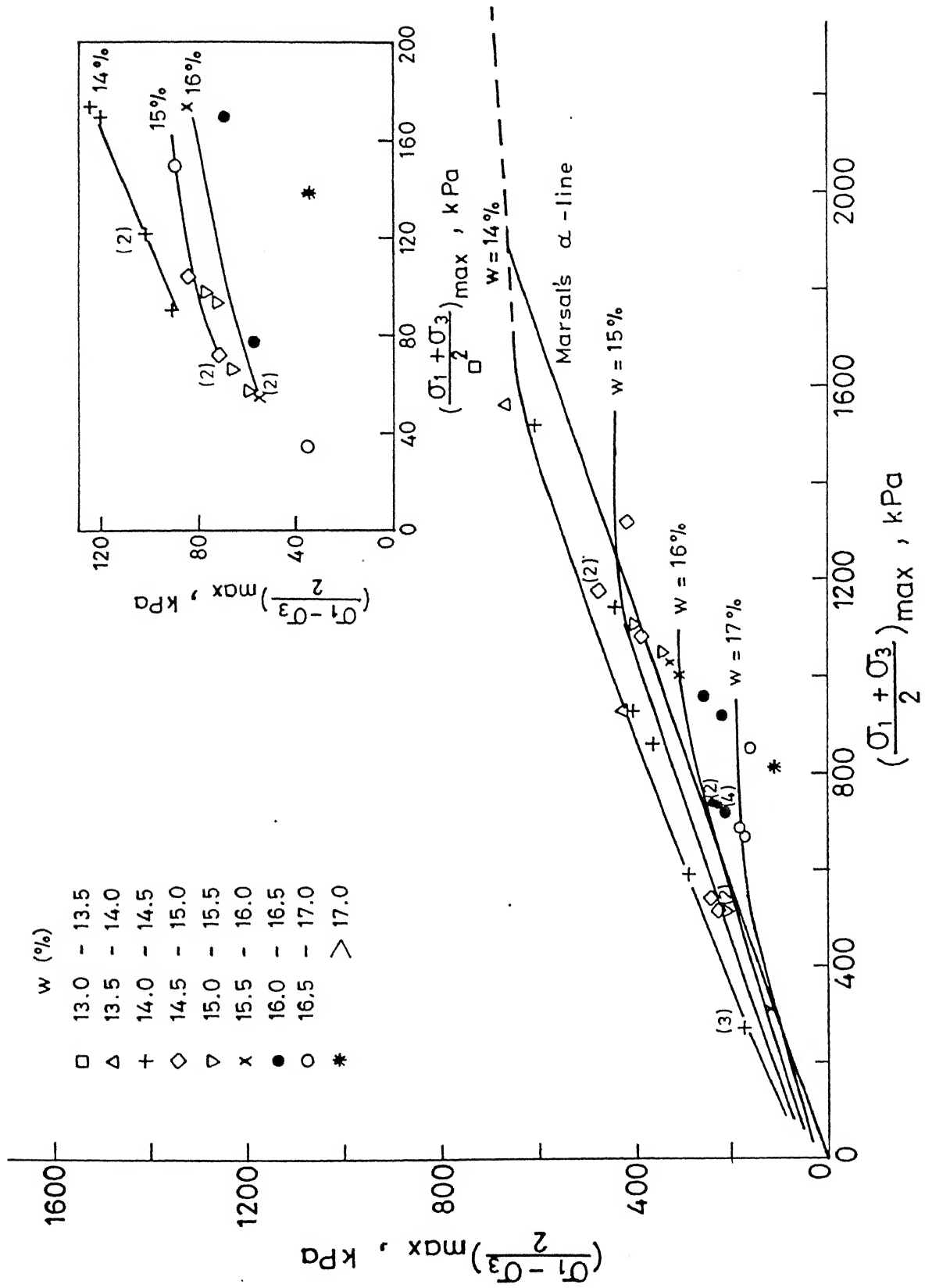


Fig. 4.65 Total stress failure envelopes.

4.8.3. Effective stress behaviour for static tests

4.8.3.1 Quasi saturated behaviour

As indicated in Sec. 4.6.4.1 in relation to testing technique for partially saturated soils, the procedure of Marsal to investigate effective stress behaviour by improving the degree of saturation at elevated cell pressure was adopted. The main argument in favour of measuring pore water pressures only in such tests is based on the premise that if the water voids are continuous then the pore pressure measurements are reliable. Before interpreting the effective stress data for test series B1 and B2, it would be desirable to examine the status of continuity of water voids in these tests.

Figure 4.66(a) presents the variation of pore pressure parameter, $B = \Delta u / \Delta \sigma_3$ (also see Fig. 4.22) with degree of saturation for all the samples with varying values of confining pressure. It will be seen that after a certain degree of saturation, the B value increases significantly with either the increase in cell pressure or water content (for the same cell pressure). For $S < 0.94$, change in B value with σ_3 does not appear to follow any trend, and for $S < 0.9$, samples compacted at optimum moisture content, OMC give the same response almost up to $\sigma_3 = 900$ kPa with B approximately equal to 0.2. Based on this limited data, it is suggested that for $S > 0.94$, $w = \text{OMC} + 1\%$, $B \geq 0.5$, the sample exhibits quasi saturated behaviour [(Cruz et al (1985))] and the water voids are continuous.

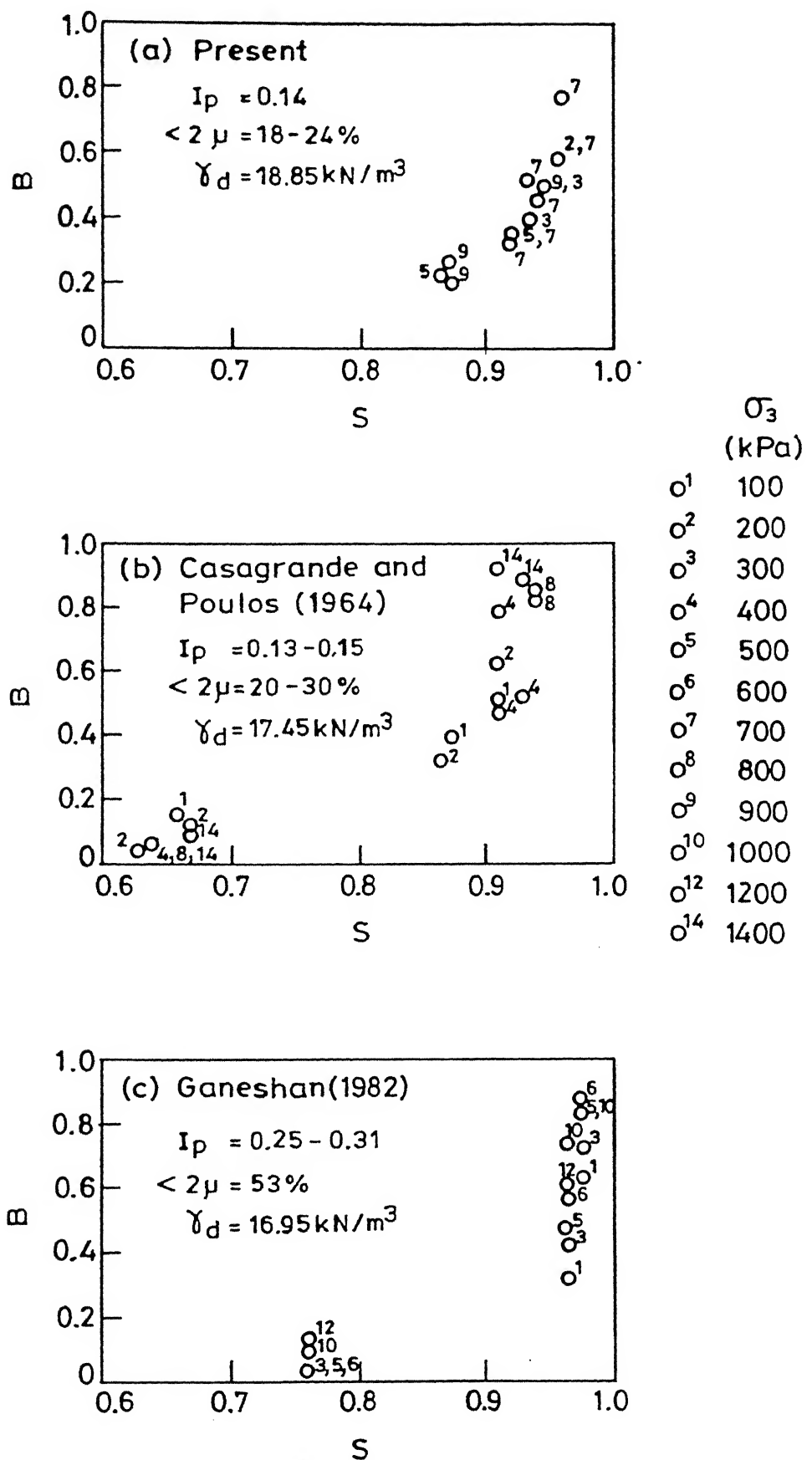


Fig. 4.66 Variation of B with S for (a) Campus silt (b) Canyon dam clay (c) Chiew Larn clay.

Consequently, For $S < 0.94$, the pore water pressure measurements may not be highly reliable especially for samples with $S < 0.9$.

Data for Canyon dam clay [Casagrande and Poulos (1964)] and Chiew Larn dam clay [Ganeshan (1982)] is also presented in Figs. 4.66(b) and (c). Similar trends can also be observed for these materials where data is available over a wider range of S values.

Canyon dam clay is practically similar to the Campus silt used in the present study (see Fig. 4.1 for particle size distribution, Fig. 4.2 for Atterberg limits and Fig. 4.3 for compaction characteristics). Not only are the physical and compaction characteristics comparable for these two materials, their pore pressure response with increasing cell pressure under undrained loading (Fig. 4.22), stress - strain and pore pressure - strain behaviour during undrained shear of samples compacted dry of optimum [OMC - 1.0 %, Fig. 4.67(a)] and wet of optimum [OMC + 2.0% , Fig. 4.67(b)] with comparable σ_3 values, and peak failure envelope (Fig. 4.68) show remarkable similarities. Because of such strong similarities, Canyon dam clay data has been used to compare out test results as discussed in later section. As shown in Fig. 4.66(b), Canyon dam clay having γ_d values less than for Campus silt, the quasi saturated behaviour during undrained shear is observed for $S > 0.9$ and $B \geq 0.5$. The water voids are continuous for $S > 0.9$ ($w = \text{OMC} + 1\%$) and consequently pore water pressure response of

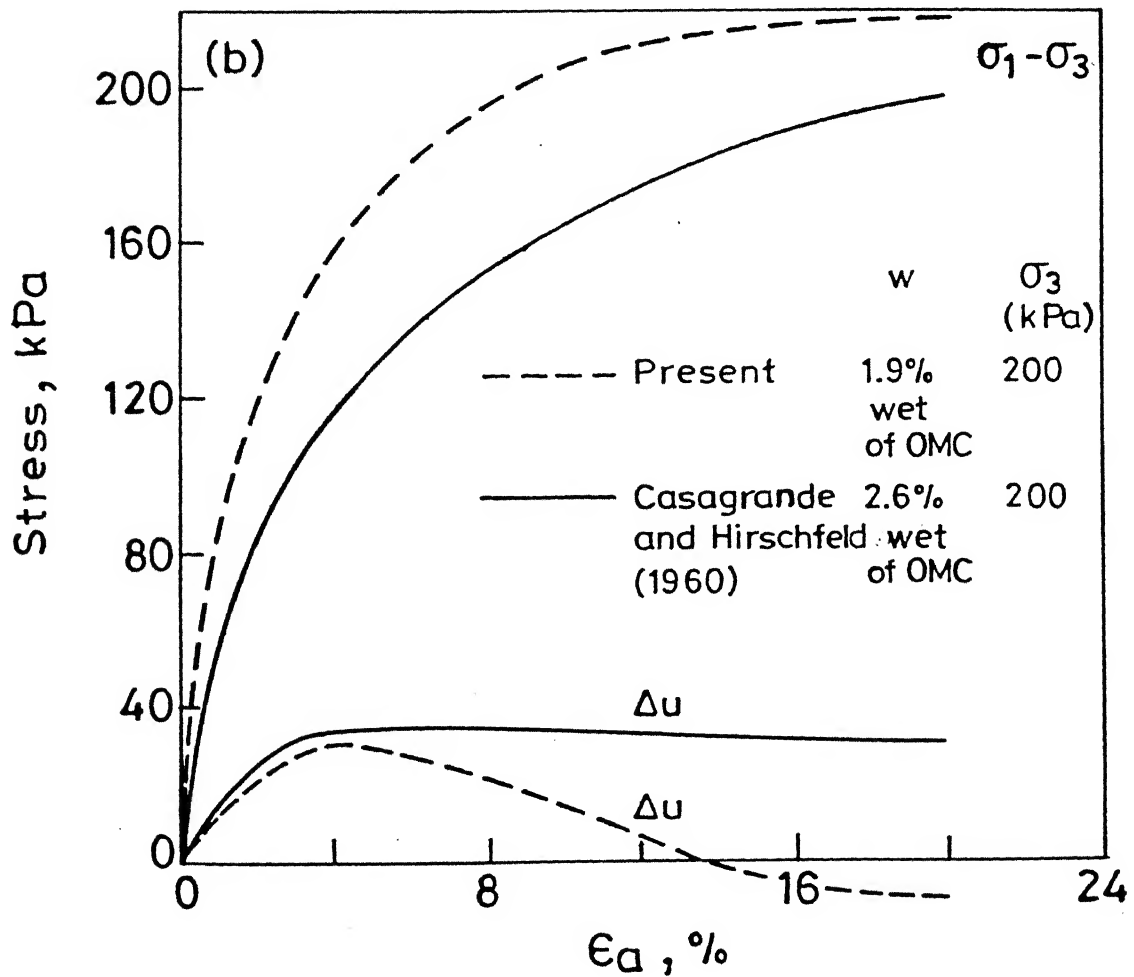
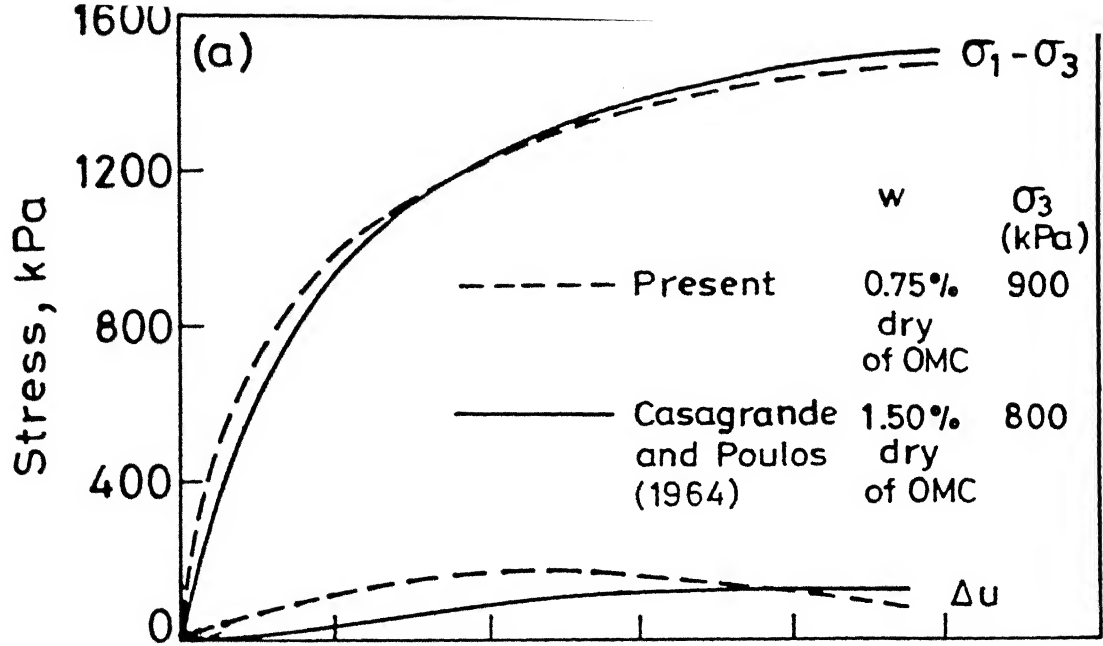


Fig. 4.67 Comparison of stress-strain and pore pressure-strain behaviour (a) dry of optimum (b) wet of optimum.

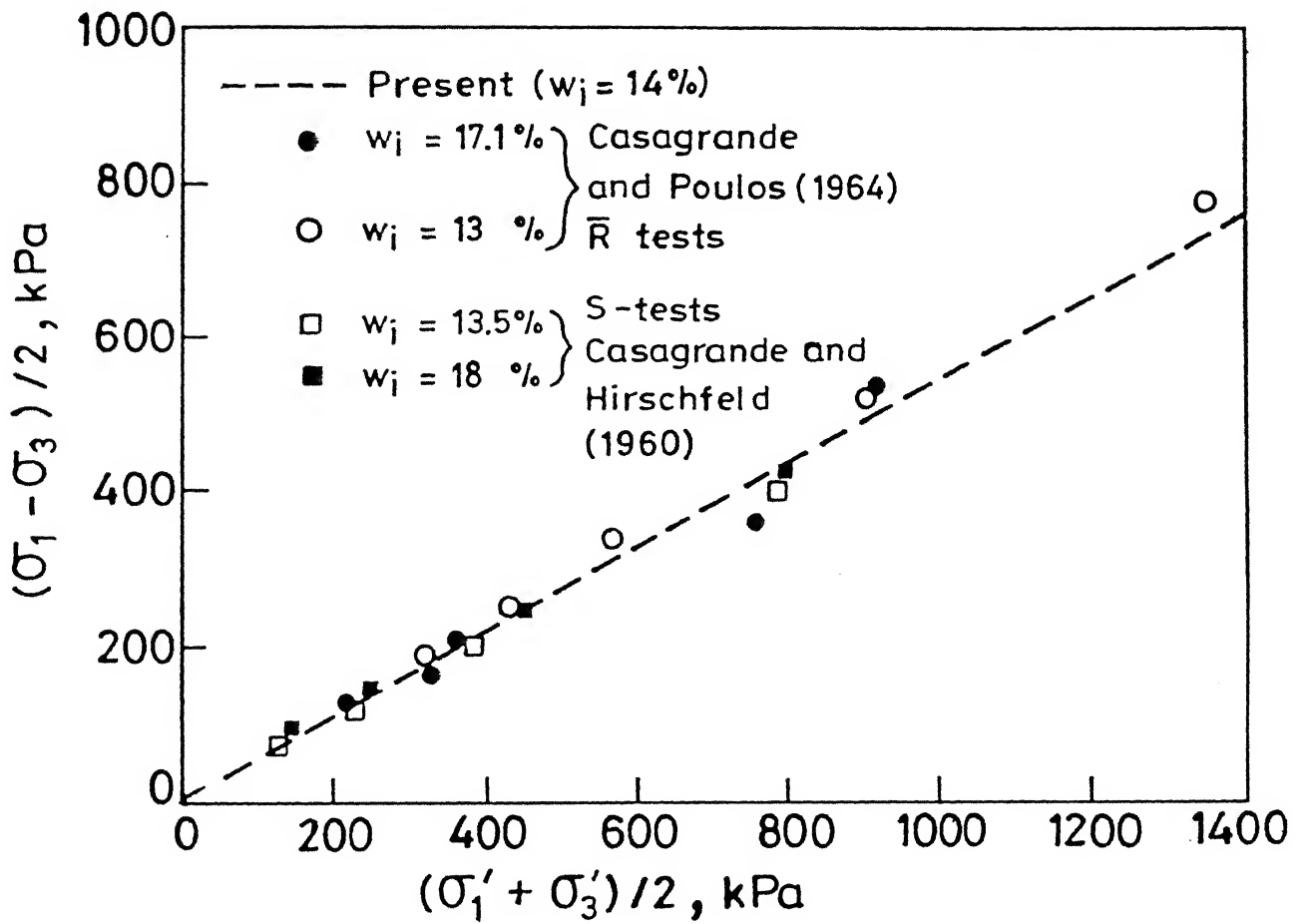


Fig. 4.68 Comparison of peak failure envelope.

samples with $S < 0.9$ is likely to be suspect in early stages of shear test.

Fig. 4.66(c) gives similar trends for Chiew Larn dam site soil in which case ($\gamma_d = 16.95 \text{ kN/m}^3$) quasi saturated behaviour is not exhibited for S values less than 0.95 %. For samples with $S \geq 0.95$ ($w = \text{OMC}$), value of $B > 0.3$ is obtained for $\sigma_3 \geq 1000 \text{ kPa}$ whereas for $S > 0.98$ ($w > \text{OMC}$), $B > 0.3$ is obtained for $\sigma_3 \geq 500 \text{ kPa}$. Here, continuous water voids appear to be established at higher degree of saturation (0.95 - 0.98) as compared to Campus silt and Canyon dam clay primarily due to higher clay content and plasticity index.

This procedure for establishing the relevant degree of saturation and cell pressure values required to ensure continuity of water voids must be followed before interpreting effective stress data obtained from undrained test assuming quasi saturated response. In a way, this is equivalent to ensuring that the sample state lies on the 45° line in the Δu vs σ_3 plot as shown in Fig. 4.22.

4.8.3.2 Samples exhibiting quasi saturated response

The effective stress data for test series B1 (Figs. 4.23 to 4.34) and B2 (Figs. 4.35 to 4.42) includes response of samples with varying degrees of saturation. In order to distinguish the samples with continuous water voids from those having low degree of saturation and only partially continuous water voids, values of maximum positive pore water pressure, Δu_{\max} produced during undrained shear as proportion of σ'_c were

computed. Figure 4.69 shows variation of $\Delta u_{\max}/\sigma_c'$ with σ_c' for all the test data from the present study and that available for Canyon dam clay. Data for sedimented Campus silt during undrained shear [Gupta (1973)] is also indicated.

It will be seen that a consistent pattern is exhibited by all the data points which satisfy the conditions for quasi saturated behaviour ($S > 0.94$ for Campus silt and $S > 0.9$ for Canyon dam clay), whereas samples A, B, C, D, E, G and J (with $S < 0.94$) exhibit no trend. A similar picture emerges (Fig. 4.70) when $\Delta u_{\max}/(\sigma_1 - \sigma_3)$ at 0 (see inset) is compared with σ_c' . It will also be seen that only at very high values of σ_c' , the effective stress paths will show a normalized behaviour as is typically exhibited by fully saturated samples. No normalized response is expected for samples tested at σ_c' values less than that required for full saturation, as is shown in Fig. 4.71 for Campus silt and Fig. 4.72 for Canyon dam clay.

Also, the behaviour shown in Figs. 4.69 and 4.70 suggests that for Campus silt and Canyon dam clay, the effective stress point for the stage of shear when Δu_{\max} is generated can be successfully predicted in the effective stress range from very low level (relevant to railway subgrade case) up to $\sigma_c' = 400$ kPa.

The non - normalizability of these test results may also be seen from Fig. 4.73 where the variation of $(\sigma_1 - \sigma_3)/2$ at failure is compared with σ_c' value for both the Campus silt and Canyon dam clay. The dotted lines show the predicted normalized response of these materials under fully saturated condition

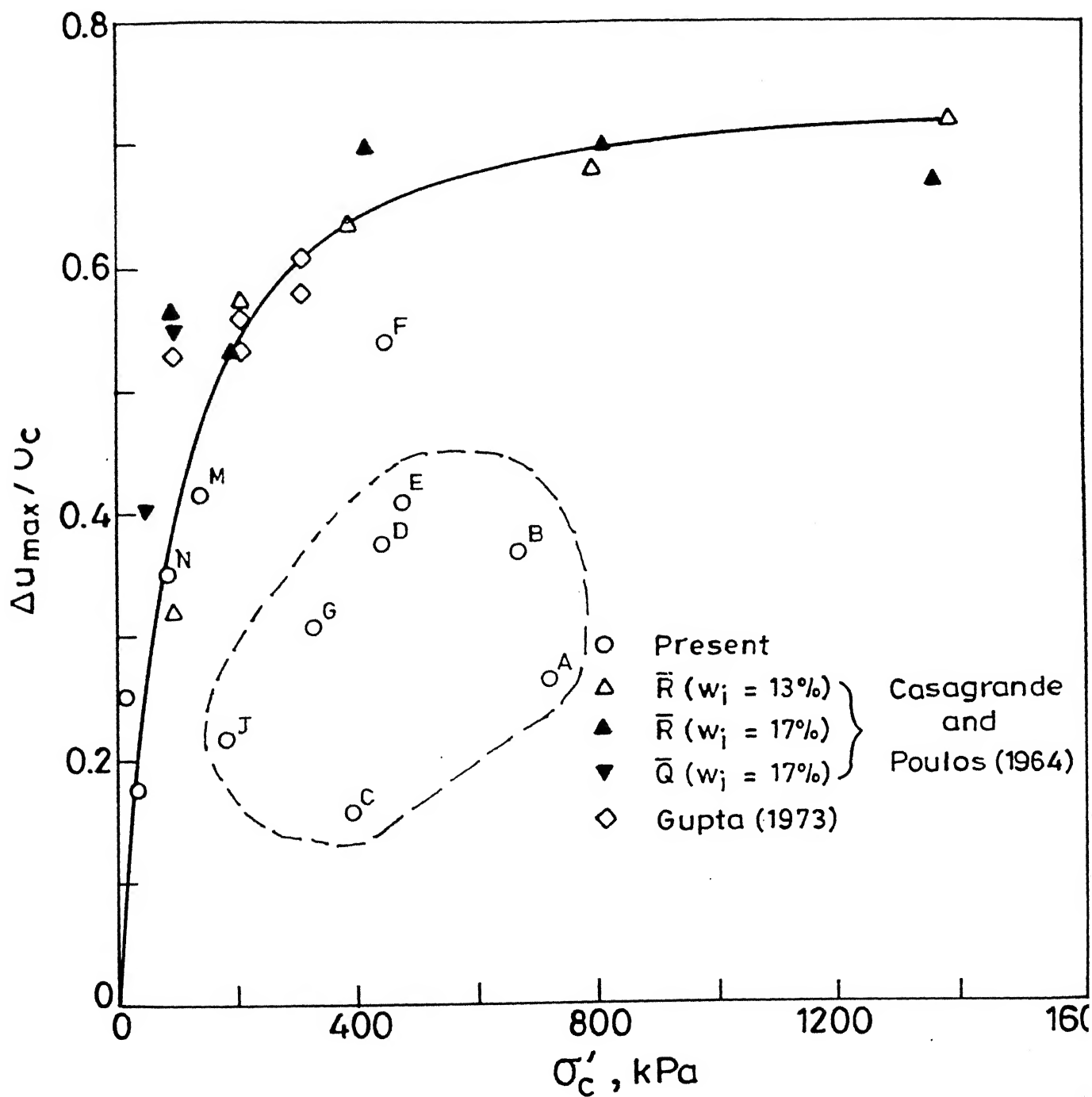


Fig. 4.69 Variation of $\Delta u_{\max} / \sigma'_c$ with σ'_c .

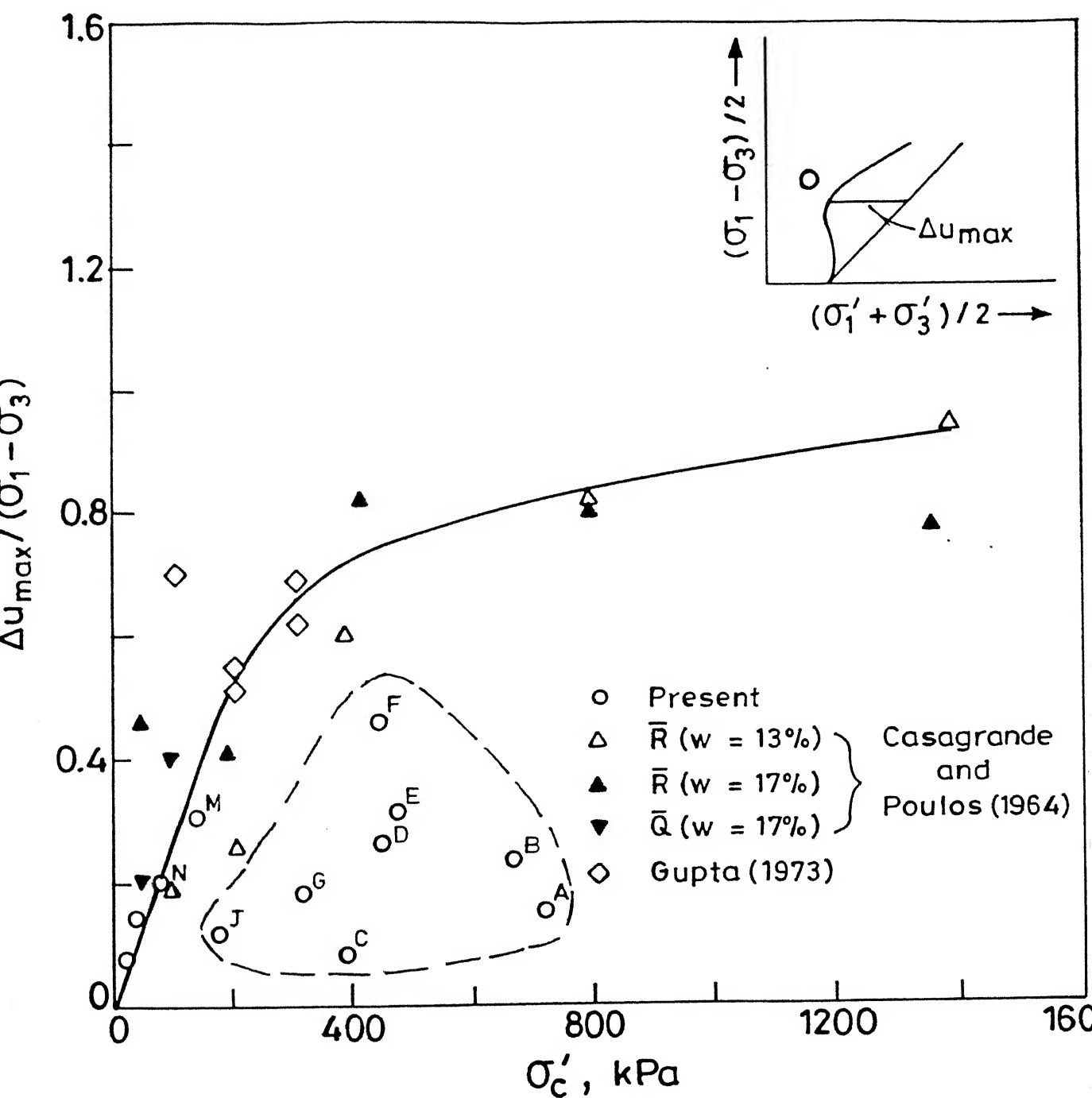


Fig. 4.70 Variation of $\Delta u_{\max} / (\sigma_1 - \sigma_3)$ with σ'_c

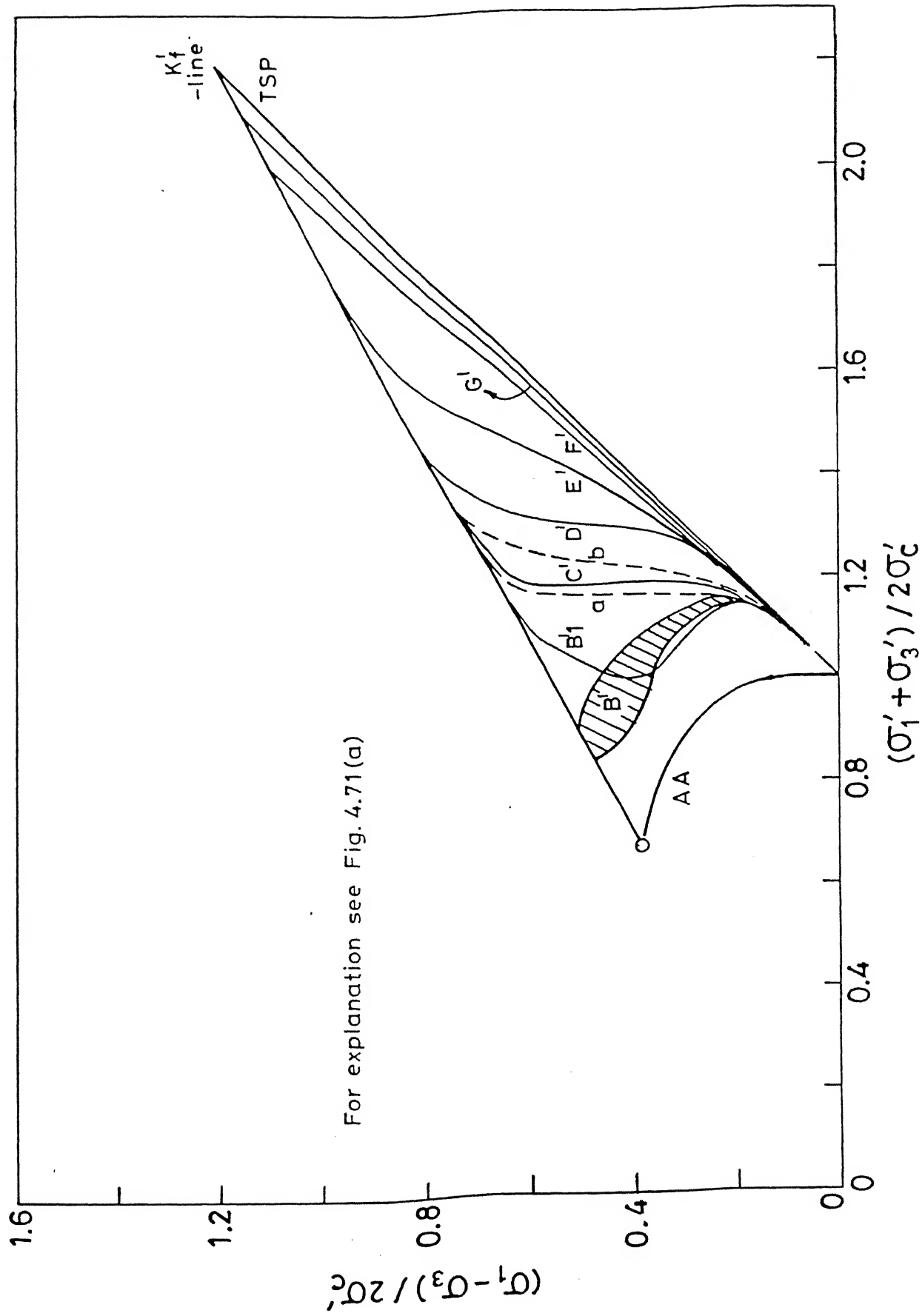


Fig. 4.71 Normalized stress paths for Campus silt.

Curve	S_i (%)	S_f (%)	σ_3 (kPa)	σ'_c (kPa)	w (%)	Test Name
AA						
B ¹		100	700	300		H, I, K, GUPTA(1973)
B1 ¹		100	700	163	15.5	L
C ¹	92	< 100	700	(452-477)	15.0	D, E
D ¹	87		900	674	13.6	B
E ¹	87		900	720	12.2	A
F ¹	87		500	392	13.5	C
G ¹	90	100	500	40	14.0	T, V, S, U
a	95		300	149	15.2	M
b	95		200	86	15.9	N

Fig. 4.71(a) Explanation for Figure 4.71.

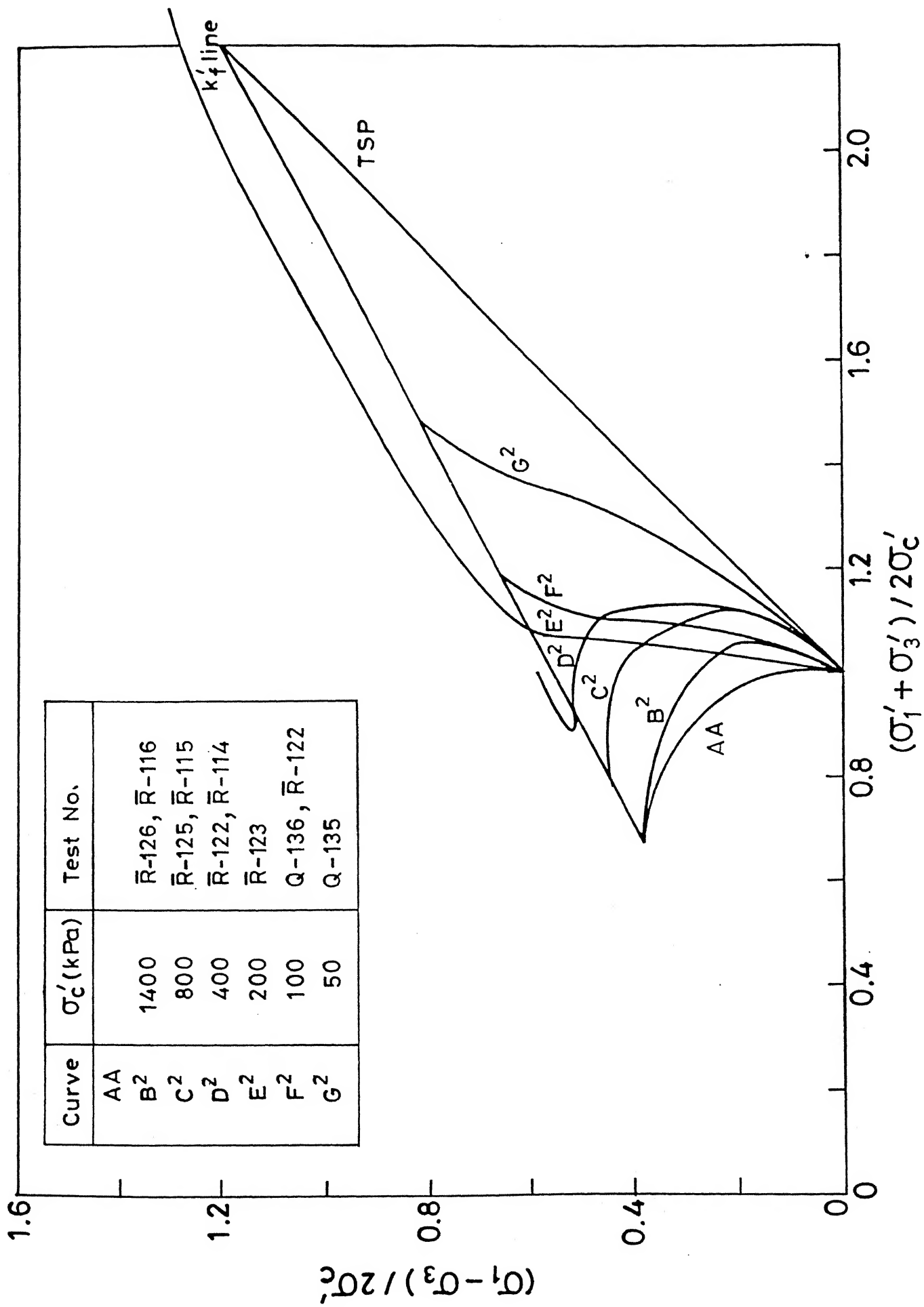


Fig. 4.72 Normalized stress paths for Canyon dam clay (Casagrande and Poulos, 1964)

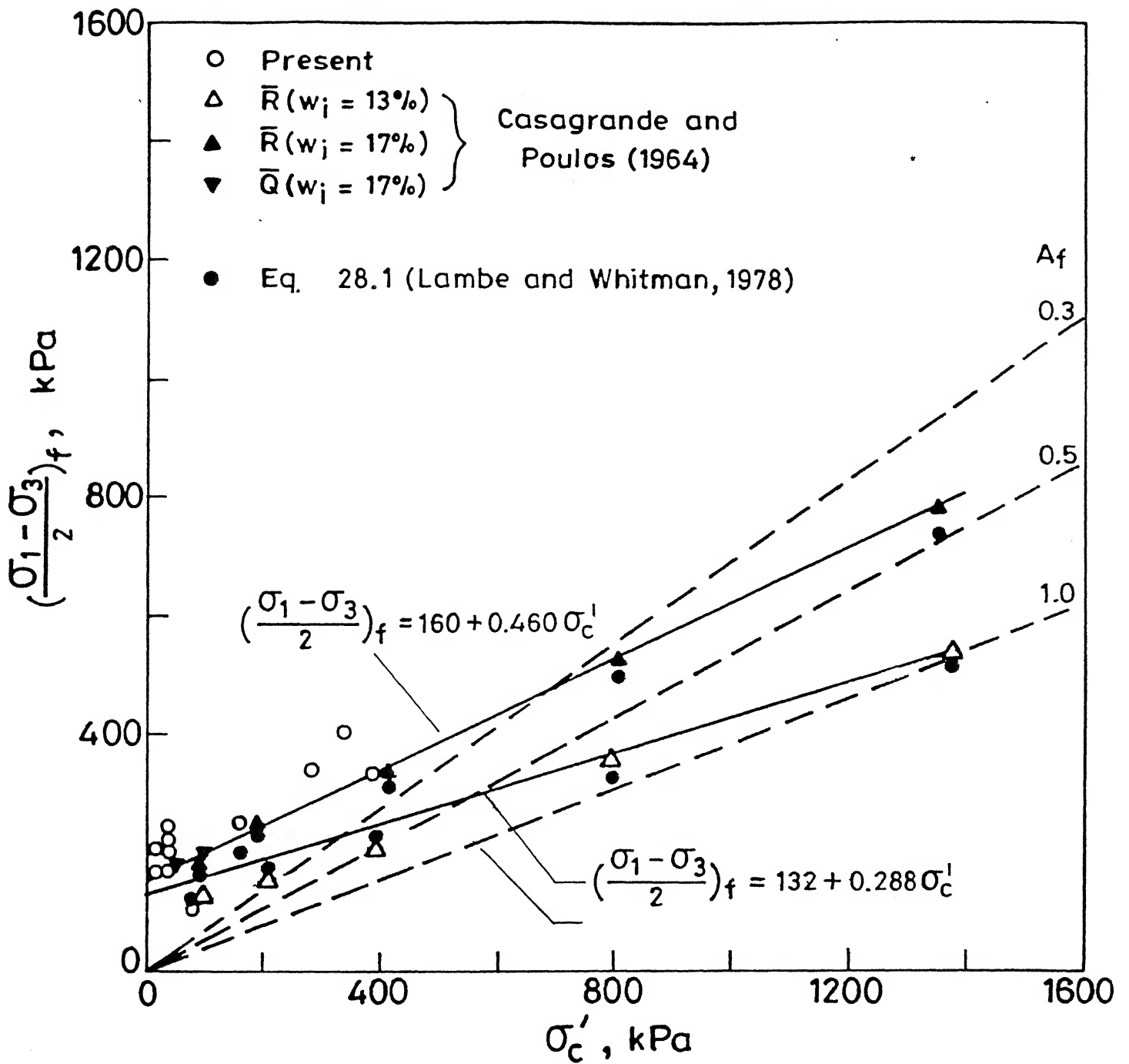


Fig.4.73 Variation of $(\frac{\sigma_1 - \sigma_3}{2})$ at failure with σ'_c .

with $c' = 0$. Incidentally, the samples compacted at OMC or OMC + 1 % for both these soils follow the relationship

$$(\sigma_1 - \sigma_3)_f / 2 = 160 + 0.460 \sigma_c' \quad (4.2)$$

as compared to samples initially compacted dry of optimum in case of Canyon dam clay which follow the relationship as given below.

$$(\sigma_1 - \sigma_3)_f / 2 = 132 + 0.288 \sigma_c' \quad (4.3)$$

It may be pointed out that for those Canyon dam clay tests where back pressure was applied for saturation, the dry of optimum samples sucked water and got softened as compared to OMC + 1 % water content samples which consolidated to lower water content values.

It is significant to note that, under both states of initial moulding water content, the compacted samples tend to approach the saturated state response at very high σ_c' values. While the initially dry samples (softened during back pressure saturation) approach $A_f = 1.0$ response at $\sigma_c' = 1400$ kPa, those compacted wet of OMC (consolidated during back pressure) exhibit stiffer response and tend to approach $A_f = 0.5$ at σ_c' values greater than 1400 kPa. In Fig. 4.73, the solid dots for both the moulding water content states represent the predicted results using actual c' and ϕ' values and A_f values as measured (see Tables 4.8 and 4.9).

Table 4.8 Calculation of ultimate stress from Eq. (28.1) from Lambe and Whitman (1978) for Campus silt.

Test No.	Δu_f	$(\frac{\sigma_1 - \sigma_3}{2})_f$ Exp	σ_c'	A_f	$(\frac{\sigma_1 - \sigma_3}{2})_f$ Cal
N26	101	415	446	0.120	420
N25	-26	202	149	0.064	169
N28A	5	109	86	0.023	115
T109	-168	212	20	-0.400	---
T115	-140	230	40	-0.305	---

* All stress units are in KPa .

Equation (28.1) [Lambe and Whitman (1978)] is given below :

$$q_f = \frac{\bar{c} \cos \bar{\phi} + (\bar{p}_0 - 2 A_f q_f) \sin \bar{\phi}}{1 - \sin \bar{\phi}}$$

Table 4.9 Calculation of ultimate stress from Eq. (28.1) from Lambe and Whitman (1978) for Canyon dam clay results

Original Test no.	Referred here as	Δu_f	$(\frac{\sigma_1 - \sigma_3}{2})_f$ Exp	σ_c'	A_f	$(\frac{\sigma_1 - \sigma_3}{2})_f$ Cal
$\bar{R}112$	R1	20	130	100	-0.077	167
$\bar{R}114$	R2	225	225	390	0.500	219
$\bar{R}115$	R3	510	312	793	0.815	325
$\bar{R}116$	R4	1000	540	1380	0.925	515
$\bar{R}122$	R5	30	187	97	-0.080	164
$\bar{R}123$	R6	12	250	102	0.024	218
$\bar{R}124$	R7	180	335	413	0.268	222
$\bar{R}125$	R8	420	520	803	0.404	330
$\bar{R}126$	R9	781	765	1356	0.501	735

* All stress units are in KPa .

4.8.3.3 Stress - strain, pore pressure - strain response with varying confining stress

As the effective stress paths are not normalizable with respect to σ_c' , a similar pattern is expected in terms of stress - strain and pore pressure - strain behaviour for all tests in series B1 and B2 since in no case, cell pressure is large enough to produce full saturation by compressing and dissolving air present in the sample. Figure 4.74 shows that for the same strain, changes in $(\sigma_1 - \sigma_3)$ are not proportional to the corresponding changes in σ_c' for quasi saturated samples. The pore pressure response also shows similar behaviour (the higher σ_c' values suppress dilatancy observed at low stress levels). Non-normalizable behaviour with σ_c' is also shown (Fig. 4.74) by two back saturated samples tested at $\sigma_c' = 20$ and 40 kPa. These very low effective stress tests demonstrate enhanced dilatancy during undrained shear.

Furthermore, it will be seen that (Fig. 4.75), as expected, the stress- strain behaviour of partially saturated soils is very sensitive to the confining stress. Two samples tested at $\sigma_3 = 0$ and 20 kPa give essentially the same result up to failure but even a small confining stress increase changes the brittle unconfined response to an elasto-plastic one which further changes to work-hardening stress strain behaviour as σ_3 is increased to 500 kPa (Fig. 4.75). Actually this change over in stress - strain behaviour occurs at $\sigma_3 > 200$ kPa (for the same water content) as can be seen in Fig. 4.74. At $\sigma_3 < 200$

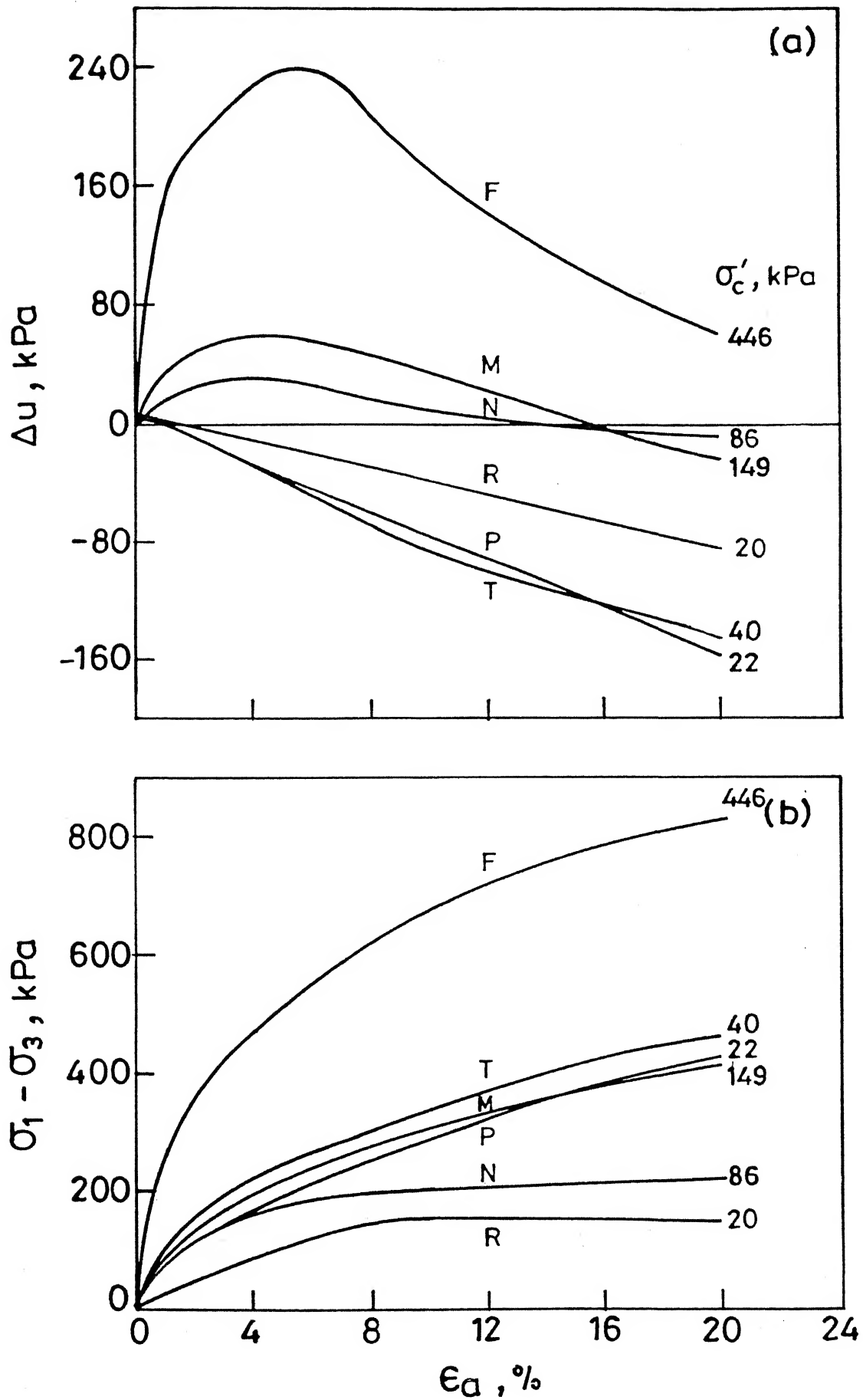


Fig. 4.74 Effect of confining pressure on (a) pore pressure-strain behaviour (b) Stress-strain behaviour.

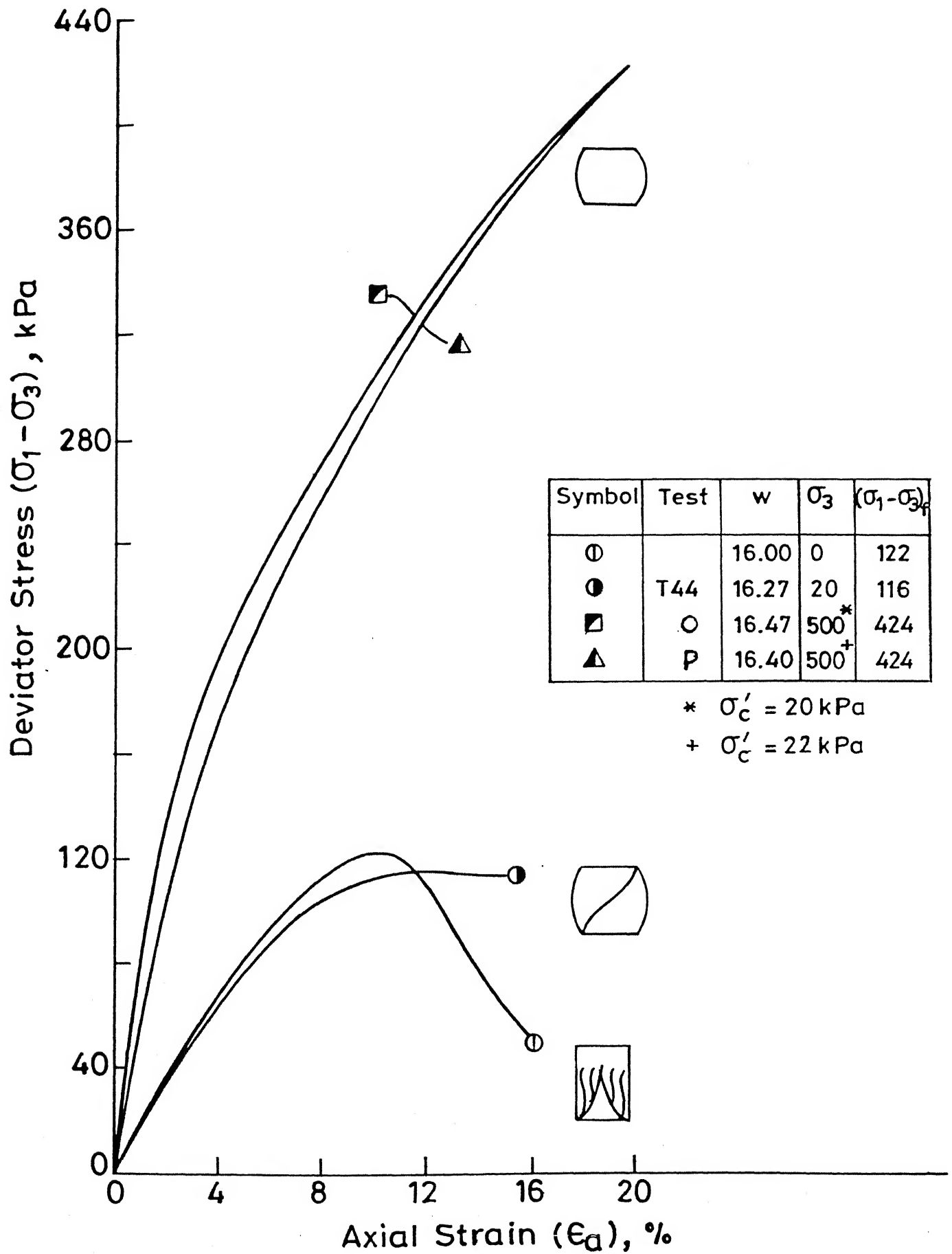


Fig.4.75 Effect of confining pressure on stress-strain behaviour.

kPa, the quasi saturated samples will give high negative pore pressure at failure but as σ_3 increases beyond 200 kPa (corresponding to $\sigma_c' = 86$ kPa), pore pressure at failure increases to zero for $\sigma_3 = 300$ kPa (σ_c' being 149 kPa) and becomes positive for higher values of confinement.

4.8.3.4 Failure envelope

The state of stress at failure has been investigated in terms of both $(\sigma_1 - \sigma_3)_{\max}$ and $(\sigma_1' / \sigma_3')_{\max}$ criteria. Results from all the tests in Series B1, B2 and B3 are plotted in terms of $(\sigma_1 - \sigma_3)/2$ and $(\sigma_1' + \sigma_3')/2$ by both the criteria. It may be seen (Fig. 4.76) that there is a unique envelope passing through all the failure states and can be represented in terms of effective shearing resistance parameters, $c' = 10.7$ kPa and $\phi' = 32.6^\circ$.

An enlargement of the failure envelope in the low effective stress range, along with the total stress failure envelopes for the range of water contents studied, is given in Fig. 4.77. As was shown earlier in Fig. 4.68, the same failure envelope and shearing resistance parameters are applicable for the results of Canyon dam clay.

Incidentally, interpretation of quasi saturated response as advocated by Marsal (1979) and further investigated by Yudhbir and Korchoke (1987) is also attempted here. As shown in Fig. 4.65, the slope of the line joining points on total stress envelopes corresponding to different water contents where saturation is obtained, gives a value of $\tan \alpha = 0.354$ ($\alpha =$

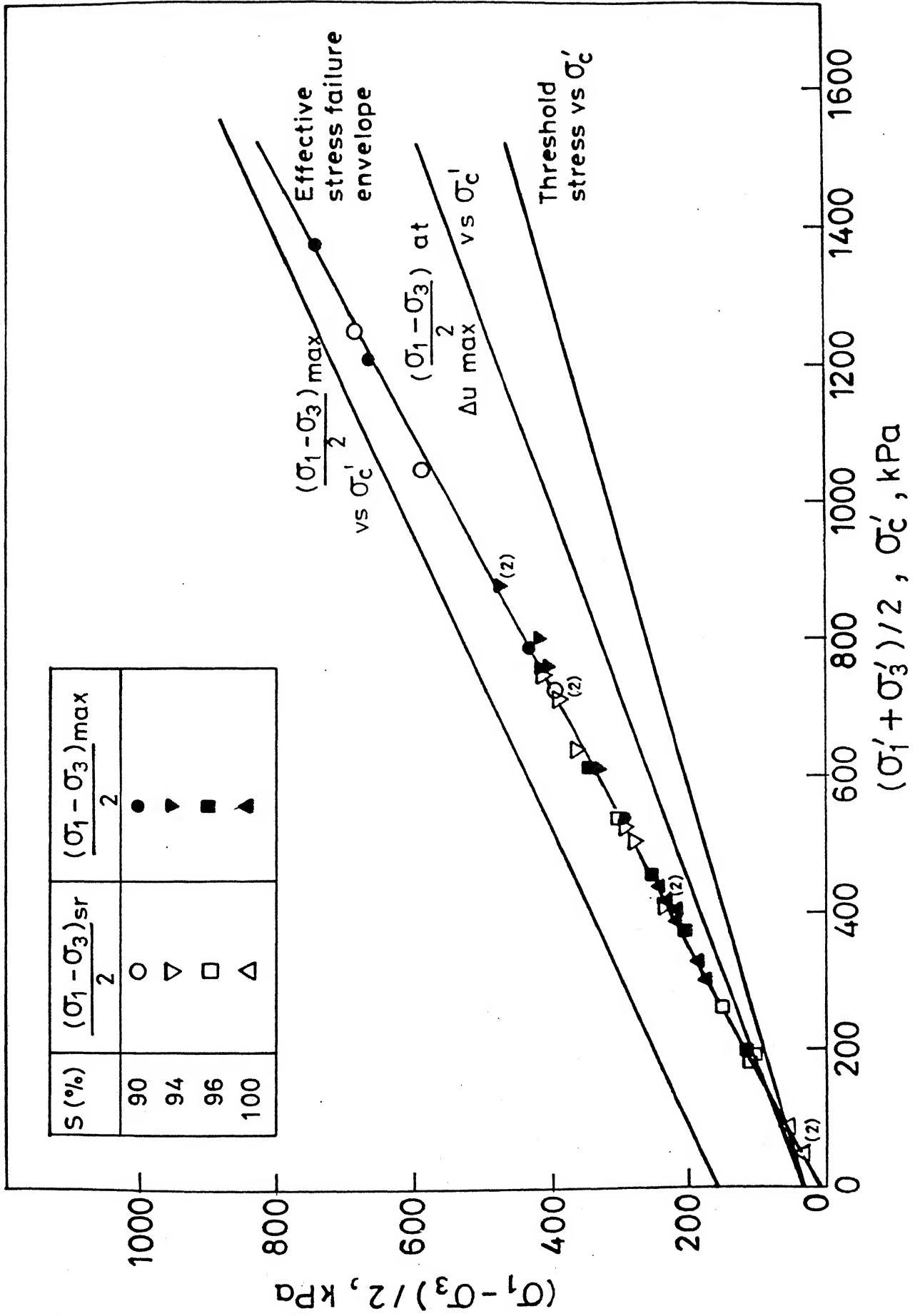


Fig. 4.76 Effective stress failure envelope .

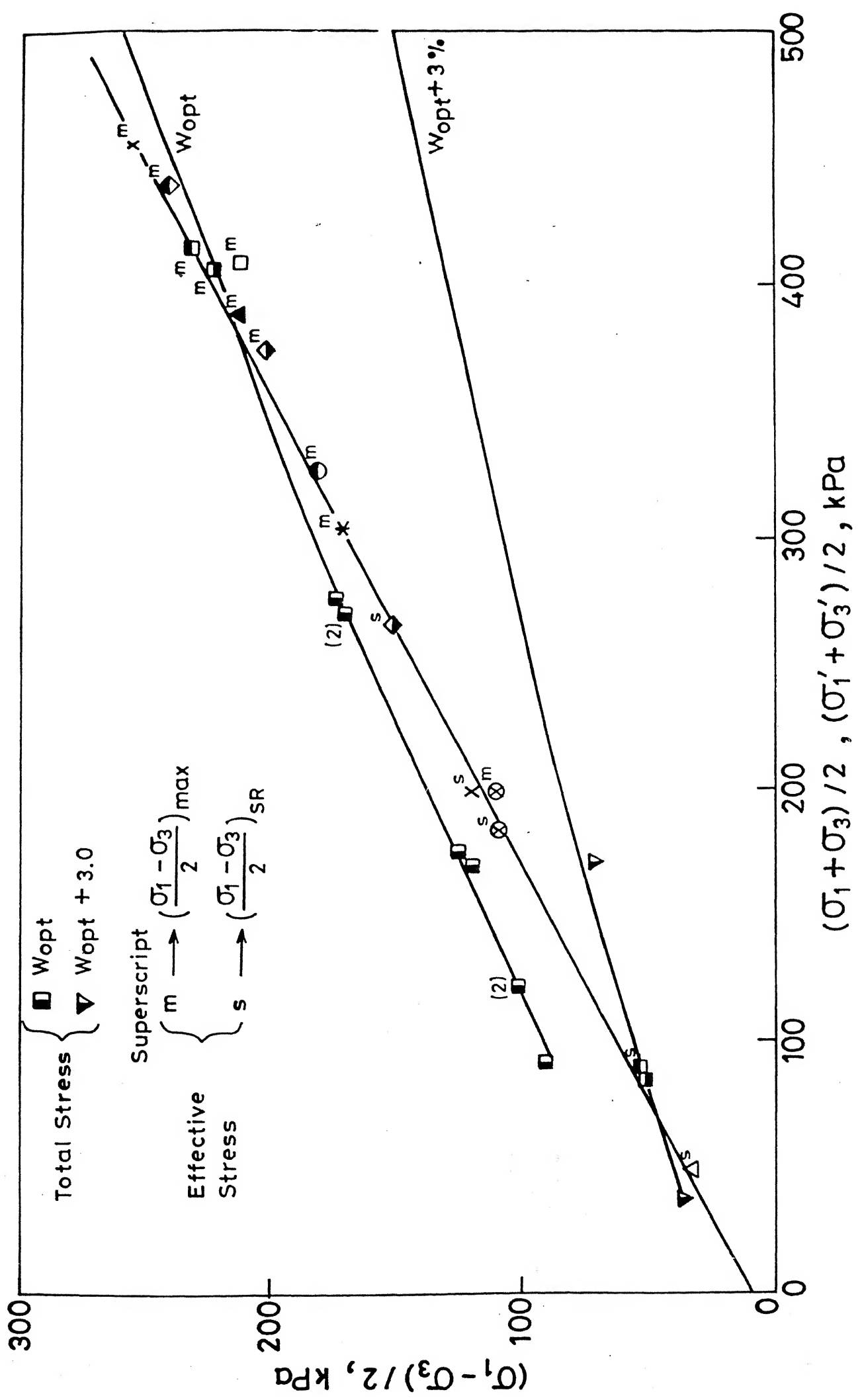


Fig. 4.77 Effective stress failure envelope (enlarged view)

19.5°). Taking $A_f = 0.5$ as suggested in this approach, the failure envelope obtained (defined by $c' = 0$ and $\phi' = 33.2^\circ$) matches reasonably well with that obtained from best fit to experimental data.

For the Campus silt, Yudhbir and Prakasa Rao (1986), on the basis of laboratory and field tests suggest $c' = 0$ and $\phi' = 35^\circ$ for saturated and $c' = 14$ kPa and $\phi' = 35^\circ$ for partially saturated undisturbed samples. This soil in the field behaves like a stiff lightly overconsolidated material as a consequence of annual water table fluctuations as reported by Yudhbir et al. (1979) who also report $A_f = 0.4$ for these soils. These shearing resistance parameter values seem to be in close agreement with those determined for compacted samples.

In case of tests where samples did not soften during back pressure saturation but instead were consolidated, the $(\sigma_1 - \sigma_3)_f / 2$ vs σ_c' relationship (Fig. 4.73) approaches the line for saturated samples with $A_f = 0.5$ and $c' = 0$ in Marsal's approach. The consolidated state of the samples before shear seems to be consistent with the Marsal's α - line (Fig. 4.65) which depicts behaviour corresponding to consolidated undrained test on samples in a saturated state. Incidentally, in Fig. 4.73, most of the data points from the present study (except for those tested at $\sigma_c' = 20$ and 40 kPa which had softened during back pressure saturation) scatter around the results for consolidated samples of Canyon dam clay. The relationship for softened samples, however, suggests $A_f = 1.0$ and $c' = 0$ under saturated conditions and once again the results for Campus silt

and the Canyon dam clay seem to scatter around a common relationship, the scatter being more pronounced at very low stress levels ($\sigma_c' = 20$ and 40 kPa).

4.8.3.5 Comparison with other results

4.8.3.5.1 Comparison with Cruz et al. (1985)

Cruz et al. (1985) report test results for a large variety of soils - both undisturbed and compacted - tested following the Marsal's quasi - saturation procedure and measuring pore water pressures only to evaluate the shearing resistance parameters.

Group IV soil (sedimentary colluvial : $w_L = 29-38\%$, $I_p = 13-19\%$, $< 2\mu = 17-32\%$, $OMC = 11-14\%$, γ_d at $OMC = 18 - 19.5$ kN/m^3) described by Cruz et al. (1985) is quite similar to the Campus silt used in the present study. The stress - strain, pore pressure - strain and stress path results for group IV soil (Fig. 4.78) show remarkable similarities with those obtained for the Campus silt as presented in Figs. 4.23 to 4.34. Cruz et al. (1985) also observe change in behaviour from dilatant response at low confining stress (< 500 kPa) to a contractive response during shear for effective confining stress in the range of 1000 kPa (as compared to 1400 kPa needed in case of Campus silt). Furthermore, for the group IV soils, the shearing resistance parameters : $c' = 5 - 20$ kPa and $\phi' = 32 - 34^\circ$ compare rather well with the results obtained for the Campus silt, ($c' = 10.7$ kPa, $\phi' = 32.6^\circ$).

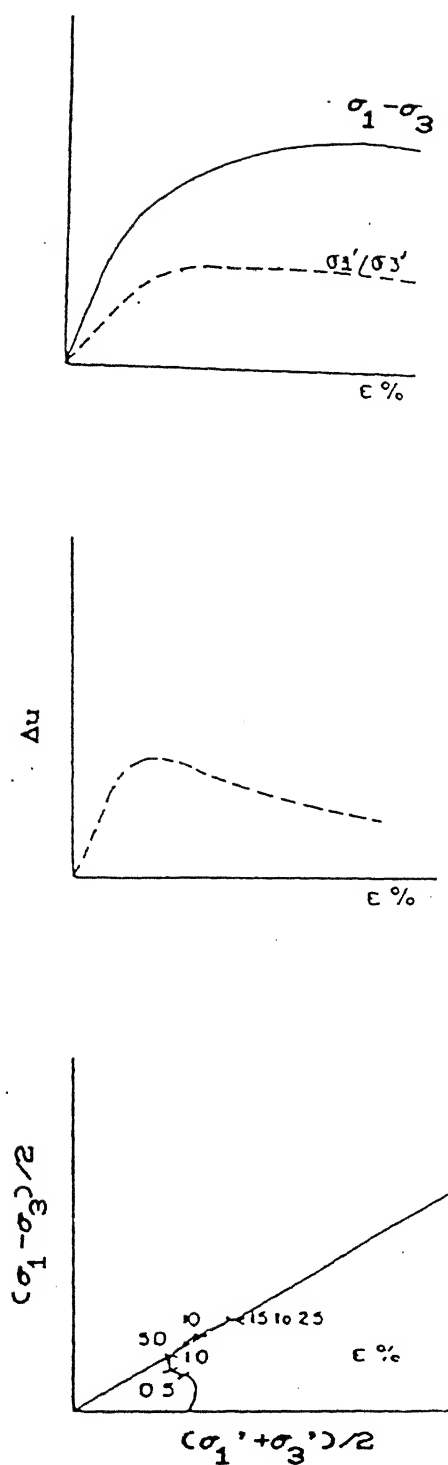


Fig. 4.78 Typical stress - strain, pore pressure - strain and stress path for Group IV soil (Cruz et al., 1985)

Incidentally, as indicated in Sec. 4.8.3.3 for Campus silt, Cruz et al. (1985) also report that unique failure envelope is obtained on the basis of both maximum deviator stress and $(\sigma_1'/\sigma_3')_{\max}$ - failure criteria for group IV soils.

4.8.3.5.2 Comparison with data for Canyon dam clay

As already illustrated in Sec. 4.8.3.1, the Campus silt and Canyon dam clay show remarkable similarities in practically all aspects of the behaviour of compacted samples.

Since very detailed undrained test results were available for the Canyon dam clay which has been shown to be quite similar to the Campus silt, it was decided to examine the effective stress data available for both soils in the general framework of critical state model.

Following Yudhbir and Wood (1989), the water content - effective stress relationship for these low plasticity soils in a normally consolidated state (starting from remoulded slurry state) was established as shown in Fig. 4.79. Also plotted in Fig. 4.79 is the experimental data for these soils. Tables 4.10 and 4.11 show the details related to critical state for Campus silt. As argued by Yudhbir and Wood (1989), these compacted states are expected to lie on the recompression line, the slope (κ) of which was again estimated from the relationships suggested by Yudhbir and Wood (1989). They had observed that the liquidity index, I_L vs effective stress plot for normally consolidated states shows considerable scatter ; the value of effective stress $P' = (\sigma_1' + 2\sigma_3')/3$ varying from 600 kPa to 1500

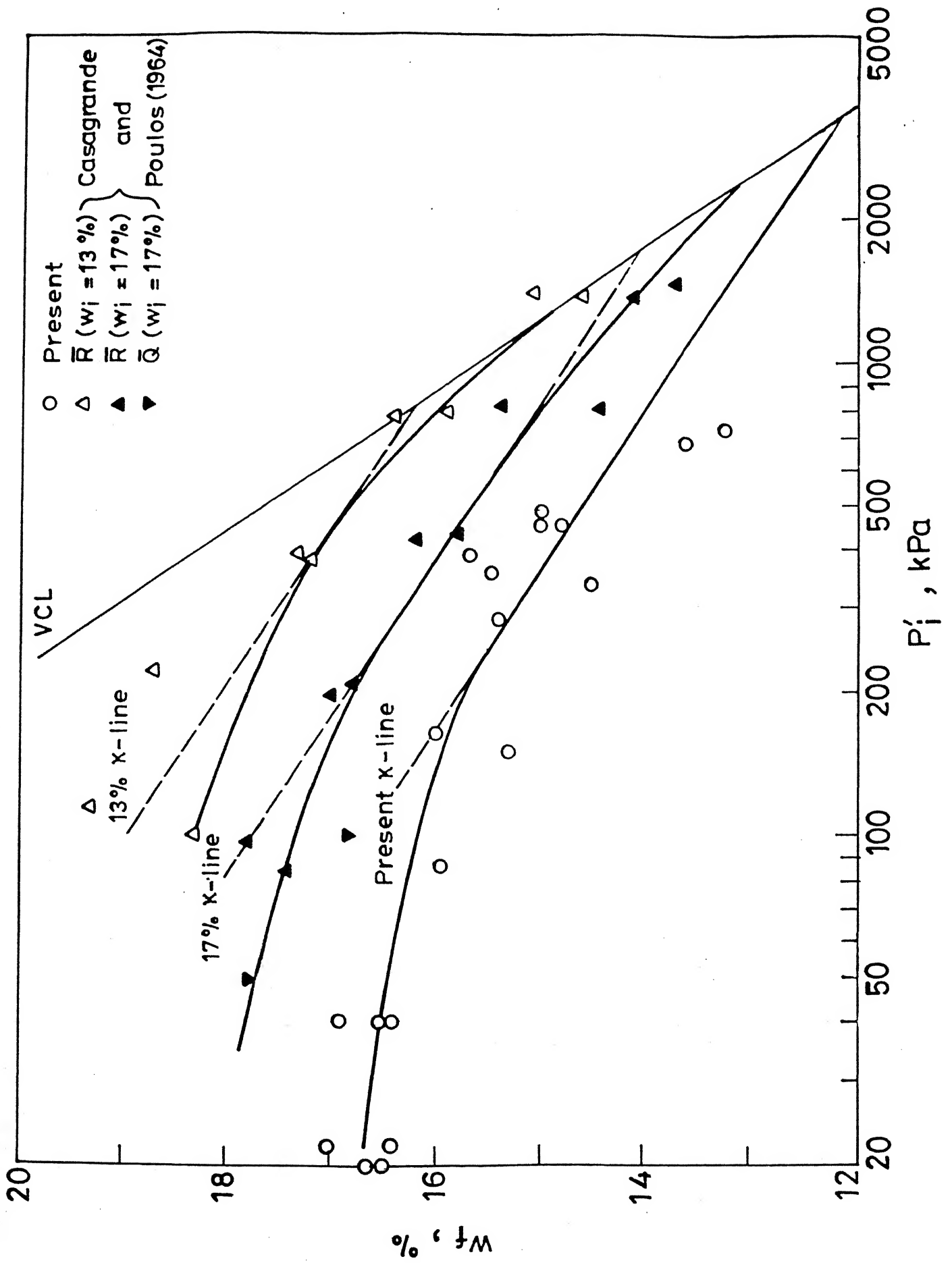


Fig.4.79 Variation of P'_i with w_f .

Table 4.10 Critical state data for Campus silt (static tests).

Test	q_f	P'_f	P_{cs}	Δu_{cs}	P_{cs}/P'_f	P'_e	q/P'_e	P'_f/P'_e
New23	1480	1129	1220	-91	1.08	2250	0.658	0.502
New1	846	648	Low Cell pressure ; low S_1			2050	0.413	0.316
New27	1330	991	1080	-89	1.09	2000	0.665	0.496
New30	580	438	Low Cell pressure ; low S_1			-----	-----	-----
New29	834	616	800	-184	1.30	1470	0.567	0.419
New26	830	659	705	-46	1.07	1310	0.634	0.503
New32	944	725	670	+55	0.92	1250	0.755	0.580
New24	942	723	670	+57	0.93	1250	0.754	0.578
New25	404	308	614	-306	1.99	1104	0.366	0.279
New28	218	166	497	-331	2.99	910	0.240	

* All stress units are in kPa

Table 4.11 Critical state data for Campus silt (cyclic and static tests).

Test	q_f	p'_f	p_{cs}	Δu_{cs}	p_{cs}/p'_f	p'_e	q/p'_e	p'_f/p'_e
High σ'_c								
T103	690	495	580	-85	1.17	1080	0.639	0.458
T104	810	626	560	+66	0.90	1050	0.750	0.580
T105	660	505	525	-20	1.04	980	0.673	0.515
T106	510	370	470	-100	1.27	880	0.580	0.420
$\sigma'_c = (20 - 22)$ KPa								
T108	424	317	410	-93	1.29	770	0.551	0.412
T109	424	337	400	-63	1.19	760	0.558	0.443
T110	344	247	330	-83	1.34	620	0.555	0.398
$\sigma'_c = 40$ KPa								
T115	460	339	395	-56	1.16	740	0.622	0.458
T116	360	269	343	-74	1.28	650	0.554	0.414
T117	480	360	410	-50	1.14	770	0.623	0.467
T119	444	332	395	-63	1.19	740	0.600	0.449

* All stress units are in kPa

kPa at $I_L = 0$ and from 6 to 15 kPa at $I_L = 1.0$. The Virgin consolidation line, VCL, best fitting the data points as shown in Fig. 4.79 would suggest slightly higher value of P' at $I_L = 0$. The compacted soil samples appear to behave like overconsolidated soils with different values of past maximum pressure (produced due to compaction) depending on the moulding water content and dry density.

The corresponding relationship between water content and effective stress at failure, P_f' is depicted in Fig. 4.80; the VCL as obtained from Fig. 4.79 is also shown. The position of the Critical state line, CSL for these soils, as suggested by Yudhbir and Wood (1989) is indicated in Fig. 4.80. Details of some of the test points are given in Fig. 4.80(a) where it is quite clear that samples of Canyon dam clay like R4, which virtually lie on VCL at the start of the test, develop positive pore pressure throughout and P' moves towards CSL. Samples like R1 (Canyon dam clay), and A, P and U (Campus silt) on the other hand dilate towards the CSL. In between these two extremes, the paths followed by other samples are shown in Fig. 4.80(a). Given the fact that there is some uncertainty about the exact location of CSL, the position as fixed according to the guideline given by Yudhbir and Wood (1989) seems to represent the test data quite satisfactorily.

Figure 4.81 depicts the failure envelope in the Cambridge stress space along with the peak failure envelope corresponding to $c' = 10.7$ kPa and $\phi' = 32.6^\circ$.

The convergence of end points for all these tests reported

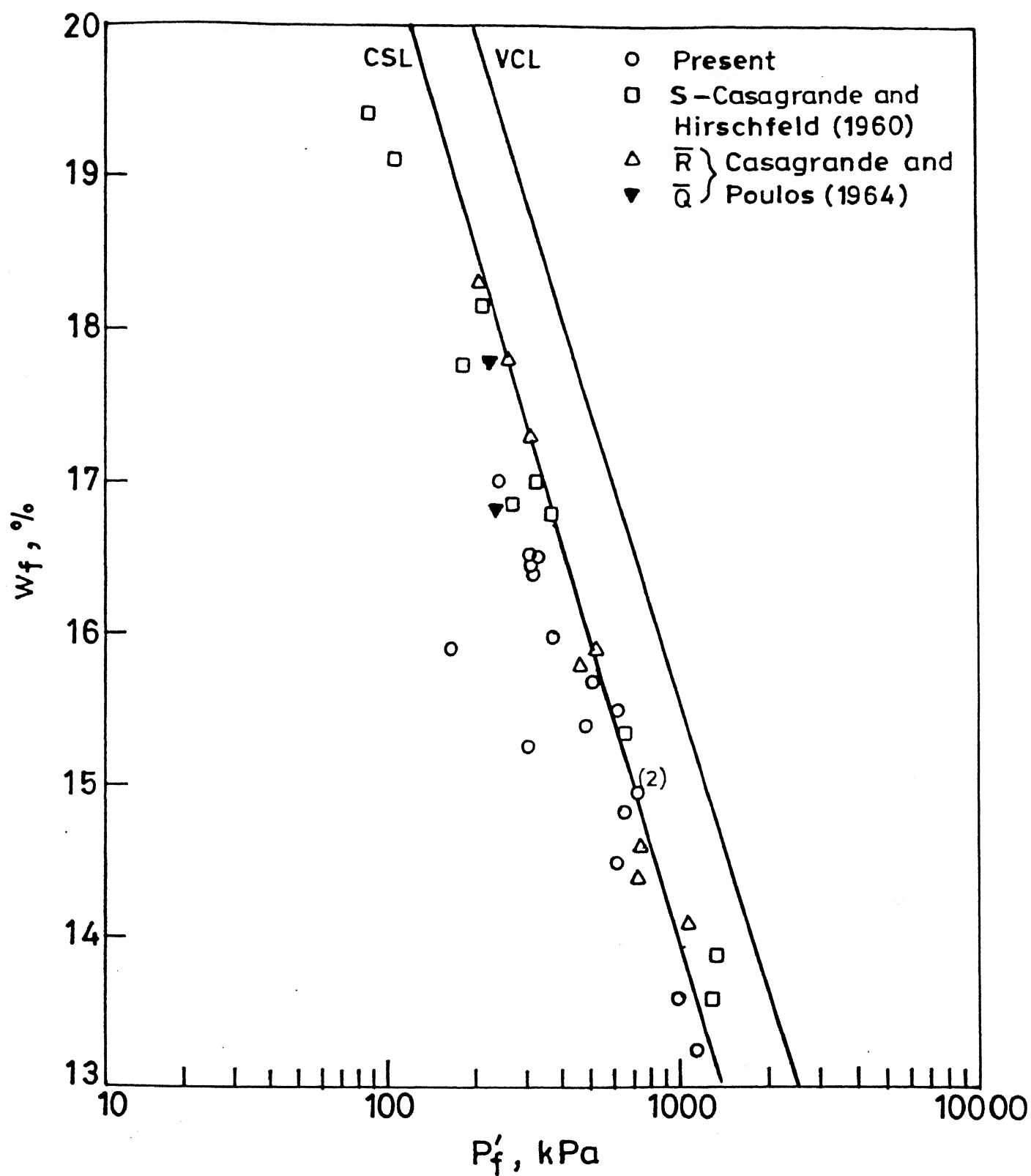


Fig. 4.80 Variation of P'_f with w_f .

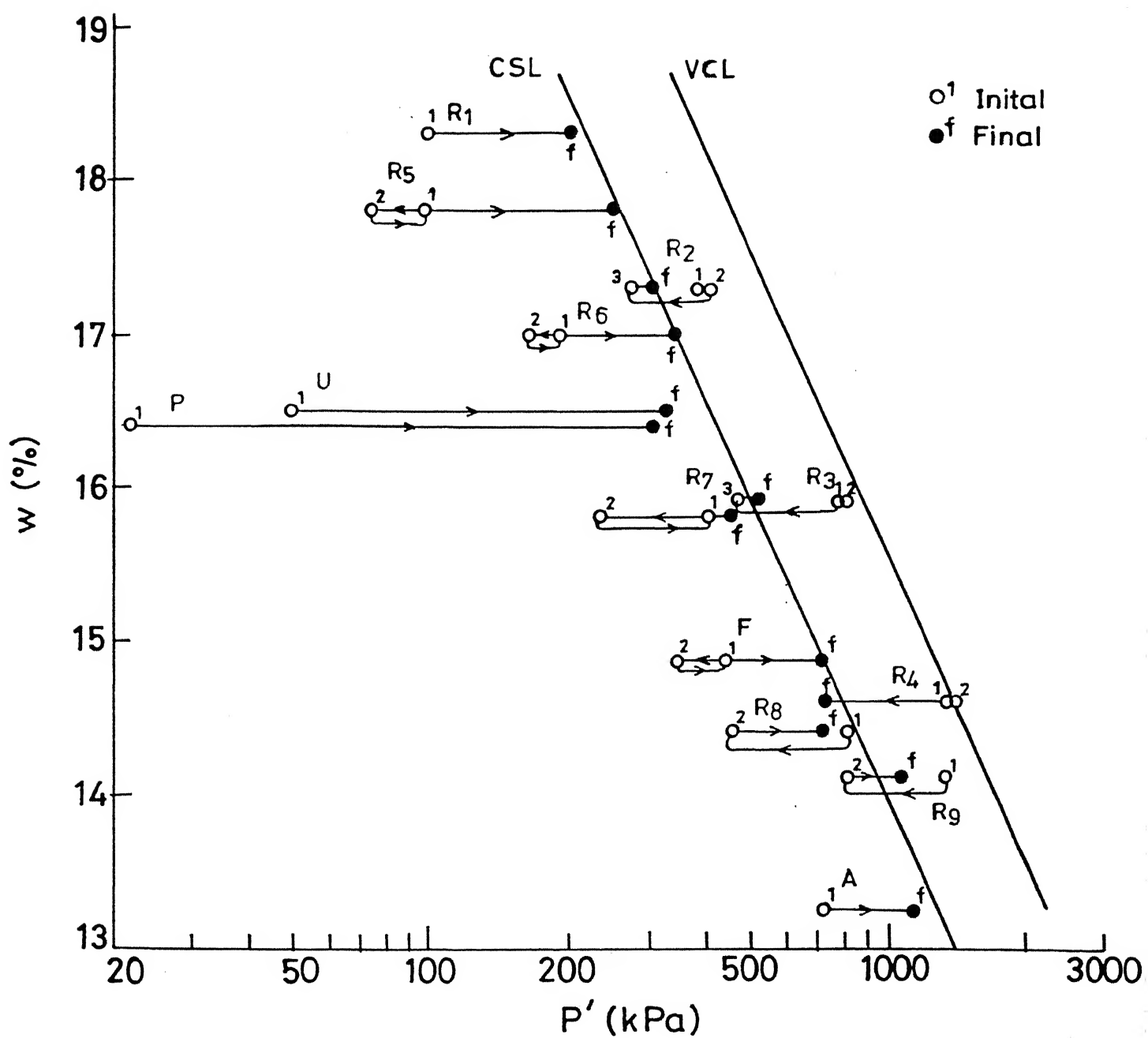


Fig. 4.80(a) Variation of P' with w .

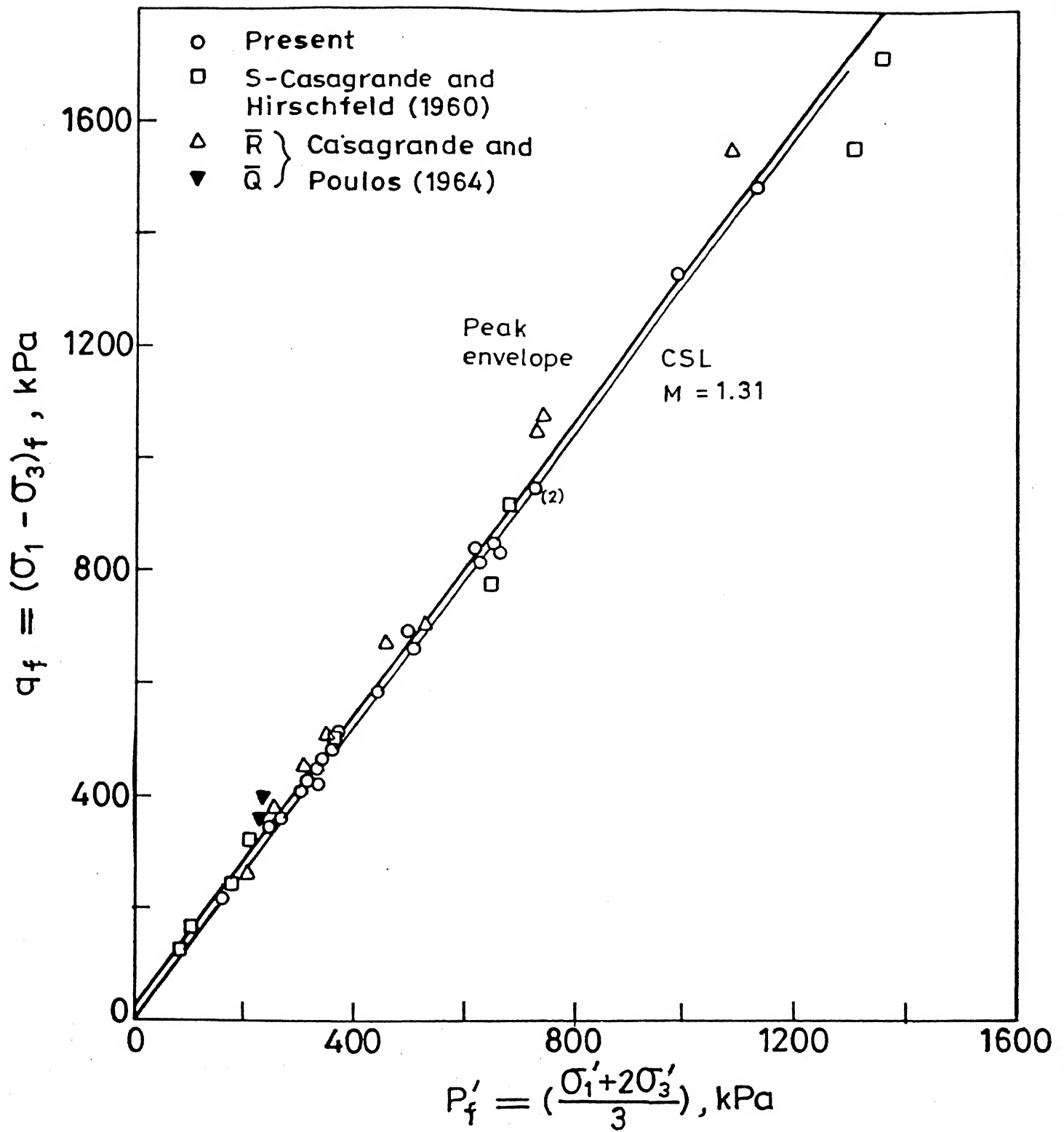


Fig. 4.81 Variation of P'_f with q_f .

for both the soils, towards CSL is also well brought out in Figs. 4.82 and 4.83 where the state paths are also indicated. The value of P_e' - Hvorslev's equivalent consolidation pressure - was evaluated from VCL shown in Fig. 4.79. Figure 4.84 shows the end points for all the undrained tests for both the soils and some drained tests (S tests) on the Canyon dam clay. Point C giving the intersection of Hvorslev surface with tension cut off was obtained by assuming P'/P_e' at C equal to $0.1 \times (P_{cs}'/P_e')$ as suggested by Yudhbir and Wood (1989) and the Hvorslev surface represented by upper line is then obtained by joining point C with the critical state line. The Hvorslev surface represented by lower line shows best fit to the experimental data. The Roscoe surface shown in Figs. 4.82 to 4.84 was predicted from modified Cam - clay model using the following critical state parameters (Table 4.12) :

$$\lambda = 0.08$$

$$\kappa = 0.018$$

$$M = 1.31$$

In spite of various difficulties in testing partially saturated soils and interpreting the test data, the picture evolved in Figs. 4.79, 4.80, 4.80a, 4.82, 4.83 and 4.84 tends to support the view that compacted soils, when tested at a degree of saturation above a certain value (which ensures quasi saturation in case of samples not back pressured) as brought out earlier in Sec. 4.8.3.1 behave like overconsolidated soils

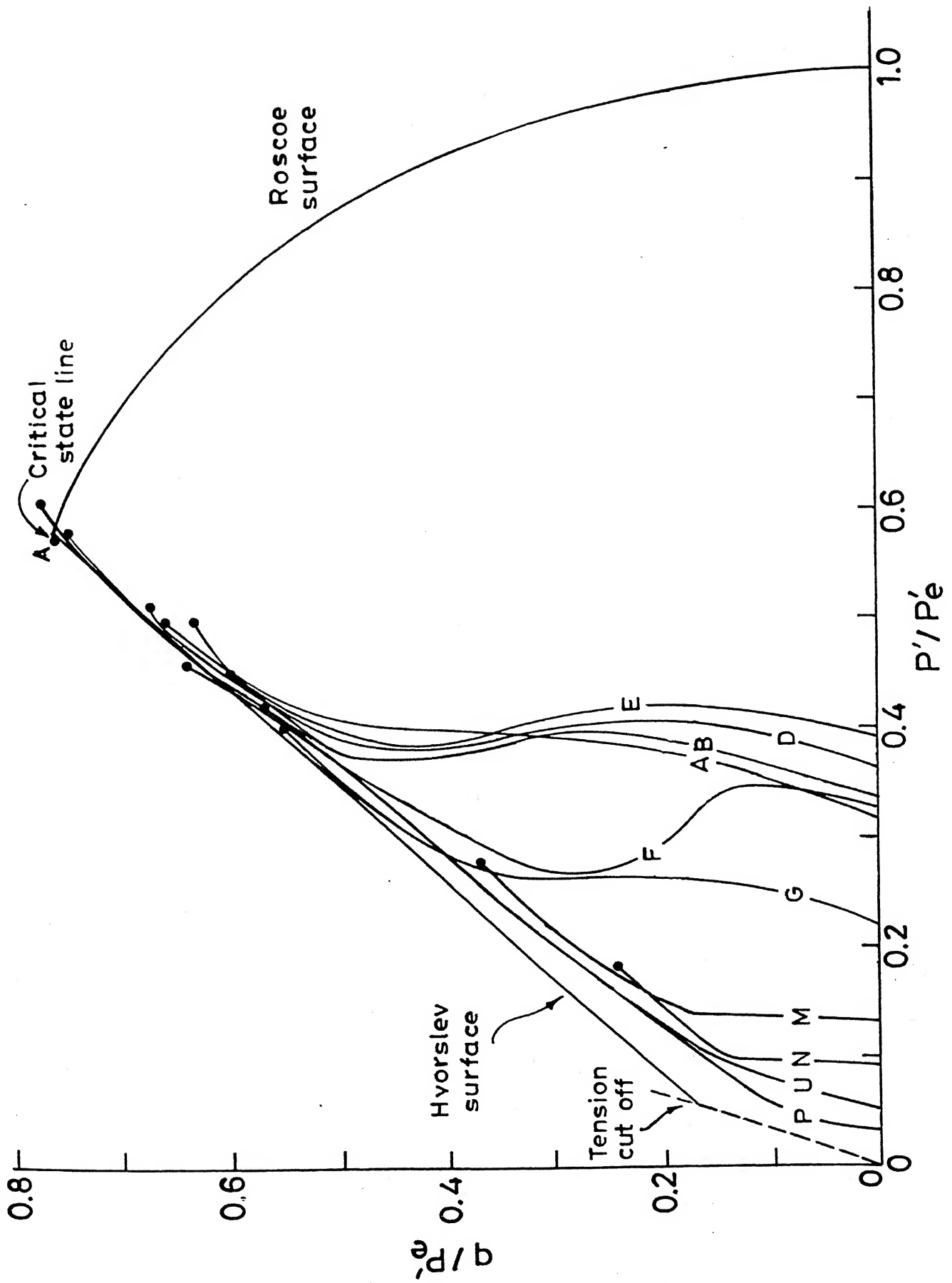


Fig. 4.82 q/P'_e versus P'/P'_e relationship for campus silt.

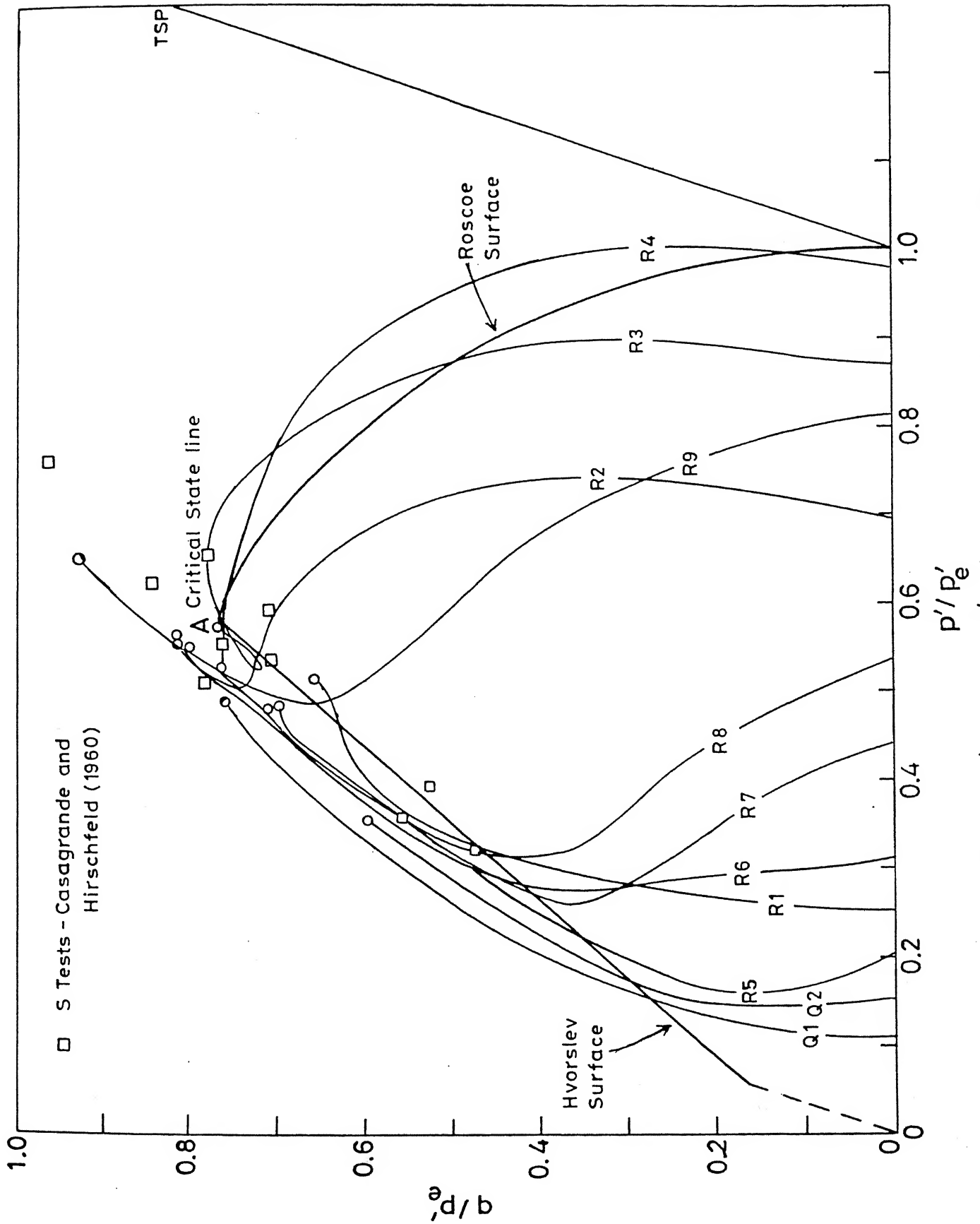


Fig. 4.83 q/P'_e versus p'/P'_e relationship for Canyon dam clay.

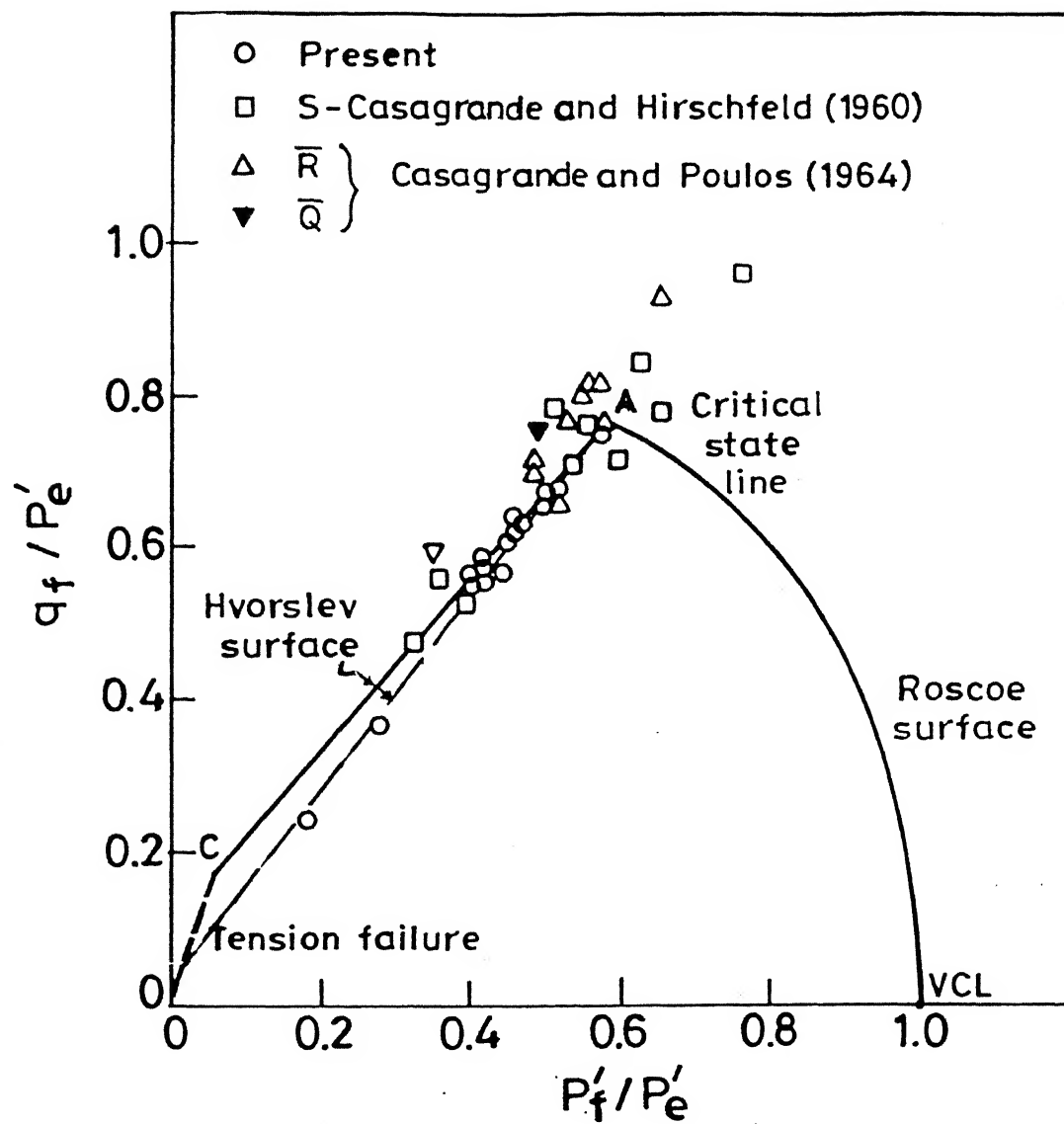


Fig. 4.84 q_f/P'_e versus p'_f/p'_e relationship.

Table 4.12 Calculation for Roscoe Surface

p'/p'_e	q/p'_e
1.00	0.000
0.95	0.325
0.90	0.450
0.85	0.537
0.80	0.600
0.75	0.658
0.70	0.700
0.65	0.733
0.60	0.758
0.58	0.766

Modified Cam Clay Equation :

$$p'/p'_e = \left[\frac{M^2}{M^2 + \eta^2} \right]^{0.78}$$

$$\eta = \frac{q/p'_e}{p/p'_e}$$

$$M = 1.31$$

up to confining stresses below that needed for complete saturation and like a normally consolidated clay when tested at effective confining stress equal to or greater than that needed for full saturation.

While all the tests in the present study depicted dilatant response similar to overconsolidated samples (Fig. 4.82), the sample R4 for Canyon dam clay (which was fully saturated) behaved almost like a normally consolidated clay and moved practically along the Roscoe surface (Fig. 4.83). Incidentally, the state paths for tests A, B, D and E in Fig. 4.82 do not reflect their exact nature as seen in corresponding samples for Canyon dam clay (Fig. 4.83) which were saturated by back pressure. This discrepancy, as explained earlier (Figs. 4.69 and 4.70) is due to the fact that given their low initial degree of saturation, they could not be quasi saturated and the pore pressure response in the early stages of the test (below the Hvorslev surface) may not be highly reliable (since the water voids are not continuous, see Fig. 4.66). However, after the state paths for these tests have reached the Hvorslev surface, they move along it towards the CSL in a manner similar to the other tests.

Notwithstanding various limitations of this analysis of available test data, one point seems quite clear that at low stress levels, the test results on compacted clays will lie on the Hvorslev surface tending to approach CSL at large strains (20 % in this case). That they behave as over consolidated soils, is also brought out in Fig. 4.85 where pore pressure

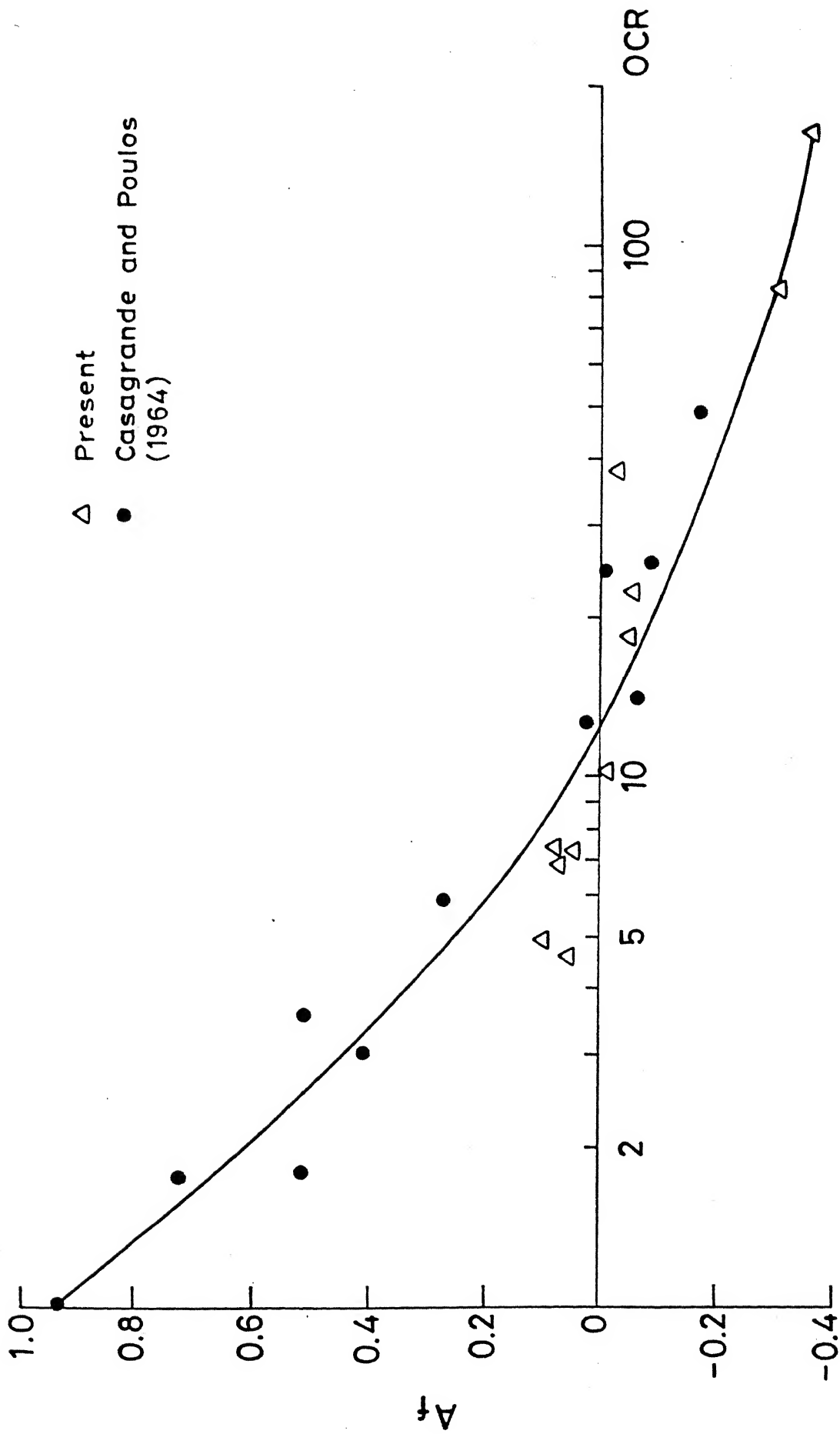


Fig. 4.85 Pore pressure parameter A_f versus OCR.

parameter A_f is plotted against over consolidation ratio, OCR. For calculating OCR, the past maximum pressure, depending on the initial moulding water content, was obtained from Fig. 4.79 as the value of P' where the recompression curve meets VCL.

4.8.3.5.3 Comparison in terms of total stress behaviour of compacted soils

Compacted soils are used for construction of embankments for transportation routes, dams, water supply reservoirs and as liners of beds of storage ponds built for containment of chemical industry effluent, mine tailings and fly ash slurry etc. Behaviour of as compacted samples, tested under - unconfined and confined conditions, in terms of total stresses hold considerable attraction for the practicing engineers since such a behaviour can be readily investigated without worrying about measurement of volume changes in drained or pore water / pore air pressure during undrained shear tests.

While simple correlations between undrained strength and index properties like plasticity index or liquidity index are available for saturated normally consolidated clays, no such simple correlations are available for compacted clays. Some suggestions in this regard [Weeraratne (1980) and Leroueil et al. (1992)] have been made which will be discussed in some detail in this section.

Leroueil et al. (1992) proposed that undrained strength of compacted samples (compacted using standard Proctor energy) based on unconfined test data, could be correlated with a

consistency index similar to the liquidity index commonly used for sedimentary soils. The index proposed is $(w - w_{opt})/I_p$, where w is the moulding water content, w_{opt} is the OMC and I_p being the plasticity index value. Based on comparison of some results for compacted clays, Leroueil et al (1992) have suggested that w_{opt} is approximately equal to water content corresponding to plastic limit. Yudhbir et al. (1980) have already proposed such an equivalence between OMC and plastic limit after examining significant data points for soil with plastic limit varying from 15 % to 85 %. Yudhbir et al. (1980) have further argued that such a relationship has a basic significance "considering the similarities between the deformation behaviour on either side of OMC and plastic limit."

Yudhbir and Weeraratne (1988) proposed that water content vs undrained strength for samples at and wet of OMC might be compared with the water content vs undrained strength relationships available for saturated remoulded soils. [For example, see Wroth and Wood (1978)].

The test results available from the present study for unconfined and confined tests, including data points for Canyon dam clay tested at high confining stress, are presented in Fig. 4.86. Results for samples that were softened at various stages (series A3), as discussed earlier, are also presented in Fig. 4.86. Some observations can be made from the trends indicated here as given below :

1. Samples compacted dry of optimum and tested either

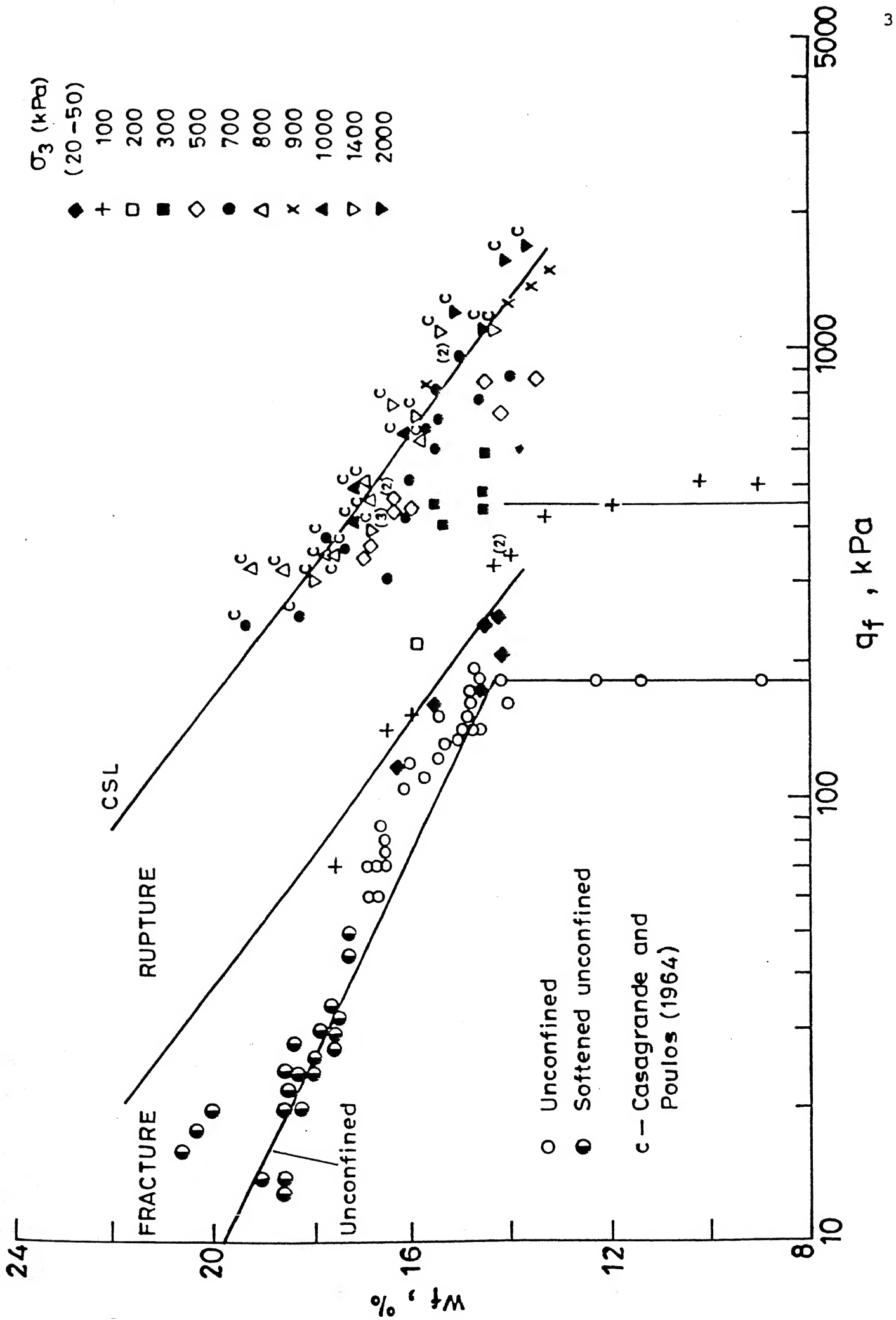


Fig.4.86 Water content versus strength relationship at failure.

unconfined or with $\sigma_3 = 100$ kPa show practically constant value of $q_f = (\sigma_1 - \sigma_3)_f$ up to OMC after which the values of q_f decrease with increasing water content. In each case for $w < \text{OMC}$, the samples experienced brittle failure with pronounced vertical splitting. At higher water content (up to 16 %) both unconfined and those with $\sigma_3 = 20$ kPa showed brittle failure with a stepped failure surface (including vertical portion also) ; for $w > 16\%$, however, samples exhibited pronounced bulging with no well defined failure plane. For $\sigma_3 > 20$ kPa and $w > \text{OMC}$, the sample showed bulging and a well defined failure plane for all the samples tested.

2. For both softened and unsoftened unconfined tests, there is a unique w vs q_f relationship which lies to the left of the fracture - rupture (F - R) boundary as suggested by Yudhbir and Wood (1989). While the low confining stress data ($20 < \sigma_3 < 100$ kPa) lies on the F - R boundary, the results for samples with $\sigma_3 \geq 700$ kPa seem to scatter along the projection of CSL in this space. The F - R boundary in this space corresponds to the projection of the tension cut off line shown in Fig. 4.84.

Figure 4.87 shows the relationship between undrained strength, s_u and $(w - w_{\text{opt}})/I_p$ for Campus silt, CL and CH soils along with the proposal made by Leroueil et al. (1992). The observations made from Fig. 4.86 are again born out by the patterns seen in Fig. 4.87. It may be suggested that for $(w - w_{\text{opt}})/I_p$ equal to -0.025 (dry of OMC), the compacted samples

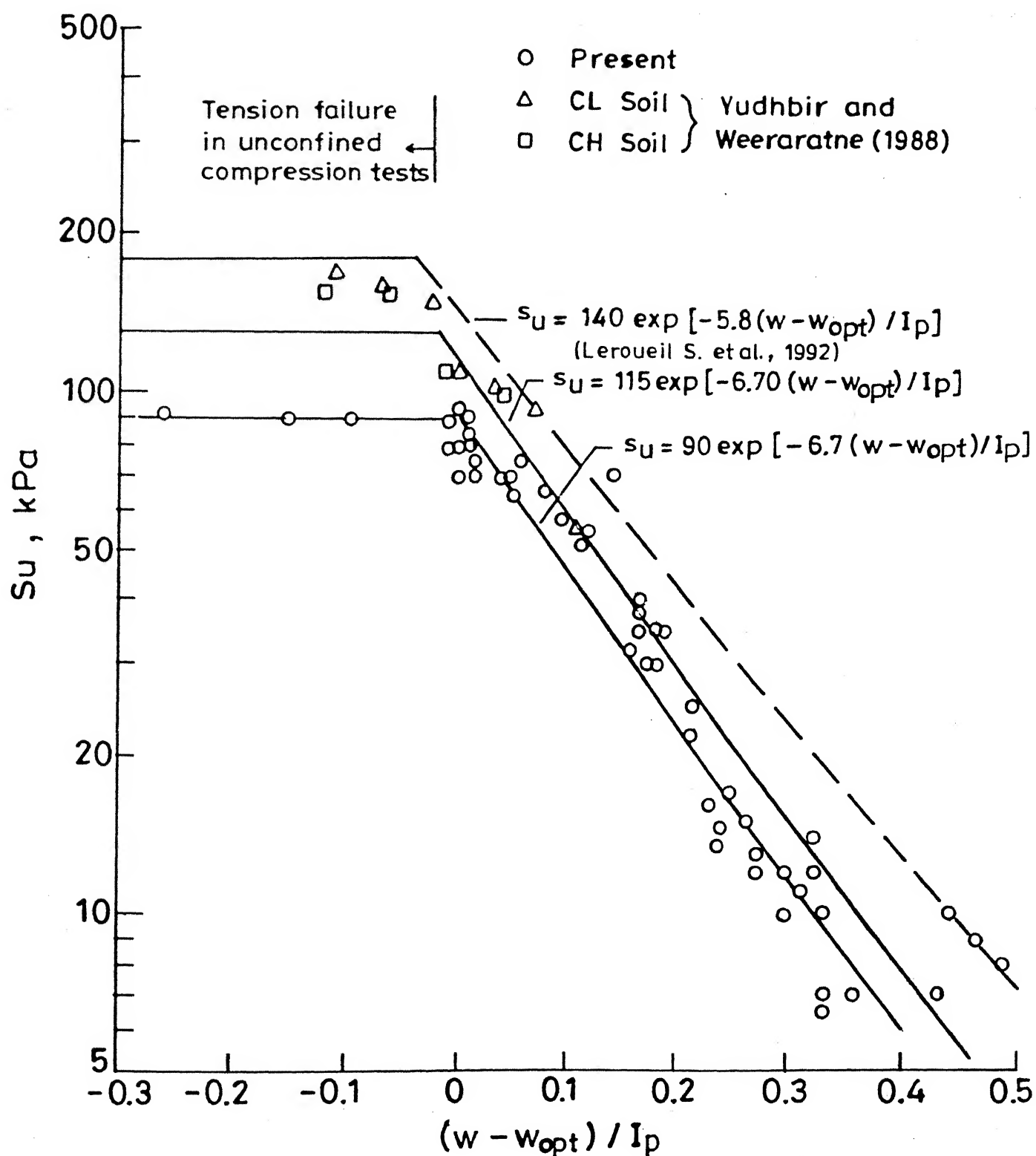


Fig. 4.87 Variation of s_u with $(w - w_{opt}) / I_p$.

will fail in tension during unconfined compression tests and the value of s_u (varying from 90 to 180 kPa) is practically constant with water content. Furthermore, a unique s_u vs $(w - w_{opt})/I_p$ relationship for compacted soils (wet of OMC) may be represented as follows :

$$s_u = 115 \exp [-6.7 (w - w_{opt})/I_p] \quad (4.4)$$

which may be expressed as :

$$(w - w_{opt})/I_p = 0.708 - 0.15 \ln (s_u) \quad (4.5)$$

It may be noted that water content vs s_u type relationships are valid for shear failure mechanism only and should not be extrapolated in the tension failure region. It will also be seen that the value of unconfined strength at OMC (standard Proctor energy level ; both Proctor and Harvard miniature tests) may be taken as 115 ± 35 kPa for a variety of soils having plasticity index values ranging from 11 % to 47 %.

4.8.4 Effective Stress Behaviour of Compacted Campus silt under Cyclic Load Condition and Evaluation of Threshold Stress

4.8.4.1 Plastic strain development

Development of plastic strain is of considerable importance in the design of railway formations and in the

prediction of maintenance life of track.

The development of cumulative plastic strain, ϵ_p , with number of load cycles during undrained shear is shown in Figs. 4.88 and 4.89 for back saturated samples (Table 4.13). It will be seen that at low values of cyclic stress level, R_f , ϵ_p values attain a maximum at N approximately equal to 50 to 60 after which practically no more increase in plastic deformation occurs. However, above a certain stress level - called threshold stress in this study - the ϵ_p value, for the same number of cycles, shows a sudden increase in magnitude. Amount of cumulative plastic strain in 100 cycles is seen to increase with increasing value of R_f .

In Fig. 4.90 are the results of tests on quasi-saturated samples (which also follow the pattern depicted in Fig. 4.69); the tests H, I and K have comparable σ_c' values 285-385 kPa where as test L was conducted at $\sigma_c' = 163$ kPa. For comparable σ_c' , the ϵ_p value shows increase with increasing R_f as noted for low σ_c' tests in Figs. 4.88 and 4.89. From these results (Figs. 4.89 and 4.90), a general expected trend of decreasing ϵ_p after 100 cycles with σ_c' is observed. This finding is same as observed by Janin et. al. (1980) during drained cyclic loading. The data for the test O with $\sigma_c' = 20$ kPa (Fig. 4.88) appears to be corresponding to R_f value slightly less than the corresponding threshold stress value. Incidentally, the corresponding value of ϵ_p after 100 cycles, at threshold stress level, in case of unconfined tests on samples compacted at OMC is of the order of 6 % (Fig. 4.91).

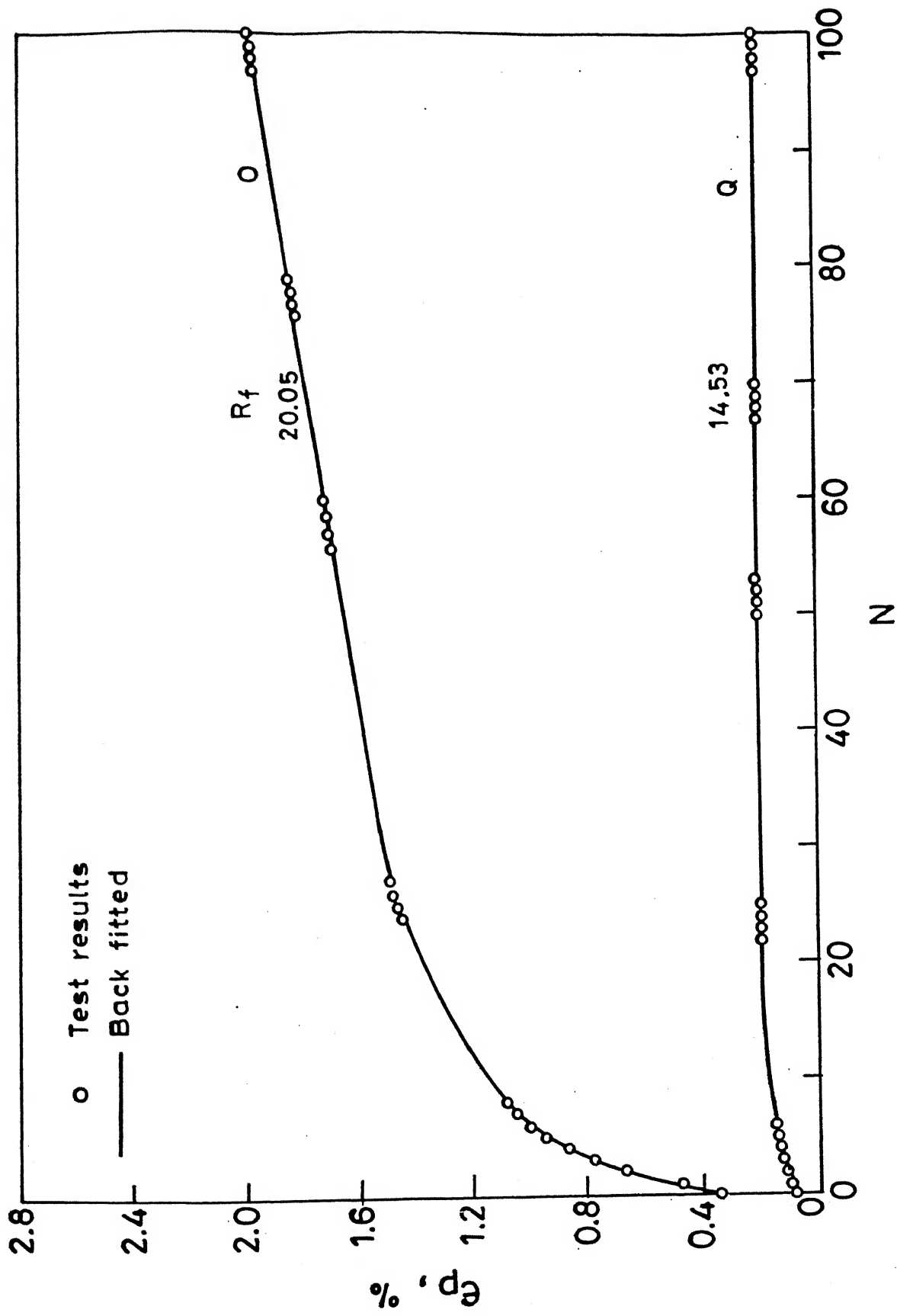


Fig. 4.88 Increase in plastic strain with cyclic loading ($\sigma'_c = 20\text{-}22\text{ kPa}$)

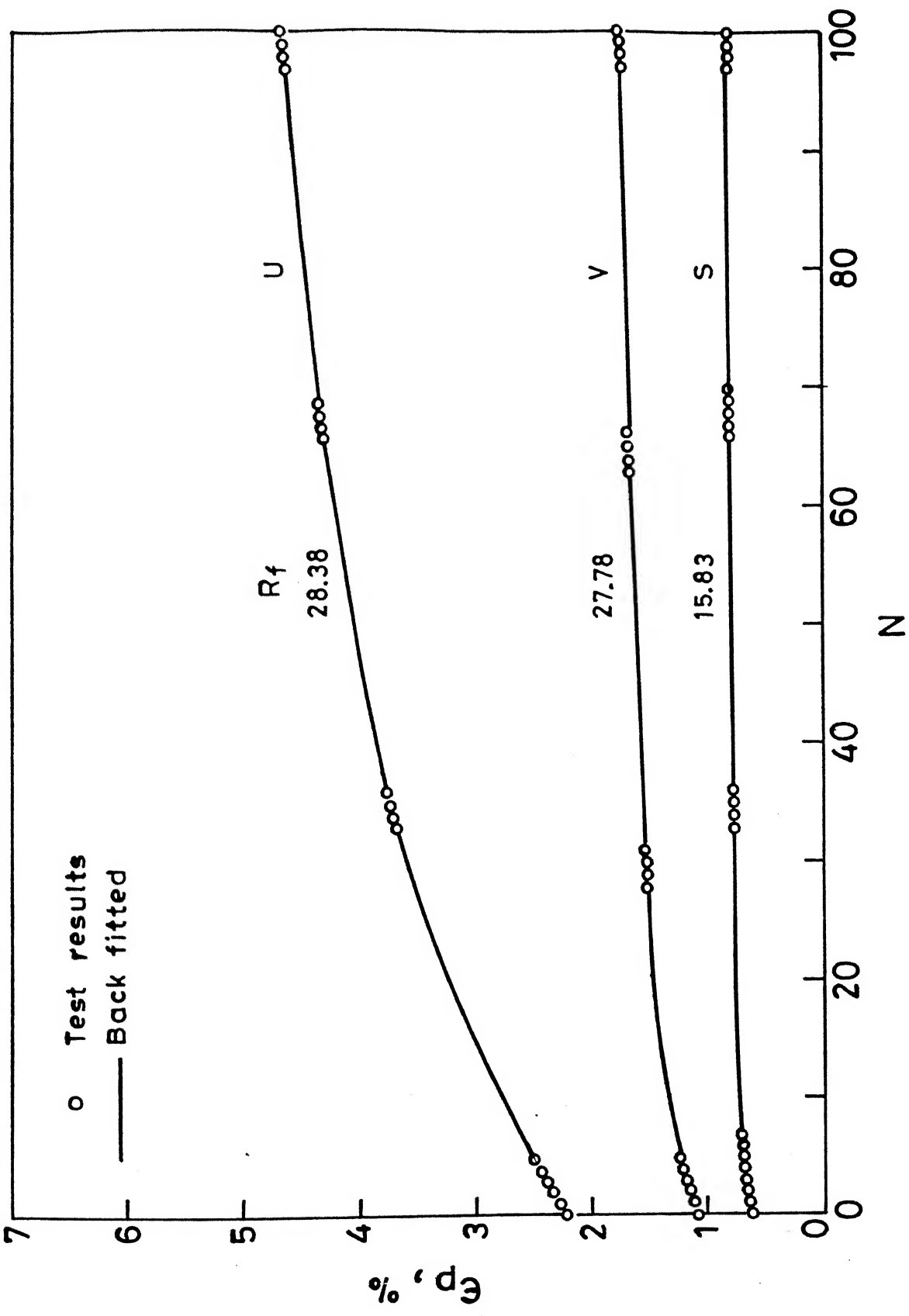


Fig. 4.89 Increase in plastic strain with cyclic loading ($\sigma'_c = 40 \text{ kPa}$)

Table 4.13 Additional data related to cyclic tests on Campus silt.

Test Curve	R _f C%	ε _p (before cyc) C%	ε _p (after 100 cyc) C%	ε _p (during 100 cyc) C%	Δu (during 100 cyc) CkPa)	Extrapolated stress level where	
						(Δu) _{max} occurs (kPa)	(σ ₁ - σ ₃)/2
High σ' _c							
K	37.68	1.37	2.91	1.54	59	260	150
H	18.52	0.20	0.53	0.33	44	290	160
I	31.82	0.45	1.10	0.65	118	330	180
L	31.37	2.00	3.90	1.90	26	160	98
σ' _c = (20 - 22) KPa							
O	20.05	0.32	1.98	1.66	--	---	---
Q	14.53	0.08	0.2	0.12	--	---	---
σ' _c = 40 KPa							
V	27.78	1.05	1.75	0.70	--	---	---
S	15.83	0.60	0.80	0.20	--	---	---
U	28.38	2.20	4.65	2.45	--	---	---

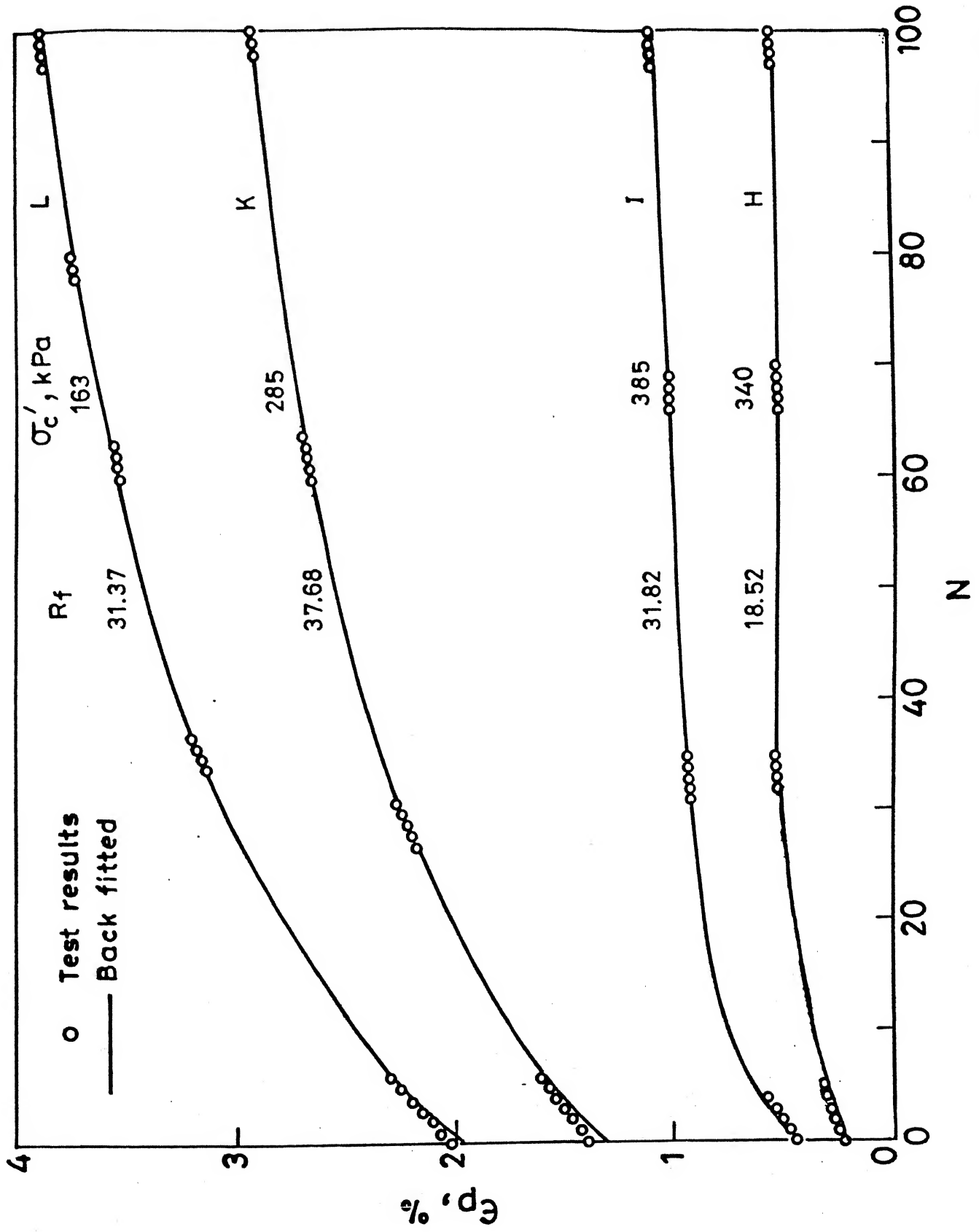


Fig. 4.90 Increase in plastic strain with cyclic loading (high confining pressure)

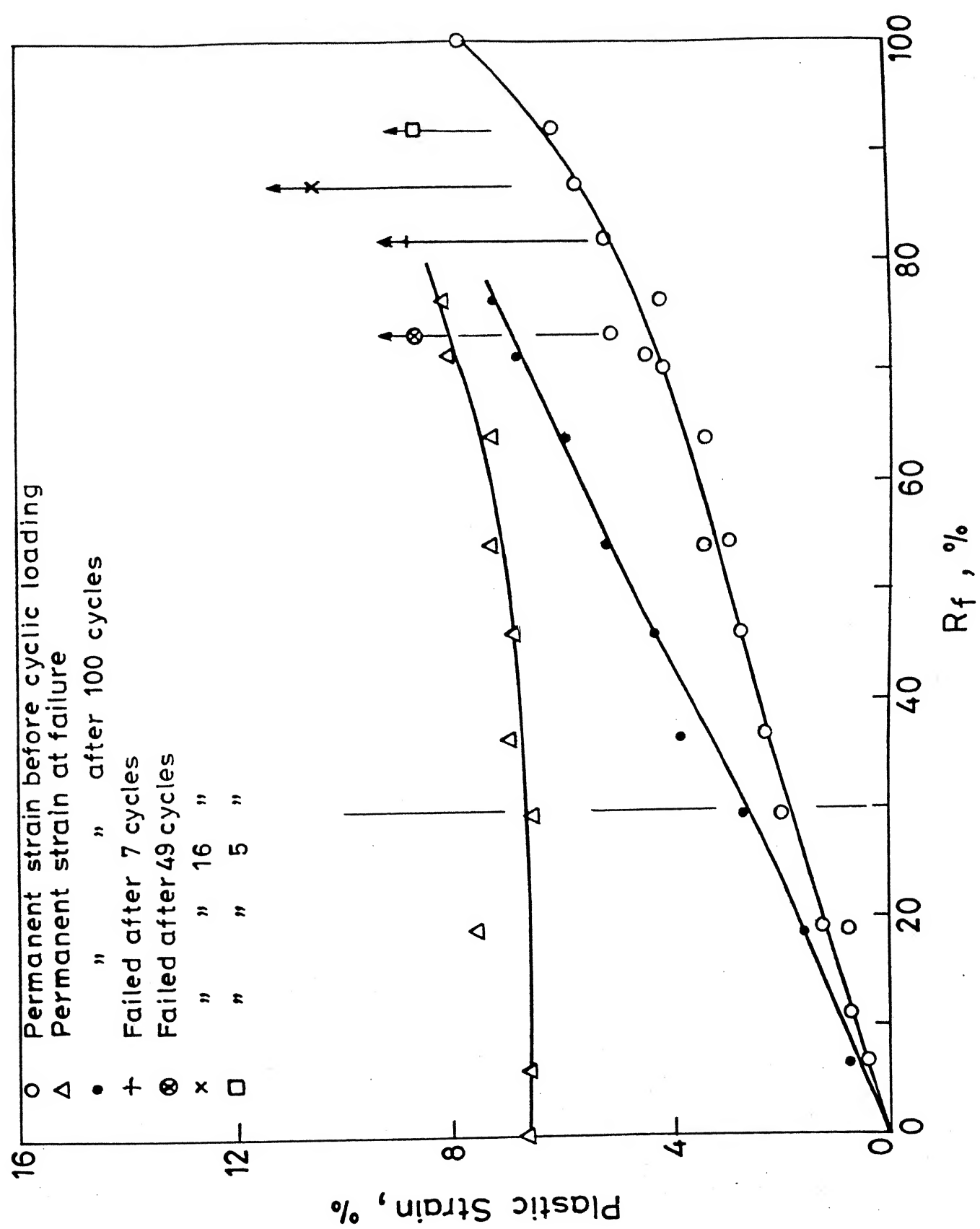


Fig. 4.91 Plastic strain versus R_f for unconfined cyclic tests.

Cumulative plastic deformation has been used as a criterion by the railway engineers for both design and maintenance aspects of the track. On the basis of results presented above and those available in literature for other soils (Figs. 4.92 and 4.93), tested in a similar manner, the following formulation to relate ϵ_p with number of cycles taking into account the effect of cyclic stress level has been suggested :

$$\log (\epsilon_p) = C_p + D_p \log (N_1) + E_p \log (N_2/N_s) \quad (4.6)$$

where $N_1 = N$ and $N_2/N_s = 1$ for $N \leq N_s$
 $N_1 = N_s$ and $N_2 = N$ for $N > N_s$

and C_p = value of $\log (\epsilon_p)$ at $N = 1$,
 D_p = first gradient of the bilinear log-log plot
between ϵ_p and N ,
 E_p = second gradient of the bilinear log-log plot
between ϵ_p and N after $N = N_2 > N_s$,
 N_s = value of N where the change in gradient from
 D_p to E_p occurs, and
 ϵ_p = plastic strain in percent.

The values of parameters C_p , D_p and E_p are shown in Table 4.14. In general, it will be seen that for samples cycled at or above threshold stress level, N_s is of the order of 2 - 8 where as for samples cycled below threshold stress level, N_s values

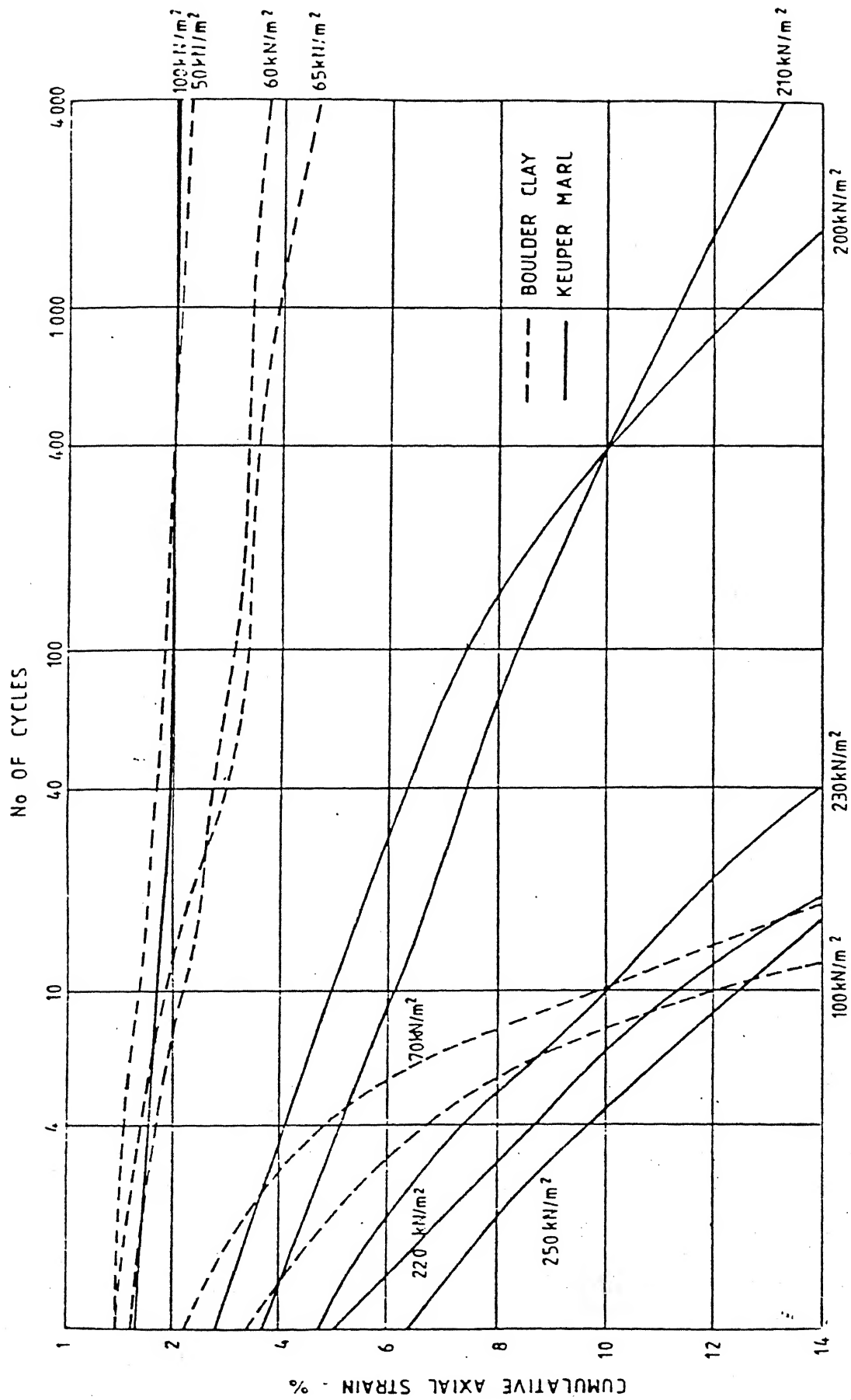


FIG. 4.92 CYCLIC LOAD TRIAXIAL TESTS - PERMANENT STRAIN v. No. OF CYCLES (JANIN ET AL., 1983A)

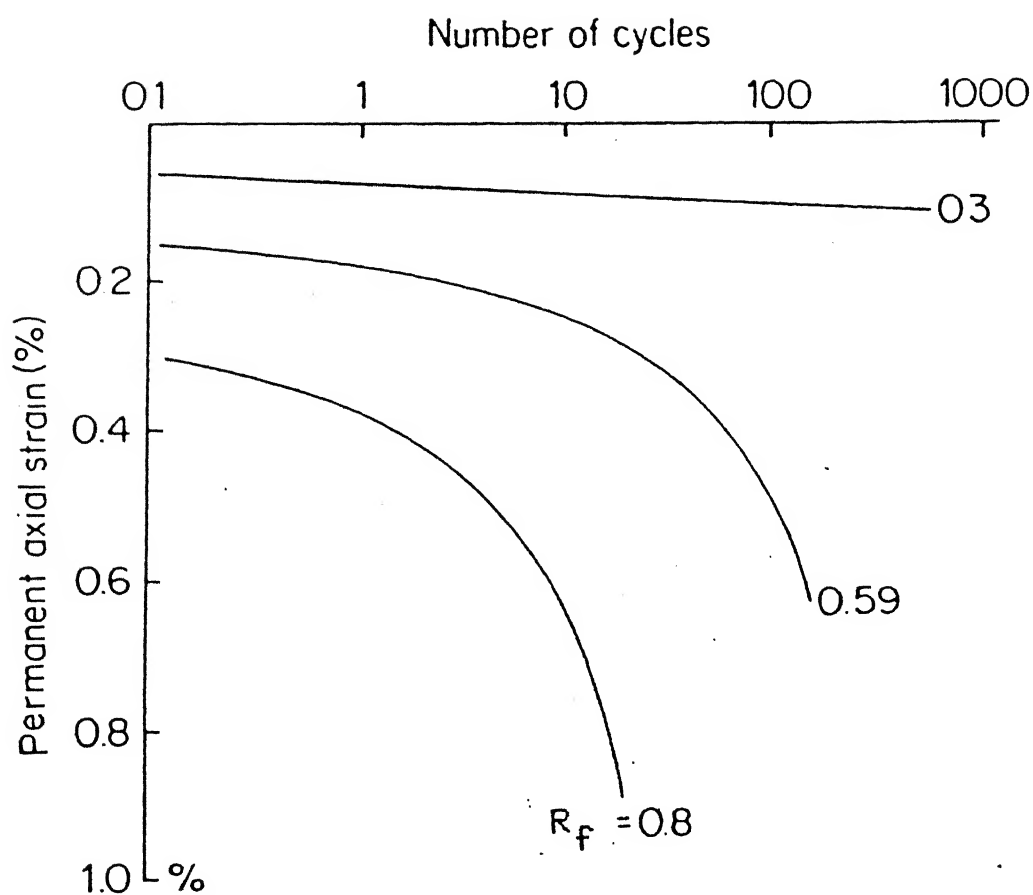


Fig 4.93 Development of permanent axial strain in cyclic triaxial undrained compression tests on lacustrine clay from Hamilton, Ontario (after Wilson and Greenwood, 1974)
Frequency 1/120 Hz

Table 4.14 Value of coefficients in plastic strain model

$$\log(\epsilon_p) = C_p + D_p \log(N_1) + E_p \log(N_2/N_s)$$

$$\text{where, } N_1 = N \text{ and } N_2/N_s = 1 \text{ for } N \leq N_s$$

$$N_1 = N_s \text{ and } N_2 = N \text{ for } N > N_s$$

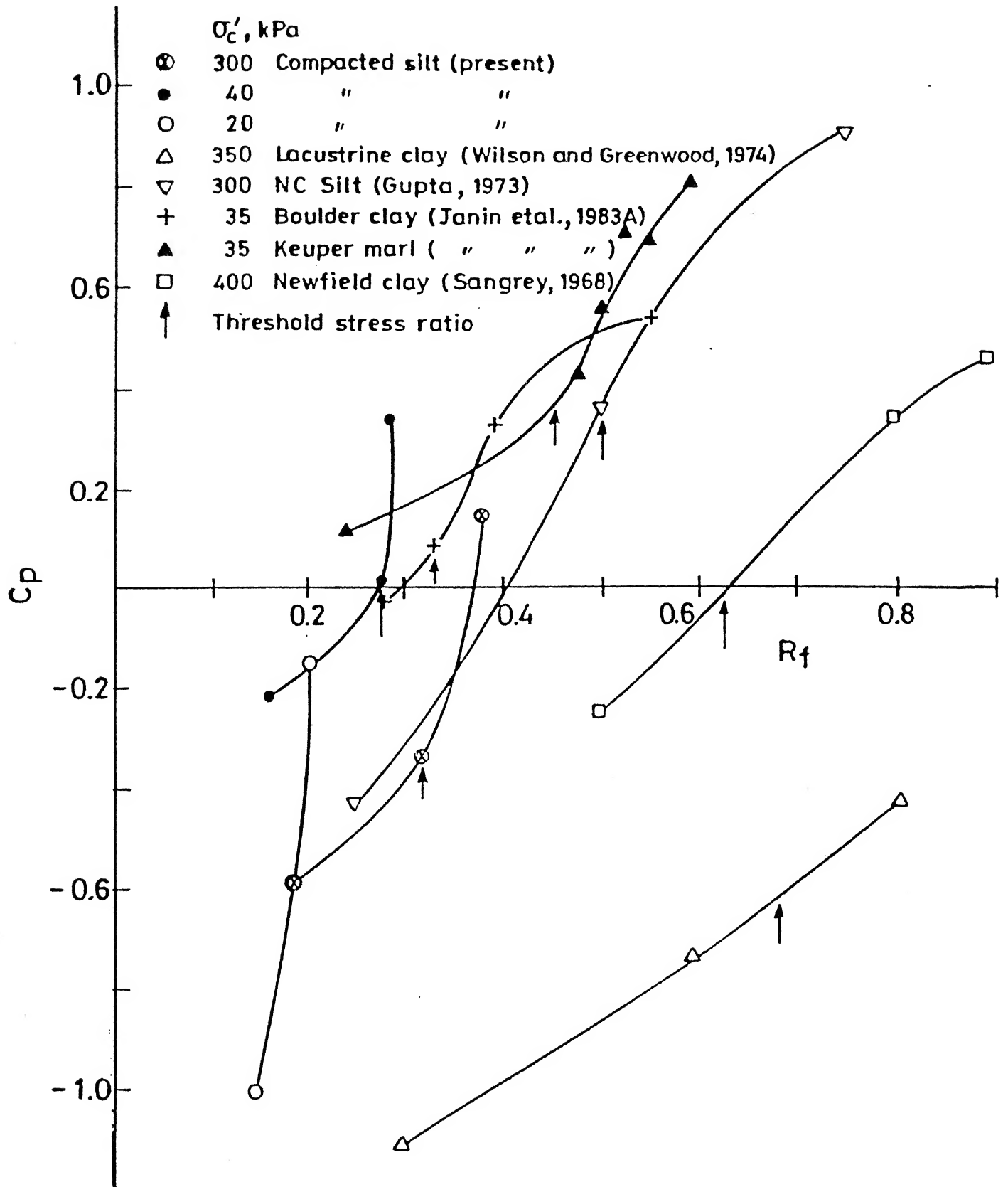
Test	R _f (%)	σ _c ' (kPa)	C _p	D _p	E _p	N _s	R _{TS} (%)	REMARK		
H	18.52	340	-0.593	0.167	0	56	0.37	COMPACTED BACKSATURATED CAMPUS SILT (PRESENT) I _p = 14		
I	31.82	385	-0.337	0.195		OOS*				
K	37.68	285	0.148	0.058	0.234	7				
L	31.37	163	0.305	0.064	0.205	8				
Q	14.53	22	-1.000	0.209	0	25	0.201			
O	20.05	20	-0.150	0.220		OOS				
S	15.83	40	-0.215	0.078	0	33	0.28			
V	27.78	40	0.013	0.117		OOS				
U	28.38	40	0.342	0.072	0.207	5				
L1	80.00	350	-0.430	0.083	0.392	5	0.68	NC UNDISTURBED LACUSTRINE CLAY, HAMILTON. I = 14 WILSON AND GREENWOOD (1974)		
L2	59.00	350	-0.740	0.111	0.462	26				
L3	30.00	350	-1.108	0.032		OOS				
B1	55.00	35	0.544		0.520	OOS	0.36	UNDISTURBED BOULDER CLAY I _p = 17 JANIN ET AL., (1983a)		
B2	39.00	35	0.332		0.520	OOS				
B3	33.00	35	0.086	0.217	0.071	40				
B4	27.80	35	-0.022	0.139	0.052	40				
K1	59.50	35	0.810		0.280	OOS	0.45	UNDISTURBED KEUPER MARL I _p = 15 JANIN ET AL., (1983a)		
K2	52.30	35	0.707		0.342	OOS				
K3	55.00	35	0.690		0.292	OOS				
K4	50.00	35	0.560		0.272	OOS				
K5	48.00	35	0.430		0.240	OOS				
K6	24.00	35	0.114	0.193	0	40				
S1	49.00	393	-0.300	0.176		OOS	0.625	NC UNDISTURBED NEWFIELD CLAY I _p = (17 - 19) % SANGREY (1968)		
S2	80.00	393	0.342	0.265	0.820	2				
S3	89.00	393	0.467		0.560	OOS				

* OOS - only one slope

are greater than 25. Thus, the contribution from the first gradient (D_p) with $N \leq N_s$ is of not much interest in estimating long term ϵ_p values. However, the second gradient (E_p) will control, depending on the cyclic stress level [i.e. C_p value in Eq. (4.6), see Fig. 4.94], the magnitude of long-term plastic deformation under large number of cycles (say 10^6).

The variation of C_p with R_f (Fig. 4.94) tends to suggest a consistent pattern for compacted and undisturbed low plasticity silty soils. The normally consolidated undisturbed and remoulded soils of comparable plasticity also show another consistent pattern.

The variation of E_p values with R_f , however, shows sudden changes in magnitude for $R_f \geq R_{TS}$. It is suggested that for $R_f < R_{TS}$, E_p value is less than D_p or equal to zero and a stable deformation behaviour is exhibited during undrained cyclic loading. For $R_f \geq R_{TS}$, both $E_p = D_p$ and $E_p > D_p$ trends are seen from the available results and the sample exhibits increasing ϵ_p value with increasing N . Here again, the stiff undisturbed and compacted samples of comparable plasticity show similar trends where as the normally consolidated undisturbed and remoulded soils of comparable plasticity depict another pattern of behaviour. From the limited test results, it would appear that for $R_f > R_{TS}$, E_p value may be taken as constant for a given soil. A similar observation on the basis of drained cyclic loading tests on undisturbed samples of London clays, has been made by Rubin et al. (1970) who suggest a similar ϵ_p vs. N relationship :

Fig. 4.94 C_p versus R_f

$$\log (\varepsilon_p) = 1.39 \varepsilon_e - 1.74 + 0.622 \log N \quad (4.7)$$

for London clay. Here ε_e is the average elastic strain in percent, which is independent of number of cycles and is function of cyclic stress level. Incidentally, the term $(1.39 \varepsilon_e - 1.74)$ in Eq. (4.7) compares with the contribution to ε_p from $C_p + D_p \log N_1$ ($N_1 = N_s$) term given in Eq. (4.6). Rubin et al. (1970) propose $E_p = 0.622$ for London clays. $E_p = 0.52$ and $E_p = 0.28$ have been evaluated for Boulder clay and Keuper marl [Janin et al. (1983a)] from drained cyclic tests on undisturbed samples. The corresponding value for the Campus silt is of the order of 0.22.

Hyde and Brown (1976) examine this problem in terms of rate of change of plastic strain, $\dot{\varepsilon}_p$ rather than ε_p . They also propose a log-log relationship of the form :

$$\log (\dot{\varepsilon}_p) = C - D \log T \quad (4.8)$$

where T is the time, in seconds of application of cyclic load of a given intensity. A similar $\dot{\varepsilon}_p$ vs N relationship was examined and the following form of the relationship is obtained

$$\log (\dot{\varepsilon}_p) = C_p + D_p \log (N_s) + E_p \log (N/N_s) + \log (E_p/N) \quad (4.9)$$

with $E_p = 0.22$, $D_p = 0.072$ and $N_s = 8$ at $R_f \geq R_{TS}$ ($\sigma_c' = 40$

kPa), for Campus silt, the value of $\dot{\epsilon}_p$ for $N = 10^6$ works out as :

$$\begin{aligned}\log(\dot{\epsilon}_p) &= 0.342 + 0.072 \log(8) + 0.22 \log(10^6/8) + \log(0.22/10^6) \\ &= 2.88 \times 10^{-6} \text{ percent per cycle.}\end{aligned}$$

which is not significant.

Plastic strain rate decreases approximately by a factor of 10 for every log cycle increase in N values. This agrees with the observations of Hyde and Brown (1976).

While the threshold stress level is being used here as the governing factor in design, the real condition governing the performance of railway track is the cumulative deformation which may be indicated in terms of ϵ_p . For example, Rubin et al. (1970) recommend $\epsilon_p < 10\%$ in 1000 cycles as a failure criterion in laboratory tests. The response of compacted Campus silt at $\sigma'_c = 40$ kPa, according to this criterion is :

(1) $R_f > R_{TS}$, Test U :

$$C_p = 0.342 ; D_p = 0.072 ; E_p = 0.207 ; N_s = 5 \text{ and } N = 1000$$

(Table 4.14),

ϵ_p from Eq. (4.6) is obtained as 10.3 percent.

(2) $R_f = R_{TS}$, Test V :

$$C_p = 0.0128 ; D_p = 0.1175 ; E_p = 0 ; N_s \text{ does not exist and } N = 1000$$

(Table 4.14),

ϵ_p from Eq. (4.6) is obtained as 2.3 percent.

(3) $R_f < R_{TS}$, Test S :

$C_p = -0.215$, $D_p = 0.078$, $E_p = 0$ and $N_s = 33$ and $N = 1000$ (Table 4.14),

ε_p from Eq. (4.6) is obtained as 0.8 percent.

This would support the suggestion in this study that the design stress level should be less than R_{TS} .

4.8.4.2 Pore pressure response during cyclic loading

In general, considerable amount of research work, related to pore pressure development during undrained cyclic loading, with special reference to problems of liquefaction in case of sands during earthquake loading and excessive deformation associated with wave loading of offshore structures for both sands and clays, has been carried out using both triaxial and cyclic simple shear equipments [see Wood (1982) ; Anderson and Hoeg (1992)].

Figure 4.95 depicts typical response of quasi-saturated compacted Campus silt samples during undrained cyclic loading. The pore pressure response is governed by the magnitude of the cyclic stress level, σ_c' value and the relative position of the cyclic stress level as compared to the failure envelope (Fig. 4.96). For example, test L has $\sigma_c' = 163$ kPa, $(\sigma_1 - \sigma_3)_{cyc} = 160$ kPa and after some number of cycles ($N \approx 80$) the pore pressures generated move point 4 in Fig. 4.96 on to the failure envelope and further cyclic loading beyond that shows slight decrease as

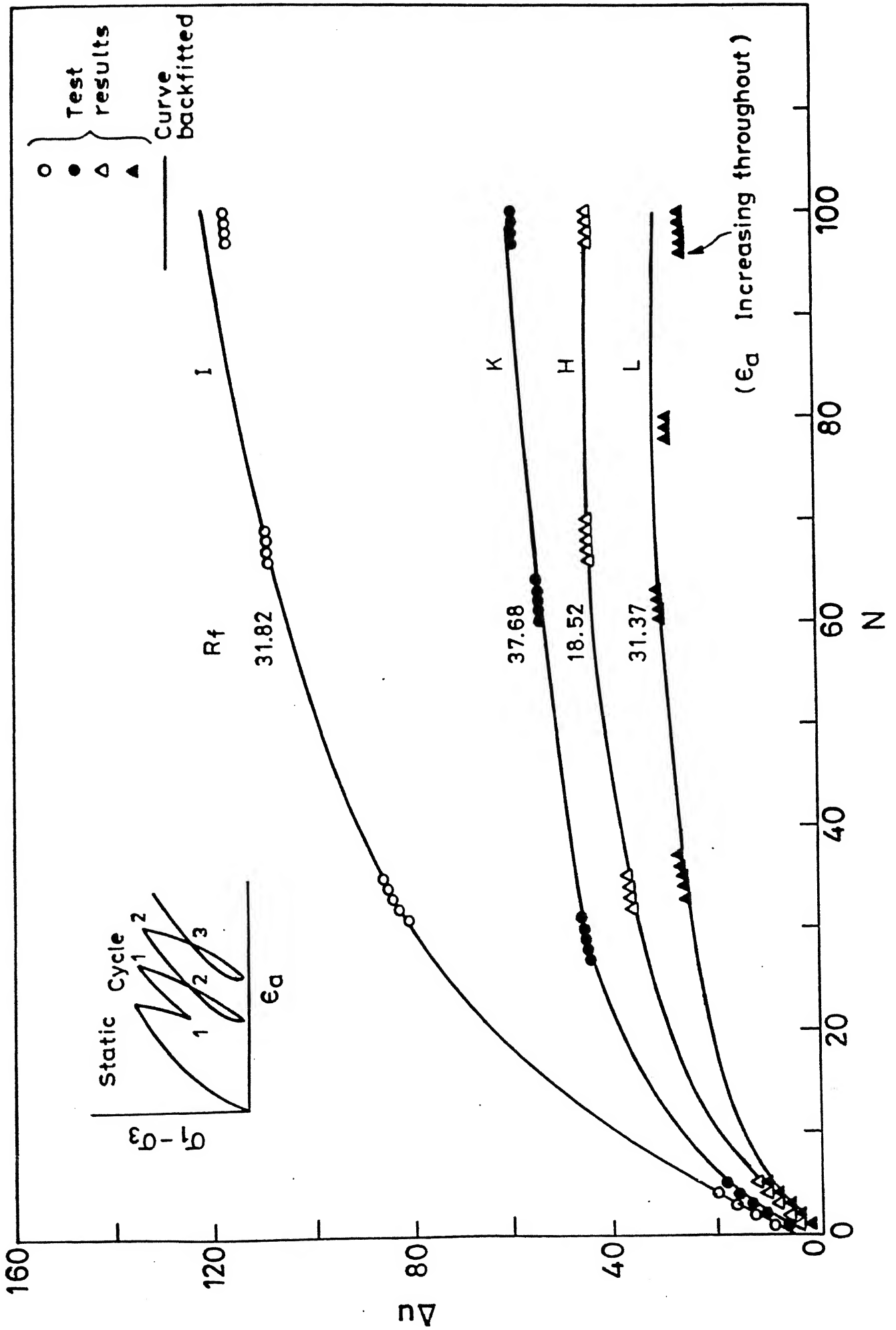


Fig. 4.95 Pore pressure rise with number of cycles.

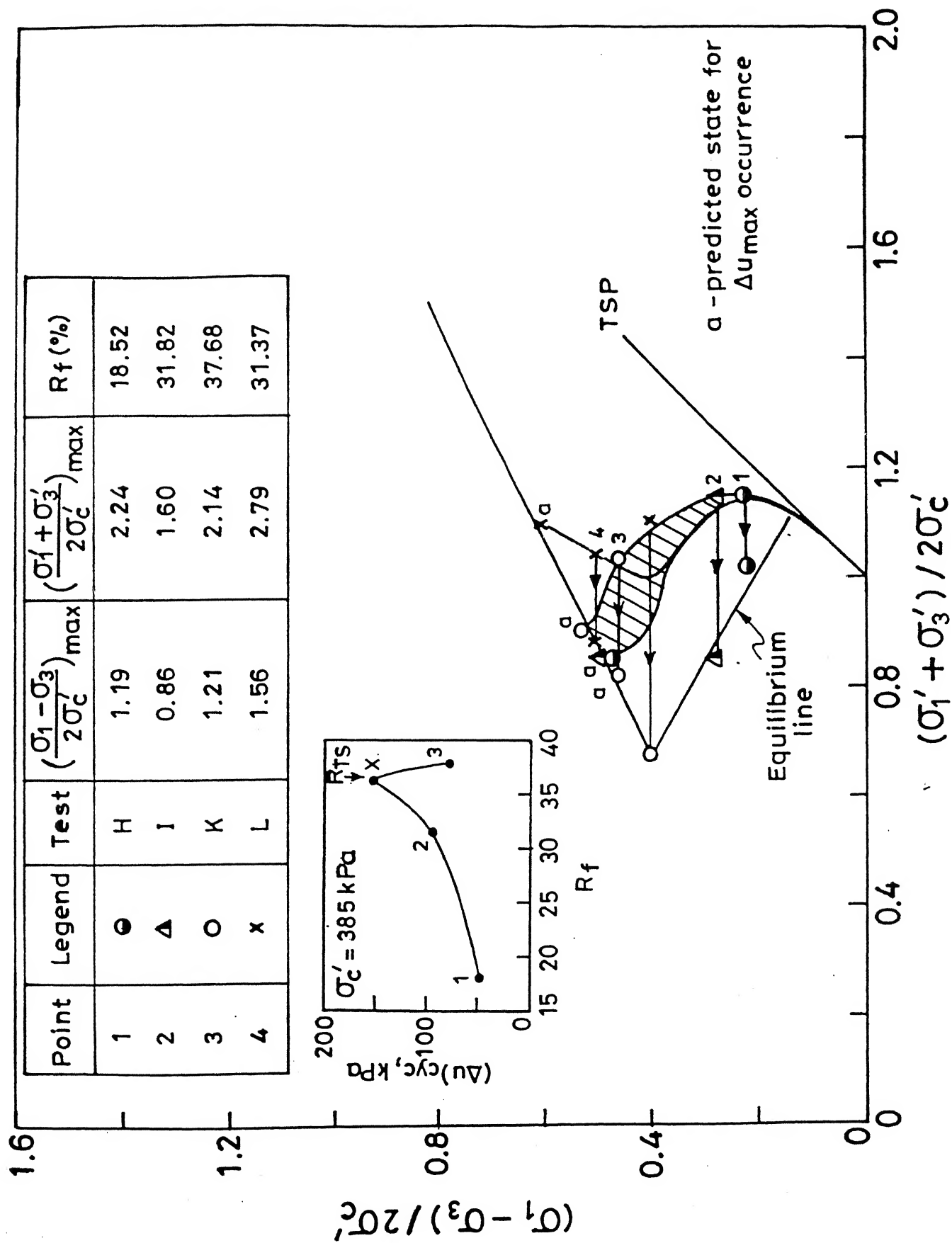


Fig.4.96 Normalized effective stress path for cyclic tests with high confining pressure.

would be expected from the highly dilatant character of the material (test K would also show similar response for $N > 100$). On the other hand, tests H and I (Figs. 4.95 and 4.96) where $R_f \leq R_{TS}$, would show a tendency to attain a constant value of pore pressure as the effective stresses approach the Sangrey's equilibrium line [Sangrey (1968)]; of course, test I, having R_f greater than the corresponding value for test H, shows larger magnitude of the pore pressures generated in 100 load cycles.

The effect of confining stress has been normalized in Fig. 4.97, the maximum dilatancy (-ve pressure) at failure is ordered according to the σ_c' values -- lowest for $\sigma_c' = 385$ kPa (test I) and highest for $\sigma_c' = 163$ kPa (test L).

Incidentally, Hyde and Ward (1985) have proposed that end points of cyclic load tests would lie on the Hvorslev surface as represented in q/P_e' vs P'/P_e' space. A similar result is indicated in Fig. 4.98 for cyclic test data for Campus silt. In fact, the location of Hvorslev surface has scope for adjustment as already seen in Figs. 4.82, 4.83 and 4.84. While fixing the position of the Hvorslev surface, location of critical state and tension cut off was obtained from the guidelines suggested by Yudhbir and Wood (1989), however, the experimental data would suggest a low intercept on q/P_e' axis and therefore a slightly steeper slope of the Hvorslev surface (Fig. 4.84). This adjustment would bring the Hvorslev surface in Fig. 4.98 close to the end points of cyclic loading in tests L and K which were cycled at $R_f > R_{TS}$.

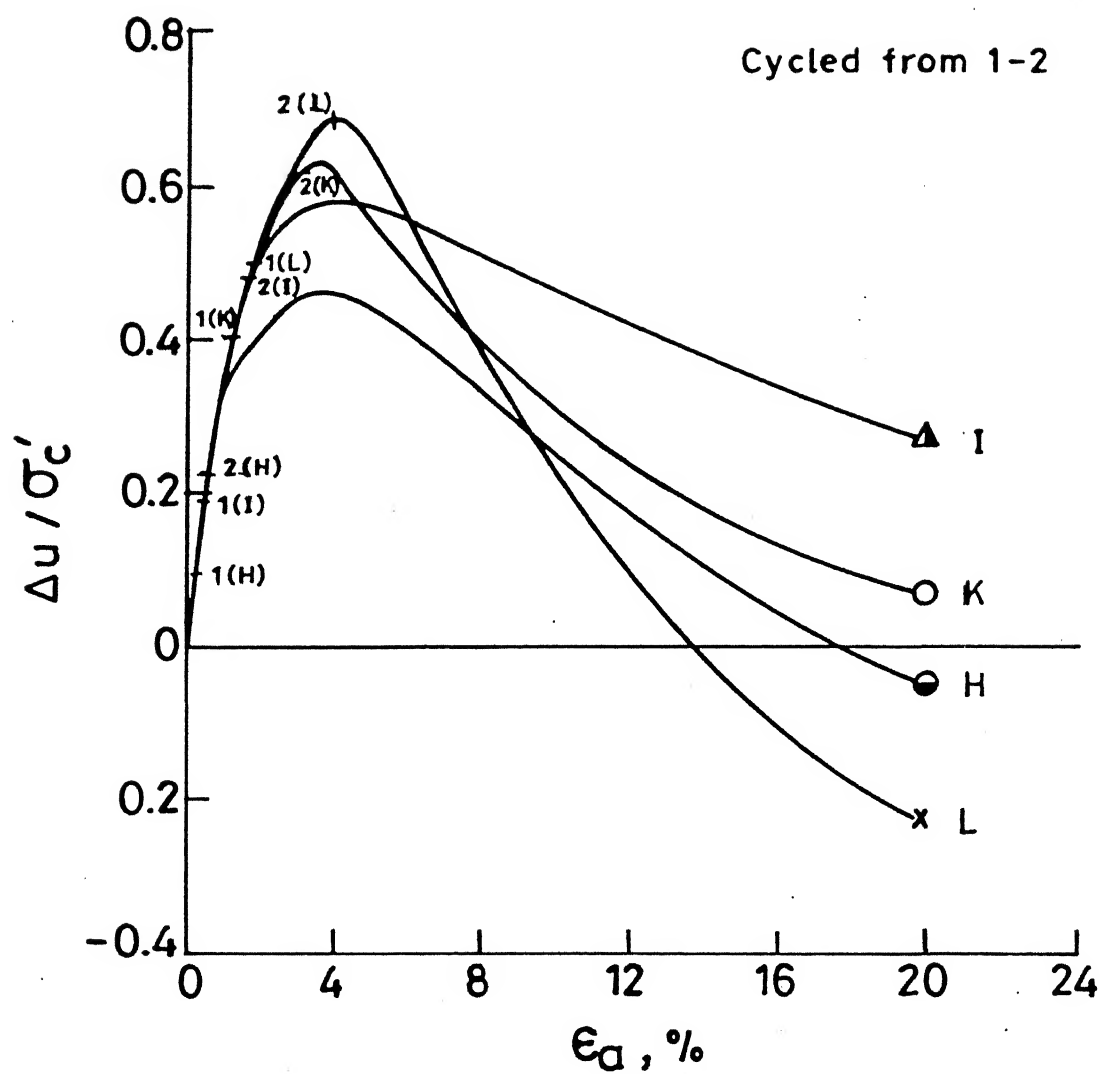


Fig. 4.97 Normalized pore pressure rise with axial strain.

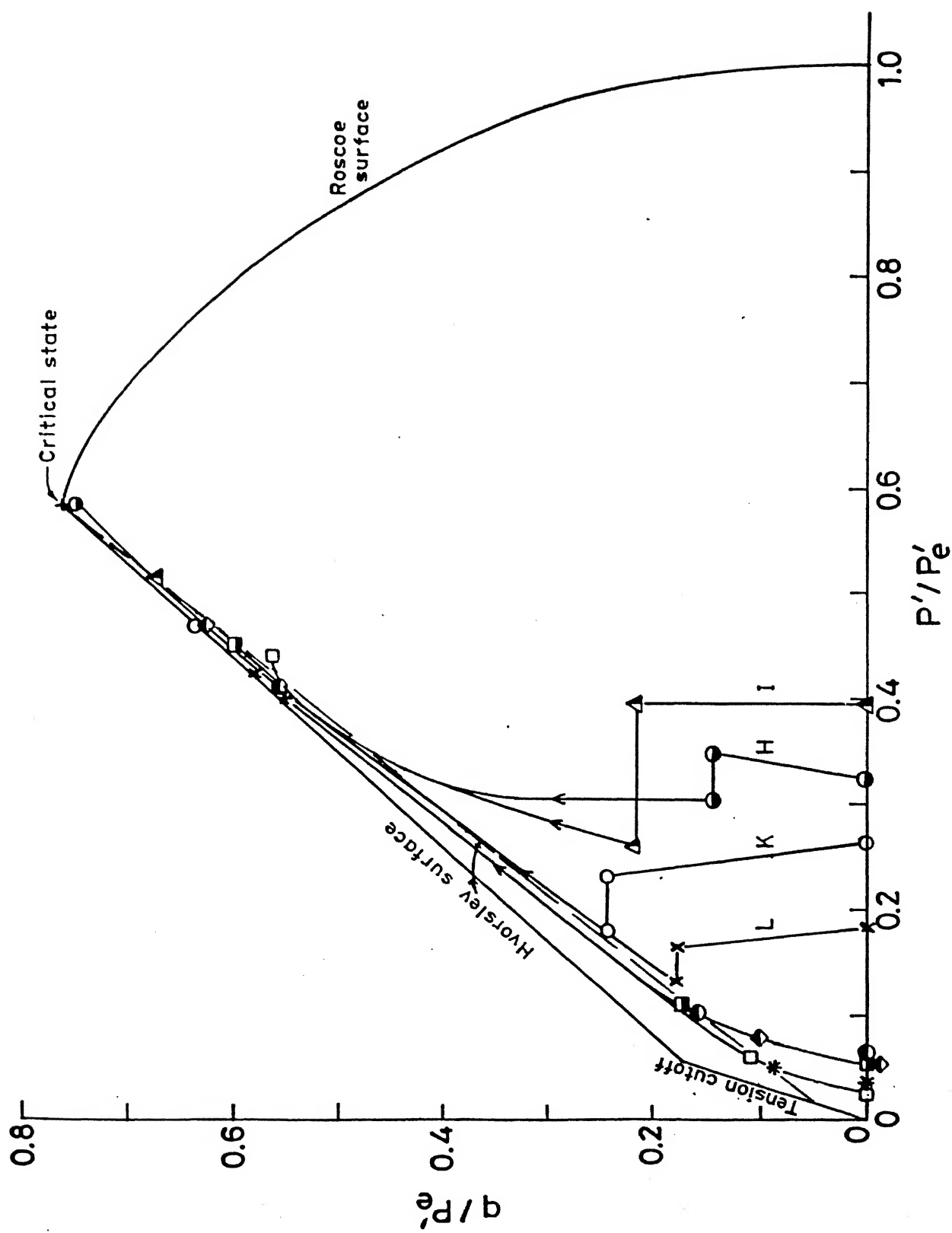


Fig. 4.98 q/P'_e versus P'/P'_e relationship for cyclic tests.

Following Hyde and Ward (1985), relationship of the form :

$$\log \dot{u}/P_e = \log \alpha - \beta \log N \quad (4.10)$$

can be used in conjunction with the equation of Hvorslev surface for a given soil to predict the pore pressure generated during N cycles at a given cyclic stress level. In the present study where the soil demonstrated highly dilatant behaviour during shear at very low confining stresses, such an approach needs further investigation with careful pore pressure measurements during cyclic loading.

4.8.4.3 Evaluation of Threshold stress and Threshold stress ratio

As already stated, threshold stress is defined as the stress level above which the cyclic loading causes rapid permanent deformation and cumulative pore pressure built up leading to the failure below the static failure value. Also, the stress ratio, R_f corresponding to $(\sigma_1 - \sigma_3)$ equal to threshold stress is called the threshold stress ratio, R_{TS} .

Rubin et al. (1970) and Janin et al. (1983a) evaluated the threshold stress for stiff undisturbed soils in the U.K. in connection with railway formation design, by using the criterion of cumulative plastic strain during cyclic drained triaxial loading at low confining stresses ($\sigma'_c = 35$ kPa). Wilson and Greenwood (1974) present results of plastic strain and pore pressure development with number of cycles of

undrained loading at different R_f values for undisturbed samples of lacustrine clay. Gupta (1973), France (1976) and Rehman (1977) followed Sangrey's approach [Sangrey (1968)] to determine the equilibrium line from which threshold stress can again be evaluated. Hyde and Ward (1985) present a simple model of soil behaviour during undrained cyclic loading which incorporates rate of development of pore pressure and the Hvorslev surface defined in terms of critical state parameters. This model can be used to predict the equilibrium line from which threshold stress can again be evaluated.

In the present study, both the threshold stress and R_{TS} have been evaluated using data from cyclic undrained triaxial tests. Threshold stress has been obtained using the plastic strain criteria - both the total value at the end of 100 cycles and the incremental value during 100 cycles - as well as the pore pressure response during cyclic loading at various values of R_f .

4.8.4.3.1 Plastic strain criterion

Figure 4.99 depicts data in terms of incremental values of ϵ_p as related to R_f for different confining stress values. Data from cyclic unconfined compression tests is also indicated. The value of R_f at which sudden increase in incremental plastic strain occurs, is taken as a measure of threshold stress ratio. These values of R_{TS} as applicable for quasi-saturated samples are given in Table 4.14. Incidentally, the R_{TS} value from unconfined test corresponds to the as compacted state of the

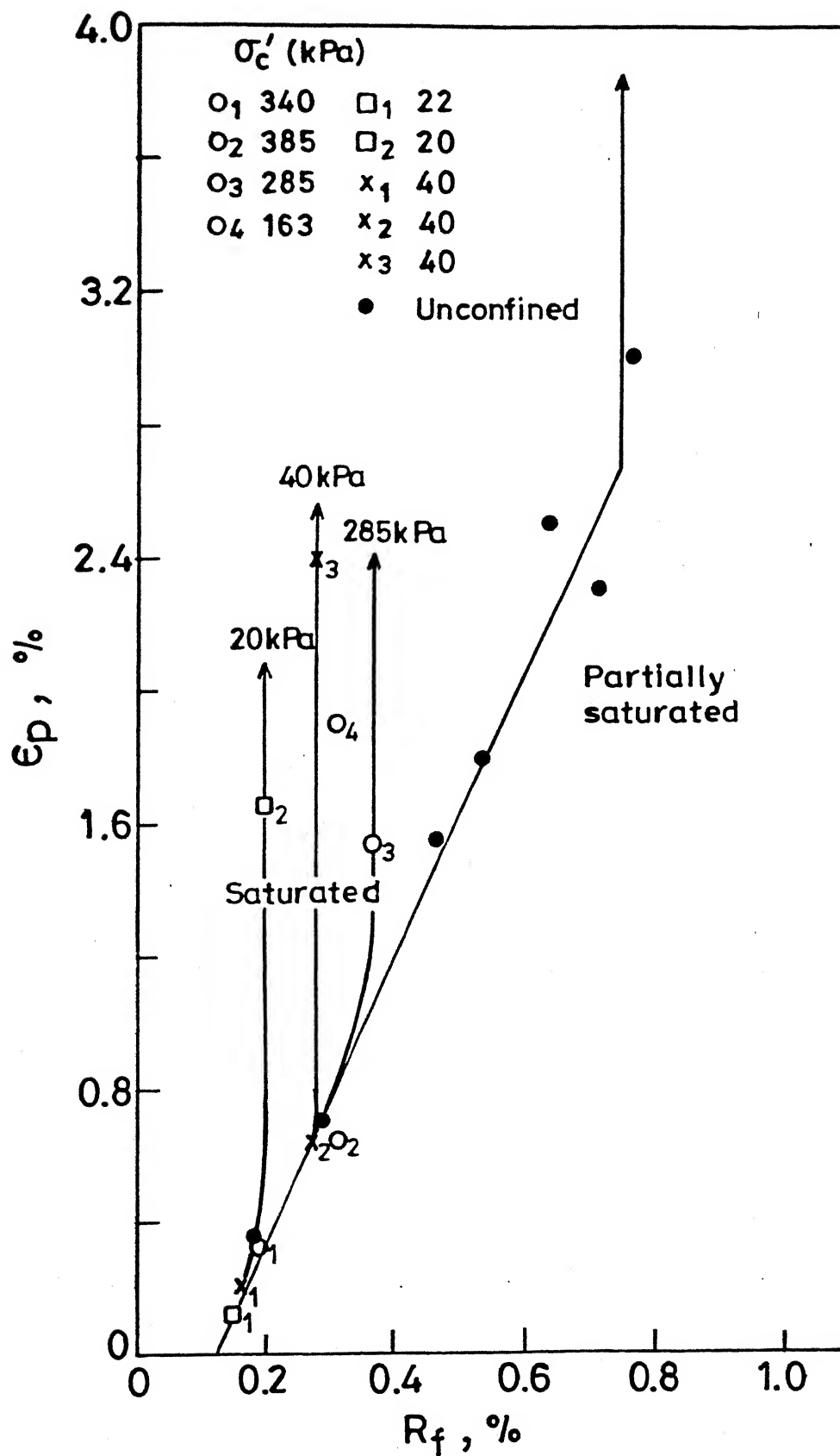


Fig. 4.99 Rise in plastic strain during 100 cycles versus R_f .

sample and is 0.75. Since the status of effective stresses during unconfined test is unknown, it is not possible to compare this value with that obtained from quasi-saturated soil behaviour.

As indicated earlier, cumulative plastic strain during cyclic undrained triaxial loading may be expressed as :

$$\log \epsilon_p = C_p + D_p \log N_1 + E_p \log N_2/N_s$$

The variation of C_p and E_p with R_f can also be used to estimate the value of R_{TS} . Figure 4.94 shows the variation of C_p with R_f for all the available test data for compacted, undisturbed stiff, undisturbed and remoulded normally consolidated soils. Here again, sudden increase in C_p value beyond a certain R_f , especially in the case of compacted and stiff undisturbed samples tested at low σ_c' values, is observed and this value of R_f is taken as a measure of R_{TS} . In the case of normally consolidated soils tested at high confining pressure, at $R_f \geq R_{TS}$, a change in the pattern of C_p vs R_f is also observed, though this change is not as abrupt as seen for compacted and stiff undisturbed samples tested at low confining stresses.

Similarly, E_p - the second gradient of ϵ_p vs N in log-log plot - can also be used to investigate the determination of R_{TS} . As indicated earlier, E_p is zero up to some value of $R_f = R_{ft}$ (indicating terminating condition for plastic strain with further cycling) after which E_p increases up to D_p . This stage

of stress level is indicative of the threshold condition and a slightly larger value of R_f would give a higher value of E_p . The variation of ϵ_p with R_f can thus be also used to determine R_{TS} . Table 4.14 lists the E_p value for different stress levels for a variety of soils. However, detailed study is required to examine the variation of E_p with R_f over a wide range of values for both compacted/stiff soils and normally consolidated soils at low confining stress values.

4.8.4.3.2. Pore pressure during cyclic loading criterion

Sangrey (1968), France (1976), Yudhbir and Rehman (1977) etc. have demonstrated the existence of equilibrium line for a variety of soils. The end point of the equilibrium line on the failure envelope is a good measure of threshold stress. This procedure could not be directly used in the present study simply because sufficient number of test results at different R_f values for samples consolidated at same σ'_c values were not available.

However, an indirect assessment of equilibrium line was made by examining the normalized effective stress paths for different σ'_c values as indicated in Fig. 4.71. It will be seen that as σ'_c increases, the effective stress path moves to the left and tends to approach the effective stress path - AA, corresponding to fully saturated condition at very high confining stress (in this case > 1400 kPa). Data for Canyon dam clay (Fig. 4.72) supports this trend.

The position of AA in Figs. 4.71 and 4.72 is based on the

Roscoe surface shown in Figs 4.82, 4.83 and 4.84. On the basis of this hypothesis, the end point of AA (in Figs. 4.71 and 4.72) is located on the normalized failure envelope for quasi-saturated compacted Campus silt as shown in Fig. 4.96. Also shown here are the normalized effective stress paths of 4 cyclic tests along with the corresponding static test stress paths. End points of tests H and I (1 and 2) are joined with this end point of AA to determine the equilibrium line. It will be seen (see inset) that a distinct change in the $(\Delta u)_{\text{cyc}} - R_f$ pattern takes place at $R_f = 36.3$ and this value is representative of R_{TS} .

Incidentally, another indirect approach to the determination of threshold stress ratio for dilative soils was attempted on the basis of deviatoric stress level at which maximum positive pore pressure develop during undrained shear (Fig. 4.70). At various values of σ'_c , the magnitude of $(\sigma_1 - \sigma_3)$ corresponding to $(\Delta u)_{\text{max}}$ was estimated from Figs. 4.69 and 4.70 and compared with the corresponding $(\sigma_1 - \sigma_3)$ at failure, $[(\sigma_1 - \sigma_3)_f]$ (see Fig. 4.73). The ratio between $(\sigma_1 - \sigma_3)$ at $(\Delta u)_{\text{max}}$ and $(\sigma_1 - \sigma_3)_f$ could also be considered as a measure of threshold stress ratio because a sample cycled from this stress level is expected to generate largest pore pressure. This estimate of R_{TS} is compared with the values obtained from plastic strain and equilibrium criteria in Fig. 4.100.

It will be seen that at low stress levels ($\sigma'_c \leq 300$ kPa), the two criteria give more or less the same value of R_{mc} .

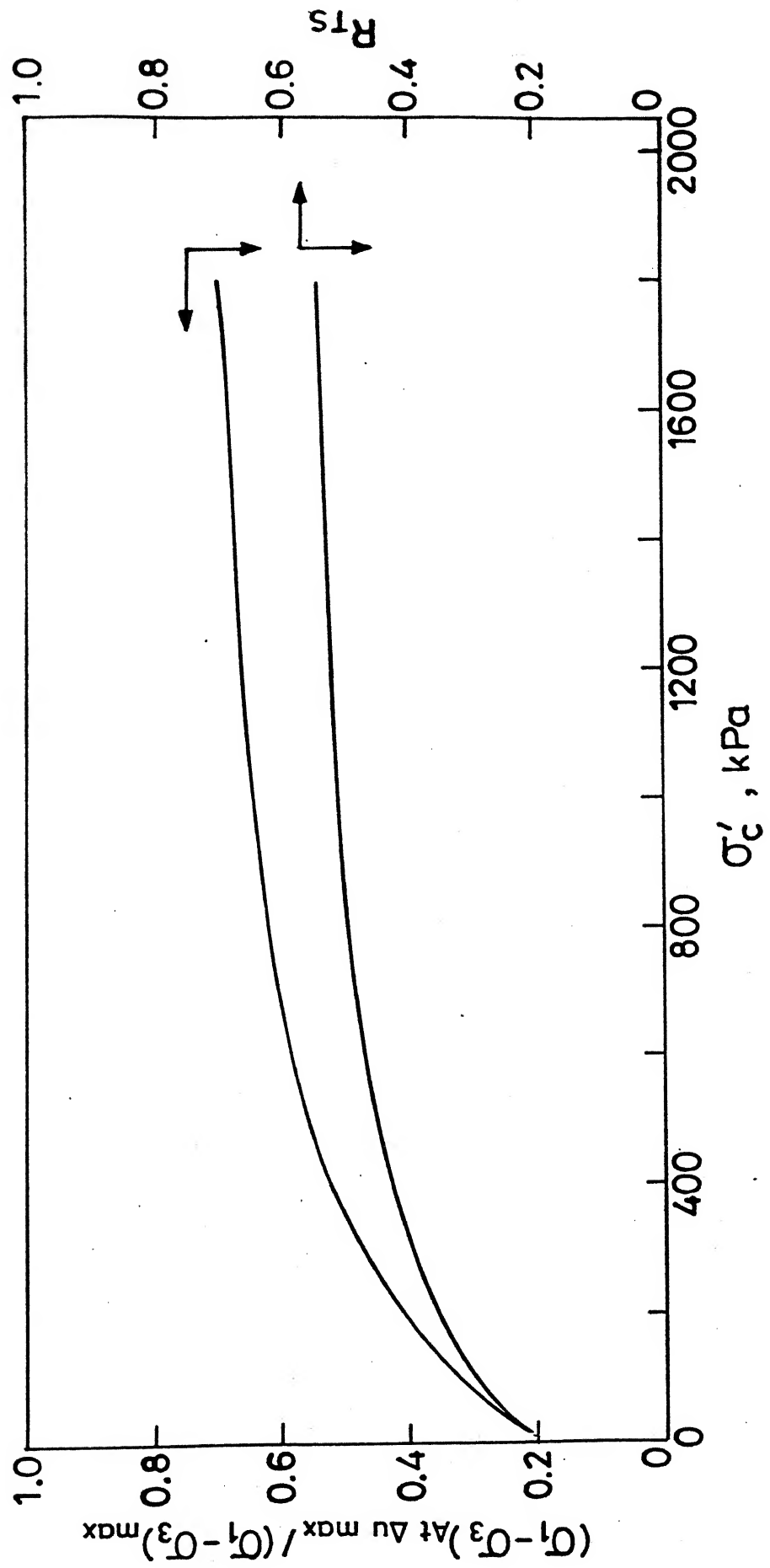


Fig.4.100 $(\sigma_1 - \sigma_3)_{\text{At } \Delta u \text{ max}} / (\sigma_1 - \sigma_3)_{\text{max}}$ and R_{Ts} versus σ'_c

whereas at high confining stresses ($\sigma_c' > 300$ kPa), $(\Delta u)_{\max}$ criterion overpredicts R_{TS} by as much as 25 % .

4.8.4.4 Guidelines for evaluation of threshold stress ratio

The test procedures to evaluate R_{TS} from plastic strain criterion and /or equilibrium line method as described here, can be readily used for each situation under consideration. However, for the purpose for routine design it would be useful to work out some empirical relationships between R_{TS} and simple soil indices. Sangrey et al. (1978) had proposed a relationship between R_{TS} and soil compressibility factor, $\kappa/(1+e_0)$ where κ is the slope of the elastic swelling line and e_0 is the initial void ratio of the soil.

Yudhbir and Kameswara Rao (1989) suggested use of such a relationship to estimate R_{TS} which decreases with decrease in plasticity index and liquid limit. As most of the test data from Sangrey et al. (1978) correspond to high effective confining stress, such a relationship would appear to be applicable only for that range of σ_c' values. Approximately, this relationship may be expressed as :

$$R_{TS} \approx 1 - \log 50 [\kappa/(1+e_0)] \quad (4.11)$$

It must be realized however, that κ determination poses certain difficulties and would have to be carried out in the range of changes in effective stress during cyclic loading.

On the suggestion of Yudhbir (1992), a relationship

between R_{TS} and plasticity index, I_p of soil was attempted. The basic logic of such a suggestion was no doubt guided by the dependence of the compressibility of the soil on I_p . Easy determination of I_p as compared to κ is no doubt a desirable feature of the proposed inter-relationship.

Figure 4.101 presents the available test data for a variety of soils (compacted, stiff, normally consolidated etc.) at low and relatively high effective confining stresses. Linear relationships between R_{TS} and I_p , with varying slopes (depending on confining stress level) are suggested. For a given σ_c' value, R_{TS} increases with increasing I_p and for the same I_p , R_{TS} increases with increasing σ_c' . The following empirical equations are suggested as guidelines to estimate R_{TS}

for $\sigma_c' = 35$ kPa,

$$R_{TS} = 0.045 + 1.29 I_p \quad (4.12)$$

for $\sigma_c' > 300$ kPa,

$$R_{TS} = 0.565 + 0.65 I_p \quad (4.13)$$

Incidentally, the range of σ_c' values for compacted low I_p soils for Eq. (4.13) may be much higher than 300 kPa.

It will be seen (Fig. 4.101) that for the range of I_p values, R_{TS} varies from 0.6 - 0.9 for high σ_c' values and from 0.25 - 0.6 for low σ_c' values. For the railway formation design, the relationship given in Eq. (4.12) is suggested for evaluation of threshold stress. However, since the σ_c' values

relevant to actual railway formation problem are smaller than 35 kPa, it would be helpful to examine the variation of threshold stress with σ_c' . Figures 4.102 to 4.104 show the variation of $(\sigma_1 - \sigma_3)/2$ at failure and $(\sigma_1 - \sigma_3)/2$ corresponding to threshold level with σ_c' for 3 soils over a wide range. The results at low effective confining stresses are depicted in Fig. 4.105. In the absence of any detailed investigation at σ_c' values less than 35 kPa, the following extrapolation relationship is suggested for railway formation design purposes

$$(\sigma_1 - \sigma_3)_{TS} = a + b \sigma_c' \quad (4.14)$$

The values of coefficients a and b depend on the soil type, its stress history and whether compacted or undisturbed. Typical values are indicated in Fig. 4.105.

As shown in Fig. 4.91, R_{TS} is 0.75 as determined from unconfined cyclic triaxial undrained tests for Campus silt. This would indicate $(\sigma_1 - \sigma_3)_{TS}$ as $0.75 \times 180 = 135$ kPa. Taking $\sigma_c' = 10$ kPa as relevant to the typical formation design (details given later) problem, $(\sigma_1 - \sigma_3)_{TS}$ can be taken as 67.4 kPa (Fig. 4.105) which is 0.499 times the value of $(\sigma_1 - \sigma_3)_{TS}$ from unconfined testing. Therefore, on the basis of this limited study, as a rule of thumb, R_{TS} value applicable to formation design on such soils may be taken as 50 % of that obtained from cyclic unconfined test. Also, $(\sigma_1 - \sigma_3)_{TS}$ is 37.5 percent of ultimate unconfined strength.

For Angul clay [Yudhbir et al. (1992)], $(\sigma_1 - \sigma_3)_{TS}$ is 53

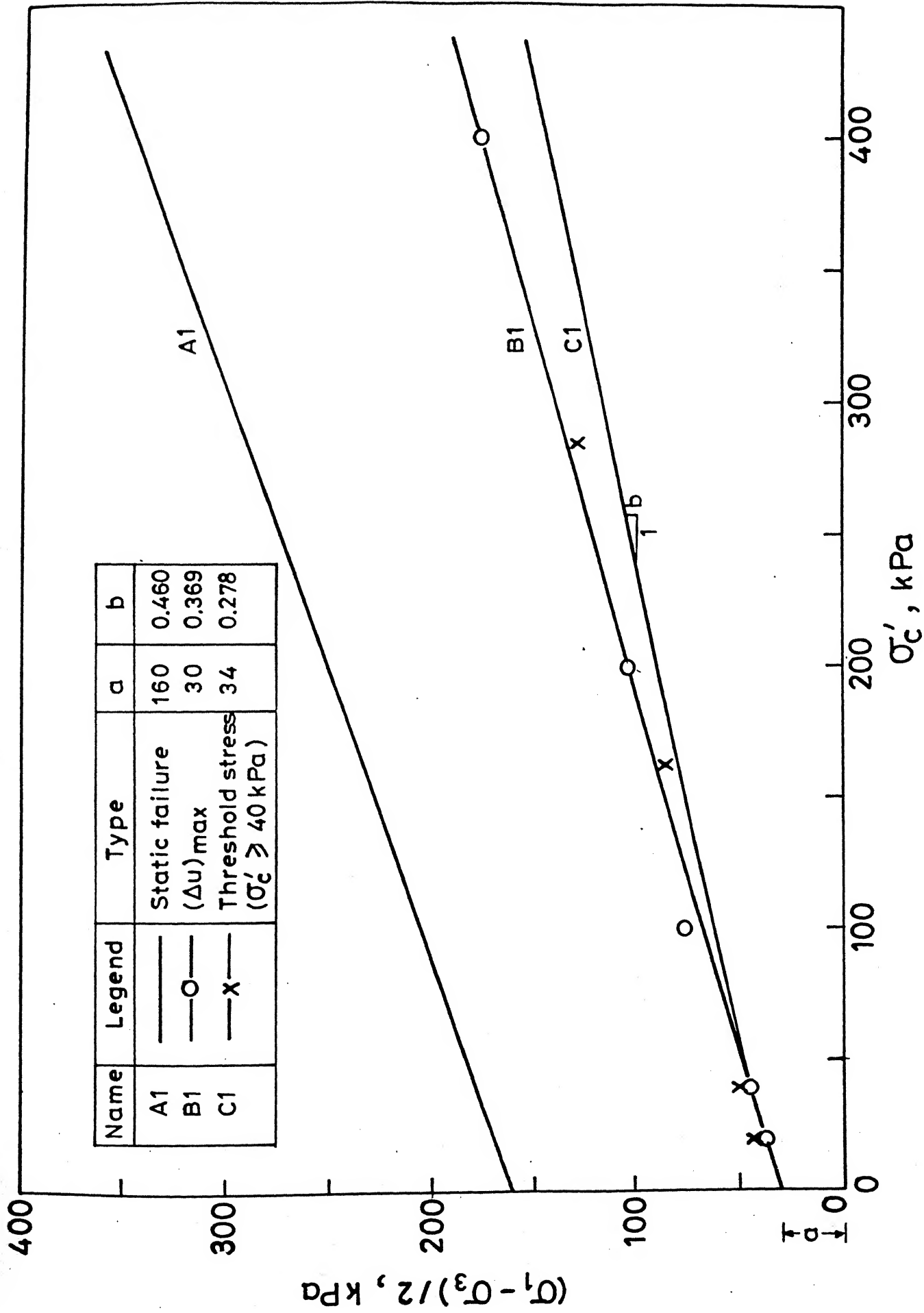


Fig. 4.102 Threshold stress versus σ'_c relationship for compacted saturated silt

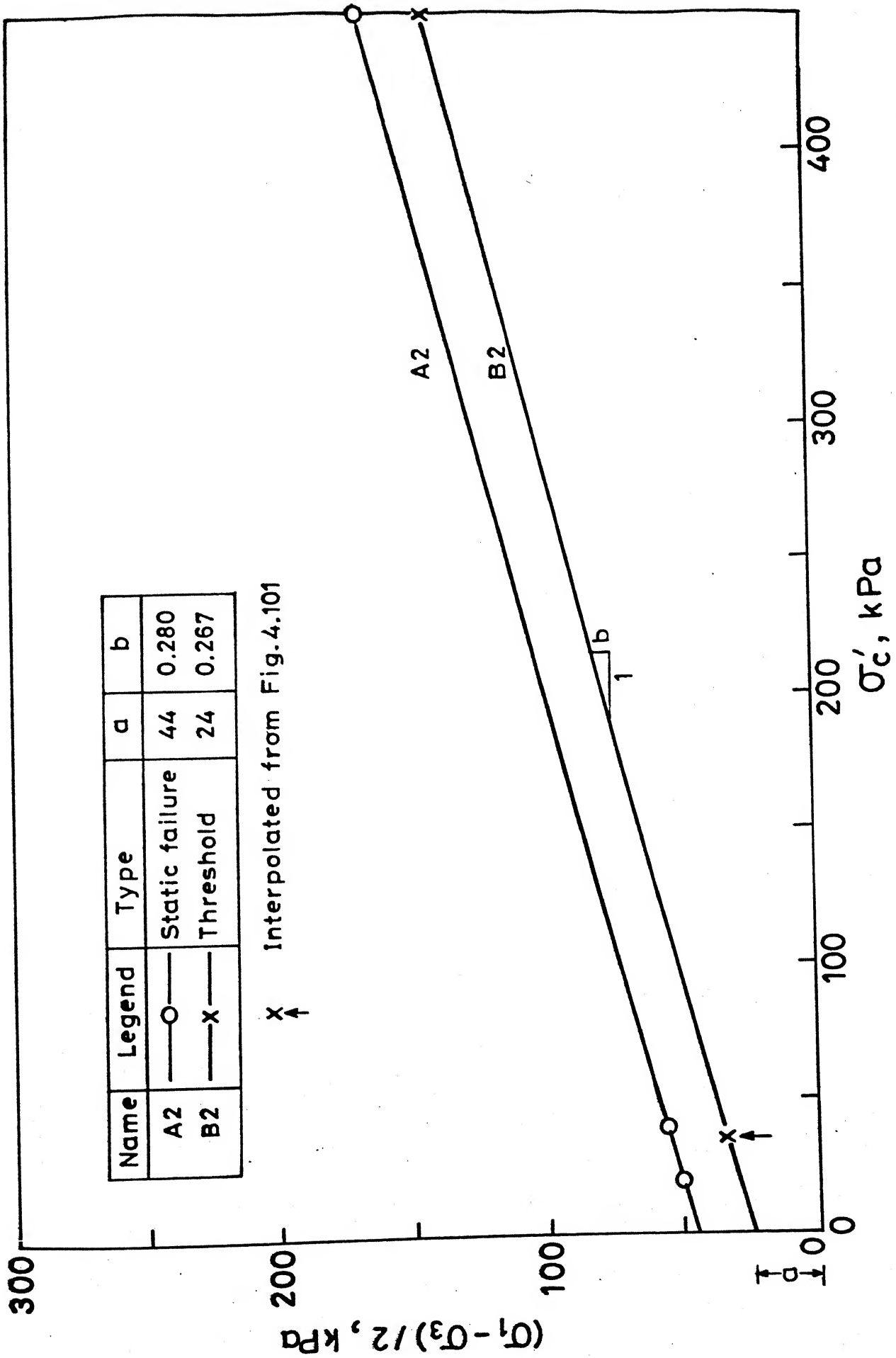


Fig. 4.103 Threshold stress versus σ'_c relationship for compacted Angul clay (Yudhbir et al., 1992)

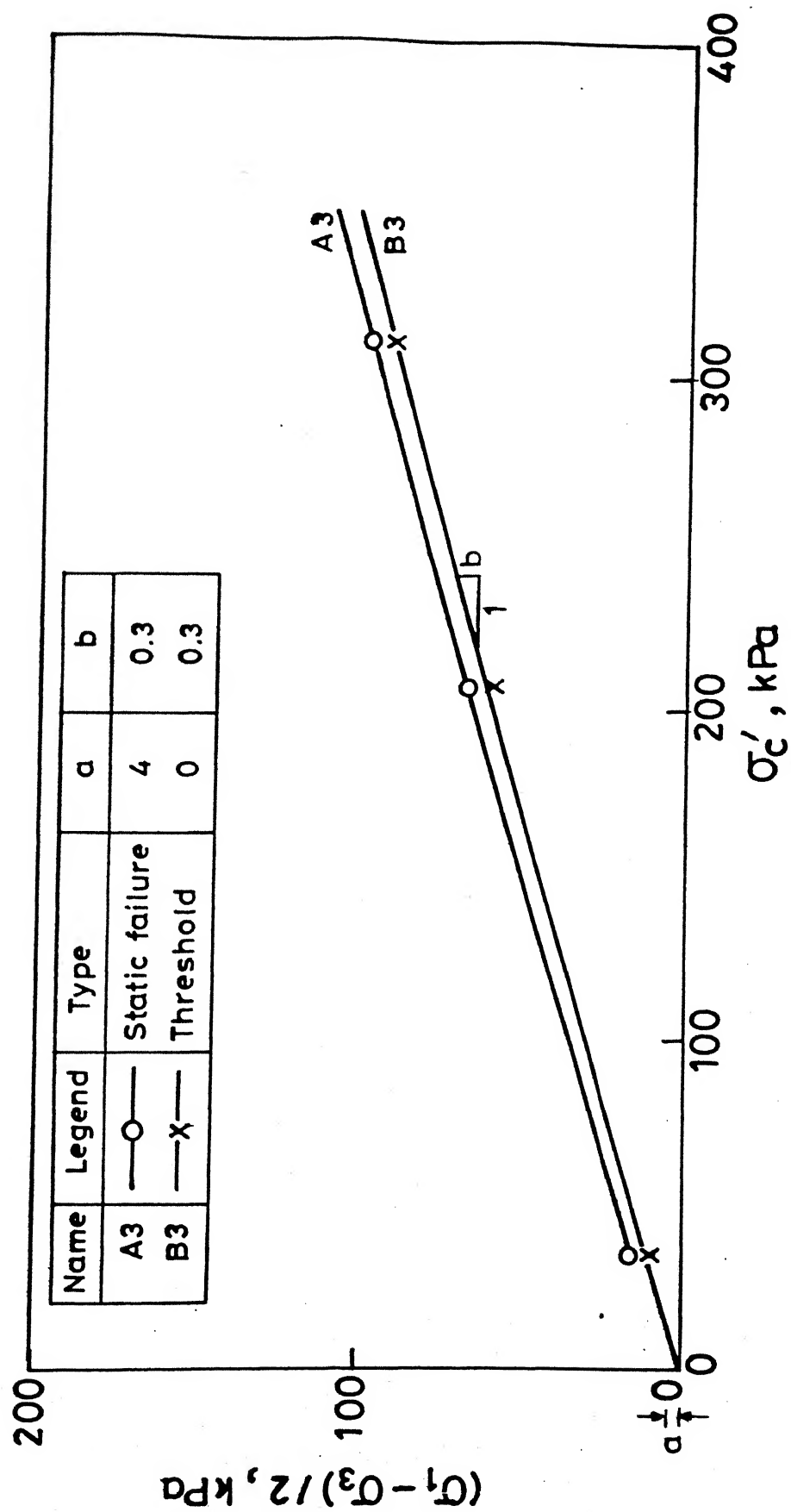


Fig. 4.104 Threshold stress versus σ'_c relationship for NC marine clay.
(Rehman, 1977)

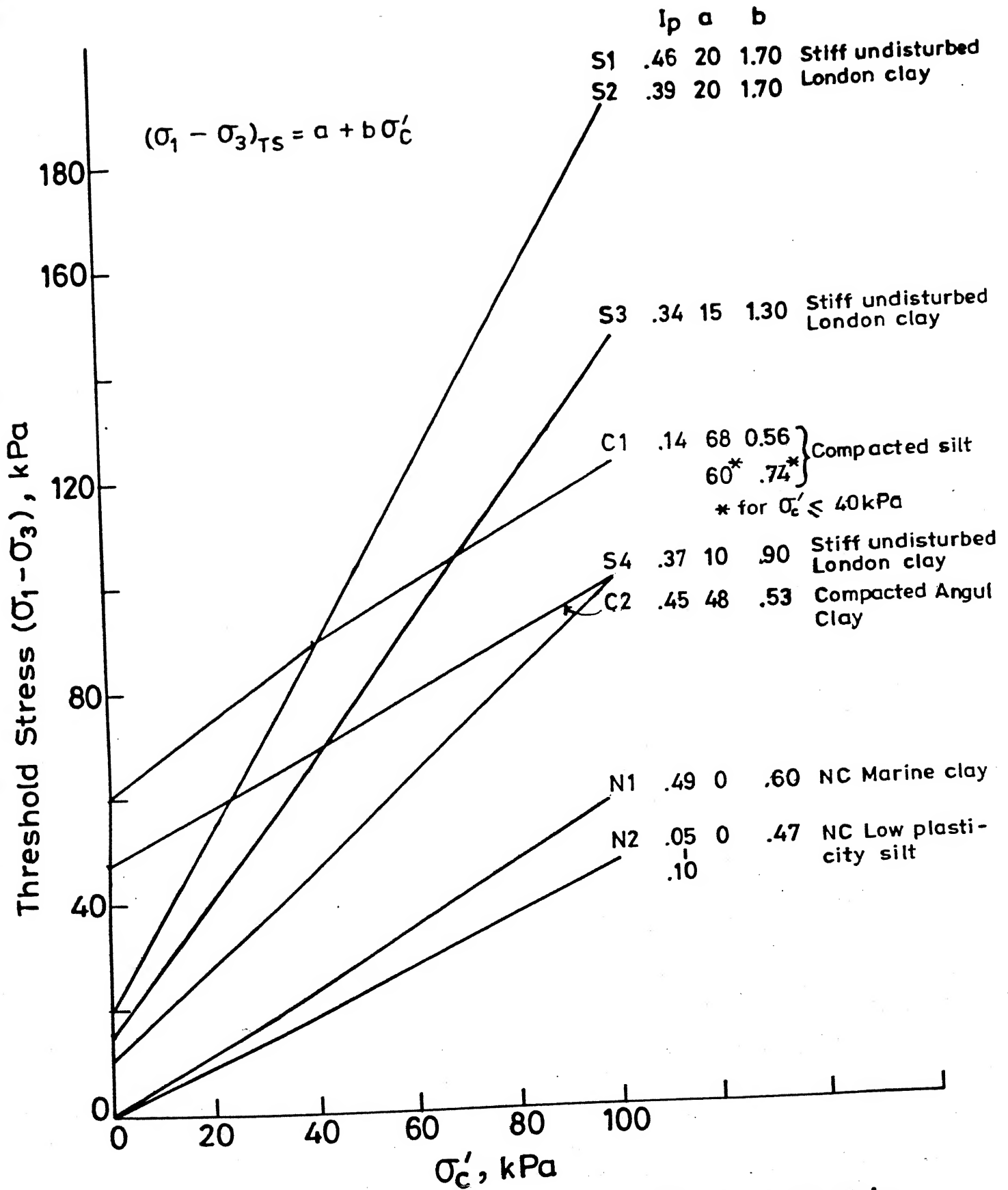


Fig. 4.105 Threshold stress versus σ'_c relationship.

kPa at σ_c' approximately equal to 10 kPa. Also, unconfined compressive strength, $(\sigma_1 - \sigma_3)$ for Angul clay is 310 kPa. So the ratio of $(\sigma_1 - \sigma_3)_{TS}$ with unconfined compressive strength, $(\sigma_1 - \sigma_3)$ for Angul clay works out to be 0.17.

CHAPTER 5

DESIGN METHODOLOGY

5.1 INTRODUCTION

Based on mathematical modelling described in Chapter 3 and experimental investigations carried out (Chapter 4), a methodology has been proposed for design of railway formation.

Track structure consists of the track equipment (tie and rail) and the formation (ballast, subballast and subgrade). All these components are shown in Fig. 1.1. Indian railways have fixed track equipment for future traffic from other criteria (65 kg rail and 65 cm tie spacing for prestressed concrete sleepers). In this section, a methodology for design of track formation is described. Conventionally, the track formation design means fixation of total depth of construction (depth of ballast and subballast) over subgrade soil. However, it must be recognized that track formation design has broader scope and in addition to the fixing of total depth of construction, it also includes gradation of material used in these layers, compaction of subgrade, drainage measures etc.

The proposed design procedure calculates the total depth of formation from 'excessive displacement' criterion because it has been recognized [Janin et al. (1983b)] that foundation should be stressed well below the limits of failure strength to prevent excessive track settlement. The basis of the proposed

design methodology is that the stress level induced by the traffic loading does not exceed the threshold stress of subgrade soil.

Moving wheel loads have been modelled as equivalent concentrated loads using impact factors [see RDSO (D) ; Eq. (5.1)]. Elastic analysis was carried out to obtain stress distribution. Soil behaviour relevant to cyclic loading was studied with reference to the results obtained in the above mentioned stress analysis using a low frequency (1/60 Hz, so as to ensure the reliability of pore pressure measurements) cyclic sinusoidal loading program available with geotechnical digital system, with a view to evaluate the threshold stress.

For a given traffic load, induced stresses on the top of subgrade can be limited or reduced by several means as given below :

- a. An increase in depth of formation.
- b. Change in track equipment e.g. sleeper spacing, sleeper size, rail size etc.
- c. Change in the track foundation structure e.g. the provision of a better load distributing layer in the ballast.

The alternative to lowering the induced stresses is to increase the magnitude of the threshold stress of subgrade by soil improvement techniques such as :

- a. lowering the water table.
- b. stabilization of the soil.
- c. geotextile

The present design procedure focusses on keeping the induced stresses below threshold stress level by providing suitable formation depth.

The methodology suggested is general in application and can be extended for any track and soil type. This methodology can also be used to design the formation for future high speed traffic and heavy axle loads. Existing track capacity can also be evaluated by this method.

5.2 BROAD OUTLINE OF DESIGN METHODOLOGY

Steps in the proposed design methodology are :

1. Estimation of induced stresses
2. Evaluation of threshold stress
3. Design of depth of formation

5.2.1. Estimation of induced stresses on the subgrade

For this purpose, a parametric study should be carried out using 3D20N model by taking different depths of formation along with different soil types. Relationship between induced stresses $[(\sigma_1 - \sigma_3)$ and/or $(\sigma_1)]$ and m values for different depth of formation, as shown in Figs. 5.1 and 5.2 [(due to 16.25 t

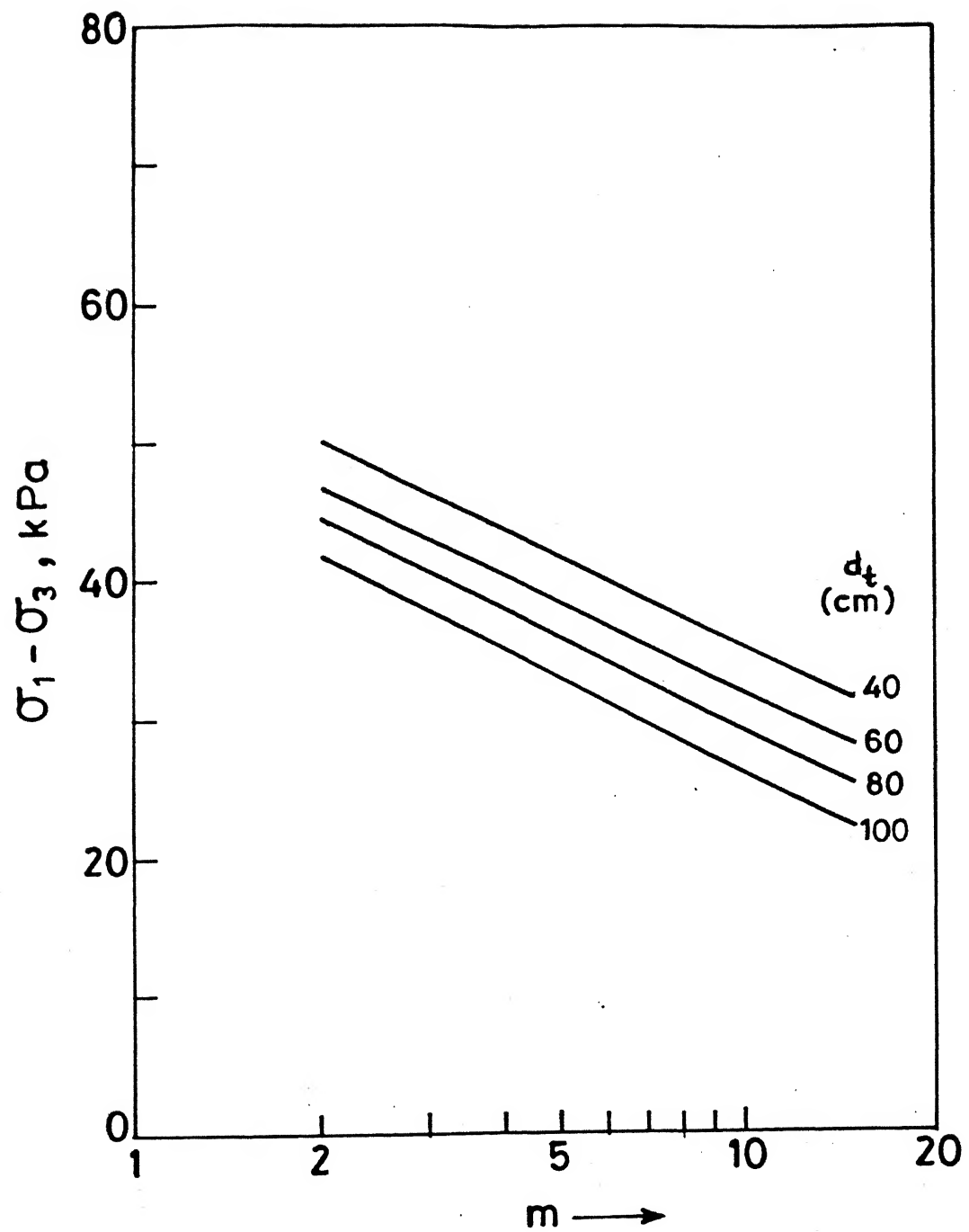


Fig.5.1 Induced stress ($\sigma_1 - \sigma_3$) versus m .

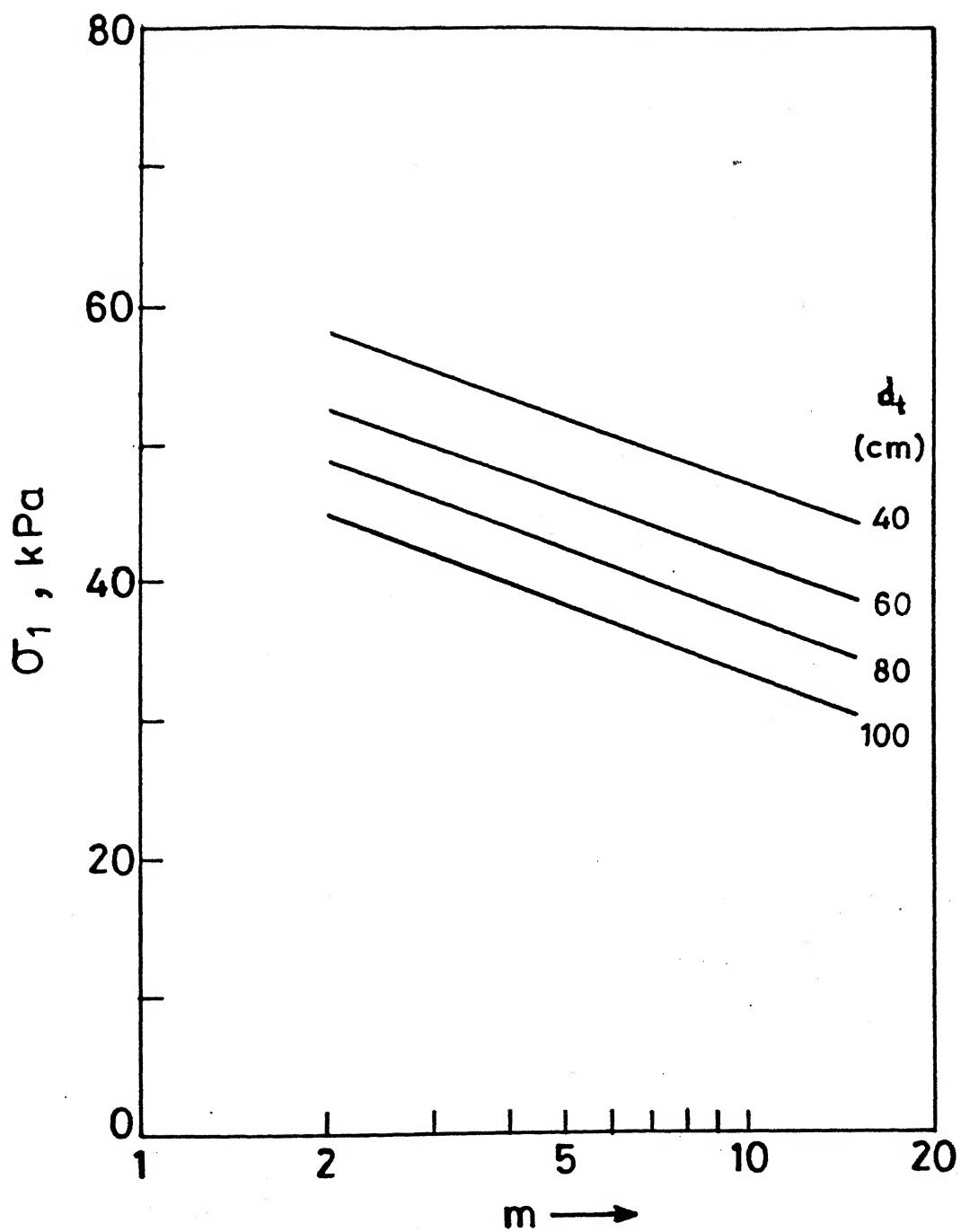


Fig. 5.2. Induced stress (σ_1) versus m .

equivalent wheel load for TRACK 1 (Appendix A1)], should be developed [Sec. 3.4 ; Eqs. (3.20) and (3.21)].

where $m = E_{\text{equ}} / E_s$,

and
$$E_{\text{equ}} = \frac{E_b d_b + E_{sb} d_{sb}}{d_b + d_{sb}}$$

with m = nondimensional factor as a measure of formation quality,

E_{equ} = equivalent Young's modulus of formation,

E_s = Young's modulus of subgrade to be evaluated by cyclic plate load test or by cross hole wave propagation test,

E_b = Young's modulus of ballast to be evaluated by triaxial test on ballast sample,

E_{sb} = Young's modulus of subballast to be determined in the same manner as E_b ,

d_b = depth of ballast layer (may be adopted equal to 25 cm), and

d_{sb} = depth of subballast layer.

Details of stress analysis have already been presented in Sec. 3.4. For the type of stress distribution analysis adopted here, it is evident that interpolation and extrapolation of results with respect to the magnitude of equivalent wheel load are valid. In fact, an influence line approach similar to the

one commonly used in structural analysis, is ideally suited, and then, results for any wheel load can be easily obtained.

5.2.2. Evaluation of threshold stress

Threshold stress is defined as the stress level above which the cyclic loading causes rapid permanent deformation and cumulative pore pressure built up leading to failure below the static failure value while threshold stress ratio, R_{TS} is the ratio of threshold stress to the ultimate static failure stress (threshold stress/ultimate static failure stress).

The procedure to be adopted for evaluation of threshold stress should be same as described in detail in Chapter 4 for series B3 tests. The main steps are briefly outlined here :

- a. Determine failure envelope in terms of effective stresses for undisturbed and/or as compacted samples by conducting consolidated undrained triaxial compression tests on saturated samples with pore pressure measurements using σ_c' values ranging from 20 kPa to 100 kPa.
- b. Conduct few constant amplitude cyclic undrained triaxial compression tests at $\sigma_c' = 20$ and 35 kPa on saturated samples at $R_f = R_{TS} \pm 0.1$; the value of R_{TS} can be obtained from Eq. (4.12). Cyclic load test should be carried out at low enough frequency so as to ensure reliable pore pressure measurement with sinusoidal wave loading.

c. Evaluate threshold stress using any or more than one of the approaches discussed in Sec. 4.8.4.3.

.2.3. Design of depth of formation

Design procedure consists of comparing $(\sigma_1 - \sigma_3)$ induced due to traffic loads with the threshold stress $(\sigma_1 - \sigma_3)$ and the minimum depth at which $(\sigma_1 - \sigma_3)$ induced due to traffic load is less than threshold stress, is adopted as depth of formation. The detailed rigorous design procedure is given below in Sec. 5.3 while the simplified procedure for routine design is described in Sec. 5.4.

5.3 RIGOROUS DESIGN

Rigorous design should be carried out for major changes in soil type and track structure.

As discussed in Chapter 4, for compacted soil, threshold stress ratio is a function of initial effective stress, σ_c' . Also, effective stresses increase as the depth of formation increases. Thus, a relationship can be proposed relating the threshold stress to the depth of formation.

Figure 5.3 shows the variation of static effective stress with depth based on the assumption that density of ballast is 17.5 kN/m^3 and the vertical stress from the track equipment is 4 kPa. Here, an isotropic state of stress has been assumed. This distribution is same as assumed by Rubin et al. (1970). Also shown on this figure is the variation of threshold stress

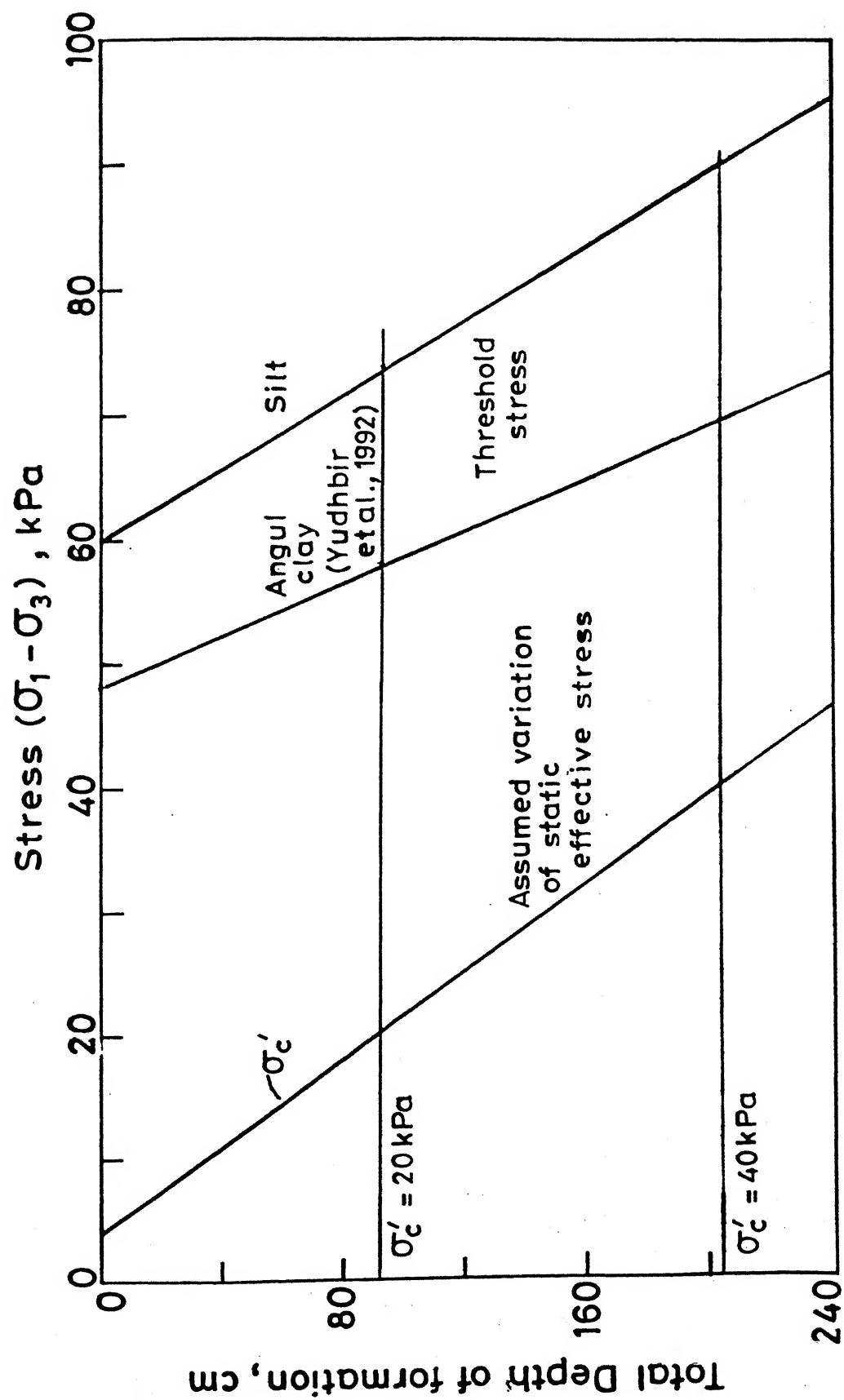


Fig.5.3 Threshold stress versus total depth of formation.

with depth for Campus soil and Angul clay reproduced from Fig. 4.105.

For any subgrade soil, threshold stress can be evaluated, using the testing methodology recommended earlier, from Eq. (4.14) as given below :

$$(\sigma_1 - \sigma_3)_{TS} = a + b \sigma_c'$$

where

σ_c' = initial consolidation stress at which the threshold stress, $(\sigma_1 - \sigma_3)_{TS}$ is needed,

a = value of $(\sigma_1 - \sigma_3)_{TS}$ at $\sigma_c' = 0$, and

b = slope of line in $(\sigma_1 - \sigma_3)_{TS}$ vs. σ_c' space (Fig. 4.105).

Values of coefficients a and b for some soils are shown in Fig. 4.105.

A flow chart for the recommended design procedure is given in Fig. 5.4.

If the formation thickness obtained by this method is less than minimum 40 cm depth of formation recommended by Indian railway, then provide formation depth equal to 40 cm.

The general scope of the proposed design methodology is illustrated in Fig. 5.5 where stress distribution data for different subgrade soils and wheel loads (two) is depicted. Also shown is the variation of threshold stress with depth for

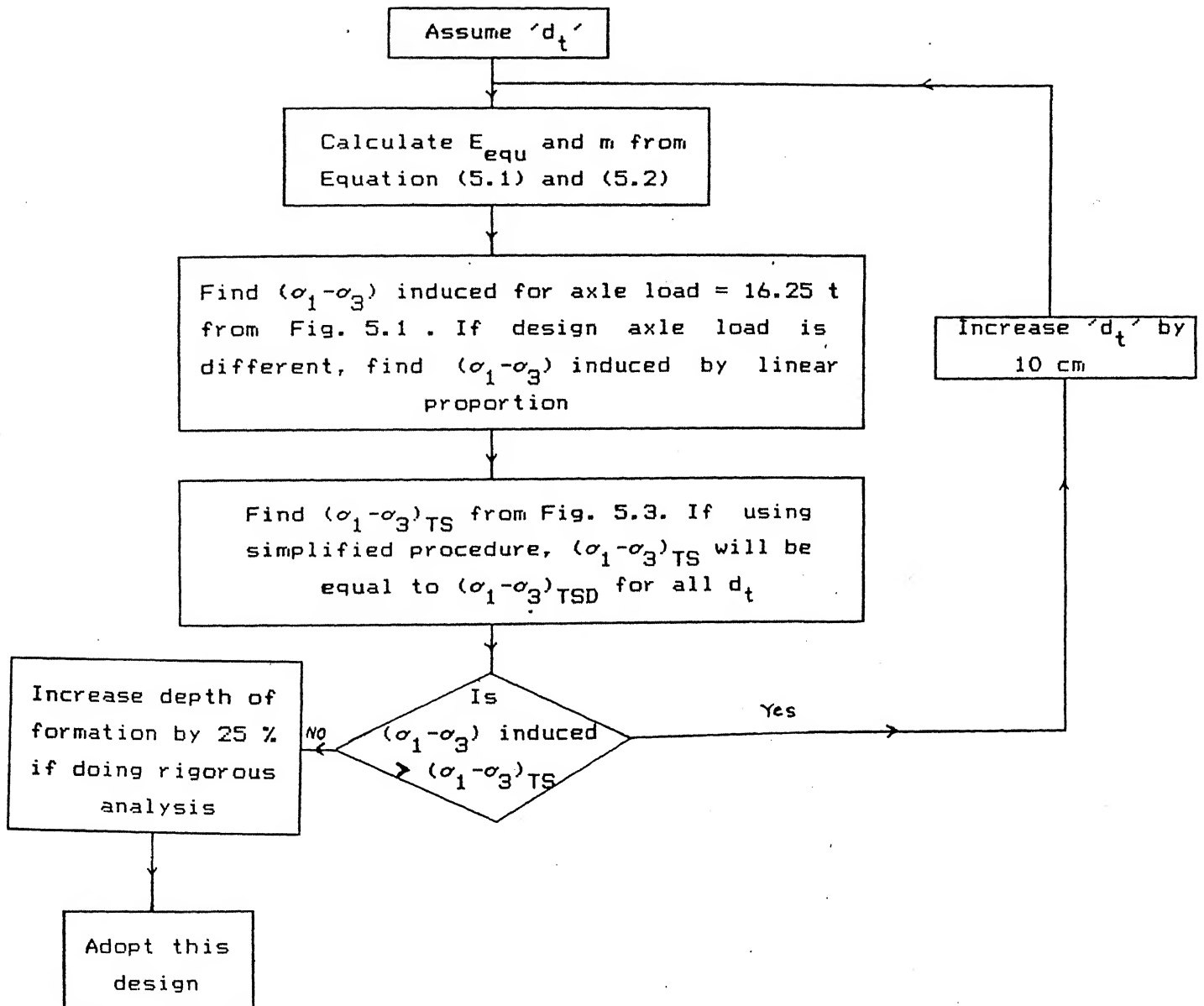


Fig. 5.4 Flow Chart

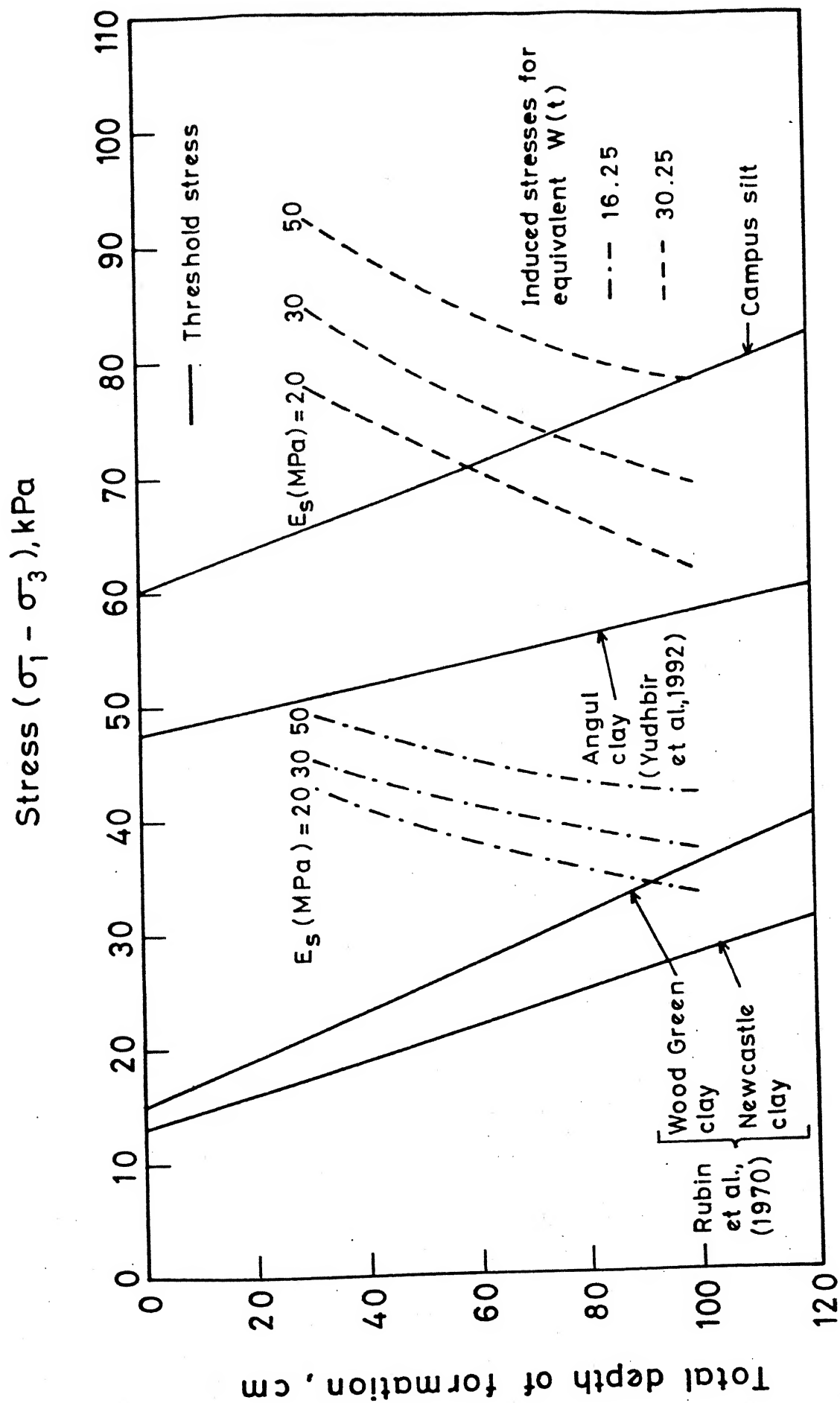


Fig. 5.5 Design chart

plasticity index. The dependence of the design formation depth on the wheel load (including speed factor) and the type of subgrade is brought out as earlier suggested by Rubin et al. (1970).

An alternative design methodology based on induced σ_1 values and bearing capacity of subgrade soil has been proposed by Janin et al. (1983c). They suggested this approach as an improvement over that proposed by Rubin et al. (1970).

In this study, the threshold stress approach is considered more suitable simply because it gives a much better insight into the soil behaviour under repeated loading. However, since the threshold stress values are based on laboratory tests conducted under idealized condition, for example 100 % Proctor compaction and no intermediate stage softening (as will occur in the field) etc., it is suggested that the design formation depth as obtained from this methodology be increased by 25 %. This added safety is primarily meant to take into account the actual track drainage conditions prevailing in the field. The laboratory test procedure does not anticipate free access of subgrade soil to water (stored in the ballast/subballast layers) in between the train loadings.

Incidentally, while the augmenting factor for speeds up to 120 kmph is based on the recommendation of Indian railway (41 % augmentation for speed equal to 120 kmph), the corresponding factor for higher speeds (300 kmph) has been obtained from the relationship suggested by the German railways and is given below [also see Eq. (2.22)] :

$$\text{Speed factor} = s \bar{t} \quad (5.1)$$

where

s = a factor which depends on track quality
and varies between 0.1 y to 0.3 y ,

$y = 1$ for speed ' V ' \leq 60 kmph,

$= 1 + (V - 60)/140$ for ' V ' $>$ 60 kmph,

and $\bar{t} = 3$ for statistical safety of 99.7 %

Thus, speed factor for $V = 300$ kmph is obtained as 1.628 for average track ($s = 0.2 y$). Axle load equal to 23 t has been used with these speed factors.

The design methodologies proposed by Rubin et al. (1970), Janin et al. (1983c) and the one suggested here are all based on deformation criterion and not on the basis of bearing capacity failure analysis, since the former intervenes long before actual strength failure occurs.

5.4 SIMPLIFIED DESIGN

In track formation design, where one is dealing with long stretches with possible variations in subsoil conditions, it is desirable to adopt a simplified design approach for initial estimate of the formation depth. Also, in case of situation where loading and speed conditions are not critical, routine design can be carried out by using such a simplified approach.

From Fig. 4.99, it is clear that threshold stress ratio, R_{TS} depends upon initial consolidation pressure, σ_c' . Also, ultimate stress at failure and threshold stress depend on σ_c' and the corresponding relationship can be expressed as follows :

$$(\sigma_1 - \sigma_3)_f / 2 = a_f + b_f \sigma_c' \quad (5.2)$$

$$(\sigma_1 - \sigma_3)_{TS} / 2 = a_{TS} + b_{TS} \sigma_c' \quad (5.3)$$

For Campus silt ($I_p = 0.14$), (Fig. 4.102)

$$\begin{aligned} a_f &= 160 ; \quad b_f = 0.460 \\ a_{TS} &= 30 ; \quad b_{TS} = 0.369 \end{aligned}$$

For Angul clay ($I_p = 0.45$), (Fig. 4.103)

$$\begin{aligned} a_f &= 44 ; \quad b_f = 0.280 \\ a_{TS} &= 24 ; \quad b_{TS} = 0.267 \end{aligned}$$

Within the range of σ_c' values relevant to the track formation design, R_{TS} varies from 0.187 (30/160) at $\sigma_c' = 0$ to $R_{TS} = 0.243$ for $\sigma_c' = 35$ kPa in case of Campus silt. The corresponding values for Angul clay are 0.54 and 0.62 respectively. Although, the actual variation of R_{TS} with σ_c' needs experimental determination, the value relevant to design σ_c' (approximately 11 kPa corresponding to 40 cm depth of

formation) may be taken as equal to the value for $\sigma_c' = 0$ as a conservative estimate. Incidentally, this value of R_{TS} is approximately 85 % of that calculated from the relationship [Eq. (4.12)] :

$$R_{TS} = 0.045 + 1.29 I_p$$

For a routine design procedure, therefore, it is suggested that based on I_p value, the corresponding R_{TS} from the Eq. (4.12) be estimated and 85 % of this value be taken as the design value.

In order to compute $(\sigma_1 - \sigma_3)_{TS}$, evaluate the $(\sigma_1 - \sigma_3)_f$ vs σ_c' relationship from consolidated undrained tests with σ_c' varying from 20 to 100 kPa.

A flow chart describing the procedure is given in Fig. 5.6.

5.5 DESIGN EXAMPLE FOR CAMPUS SILT

As it is observed (Fig. 5.5) that for Campus silt under compacted conditions, depth of formation equal to 40 cm is sufficient for equivalent wheel load = 16.25 t, design example given below has been worked out for equivalent wheel load = 30.25 t.

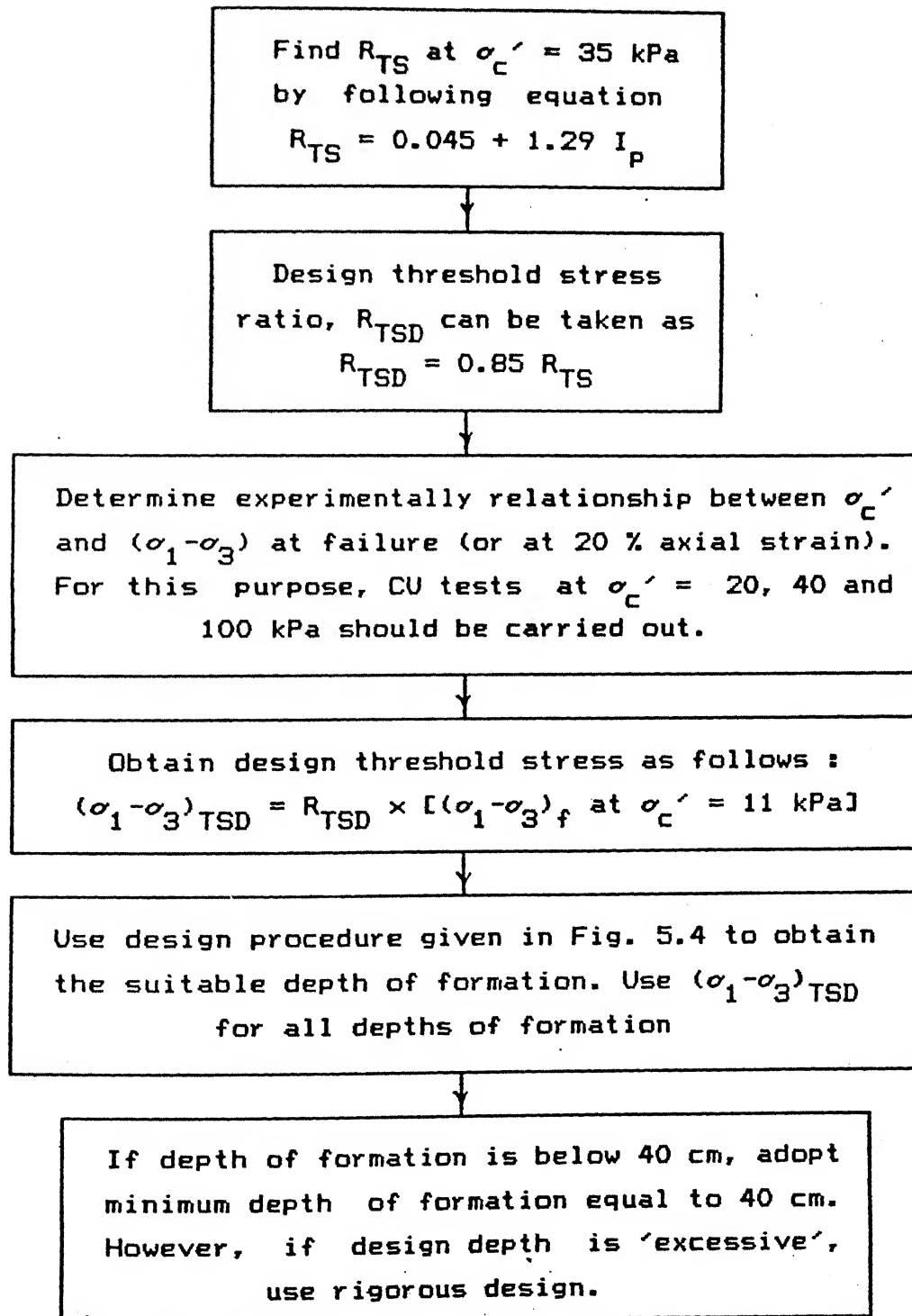


Fig. 5.6 Flow chart for simplified design

5.5.1. Rigorous Design

Trial 1 :

Take $d_t = 40$ cm

let $E_b = 150$ MPa ; $d_b = 25$ cm ; $E_{sb} = 80$ MPa

$\therefore d_{sb} = 15$ cm

$\therefore E_{equ} = 123.75$ MPa

let, $E_s = 20$ MPa

$\therefore m = 6.187$

$\therefore (\sigma_1 - \sigma_3)$ induced = 40 kPa (from Fig. 5.1)

Therefore, $(\sigma_1 - \sigma_3)$ induced for 30.25 t equivalent load works out to be 74.46 t.

From Fig. 5.3, for $d_t = 40$ cm ,

threshold stress level = 66 kPa

As $(\sigma_1 - \sigma_3)$ induced is greater than threshold stress level,

$d_t = 40$ cm is not safe.

Trial 2 :

$d_t = 50$ cm

$m = 5.75$

$(\sigma_1 - \sigma_3)$ induced = 39 kPa (by interpolation)

$(\sigma_1 - \sigma_3)$ induced for 30.25 t load = 72.6 kPa

Threshold stress = 67 kPa

As $(\sigma_1 - \sigma_3)$ induced is greater than threshold stress level,

$d_t = 50$ cm is not safe.

Trial 3 :

$d_t = 60$ cm

$$m = 5.46$$

$$(\sigma_1 - \sigma_3) \text{ induced} = 37 \text{ kPa}$$

$$(\sigma_1 - \sigma_3) \text{ induced for } 30.25 \text{ t load} = 68.9 \text{ kPa}$$

$$\text{Threshold stress} = 69 \text{ kPa}$$

As $(\sigma_1 - \sigma_3)$ induced is equal to threshold stress level,

$$d_t = 60 \text{ cm can be chosen.}$$

As a measure of factor of safety, increase the depth of formation by 25 % . Therefore, recommended depth of formation is 75 cm. Provide ballast depth equal to 25 cm and subballast depth equal to 50 cm.

Compact the subgrade soil up to 1.5 m depth before laying out the formation to the 90 % of maximum dry density.

5.5.2. Simplified Design

Step 1. Obtain R_{TS} corresponding to $\sigma_c' = 35 \text{ kPa}$ from Eq. (4.12) as given below :

$$\begin{aligned} R_{TS} &= 0.045 + 1.29 \times 0.14 \\ &= 0.225 \end{aligned}$$

Step 2. Obtain design threshold stress ratio, R_{TSD} as given below :

$$\begin{aligned} R_{TSD} &= 0.85 \times 0.225 \\ &= 0.191 \end{aligned}$$

Step 3. The relationship between σ_c' and $(\sigma_1 - \sigma_3)_f$ is given

in Fig. 4.102. From this figure, $(\sigma_1 - \sigma_3)_f$ corresponding to $\sigma_c' = 11$ kPa is equal to 330.2 kPa.

Step 4. Thus, obtain design threshold stress, $(\sigma_1 - \sigma_3)_{TSD}$ as given below :

$$\begin{aligned} (\sigma_1 - \sigma_3)_{TSD} &= R_{TSD} [(\sigma_1 - \sigma_3)_f \text{ at } \sigma_c' = 11 \text{ kPa}] \\ &= 0.191 \times 330.2 \\ &= 63.07 \text{ kPa} \end{aligned}$$

Step 5. Use the design procedure given in Fig. 5.4.

Trial 1 :

Assume $d_t = 70$ cm

$m = 5.25$

$(\sigma_1 - \sigma_3)$ induced for 30.25 t load = 67.9 kPa

Design threshold stress = 63.07 kPa

As induced stress is greater than design threshold stress, $d_t = 70$ cm is not safe.

Trial 2 :

Assume $d_t = 80$ cm

$m = 5.09$

$(\sigma_1 - \sigma_3)$ induced for 30.25 t load = 66 kPa

Design threshold stress = 63.07 kPa

As induced stress is greater than design threshold stress, $d_t = 80$ cm is not safe.

Trial 3 :

Assume $d_t = 90$ cm

$m = 4.97$

$(\sigma_1 - \sigma_3)$ induced for 30.25 t load = 63 kPa

Design threshold stress = 63.07 kPa

As induced stresses are equal to design threshold stress, $d_t = 90$ cm is safe.

As this design already gives conservative estimate, no increase in depth of formation is needed.

While suggesting above design procedures, it has been assumed that drainage conditions in the subgrade are perfect. However, if drainage conditions are poor, mud pumping will occur in most situations and the ballast and subballast layers will no longer meet the design specifications. Young's modulus of ballast and subballast layers will reduce significantly and thus, in Eq. (3.21), E_{equ} will decrease leading to increase in induced stresses. Poor drainage conditions will also lead to reduction in both the threshold stress value and soil modulus. Thus, the progressive degradation of subgrade, ballast and subballast will occur and the present design charts will not be applicable.

This focusses on the need to provide filters and subballast layer in the track structure in order to maintain the good drainage conditions. A typical track section incorporating filters has been shown in Fig. 5.7 wherein

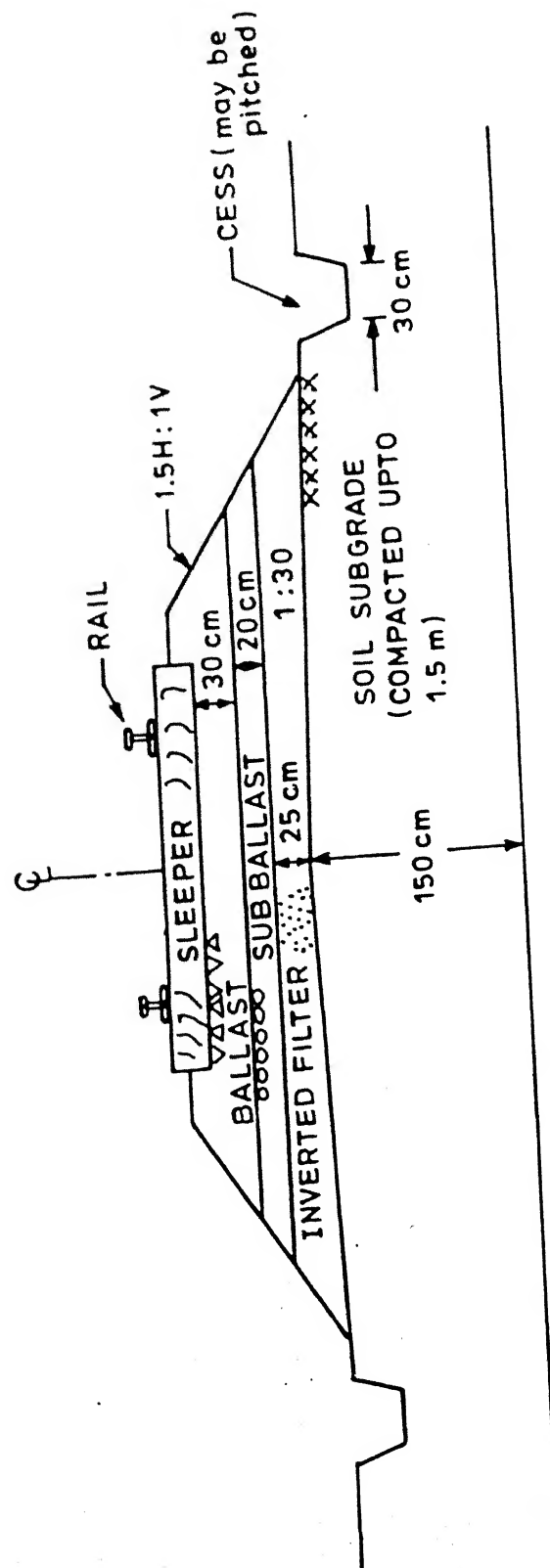


Fig. 5.7 Cross-section of a typical formation

provision of lateral drains at different intervals along the track has been suggested. The typical values in Fig. 5.7 are only valid for a specific site.

CHAPTER 6

CONCLUSIONS AND RECOMMENDATIONS

6.1 GENERAL

On the basis of the detailed analysis to estimate the stresses induced in the railway formation and experimental investigations undertaken to study the effect of these induced stresses on subgrade soil, following aspects are established. These aspects have been described below under the following heads.

1. Mathematical modelling
2. Geotechnical investigations
3. Design methodology

6.2 MATHEMATICAL MODELLING

In the present study, three models viz. ELASTIC.F, 2D8N and 3D20N have been developed for calculating the stresses in the track structure. Based on the mathematical modelling carried out in this study, following conclusions are arrived at :

1. Maximum major principal stress on top of subballast and ballast is found to be slightly on the right side of the rail

seat (Fig. 3.50). However, on top of subgrade, maximum stress occurs below the rail seat (Figs. 3.50 and 3.52).

2. Maximum τ_{\max} on top of subgrade occurs slightly to the right of the rail seat. However, the difference between maximum τ_{\max} and τ_{\max} below the rail seat is insignificant and for all practical purposes, τ_{\max} below the rail seat may be taken as maximum τ_{\max} on top of subgrade.

3. Around 68 % of major principal stress on top of subgrade disperses within 1 m depth of subgrade for single wheel load case while for double wheel load case, the corresponding dispersion is only 14 % [Fig. 3.49(a)].

4. The following general conclusions can be made from the results of parametric studies :

(a) Depth of formation and type of subgrade are the most important factors affecting the vertical stress coming on the subgrade.

(b) Tie spacing moderately affects the vertical stress on top of subgrade.

(c) Type of rail has negligible influence on vertical stress on top of subgrade.

5. Major principal stress on top of subgrade under the rail seat, σ_{1t} increases with increase in Young's modulus of

subgrade, E_s while minor principal stress on top of subgrade under the rail seat, σ_{3t} decreases with increase in E_s . However both σ_{1t} and σ_{3t} decrease with increase in depth of formation (Fig. 3.40).

6. Gain achieved by increasing the depth of ballast (keeping total depth of formation constant) in terms of reduction of settlement or major principal stress on top of subgrade is not significant (Fig. 3.42).

7. Displacement of track, δ is the function of type of subgrade only while other track parameters and depth of formation have negligible effect on δ (Fig. 3.41).

8. The effect of joint elements is to reduce both Major and Minor principal stresses on top of subgrade under the rail seat marginally and to increase the displacement of top of sleeper (Figs. 3.40 and 3.41).

9. Results predicted by all the three models (ELASTIC.F, 2D8N and 3D20N) have been compared with results predicted by other models, measured results in the field by ORE (Office for Research and Experiments, International railways) and Indian railways, full scale model test results by ORE and semi-empirical methods available in literature. It has been found that all the three models predict the results quite satisfactorily.

However, semi-empirical methods available in literature predict stresses two to four times higher than those measured in the field for certain Indian tracks while ELASTIC.F and 3D20N models predict stresses for the same tracks within 20 % of the measured stresses which is the range of measurement for these results. Thus, the need to carry out detailed stress analysis in the present study is well brought out.

10. Results obtained from ELASTIC.F model lie within 5-20 % of results obtained by 3D20N model in general and vary up to 90 % for high values of Young's modulus of subgrade and low values of depth of formation.

11. Results obtained by 2D8N model lie within 10 % of results obtained by 3D20N model. However, it may be noted that 2D8N will underpredict stresses on top of subgrade for smaller depth of formation and will overpredict it for large depths due to two dimensional nature of this model. However, to rectify this shortcoming, a semi-analytical modification has been suggested.

12. 3D20N model predicts results quite similar to MULTA model [Selig et al. (1979)] which is like a closed form solution.

13. It is shown that the vertical and horizontal stresses inside the subgrade predicted by elastic analysis compare well

with those obtained by elasto-plastic analysis which takes into consideration 'no tension' condition in granular material.

14. Tensile minor principal stresses are predicted by this model in the ballast and subballast layers which is the disadvantage of elastic analysis. However, it is shown that minor principal stresses inside the subgrade predicted by elastic analysis compare well with elasto-plastic analysis.

15. A non - dimensional parameter, m has been introduced as a measure of ballast, subballast and subgrade characteristics (i.e. the formation quality), in a simple way, as

$$m = E_{\text{equ}} / E_s ,$$

and
$$E_{\text{equ}} = (E_b d_b + E_{sb} d_{sb}) / (d_b + d_{sb})$$

The effectiveness of using m in design has been clearly brought out in Chapters 3 and 5.

6.3 GEOTECHNICAL TESTING

The conclusions arrived at from the geotechnical testing carried out in the present study (Chapter 4) have been given below under the different heads :

1. Unconfined tests
2. Effective stress static tests
3. Effective stress cyclic tests

6.3.1 Unconfined tests

1. The relationship between incremental plastic strain, $\delta\epsilon_p$ after 100 load cycles on unconfined compacted samples and the corresponding increase in incremental water content on softening has been developed (Fig. 4.57). Such a relationship, if developed on undisturbed sample, would offer a simple methodology to predict the expected changes in the water content due to cyclic loading on the basis of incremental plastic strain data.

2. Soil samples subjected to unconfined cyclic loading undergo changes in stiffness (Fig. 4.59). E-value increases with cyclic stress ratio, R_f up to a certain level after which no more stiffening takes place as a result of cyclic loading. However, reduction in E-value takes place for softened state due to reduction in effective stresses.

3. Value of ultimate failure stress of samples is practically independent of the cyclic stress history (Fig. 4.58).

4. The explanation of mudpumping problems encountered by Indian railways under the tracks in alluvial soil deposits has

been well brought out by observing the significant degradations in both stiffness and strength following the transient loading and softening.

5. Threshold stress ratio for alluvial silt under unconfined conditions for compacted samples has been obtained as 0.75.

6.3.2 EFFECTIVE STRESS STATIC TESTS

1. A simple procedure to ensure quasi-saturated behaviour for partially saturated sample is given (Fig. 4.66). Following this procedure, for Campus silt, it is observed that samples with $S > 0.94$, $w = \text{OMC} + 1\%$ and $B \geq 0.5$ would exhibit quasi saturated behaviour and continuous water voids. For Canyon dam clay [Casagrande and Hirschfeld (1960); Casagrande and Poulos (1964)], samples with $S > 0.9$ and $B \geq 0.5$ and for Chiew larn dam clay [Ganeshan (1982)], $S > 0.95$ and $B \geq 0.3$ are expected to show quasi saturated behaviour.

2. It has been shown that effective stress paths for compacted samples will show a normalized behaviour as is typically exhibited by saturated samples only at very high values of σ_c' (Figs. 4.71 and 4.72). It is observed that stress - strain and pore pressure - strain response for these samples also follow non - normalized behaviour. Back saturated samples at low confining pressures follow non - normalized behaviour (Fig. 4.74).

3. Samples of Campus silt and Canyon dam clay compacted at OMC or OMC + 1% follow the following relationship for fully saturated condition (Fig. 4.73) :

$$(\sigma_1 - \sigma_3)_f / 2 = 160 + 0.460 \sigma_c'$$

4. A unique effective stress failure envelope is obtained from both $(\sigma_1 - \sigma_3)_{\max}$ and $(\sigma_1' / \sigma_3')_{\max}$ criteria for Campus silt which can be represented in terms of effective stress shearing resistance parameters, $c' = 10.7$ kPa and $\phi' = 32.6^\circ$ (Fig. 4.76). Incidentally, it has been shown that evaluation of failure envelope by Marsal's procedure [Marsal (1970)] gives satisfactory result.

5. The stress - strain, pore pressure - strain, stress path and other results for Campus silt show remarkable similarities with group IV soils [Cruz et al. (1985)] as shown in Figs. 4.23 to 4.34.

6. It is observed that Campus silt and Canyon dam clay [Casagrande and Hirschfeld (1960); Casagrande and Poulos (1964)] show remarkable similarities in practically all aspects of the behaviour of compacted samples. Effective stress data available for both soils on compacted samples has been examined in the general framework of critical state model (Figs. 4.79 to 4.85).

Guidelines given by Yudhbir and Wood (1989) have been followed in drawing VCL, CSL, Recompression lines, Tension cut off etc. It has been observed that these lines show reasonable fit with the actual experimental data (Figs. 4.79 to 4.84).

These results suggest that compacted soil behaviour may also be successfully interpreted using the critical state model. It is shown that for low confining stress levels, the compacted samples at failure tend to lie on Hvorslev surface.

7. While comparing data in terms of total stress behaviour of compacted soils, following observations have been made :

a. Samples compacted dry of optimum and tested either unconfined or with $\sigma_3 = 100$ kPa show practically constant value of q_f up to OMC after which q_f decreases with increasing water content while failure mode changes from brittle to the bulging type.

b. For both softened and unsoftened unconfined tests, there is a unique w vs q_f relationship which lies left of the fracture-rupture boundary as suggested by Yudhbir and Wood (1989).

The generalized relationship initially proposed by Leroueil et al. (1992) between $(w - w_{opt})/I_p$ and s_u has been modified as given below (Fig. 4.87) :

$$s_u = 115 \exp [-6.7 (w - w_{opt})/I_p]$$

It is proposed that this relationship may be used for estimating undrained strength of compacted clays at OMC or wet of OMC.

6.3.3 EFFECTIVE STRESS CYCLIC TESTS

1. For cyclic stress ratio, R_f below threshold stress ratio R_{TS} , cumulative plastic strain, ϵ_p attains a maximum value at N approximately equal to 50 to 60 after which practically no more increase in ϵ_p occurs. However, for $R_f > R_{TS}$, ϵ_p values for the same number of cycles, show sudden increase in magnitude.

ϵ_p after 100 cycles shows decreasing trend with σ'_c values as also observed by Janin et al. (1980).

The following relationship to relate ϵ_p with N has been suggested :

$$\log(\epsilon_p) = C_p + D_p \log(N_1) + E_p \log(N_2/N_s)$$

where $N_1 = N$ and $N_2 / N_s = 1$ for $N \leq N_s$, and
 $N_1 = N_s$ and $N_2 = N$ for $N > N_s$

For $R_f < R_{TS}$, E_p value is less than D_p or equal to zero while for $R_f \geq R_{TS}$, both $E_p = D_p$ and $E_p > D_p$ trends are observed.

From the limited results, it would appear that for $R_f > R_{TS}$, E_p value may be taken as constant for a given soil type. E_p value was found to be 0.622 for undisturbed London clays. E_p

= 0.52 and $E_p = 0.28$ have been evaluated for undisturbed stiff Boulder clay and Keuper marl [Janin et al. (1983a)]. The corresponding E_p value for the Campus silt is of the order of 0.22.

Published results for other types of soils viz. stiff undisturbed, normally consolidated (undisturbed and remoulded), etc. have also been analyzed and it is observed that variation of C_p and E_p values with R_f (Fig. 4.94) tends to suggest a consistent pattern for compacted and undisturbed low plasticity silty soils. The normally consolidated undisturbed and remoulded soils of comparable plasticity also show another consistent pattern.

Plastic strain rate decreases approximately by a factor of 10 for every log cycle increase in N values. This agrees with the observations of Hyde and Brown (1976).

2. Hyde and Ward (1985) have proposed that end points of cyclic loading tests on normally consolidated and over consolidated tests would lie on the Hvorslev surface as represented in q/P_e' vs P'/P_e' space. A similar result is obtained for cyclic test data for compacted Campus silt (Fig. 4.98).

3. Incremental plastic strain during 100 cycles shows sudden increase after certain value of R_f which may be taken as a measure of threshold stress ratio (Fig. 4.99).

Similarly, variation of C_p and E_p with R_f can also be used

to estimate the value of R_{TS} . Both C_p and E_p values show sudden increase beyond a certain R_f which may be taken as threshold stress ratio. In case of normally consolidated soils, change in C_p values is not as abrupt as observed for compacted and stiff undisturbed samples tested at low confining stresses.

4. It has been shown that threshold stress and equilibrium line can be obtained by examining the normalized effective stress paths for different σ_c' values (Fig. 4.96).

An indirect approach to the determination of threshold stress ratio for dilative soils on the basis of stress level at which maximum positive pore pressure develop has been made. For σ_c' up to 40 kPa, threshold stress level corresponds to stress level at which maximum positive pore pressure develops but at relatively, high σ_c' values, R_{TS} is overpredicted by as much as 25 % .

5. Sangrey et al. (1978) have proposed a relationship between R_{TS} and κ for the range of σ_c' values where κ , the measure of soil compressibility is dependent on I_p . On suggestion of Yudhbir (1992), a relationship between R_{TS} and I_p has been developed for a variety of soils (compacted, stiff, normally consolidated etc.) at low and relatively high effective confining stresses. Based on this, the following empirical equations are suggested as guidelines to estimate R_{TS} (Fig. 4.101) :

for $\sigma_c' = 35$ kPa,

$$R_{TS} = 0.045 + 1.29 I_p$$

for $\sigma_c' > 300$ kPa,

$$R_{TS} = 0.565 + 0.65 I_p$$

For railway formation design, the relationship given in Eq. (4.12) may be used for evaluation of threshold stress for routine works on the basis of plasticity index of the soil.

Relationship of the form $(\sigma_1 - \sigma_3)_{TS} = a + b \sigma_c'$ has also been given for a variety of soil types at low effective stress ranges. Values of coefficients a and b depend on the soil type, its stress history and whether compacted or undisturbed.

Also, as a rule of thumb, it is observed that threshold stress $(\sigma_1 - \sigma_3)$ for railway design could be taken as 36 percent of ultimate unconfined strength, $(\sigma_1 - \sigma_3)$ for Campus silt while for Angul clay, this works out to be 17 percent of ultimate unconfined strength for Angul clay.

A design methodology based on stresses induced and threshold stress has been proposed. A detailed step by step procedure (flow chart) has been outlined and a simplified method for routine design of formation depth has been recommended.

6.4 RECOMMENDATIONS FOR FURTHER STUDIES

1. The performance of the new tracks built according to design proposed above should be carefully monitored for few years. This will help in evaluating the efficacy of the proposed design methodology and will give the required confidence.

2. Design charts similar to Figs. 5.1 or 5.2 may be plotted by carrying out elasto-plastic analysis of track structure. However, this should be done only when the detailed careful monitoring of track structure built on present design help increase the knowledge about actual failure mechanism and suggests the need for elasto-plastic analysis.

3. In the present study, dynamic wheel load is calculated from the static wheel load by empirical method (either by formulae or by charts). However, it is well known that this dynamic wheel load is dependent upon track quality, stiffness, deflection and type of subgrade. Hence, a rational method should be evolved to convert static wheel load into dynamic wheel load which considers all the factors mentioned above.

4. Presently, ballast depth is being taken as 25 cm on empirical basis. However, fatigue strength of ballast and subballast should be properly evaluated and proportioning for them should be based on this strength.

5. Study regarding existing status of formation at different locations may be taken up according to proposed design methodology. For this purpose, instead of evaluating threshold stress for compacted samples, undisturbed samples will be used for testing. This will help in following ways :

a. This will improve the performance of Indian tracks in terms of riding comfort and accidents.

b. This will help in reducing the maintenance cost enormously.

c. This will provide the feedback for the proposed design methodology and then, further improvements can be made accordingly, based on this experience.

6. The relationship between threshold stress and depth of formation has been given in Fig. 5.5 for four soil types. It is highly desirable to have this data for different soil types for both compacted and undisturbed samples. This will be helpful in developing still better simplified design procedures.

REFERENCES

- Agarwal, V. K., and Yog, A. K. (1975). "New approach to the design of railway track foundation." *Indian Railway Technical Bulletin*, XXXII, 198, 66-78.
- Andersen, K. H., et al. (1976). "Effect of cyclic loading on clay behaviour." *Norwegian Geotech. Inst. Pub.*, 113, 1-6.
- Andersen, K. H., et al. (1980). "Cyclic and static laboratory tests on Drummen clay." *Norwegian Geotech. Inst. Pub.*, 131, 1-31.
- Andersen, K. H., et al. (1988). "Cyclic soil data for design of gravity structures." *Norwegian Geotech. Inst. Pub.*, 175, 1-23.
- Andersen, K. H., and Hoeg, K. (1992). "Deformation of soils and displacements of structures subjected to combined static and cyclic loads." *Norwegian Geotech. Inst. Pub.*, 185, 1-12.
- Baldi, G., Hight, D. W., and Thomas, G. E. (1988). "A reevaluation of conventional triaxial test methods." *Advanced triaxial testing of Soil and Rock*, STP 977, Amer. Soc. Testing and Materials, 82-94.
- Bishop, A. W., and Henkel, D. J. (1953). "Pore pressure changes during shear in two undisturbed clays." *Proc. 3rd Int. Conf. on Soil Mech. and Found. Engrg.*, Zurich, 1, 94-99.
- Bishop, A. W., Alpan, I., Blight, G. E., and Donald, I. B. (1960). "Factors controlling the strength of partly saturated cohesive soils." *Proc. Res. Conf. on Shear Strength of Cohesive Soils*, ASCE, Univ. of Colorado, Boulder, 503-532.
- Bishop, A. W., and Henkel, D. J. (1962). *The measurement of soil properties in the triaxial test*. Second edition, Edward Arnold publishers Ltd., London.
- Bishop, A. W., and Wesley, L. D. (1975). "A hydraulic triaxial apparatus for controlled stress path testing." *Geotechnique*, London, England, 25(4), 657 - 670.
- Bowles, J. E. (1984). *Foundation analysis and design*. McGraw-Hill Inc., International Student Edition, New York, N.Y.

- Burgohain, D. N., and Shah, V. L. (1977). "Curved interface elements for interaction problems." *Proc. Int. Symp. on Soil - Struct. Interaction*, Univ of Roorkee, Roorkee, India, Jan, 1, 197-201.
- Burgohain, D. N., and Shah, V. L. (1978). "Curved isoparametric interface surface elements." *J. Struct. Div.*, ASCE, 104(1), 205-209.
- Burmister, D. M. (1945). "The general theory of stresses and displacements in layered systems -- I, II and III." *J. Appl. Physics*, (Feb., Mar., May), 16(2,3,5), 88-94, 126-128, 296-302.
- Casagrande, A., and Hirschfeld, R. C. (1960). "First progress report on investigation of stress, deformation and strength characteristics of compacted clays." A research project sponsored by 'The Waterways Experiment Station' in co-operation with Harvard University, Pierce Hall, Harvard University, Cambridge, Massachusetts, May.
- Casagrande, A., and Poulos, J. (1964). "Fourth progress report on investigation of stress, deformation and strength characteristics of compacted clays." A research project sponsored by 'The Waterways Experiment Station' in co-operation with Harvard University, Pierce Hall, Harvard University, Cambridge, Massachusetts, October.
- Chang, S. C., Adegoke, C. W., and Selig, E. T. (1980). "Geotrack model for railroad track performance." *J. Geotech. Engrg.*, ASCE, 106(11), 1201-1217.
- Cook, R. D., Malkus, O. S., and Plesha, M. E. (1989). *Concepts and applications of finite element analysis*. Third Edition, John Wiley and Sons, New York, N.Y.
- Cruz, P. T., et al. (1985). "Peculiarities of tropical lateritic and saprolitic soils used as construction materials : Selection, control and acceptance criteria -- Dams." *Progress Report of Committee on Tropical Lateritic and Saprolitic Soils*, Brazilian Soc. of Soil Mech., 275-327.
- Curnier, A. (1983). "A static infinite element." *Int. J. Numer. Methods Engrg.*, 19, 1479-1488.
- Desai, C. S., and Siriwardane, H. J. (1982). "Numerical models for track support structures." *J. Geotech. Engrg.*, ASCE, 108(3), 461-480.
- Fenner, R. T. (1986). *Engineering elasticity - application of numerical and analytical techniques*. John Wiley and Sons, New York, N.Y.

- France, J. W. (1976). "An investigation of the effects of the drainage on the repeated load behaviour of soils," thesis presented to the Cornell University at Ithaca, U.S.A., in partial fulfillment of the requirements for the degree of Master of Science.
- Fredlund, D. G., Morgenstern, N. R., and Widger, R. A. (1978). "The shear strength of unsaturated soils." *Can. Geotech. J.*, 15(3), 314-321.
- Ganeshan, V. (1982). "Strength and collapse characteristics of compacted residual soils," thesis presented to the Asian Institute of Technology at Bangkok, Thailand, in partial fulfillment of the requirements for the degree of Master of Engineering, GT-18-16.
- Goodman, R. E., Taylor, R. L., and Brekke, L. (1968). "A model for the mechanics of jointed rock." *J. Soil Mech. and Found. Engrg. Div.*, ASCE, 94(3), 637 - 659.
- Gupta, S. K. (1973). "Undrained behaviour of a silt from Indo - Gangetic alluvium," thesis presented to the Indian Institute of Technology at Kanpur, India, in partial fulfillment of the requirements for the degree of Master of Technology.
- Hall, B. E. (A). "Richards bay coal line formation design and material standards." *Abstract of Seminar on Long haul in Canada*, IIB - 50 - 1, IIB - 50 - 17, Report supplied by RDSO, India.
- Harr, M. E. (1966). *Foundations of theoretical soil mechanics*. McGraw-Hill, New York, N.Y.
- Head, K. H. (1982). *Manual of soil laboratory testing*. Volume 1, 2, and 3, Engineering Laboratory Equipment Limited, London.
- Ho, David, Y. F., and Fredlund, D. G. (1982). "Increase in strength due to suction for two Hongkong soils." *Proc. Conf. Engrg. and Const. in Tropical and Residual Soils*, Honolulu, 263-295.
- Hetenyi, M. (1961). *Beams on elastic foundation*. Univ of Michigan Press, Ann Arbor, Mich.
- Hyde, A. F. L., and Brown, S. F. (1976). "The plastic deformation of a silty clay under creep and repeated loading." *Geotechnique*, London, England, 26(1), 173-184.
- Hyde, A. F. L., and Brown, S. F. (1976). "A pore pressure and stability model for a silty clay under repeated loading." *Geotechnique*, London, England, 35(2), 113-125.
- IS : 5249 - 1977. "Method of test for determination of in situ dynamic properties of soils." I.S.I., New Delhi.

IS : 1888 - 1982, "Method of load test on soils." Second Edition, I.S.I., New Delhi.

Janin, et al. (1980). "Question D 117 -- Optimum adoption of the conventional track to future traffic. Report No. 14 -- Performance of soil under the effect of repetitive stresses as a function of particle size and water content." Report No. D117 / RP 14, ORE, Utrecht, Netherlands.

Janin, et al. (1982). "Question D 117 -- Optimum adoption of the conventional track to future traffic. Report No. 18 -- The behaviour of track bed structure under repeated loading (First phase - Vienna arsenal tests)." Report No. D117 / RP 18, ORE, Utrecht, Netherlands.

Janin, et al. (1983a). "Question D 117 -- Optimum adoption of the conventional track to future traffic. Report No. 25 -- The behaviour of the track bed structure under repeated loading (Tests at Vienna arsenal and Derby)." Report No. D117 / RP 25, ORE, Utrecht, Netherlands.

Janin, et al. (1983b). "Question D 117 -- Optimum adoption of the conventional track to future traffic. Report No. 27 -- The behaviour of track bed structure under repeated loading." Report No. D117 / RP 27, ORE, Utrecht, Netherlands.

Janin, et al. (1983c). "Question D 117 -- Optimum adoption of the conventional track to future traffic. Report No. 28 -- Design charts for the track / foundation system." Report No. D117 / RP 28, ORE, Utrecht, Netherlands.

Jumikis, A. R. (1966). *Soil mechanics*. D. Von Nostrand Company Inc., Princeton, New Jersey.

Kapoor, O. P., et al. (1967a). "Investigations on the determination of intensity of pressure on railway formation - BG track." Progress Report No. 1 - Civ. Engrg. Report No. C-55, RDSO, India.

Kapoor, O. P., et al. (1967b). "Investigations on the determination of intensity of pressure on railway formation - BG track." Progress Report No. 2 - Civ. Engrg. Report No. C-56, RDSO, India.

Kumar, P., et al. (1990). "To study the effect of repetitive loading on railway formation - Cyclic plate load test determination of dynamic moduli." Progress Report No. 1/2 - Subproject I, Geotech. Engrg. Directorate, RDSO, India, October.

- Kumar, P., et al. (1991a). "To study the effect of repetitive loading on railway formation - Cyclic plate load test determination of dynamic moduli." *Progress Report No. 1/3 - Subproject I, Geotech. Engrg. Directorate, RDSO, India, March.*
- Kumar, P., et al. (1991b). "To study the effect of repetitive loading on railway formation - Wave propagation meter test determination of dynamic moduli." *Progress Report No. 2/3 - Subproject II, Geotech. Engrg. Directorate, RDSO, India, March.*
- Lambe, T. W. (1960). "A mechanistic picture of shear strength in clay." *Res. Conf. on Shear Strength of Cohesive Soils, ASCE, Univ of Colorado, Boulder, 555-580.*
- Lambe, T. W., and Whitman, R. V. (1978). *Soil Mechanics*. Wiley Eastern Limited, New Delhi.
- Leroueil, S., et al. (1992). "Remarks on the design of clay liners used in lagoons as hydraulic barriers." *Communicated for Publication. Preprint.*
- Marsal, R. J. (1979). "Analysis of fundamentals of compacted cohesive soils." *General report, Main session IV, Proc. 6th Pan-Am conf. on Soil Mech. and Found. Engrg., Lima, Peru, 1, 143-222.*
- Menzies, B. K. (1988). "A computer controlled hydraulic triaxial testing system." *Adv. Triaxial testing of Soil and Rock - STP 977, Amer. Soc. Testing and Materials, 82-94.*
- Mukerji, A. K., and Yog, A. K. (1974). "Intensity and pattern of distribution of pressure coming on the railway formation under various depths of ballast and blanket with different packing conditions on broad gauge - static test." *Civ. Engrg. Report No. C-131, Geotech. Engrg. Directorate, RDSO, India.*
- Mundrey, J. S. (1988). *Railway track Engineering*. Tata McGraw-Hill Publishing Co. Ltd., New Delhi.
- Prakasa Rao, A. V. N. S. (1985). "Effective stress interpretation of in situ stress data," thesis presented to the Indian Institute of Technology at Kanpur, India, in partial fulfillment of the requirements for the degree of Master of Technology.
- Rao, S. S. (1987). *The finite element method in engineering*. Second Edition, Pergamon Press, Oxford.
- RDSO (A). "State of art - shear strength of soils under cyclic loading." *communicated in written by Joint Director, Geotech. Engrg. Directorate, RDSO, India.*

- RDSO (B). "Track in the system railway." O. Univ. - Prof. Dipl. - Ing. Dr. Techn. Klaus RieBberger, Technische Universitat Graz, Report supplied by RDSO, India.
- RDSO (C). "M/s RITES report." Report supplied by Geotech. Engrg. Directorate, RDSO, India.
- RDSO (D). "B.S. Mundy -- CRA/GE's copy." Report supplied by Geotech. Engrg. Directorate, RDSO, India.
- RDSO (1987). "Interim report II for the feasibility study on railway improvement plan of transport capacity and train speed on Delhi - Kanpur section in India - Appendix - II." Japan Int. Cooperation Agency (JICA), Report supplied by RDSO, India.
- Reddy, J. N. (1986). *An introduction to the finite element method*. International Edition, McGraw-Hill Inc., New York, N.Y.
- Rehman, M. S. (1977). "Undrained behaviour of saturated normally consolidated clay under repeated loading," thesis presented to the Indian Institute of Technology at Kanpur, India in partial fulfillment of the requirements for the degree of Master of Technology.
- Rubin, et al. (1970). "Question D71 -- Stresses in the rails, the ballast and in the formations resulting from traffic loads. Report No. 12 -- Repeated loading of clay and track foundation design." Report No. D71 / RP12, ORE, Utrecht, Netherlands.
- Sangrey, D. A. (1968). "The behaviour of soils subjected to the repeated loading," thesis presented to the Cornell University at Ithaca, U.S.A., in partial fulfillment of the requirements for the degree of Doctor of Philosophy.
- Sangrey, D. A., Castro, G., Poulos, S. J., and France, J. W. (1978). "Cyclic loading of sands, silts and clays." *Proc., ASCE Spec. Conf. on Earthquake Engrg and Soil Dynamics*, Pasadena, 2, 836-51.
- Saxena, S. C., and Arora, S. (1987). *A text book of railway engineering*. Dhanpat Rai and Sons, Delhi.
- Schjetne, K. (1976). "Foundation engineering for gravity structures in the north sea." *Norwegian Geotech. Inst. Pub.*, 113, 23-33.
- Selig, E. T., Chang, C. S., Adegoke, C. W., and Alwa - Hurtado, J. E. (1979). "A theory for track maintenance and life prediction." *Technical Report DOT / RSPA / DPB - 50 / 79 / 22*, Civ. Engrg. Dept., State Univ of New York at Buffalo.

Senac, G. (1984). "Increasing speeds on existing lines." *French Railway Review*, 2, 123-130.

Shew, W. Y., and Chang, N. Y. (1987). "Cyclic behaviour of a clay : experiment and modelling." *Soil Dynamics and Liquefaction, Developments in Geotech. Engrg.*, Elsevier Comp. Mech. Pub., 42, 269 - 282.

So, W. (1978). "Track structure design using mathematical models." *Technical Report No. FRA/ ORD - 78/08*, Association of American Rail road.

Srivastava, N. K. (1977). "Laboratory determination of in-situ parameters of alluvium soils," thesis presented to the Indian Institute of Technology at Kanpur, India, in partial fulfillment of the requirements for the degree of Master of Technology.

Stewart, H. E., and Selig, E. T. (1982). "Predicted and measured resilient response of track." *J. Geotech. Engrg.*, ASCE, 108(11), 1423-1442.

Tadatoshi, I., et al. (A). "Measures for stabilization of railway earth structures." *Japan Railway Technical Service*, Report supplied by RDSO, India.

Talbot, A. N., et al. (1923). "Third progress report of the special committee to report on stresses in railroad track." *Trans. ASCE*, LXXXVI, 907-1068.

Timoshenko, S., and Langer, B. F. (1932). "Stresses in railroad track." *Appl. Mech. Div., Trans. Am. Soc. of Mechanical Engrg.*, 54, 272-302.

Vijayan, C. (1981). "Finite element analysis of strip and circular plate anchors," thesis presented to the Indian Institute of Technology at Kanpur, India, in partial fulfillment of the requirements for the degree of Doctor of Philosophy.

Weeraratne, S. J. (1982). "Compaction and strength characteristics of a compacted residual soil," thesis presented to the Asian Institute of Technology at Bangkok, Thailand, in partial fulfillment of the requirements for the degree of Master of Technology, GT-18-16.

Wilson, N. E., and Greenwood, J. R. (1974). "Pore pressures and strains after repeated loading of saturated clay." *Can. Geotech. J.*, 11(2), 269-277.

Wood, D. M. (1982). "Laboratory investigations of the behaviour of soils under cyclic loading : A review." *Soil Mechanics - Transient and Cyclic loads*, G. N. Pande and O. C. Zienkiewicz.. eds.. John Wiley and Sons. Inc., 513-582.

- Wroth C. P., and Wood D. M. (1978). "The correlation of index properties with some basic engineering properties of soils." *Can. Geotech. J.*, 15(2), 137-145.
- Yudhbir (1992). "Relationship between threshold stress ratio and plasticity index at different confining pressures" *Personal Communication*.
- Yudhbir, and Korchoke, C. (1987). "Evaluation of effective stress strength parameters of partially saturated soils." *Proc. Indian Geotech. Conf.*, Bangalore, 1, 35-40.
- Yudhbir, et al. (1979). "Design parameters for shallow foundations on alluvium." *Proc. 6th Asian regional conf. on Soil Mech. and Found. Engrg.*, Singapore. Preprint.
- Yudhbir, and Prakasa Rao, A. V. N. S. (1986). "Effective stress interpretation of in situ tests" *Use of in-situ tests in geotechnical engineering*, S. P. Clemence, ed., ASCE, Geotech. Special Pub. No. 6, 1189-1200.
- Yudhbir, and Kameswara Rao, N. S. V. (1989). "An approach paper for a rational criterion for design and construction of railway formations." *Report submitted to RDSO, India*, May.
- Yudhbir, Kameswara Rao, N. S. V., and Shahu, J. T. (1991). "A rational criterion for design and construction of railway formations." *Report No. 1, Volume 1, Technical Report submitted to RDSO, India*, May.
- Yudhbir, Kameswara Rao, N. S. V., and Shahu, J. T. (1992). "Design of track formation at Angul for NALCO (Orissa)." *Dept. of Civ. Engrg., IIT, Kanpur, India*.
- Yudhbir, Raymahashay, B. C., and Sahu (1980). "Compaction characteristics of clay mineral mixtures." *Proc. Int. Conf. on Compaction*, Paris, 93-98.
- Yudhbir, and Rehman, M. S. (1977). "Deformation and pore pressure response of a soft clay subjected to the repeated loading." *Proc. Int. Symp. on Soft Clay*, Bangkok, Thailand, 181 - 191.
- Yudhbir, and Weeraratne, S. P. (1988). "Aging and air drying of wet side compacted soils." *Int. Conf. on Engrg. Problems on Regional Soils*, Beijing, China. Preprint.
- Yudhbir, and Wood, D. M. (1989). "Recent developments in laboratory strength and deformation testing." *General report, 12th Int. Conf. on Soil Mech. and Found. Engrg.*, Rio de Janeiro, Brazil, August. Preprint.

Zienkiewicz, O. C., Emson, C., and Bettess, P. (1983). "A novel boundary infinite element." *Int. J. Numer. Methods Engrg.*, 19, 393-404.

Zienkiewicz, O. C., and Taylor, R. L. (1989). *The finite element method*. Fourth Edition, Vol. 1, McGraw-Hill Inc., London.

APPENDIX A1

Details of TRACK 1

1. Rail :

$$E_r = 206990 \text{ MPa}$$

$$I_r = 2158 \times 10^4 \text{ mm}^4$$

distance of rail from center line of tie = 0.825 m

2. Tie :

$$\text{spacing} = 0.65 \text{ m}$$

$$\text{thickness} = 0.21 \text{ m}$$

$$\text{width} = 0.249 \text{ m}$$

$$\text{length} = 2.75 \text{ m}$$

$$E_t = 10550 \text{ MPa}$$

$$\mu_t = 0.37$$

3. Ballast :

$$d_b = 0.25 \text{ m}$$

$$E_b = 150 \text{ MPa}$$

$$\mu_b = 0.37$$

4. Subballast :

$$d_{sb} = 0.35 \text{ m}$$

$$E_{sb} = 80 \text{ MPa}$$

$$\mu_{sb} = 0.37$$

5. Subgrade :

$$E_s = 20 \text{ MPa}$$

$$\mu_s = 0.33$$

6. Load :

$$\text{wheel load} = 159.4 \text{ kN}$$

$$\text{wheel load spacing} = 1.7 \text{ m (double wheel load)}$$

APPENDIX A2

Details of TRACK 2 [same as FAST TRACK , Selig et al. (1979)]

1. Rail :

$$E_r = 211000 \text{ MPa}$$

$$I_r = 3.95 \times 10^7 \text{ mm}^4$$

2. Tie :

$$\text{spacing} = 0.50 \text{ m}$$

$$\text{thickness} = 0.178 \text{ m}$$

$$\text{width} = 0.254 \text{ m}$$

$$\text{length} = 2.743 \text{ m}$$

$$E_t = 10349 \text{ MPa}$$

$$\mu_t = 0.37$$

3. Ballast :

$$d_b = 0.381 \text{ m}$$

$$E_b = 207 \text{ MPa}$$

$$\mu_b = 0.37$$

4. Subballast :

$$d_{sb} = 0.1524 \text{ m}$$

$$E_{sb} = 138.0 \text{ MPa}$$

$$\mu_{sb} = 0.37$$

5. Subgrade :

$$E_s = 34.5 \text{ MPa}$$

$$\mu_s = 0.33$$

6. Load :

$$\text{Wheel load} = 144.556 \text{ kN}$$

$$\text{Wheel load spacing} = 1.7 \text{ m}$$

Double wheel load considered

APPENDIX A3

So (1978) TRACK and the range of parameters varied

1. Rail :

132 lb rail

$$I_r = 3950 \times 10^4 \text{ mm}^4$$

2. Tie :

spacing = 0.305 m

thickness = 0.178 m

width = 0.229 m

length = 2.59 m

Wooden Ties

3. Subgrade :

$$E_s = 27.58 \text{ MPa}$$

4. Load :

Wheel load = 44.498 kN

Wheel load spacing = 1.78 m

Double wheel load

So (1978) has considered following range of variations for parametric studies :

Tie Spacing : 0.508, 0.609, 0.711 m

Ballast depth : 0.152, 0.305, 0.457, 0.609 m

Young's modulus of subgrade : 13.79, 27.85, 41.37, 55.16 MPa

APPENDIX A4

Details of Derby and Vienna TRACKS

Details of Derby TRACK

1. Rail :

$$E_r = 211000 \text{ MPa}$$

$$I_r = 2158 \times 10^4 \text{ mm}^4$$

2. Tie :

$$\text{spacing} = 0.60 \text{ m}$$

$$\text{thickness} = 0.18 \text{ m}$$

$$\text{width} = 0.25 \text{ m}$$

$$\text{length} = 2.40 \text{ m}$$

$$E_t = 10550 \text{ MPa}$$

$$\mu_t = 0.33$$

3. Ballast :

$$E_b = 180 \text{ MPa}$$

$$\mu_b = 0.2$$

4. Subballast :

$$E_{sb} = 150 \text{ MPa}$$

$$\mu_{sb} = 0.4$$

5. Subgrade :

For Keuper marl subgrade :

$$E_s = 30 \text{ MPa}$$

$$\mu_s = 0.49$$

For Boulder clay subgrade :

$$E_s = 11 \text{ MPa}$$

$$\mu_s = 0.49$$

6. Load :

wheel load = 78.48 kN

wheel load spacing = 1.75 m

double wheel load

Details of Vienna TRACK

1. Rail :

$$E_r = 211000 \text{ MPa}$$

$$I_r = 2158 \times 10^4 \text{ mm}^4$$

2. Tie :

spacing = 0.60 m (for track with panel)

thickness = 0.215 m

width = 0.29 m

length = 2.24 m

$$E_t = 211000 \text{ MPa}$$

$$\mu_t = 0.33$$

3. Ballast :

$$E_b = 250 \text{ MPa}$$

$$\mu_b = 0.2$$

4. Subballast :

$$E_{sb} = 100 \text{ MPa}$$

$$\mu_{sb} = 0.2$$

5. Subgrade :

$$E_s = 20 \text{ MPa (Vienna clay subgrade)}$$

$$\mu_s = 0.49$$

6. Load :

wheel load = 90 kN per sleeper

APPENDIX A5

DETAILS OF TRACKS TESTED IN INDIA

1. Details of TRACK along with the measured results on section no. 2 on Ambala - Ludhiana section (1964-1967) : [Kapoor et al. (1967a) and Kapoor et al. (1967b)]

1. Rail :

$$E_r = 211000 \text{ MPa}$$

$$I_r = 1600 \times 10^4 \text{ mm}^4$$

2. Tie :

$$\text{spacing} = 0.81 \text{ m}$$

$$\text{thickness} = 0.18 \text{ m}$$

$$\text{width} = 0.245 \text{ m}$$

$$\text{length} = 2.74 \text{ m}$$

$$E_t = 10550 \text{ MPa}$$

3. Ballast :

$$E_b = 150 \text{ MPa}$$

$$d_b = 0.2 \text{ m}$$

4. Sand layer :

$$E_{\text{sand}} = 40 \text{ MPa (assumed)}$$

$$d_{\text{sand}} = 0.1524 \text{ m}$$

Pressure was measured at midheight in sand layer.

5. Subgrade :

Sandy loam subgrade .

Elastic track modulus being equal to 34.5 MPa (lowest value measured). Based on this, E_s is taken as 40 MPa.

6. Load :

wheel load = 68.67 kN

single wheel load considered.

2. Details of TRACK along with the measured results on section no. 6 on Ambala - Ludhiana section (1964-1967) : [Kapoor et al. (1967a) and Kapoor et al. (1967b)].

All other track details remain same as for section no. 2 on Ambala - Ludhiana section (1964-67) except the following :

Ballast depth = 0.305 m

CST sleeper

$$E_s = 211000 \text{ MPa}$$

3. Details of TRACK along with the results measured for tests conducted on a dead-end siding near canal bed site at RDSO, Lucknow : [Mukerji and Yog (1974)]

a. Track details : All track details are same as for track at section no. 2 on the Ambala - Ludhiana section. However, six different formation thicknesses as mentioned in Table 3.12 have been used in these tests.

Pressure cells for these tests were embedded at 76 mm inside sand layer below blanket (Table 3.12). Young's modulus for sand is taken as 40 MPa and for blanket 80 MPa.

b. Results observed : Tests were carried out under 4 wheel loads viz. 9t, 12t, 15t, and 18t. However results of all tests under different wheel loads are normalized for 18 t wheel load and average value of normalized formation pressure for 18t load was obtained. The results for different track structures are shown in Table 3.13.

4. Details of track for field measurement of formation pressure due to long haul train trials at Mandah road station, Allahabad division : [RDSO (C)]

a. Track properties : All track properties are same as that of Ambala Ludhiana section except the following :

Sleepers :

Prestressed concrete

$$E_t = 10550 \text{ MPa}$$

Spacing = 0.65 m

Ballast depth = 0.30 m

Load :

Wheel load = 161.57 kN

Double wheel load

APPENDIX B1

TESTING OF 2D8N FINITE ELEMENT ROUTINE

The results obtained by solving Boussinesq's line load problem [Jumikis (1966)] by 2-D Finite element analysis using 2D8N routine are shown in Figs. B1.1 to B1.4 along with the exact solution obtained by solving Boussinesq's equation. Exact results have been shown by full line while points represent results obtained by finite element analysis. Figure B1.1 shows vertical, lateral and shear stress profiles (distribution along depth) under the load. Finite element results and exact results match well.

Figures B1.2 to B1.4 show stress-distribution at 45.72 cm and 76.2 cm (as these are the representative depths where our primary interest lies). It is obvious that 2D8N module is able to reproduce accurate results. Mesh discretization used for this testing is shown in Fig. B1.5.

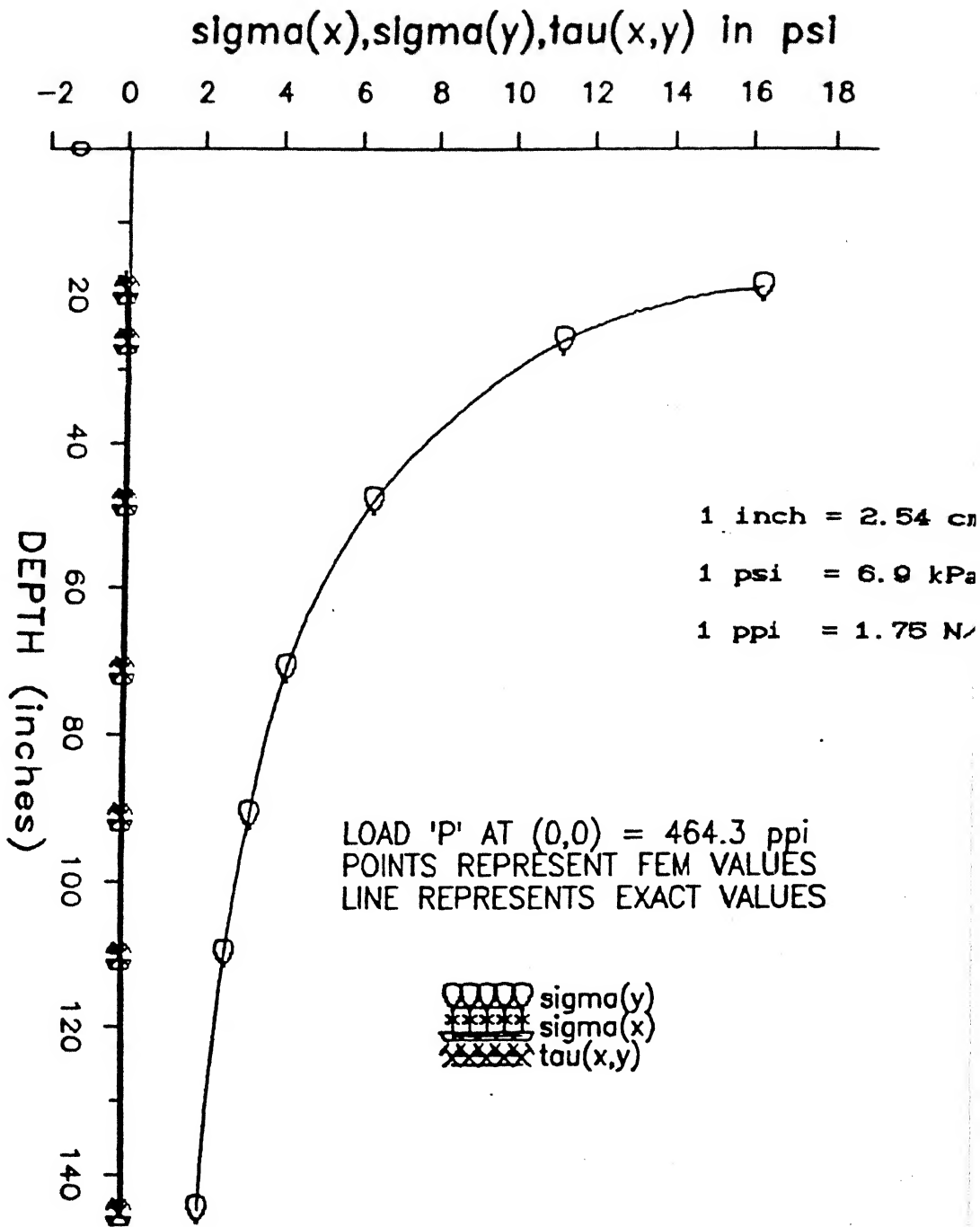


FIG. B1.1 COMPARISON OF EXACT
AND FE SOLUTIONS--STRESS PROFILES
UNDER THE LOAD -- 2-D CASE

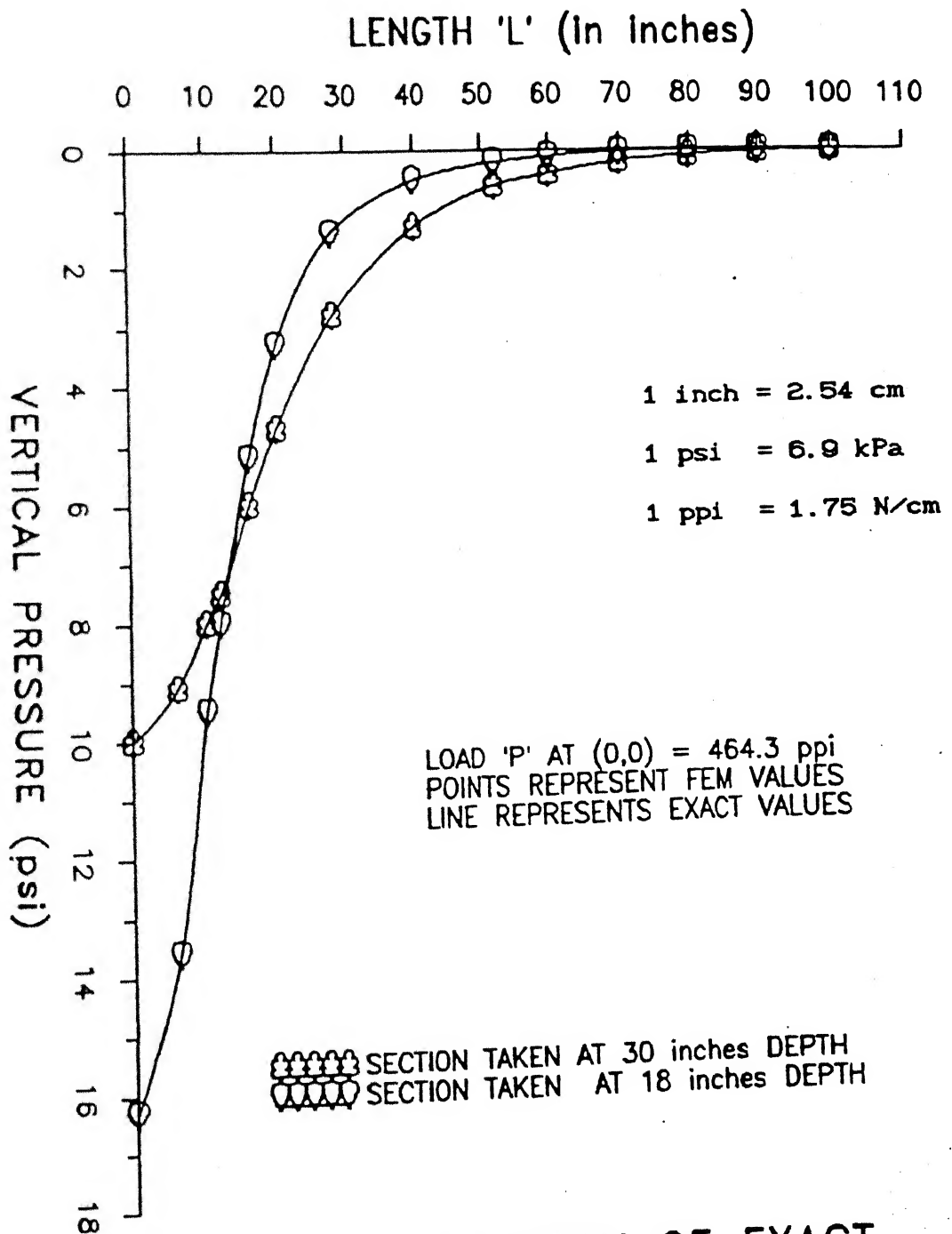


FIG. B1.2 COMPARISON OF EXACT AND FE SOLUTIONS FOR VERTICAL PRESSURE DISTRIBUTION -- 2-D CASE

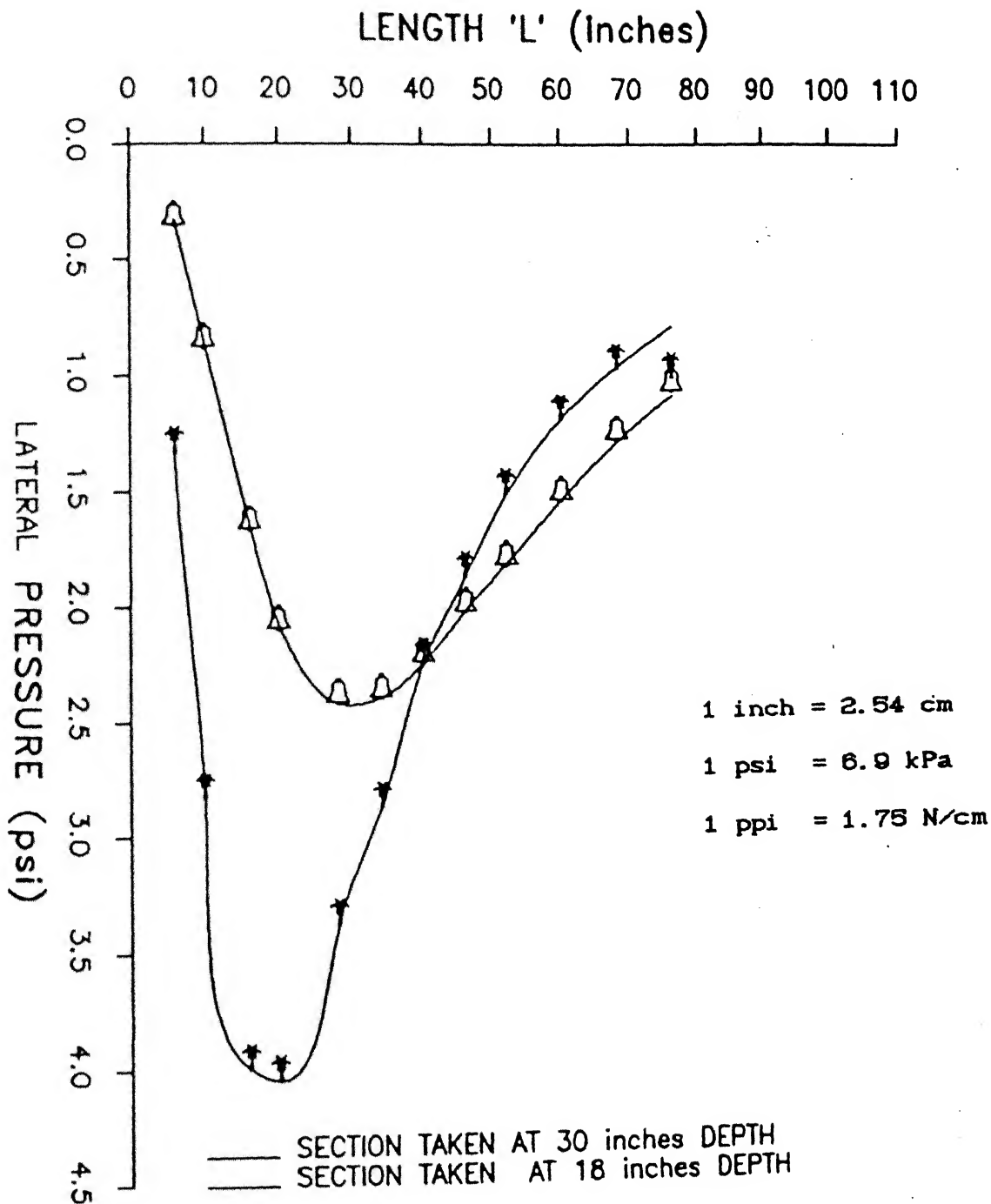


FIG. B1.3 COMPARISON OF EXACT
AND FE SOLUTIONS FOR LATERAL
PRESSURE DISTRIBUTION -- 2-D CASE

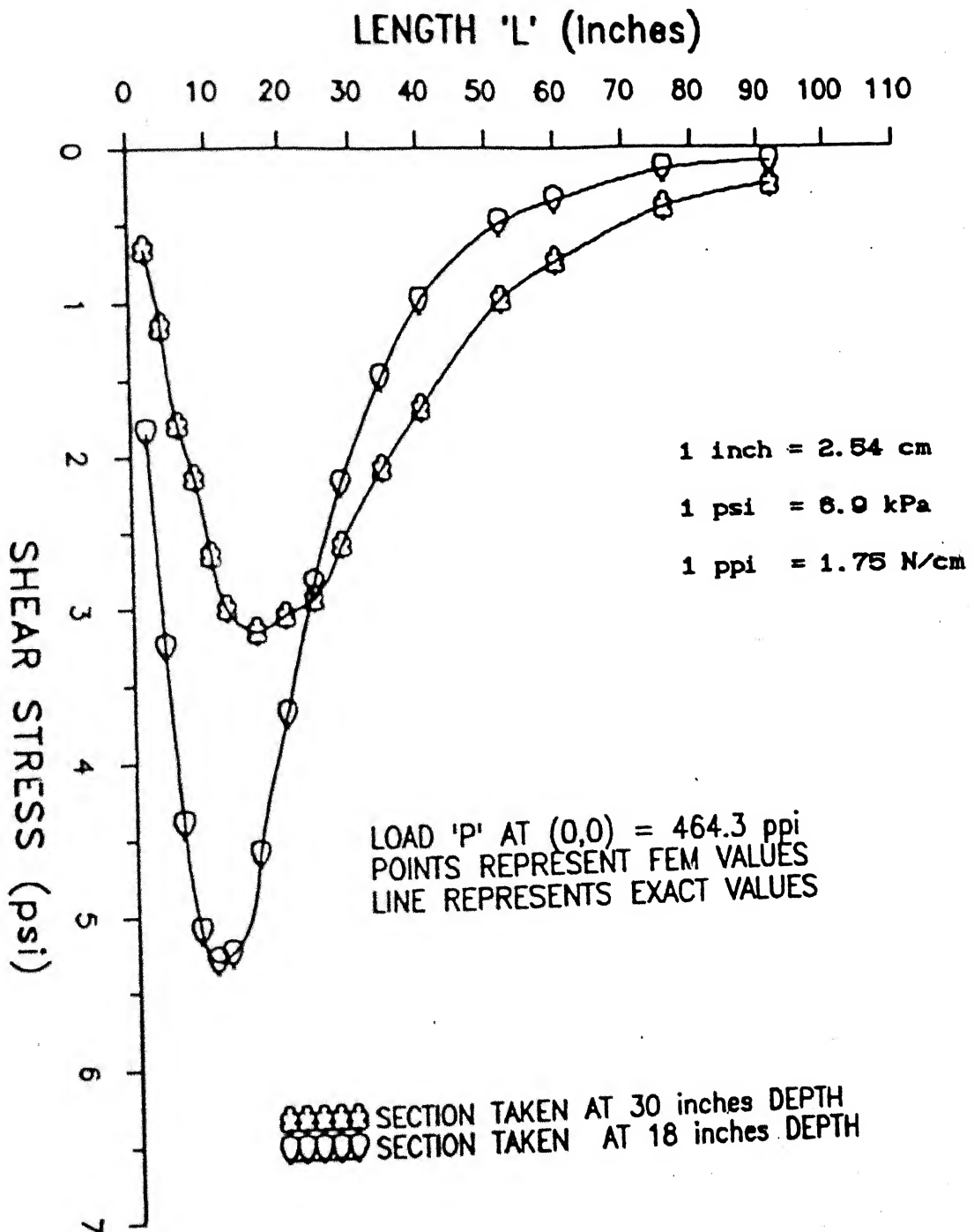


FIG B1.4 COMPARISON OF EXACT
AND FE SOLUTIONS FOR SHEAR STRESS
DISTRIBUTION -- 2-D CASE

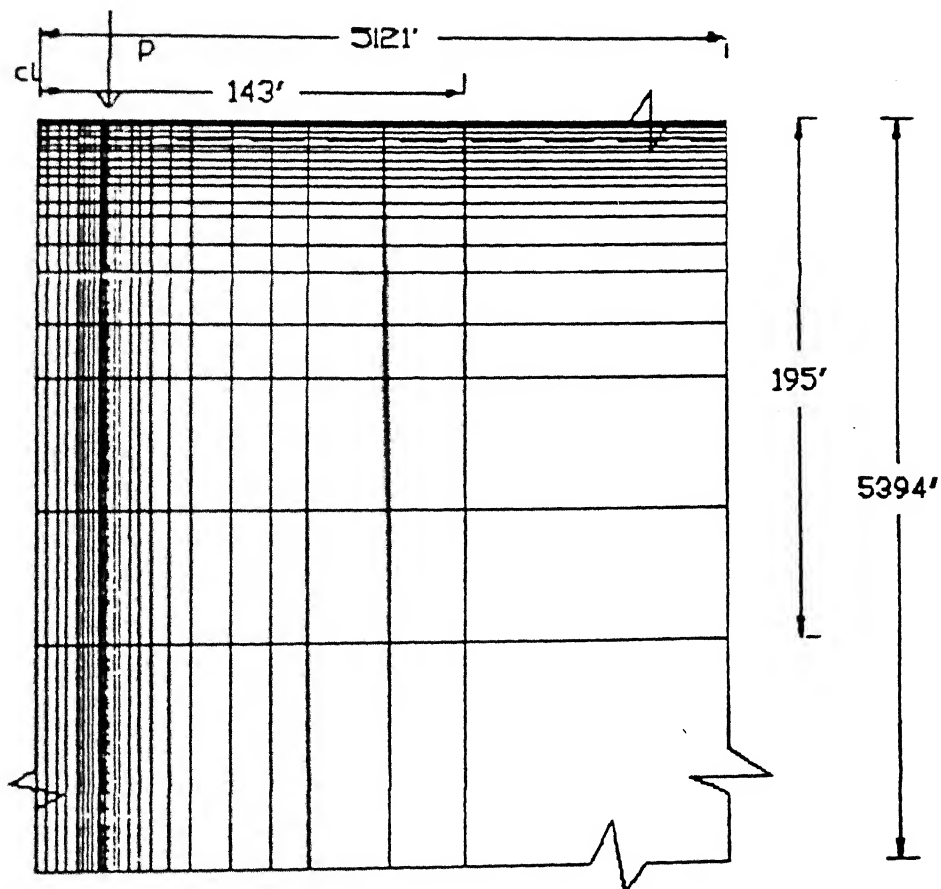


Fig. B1.5 FINITE ELEMENT MESH FOR 2-D ANALYSIS

APPENDIX B2

TESTING OF 3D20N FINITE ELEMENT ROUTINE

The results obtained by solving Boussinesq's concentrated load problem [Jumikis (1966)] by 3-D finite element analysis using 3D20N routine are shown in Figs. B2.1 to B2.2.

Figure B2.1 shows comparison of exact and predicted vertical stress distribution along the depth by using $(4 \times 4 \times 4)$ mesh discretization for 3 sections viz.

1. $x = 0.0$, $y = 0.0$
2. $x = 88.9 \text{ cm}$, $y = 0.0$
3. $x = 177.8 \text{ cm}$, $y = 0.0$

Figure B2.2 shows comparison of exact vertical stress distribution for Boussinesq's concentrated load problem with computed results for $(4 \times 4 \times 4)$ mesh discretization and for $(7 \times 7 \times 7)$ mesh discretization at section $y = 8.05 \text{ cm}$ and $z = 78.15 \text{ cm}$.

Material properties are taken as $E_s = 34.45 \text{ MPa}$ and $\nu_s = 0.33$. Load is vertical and is equal to 144.56 kN . It can be seen that computed results match very well with the exact results.

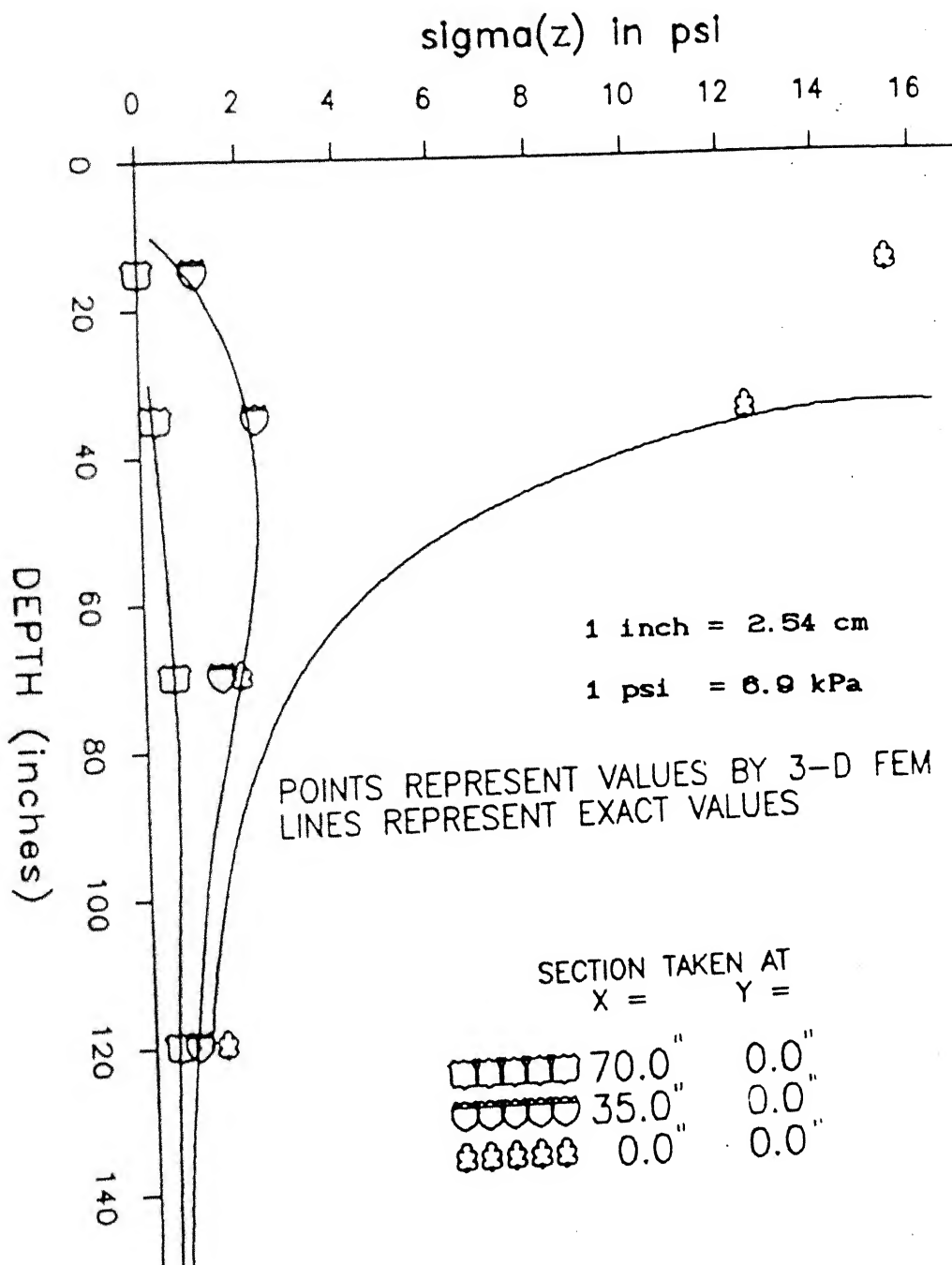


FIG. B2.1 COMPARISON OF EXACT
AND FE SOLUTIONS FOR VERTICAL
STRESS PROFILE -- 3-D CASE

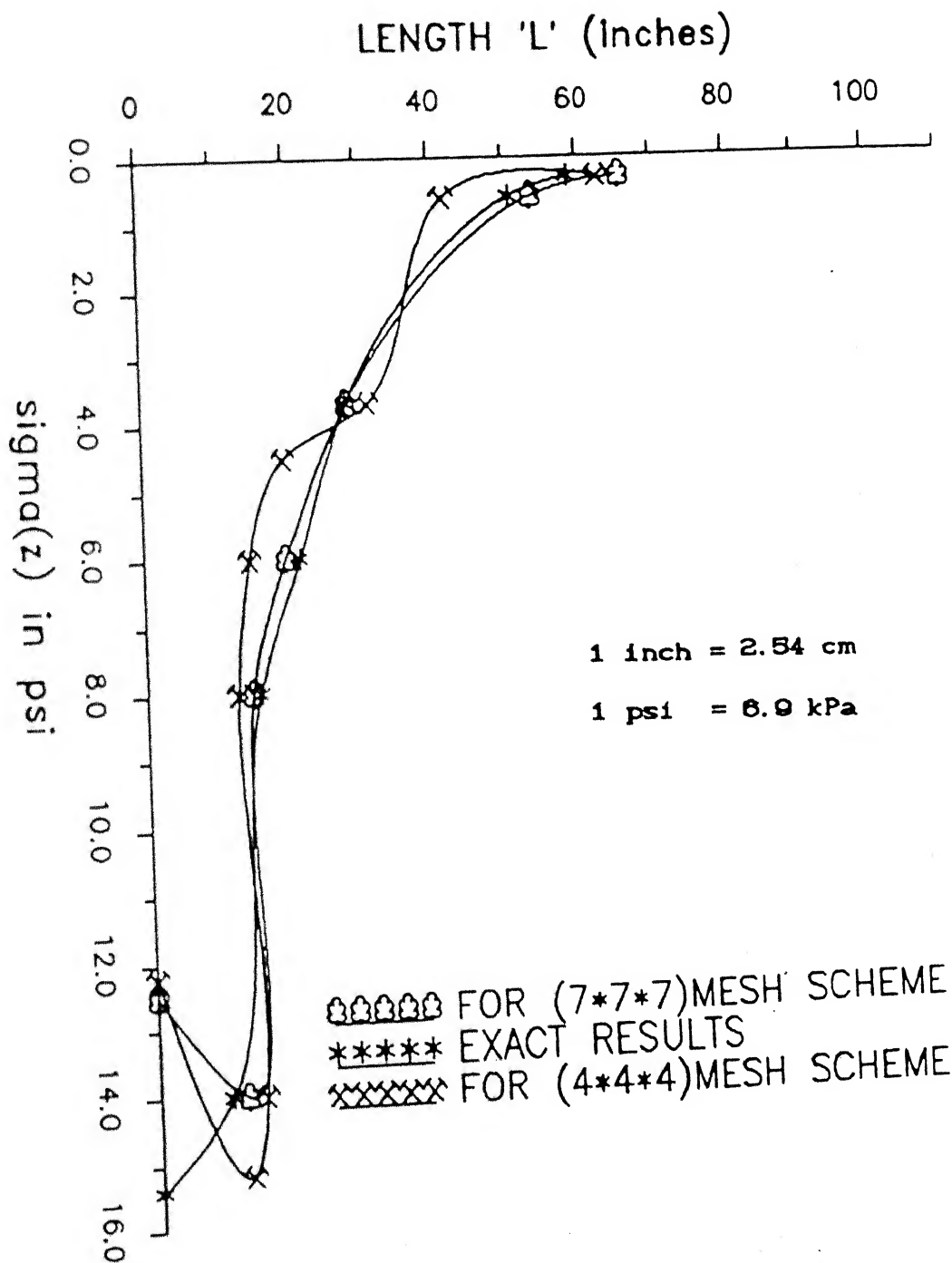


FIG. B2.2 COMPARISON OF EXACT AND FE SOLUTIONS FOR VERTICAL PRESSURE DISTRIBUTION -- 3-D CASE.